Suffusion and its effects on the mechanical behavior of granular soils : numerical and experimental investigations

Rodaina Aboul Hosn

Communauté UNIVERSITÉ Grenoble Alpes

THÈSE

Pour obtenir le grade de

DOCTEUR DE L' UNIVERSITE GRENOBLE ALPES

Spécialité: 2MGE : Matériaux, Mécanique, Génie civil, Electrochimie

Arrêté ministériel: 25 mai 2016

Présentée par

Rodaina ABOUL HOSN

Thèse dirigée par **Luc SIBILLE**
et co-encadrée par **Nadia BENAHMED**

préparée au sein du **Laboratoire Laboratoire Sols, Solides, Structures et Risques** dans **l'École Doctorale I-MEP2 - Ingénierie – Matériaux, Mécanique, Environnement, Energétique, Procédés, Production**
et en collaboration avec **IRSTEA à Aix-en-provence**

Suffusion and its effects on the mechanical behavior of granular soils: numerical and experimental investigations

Thèse soutenue publiquement le **16 novembre 2017**,
devant le jury composé de:

M Jean-Yves DELENNE
Directeur de Recherche, INRA - Université de Montpellier 2, Président
M Pierre BREUL
Professeur, Université Clermont Auvergne, Rapporteur
M Eric VINCENS
Professeur, Ecole centrale de Lyon, Rapporteur
M Bruno CHAREYRE
Maître de Conférences, Institut Polytechnique de Grenoble, Examinateur
Mme Nadia BENAHMED
Chargée de Recherche, IRSTEA - Unité de Recherche RECOVER, Co-encadrante de thèse
M Luc SIBILLE
Maître de Conférences, Université Grenoble Alpes, Directeur de thèse
M David MUIR WOOD
Professeur, University of Dundee, Invité

Acknowledgements

"If I have seen further it is by standing on the shoulders of giants" (Isaac Newton). So I take this opportunity to express my gratitude to all those people who have been instrumental in the successful completion of this research.

My deepest gratitude is to my supervisors, Dr. Luc SIBILLE and Dr. Nadia BE-NAHMED. I have been amazingly fortunate to work with supervisors who gave me the freedom to explore on my own, and at the same time the guidance to recover when my steps faltered. You taught me how to question my thoughts and express ideas. Your patience, support, comments, remarks and engagement during the past three years helped me finish this dissertation.

Moreover, I would like to thank Dr. Bruno CHAREYRE for following my research work and for his insightful comments on my study. I would like also to thank Prof. Jean-Yves DELENNE, Prof. Pierre BREUL, Prof. Eric Vincens, Prof. David MUIR WOOD for being members of the jury.

I am also thankful to the staff system at 3SR and IRSTEA who maintained all the requirements needed in my work. Moreover, I am grateful to the friendly and cheerful group of the fellow students that I was blessed to meet in my daily work. I would like as well to thank all my friends who were away physically but there presence was personalized by their support and encouragement.

Most importantly, none of this would have been possible without the love and patience of my family. My family, to whom I dedicate this dissertation, has been a constant source of love, concern, support and strength all these years. A special gratitude to my parents for instilling the importance of hard work and higher education and to my sisters for opening my eyes to the world, for their patience, understanding and encouragement.

Finally, sincere appreciation is to my fiancé, Salim BOU HAMDAN, for his constant love, support and faithful encouragement throughout the course of this research.

Contents

List of Figures

List of Tables

Abstract

Suffusion is a particular case of internal erosion taking place in hydraulic earth structures. It is characterized by the detachment and migration of fine particles by interstitial flow leaving behind the granular skeleton. Such modifications in the soil microstructure may lead to deformations at the macroscopic scale and may influence the mechanical behavior of the soil. This research was devoted to investigate the suffusion mechanism and its impact on the mechanical properties of cohesionless soils. To achieve this objective, two approaches were followed in this work: numerical and experimental approaches. A discrete numerical model was defined to describe quantitatively the soil macroscopic behavior and to analyze the microstructure of granular assemblies. It is based on the use of spherical particles and contact rolling resistance, as well as a new method of compaction to mimic the one used in laboratory and to reach a wide range of initial densities. The model was validated through comparison of numerical results with experimental data. This model was first applied on granular assemblies with different fines contents to study the role of fine particles with respect to a given soil microstructure, without taking into account an erosion process. It was shown that there exists a fines content, below the threshold, where fine particles may start to participate in the force transfer that if suffusion initiates and mobilizes these particles, it may affect the macroscopic behavior of the soil. Thereafter, a simplified kinetics of grain extraction was proposed to describe the suffusion process. It was based on a one-way fluid-solid coupling approach. The importance of this extraction procedure is that, on one hand, it takes into account complex geometric and hydraulic criteria; on the other hand, the model involves an affordable computational cost. This procedure was validated based on experimental tests carried out using a newly developed suffusion apparatus. Consequences of this erosion on the mechanical properties of soils were characterized from experimental and simulated triaxial compression tests. Suffusion development and its consequences on the macroscopic behavior are discussed from the results obtained in terms of the initial soil density and gradation, the hydraulic loading and the type of eroded particles (active or inactive in the force transfer).

Key words: internal erosion . discrete numerical model . mechanical characterization . granular soils . suffusion tests . fluid-solid coupling

Résumé

La suffusion est un cas particulier d'érosion interne qui apparait dans les ouvrages hydrauliques. Elle se caractérise par le détachement et le transport des particules fines à travers les gros grains sous l'action d'un écoulement hydraulique en laissant derrière un squelette granulaire dont les caractéristiques en termes de densité et d'arrangement géométrique granulaire ont été changées. De telles modifications dans la micro-structure du sol peuvent conduire à des déformations à l'échelle macroscopique et peuvent influencer le comportement mécanique du sol. Ce travail a été consacré à l'étude du mécanisme de suffusion et à son impact sur les propriétés mécaniques des sols non-cohésifs. Pour atteindre cet objectif, deux approches ont été suivies dans ce travail: l'une numérique et l'autre expérimentale. Un modèle numérique discret a été défini pour décrire quantitativement le comportement macroscopique du sol et analyser la micro-structure des assemblages granulaires. Il est basé sur l'utilisation de particules sphériques et la résistance au roulement aux contacts, ainsi que sur une nouvelle méthode de compactage des échantillons pour simuler celle utilisée au laboratoire, et atteindre une large gamme de densités initiales. Le modèle a été validé par comparaison de résultats numériques et de données expérimentales. Ce modèle a d'abord été appliqué sur des assemblages granulaires avec des teneur en fines différentes afin d'étudier le rôle des particules fines pour une micro-structure de sol donnée, sans tenir compte d'un processus d'érosion. Il a été montré qu'il existe un pourcentage de fines, en dessous de la teneur seuil, où des particules fines peuvent commencer à participer au transfert de force, et que, si la suffusion s'initie et mobilise ces particules, ceci pourra affecter le comportement macroscopique du sol. Par la suite, une cinétique simplifiée d'extraction du grain a été proposée pour décrire le processus de suffusion. Elle est basée sur une approche de couplage fluide-solide partielle. L'intérêt de cette procédure d'extraction est que, d'une part, elle tient en compte des critères géométriques et hydrauliques complexes; d'autre part, le modèle induit un coût de calcul raisonnable. Cette procédure a été validée sur la base d'essais expérimentaux de suffusion effectués avec un dispositif nouvellement développé. Les conséquences de cette érosion sur les propriétés mécaniques des sols ont été caractérisées par la réalisation en laboratoire et la simulation d'essais de compression triaxiale. Le développement de la suffusion et ses conséquences sur le comportement macroscopique sont discutés en terme de densité et granulométrie initiale du sol, de chargement hydraulique et du type de particules érodées (actives ou inactive vis-à-vis du transfert de force).

Mots clés: érosion interne . modèle numérique discret . caractérisation mécanique . sols granulaires . essais de suffusioon . couplage fluide-solide

General introduction

Research motivation

Internal erosion in soils is a phenomenon defined as the migration of soil particles through a porous medium by a fluid flow. It is, therefore, a multidisciplinary process which is governed by soil mechanics and hydraulics principles. Internal erosion poses serious problems in different engineering fields. Sand production is a major issue in petroleum engineering where the migration of fine particles may lead to the clogging of the soil reservoir such that it can reduce the oil production (Papamichos et al. (2001)). In geotechnical engineering, the migration of fine particles may lead to the collapse of soil structures such as embankment dams and levees. The floods induced by these failures can cause catastrophic disasters described by enormous amounts of damage to infrastructures and a significant risk to human and animal life (for example, the collapse of Teton dam (Seed & Duncan (1987)) as shown in Figure 1). Statistical analysis show that internal erosion is the major cause of approximately half of the failures of embankment dams (Foster et al. (2000)).

Internal erosion presents itself in many different forms. Of particular concern is the effect of internal erosion by suffusion on the mechanical properties of the soil. This study focuses on the suffusion process involving the selective erosion of fine particles within the matrix of coarse particles. Such a particle-scale mechanism is characterized by the detachment and the migration of fine grains by the interstitial flow leaving behind the granular skeleton. These modifications in the soil microstructure may lead to deformations at the macroscopic scale and may influence significantly the mechanical behavior of the soil. An under-studied aspect in the geotechnical field is the lasting effects that suffusion may have on the soil shear strength. Additional insight into this topic can facilitate further understanding of the involved mechanisms and processes and will lead to more adequate design, maintenance and protection of many hydraulic earth structures against the destructive forces of suffusion.

During the suffusion process, the soil structure is modified and the post-suffusion behavior may be strongly affected. Intensive research has been devoted to study the role of fine particles in the soil structure. Studies showed that the fines content may influence significantly the microstructure of the soil. The participation of particles of different sizes in the inter-particle contact force network changes with the fines content (Thevanayagam (1998, 2000); Shire et al. (2014, 2015)). Moreover, the fines content has a strong influence on the shear strength and the onset of mechanical instabilities in soils as well as on the position of the critical state line of silty sands (Benahmed et al. (2015); Yin et al. (2014a)). Therefore, the soil behavior seems to be dependent on the range of fines content, which may explain the changes in the soil strength after suffusion. Nevertheless, volumetric
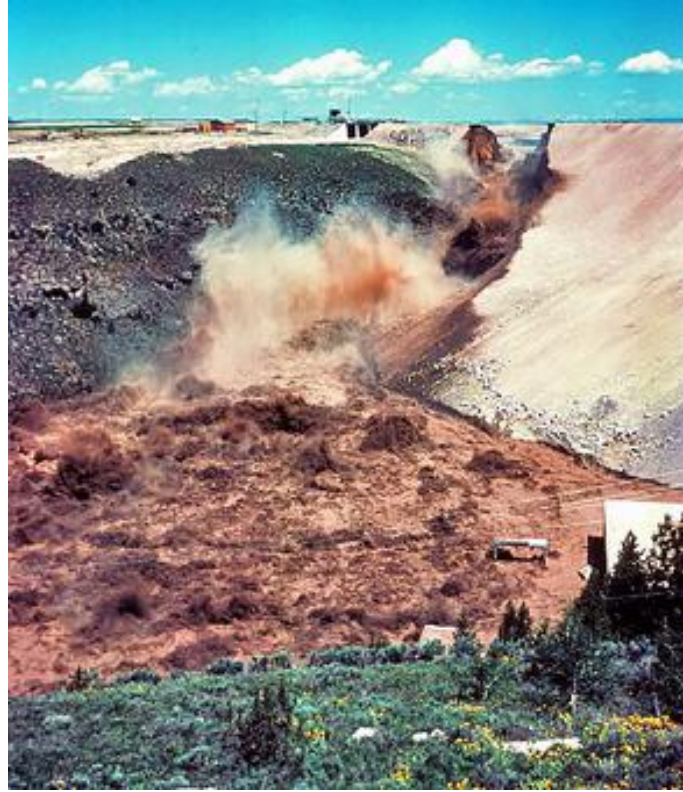
Figure 1: Catastrophic failure of the Teton Dam (picture from wikipedia).

deformation of soil (subjected to its own weight and/or an external loading) may also be induced by suffusion development and changes in soil mechanical properties may not be deduced from considerations of the fines content only. Soils reconstituted with different fines contents can help understand the role of fines in the mechanical behavior of soil but they may not be representative of eroded soils. Induced modifications in the microstructure due to the selective erosion of fine particles should be taken into consideration.

Besides, several laboratory investigations have been carried out to study the development of suffusion and its induced effects on the soil properties. Erosion tests, by developing suitable apparatus for that purpose, showed the influence of soil gradation and hydraulic gradient on erosion rates. Changes in the void ratio and the hydraulic conductivity were also reported. It was found by Sibille et al. (2015) that the initial fines content and the history of the hydraulic loading play a major role in the suffusion development and an expression of the erosion rate was proposed to predict the cumulative eroded mass. Concerning the mechanical behavior, contradictory conclusions were found. An increase or a decrease in the soil strength may occur (Ke & Takahashi (2012b, 2014a,b); Xiao & Shwiyhat (2012); D. Chang & Zhang (2011); D. Chang et al. (2012)). Therefore, further investigations are necessary in order to describe and model how a suffusive erosion affects the constitutive behavior of soils.

In addition to experimental studies, few numerical studies are available to describe qualitatively the relation between the removal of soil particles and its consequences at the macroscopic scale. Few studies include direct coupling between solid and liquid phases to analyze the migration and filtration processses during internal erosion (Sari et al. (2011)).

More recently, Tejada et al. (2016) investigated the effects of the intermittent blockage of constrictions and its consequences on the particle transport showing an exponential decay between consecutive trapping events. Other numerical studies immitate erosion by defining a procedure allowing the removal of particles without considering a fluid phase (Scholtès et al. (2010); Muir Wood & Maeda (2007); Muir Wood et al. (2010)). The latter is an efficient method from a numerical point of view, being simple and requiring less computational resources. However, the removal of particles is usually based on the particle's size and the stress that a particle holds. So this method lacks other criteria that play a major role in the erosion of fine particles, such as, the constriction sizes to allow particles to pass through or the driving fluid forces to cause particles to move.

Therefore, motivated by finding a clear relation between the erosion of fine particles and the mechanical properties of soils, this study introduces a numerical approach based on the discrete element method (DEM) and an experimental approach using a newly developed suffusion apparatus.

Research objectives

The main objective of this study is to describe the changes in the mechanical properties of eroded soils by suffusion. To achieve that, numerical and experimental approaches will be considered:

- a DEM model will be defined to attempt to describe quantitatively the modifications in the soil microstructure by a seepage flow;

- a simplified kinetic of grain extraction describing the suffusion process to be able to perform quantitative simulations with realistic computational costs will be proposed;

- experimental tests will be performed to validate the numerical model (if possible). Laboratory tests will be used to build a global conclusion of the effect of suffusion on the soil mechanical properties in addition to numerical results;

- since the evolution of the soil properties with suffusion is directly related to the role of fine particles (potentially erodible) in soils, the role of fine particles with respect to a given soil microstructure (i.e. without taking into account an erosion process) will be investigated;

- all the obtained data will be devoted to conclude the impact of suffusion on the soil macroscopic properties.

Thesis outline

This thesis is organized in five chapters grouped in three parts:

- **Part I** provides a literature review of the main findings of previous studies about internal erosion and more particularly suffusion. It consists of **Chapter 1** which introduces the suffusion phenomenon and highlights the main challenges facing researchers in studying the effect of suffusion on the mechanical properties of the soil.

- **Part II** is dedicated to the definition of the numerical tools used in this study. It comprises two chapters:

  – **Chapter 2** introduces the discrete numerical model followed in this study using spherical particles and inter-particle rolling friction. This model was then used to analyze polydisperse granular assemblies with different fines contents.

  – **Chapter 3** introduces the numerical extraction procedure followed in this study to mimic the suffusion process. An original approach which is a compromise between very simplified existing extraction procedures and complete hydromechanical coupling is defined. It is based on a one-way fluid-solid coupling which allows taking into account both hydraulic and geometric criteria to describe the detachment and the migration of fine particles with a reasonable computational cost. Moreover, the defined extraction procedure is applied on a narrow grading to assess in such a simplified case the potentiality of the proposed methodology.

- **Part III** presents the results of the experimental and numerical approaches to study the consequences of suffusion on the mechanical behavior of an internally unstable granular soil. It comprises two chapters:

  – **Chapter 4** introduces the experimental approach using a suffusion apparatus newly developed in IRSTEA to investigate the initiation and development of internal erosion. Thereafter, eroded soil samples were subjected to triaxial compression tests to study the effects of suffusion on the soil mechanical properties.

  – **Chapter 5** presents the numerical suffusion results and the characterization of the mechanical properties for discrete models calibrated on the experimental data. The numerical extraction procedure defined in Chapter 3 is applied on a grain size distribution similar to that used experimentally. A combined analysis of the suffusion results is given by comparing both the experimental and the numerical data.

Finally, a general conclusion summarizes the main outcomes of this thesis and provides recommendations for future research works.

Part I
Literature review

Chapter 1

Internal erosion of soils by suffusion: elements from the literature

1.1 Introduction

This Chapter introduces elements from the literature concerning an internal erosion process by suffusion. First, in Section 1.2, a description of the suffusion phenomenon is given. Then, the different factors that affect the initiation of suffusion are discussed in Section 1.3 including geometric, stress and hydraulic conditions. Thereafter, the description of the suffusion development is presented in Section 1.4. Due to the loss of fine particles, the mechanical behavior of the soil is modified. Thus, Section 1.5 presents the effects of suffusion on the mechanical properties of the soil. Finally, a review of the main results concluded from the literature is given in Section 1.6.

1.2 Suffusion, a particular case of internal soil erosion

Internal erosion phenomena occur in soils when solid particles are detached from the solid phase and transported by the seepage flow due to a hydraulic load that exceeds the erosion resistance of the material. These phenomena are widely observed in hydraulic earth structures, such as embankment dams and levees, and imply a particular threat (Stewart & Watts (2000); Zhang & Chen (2006); Fell & Fry (2007)). Statistical analysis showed that internal erosion is the governing failure mode of approximately half of the failures of embankment dams (Foster et al. (2000); Richards & Reddy (2007)).

Internal erosion can be initiated in four different forms: concentrated leak, backward erosion, contact erosion, and suffusion (Fell & Fry (2007); Bonelli (2012)). This study focuses on the suffusion process involving the selective erosion of fine particles within the matrix of coarse particles. Soils vulnerable to suffusion are often considered internally unstable, indicating that the constrictions formed by the coarser fraction, which constitutes the soil skeleton, are sufficiently large to allow the migration of fine particles. Broadly graded soils and gap-graded soils are usually susceptible to suffusion (Wan & Fell (2008)).

Different terms and definitions have been used in the literature to describe such a particle-scale mechanism. Kovacs (1981) gave two terms: internal suffusion and external suffusion.

The first is defined as the "redistribution of fine grains within the layer, when the solid volume of the layer is not changed, only the local permeability is altered"; while external suffusion is "scouring of fine grains, when the volume of the solid matrix is reduced, accompanied by an increase in the permeability, but the stability of the skeleton composed of the coarse grains is unaffected". Chapuis (1992) defined another term, "suffosion" as "the transport of small particles from a soil, which leaves large openings between the particles". Fell et al. (2005) defined suffusion as the inability of the coarser fraction of a soil to prevent migration of its finer fraction as a result of seepage flow. Moffat & Fannin (2006) separated the phenomenon of internal instability into "suffusion" and "suffosion". Suffusion is when the finer fraction of an internally unstable soil moves within the coarser fraction without any change in total volume, while suffosion, is when the particle migration yields a reduction in total volume and maybe collapse of the soil matrix. Wan & Fell (2008) defined suffusion as the process by which finer soil grains move through constrictions between larger soil grains by seepage forces. To avoid confusion, "suffusion" is considered in this study to describe internally unstable soils as defined by Fell et al. (2005) and Wan & Fell (2008) without any distinction between suffusion or suffosion.

The suffusion mechanism is characterized by the detachment and the migration of fine grains by interstitial flow leaving behind the granular skeleton. Figure 1.1 illustrates the suffusion process. During such a strongly coupled fluid-solid interaction process, the coarse
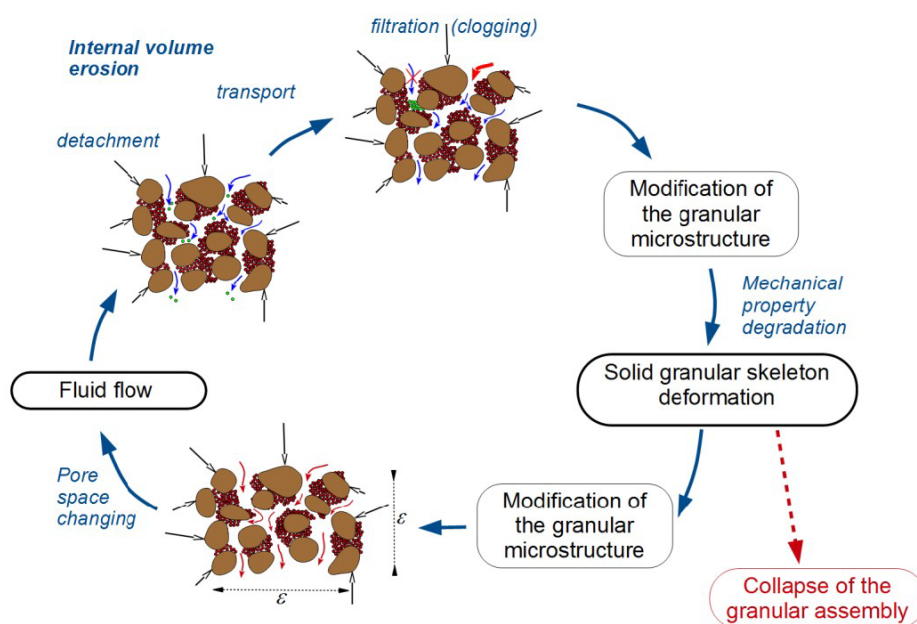
Figure 1.1: Illustration of the suffusion process (Sibille (2016)).

matrix stays intact while fine particles in the pore spaces are mobilized if smaller than the pore constriction sizes. By modifying the microstructure of the soil through the evacuation or the displacement of fines, suffusion can induce locally some mechanical degradations of the soil, which under a constant external mechanical load may present some deformations. These deformations may lead, on one hand, to the modification of the pore spaces, thus resulting in obvious changes in the porosity and the hydraulic conductivity. On the other hand, suffusion may lead to the loss of the mechanical resistance of the soil and may

eventually lead to its collapse. Although it takes years, or even decades, for a problem to develop, this phenomenon can be highly destructive (see for instance the collapse of Dychow dam (Dluzewski & Hrabowski (1998))). Moreover, if the fine particles are not small enough to pass through constrictions, clogging (at least partially) of constrictions may take place, hindering thereby, the continued erosion. Hence, suffusion may lead to clogging of the pore space accompanied with an excess pore water pressure which may also have devastating consequences if not alleviated.

1.3 Factors affecting the initiation of suffusion

Suffusion occurs if the following criteria are satisfied (Wan (2006)):

- the size of fine particles is smaller than the size of the constrictions between coarse particles, which form the skeleton of the soil (geometric criterion);

- the amount of fine particles is less than enough to fill the voids between the coarse particles (stress criterion);

- the hydraulic loading is strong enough to move fine soil particles through the voids between coarse particles (hydraulic criterion);

In what follows, the different geometric criteria based on the particle size distribution, PSD, and the constriction size distribution, CSD, will be presented. Then, the stress criteria will be addressed. For that purpose, the role of fine particles in the stress transfer in the granular assembly is highlighted and the microstructure of polydisperse granular assemblies is described. Finally, the hydraulic loading responsible for the initiation and the development of suffusion is discussed.

1.3.1 Geometric criteria of potentially erodible soils

A variety of empirical methods have been proposed to assess the potential for internal stability of soils. Some of these methods are presented in this section. These investigations are based on the "filter" concept whereby coarser fractions serve as a filter when water flows through. The potential that the finer fraction is flushed out depends on the grain size ratio between the filter and the fines layer which should not exceed an empirically derived threshold. Terzaghi & Peck (1948) proposed $\frac{D_{15}^f}{4}$ to characterize the constriction size in a filter where D_{15}^f is the particle diameter for which 15% of the mass of the filter is finer than. Then, the soil retention criterion $\frac{D_{15}^f}{4} < d_{85}$ is derived, where d_{85} is the particle diameter for which 85% of the mass of the fine fraction is finer than (Terzaghi & Peck (1948)). Later, for internal stability problems, Kezdi (1979) adopted the index ratio $\frac{D_{15}^{'}}{d_{85}^{'}}$ proposed by Terzaghi, based on splitting the gradation to distiguish between $D_{15}^{'}$ of the coarse fraction and $d_{85}^{'}$ of the finer fraction. $D_{15}^{'}$ was considered as an approximation of the constriction size in the coarse fraction. If $\frac{D_{15}^{'}}{d_{85}^{'}} < 4$, the soil is deemed internally stable. Fannin & Moffat (2006) demonstrated experimentally that gradations close to that limit value appear stable, whereas a soil with $\frac{D_{15}^{'}}{d_{85}^{'}} \approx 7$ exhibited internal instability at relatively a low hydraulic gradient.

In addition to that, Istomina (1957) evaluated the internal stability as well but using the coefficient of uniformity (Cu) as a basic index of the grain size distribution curve. If Cu $\leq$ 10, the soil is internally stable; if Cu $\geq$ 20, the soil is internally unstable; if 10 $\leq$ Cu $\leq$ 20, the soil is deemed a transitional material.

Another alternative index ratio, $\frac{H}{F}$, was proposed by Kenney & Lau (1985, 1986) based on the interpretation of laboratory suffusion tests. H is the mass fraction of grains with a diameter in the interval D to 4D and F is the mass fraction of grains smaller than D. The lowest value of $\frac{H}{F}$ is sought for D taking successively the different particle sizes constituting the considered soil. A threshold value of $\frac{H}{F} > 1$ was advocated at F < 0.2 in soils having a widely graded coarse fraction and at F < 0.3 in soils with a narrowly graded coarse fraction.

Chapuis (1992), later, analyzed several empirically derived methods for the internal stability assessment of granular soils and unified the criteria to one parameter which is the slope of the grading curve. It was found that soils with a particle size distribution which is linear or slightly concave is stable against suffusion; However, as the gradation becomes more concave, the soil becomes more internally unstable.

Recently, D. Chang & Zhang (2013b) evaluated three commonly used geometric criteria: Istomina's criterion, Kenney and Lau criterion and Kezdi's criterion. Then, they identified control variables based on the physical understanding of the microstructure. The following extended internal stability criterion was then defined for well-graded and gap-graded soils:

- a well-graded soil with a fines content less than 5% is internally stable if it satisfies $(\frac{H}{F})_{min} > 1$;

- a gap-graded soil with a fines content less than 10% is internally stable if its gap ratio is smaller than 3;

- a well-graded soil with a fines content greater than 20%, or a gap-graded soil with a fines content greater than 35%, is deemed to be internally stable;

Thus, several geometric methods have been defined in the literature. However, laboratory observations of self-filtration done by Raut (2006) showed that these methods are likely conservative, as also confirmed by Wan & Fell (2008). Moreover, from a database of 57 gradations from eight published laboratory studies, Li (2008a) demonstrated that Kezdi's method is relatively more conservative for F < 0.15 and the Kenney and Lau method is more conservative for F >0.15.

In fact, such geometric methods are based on the particle size distribution. However, according to Kenney et al. (1985), the controlling void entities in the filtration process are the constrictions, defined as the narrow sections between pores. Therefore, recent research works based on geometric criteria (Vincens et al. (2014); Silveira (1965); Locke & Indraratna (2001)) take directly into account the constriction size distribution, CSD, instead of using the particle size distribution, PSD. Accordingly, detached particles should overcome such key obstacles to pass through the filter. Reboul et al. (2010) and Vincens et al. (2012, 2014) summarized the methods for evaluating the constriction size distributions of a numerical assembly of spheres which were generated by the Discrete Element Method

(DEM) and where the void geometry was evaluated by a radical Delaunay triangulation. Since such an evaluation requires a high computational cost, simple probabilistic alternative methods are commonly used. Silveira (1965) assessed the soil filtration by analyzing the cumulative constriction size distribution (CSD) derived from the grain size distribution with assumptions about the geometric packing. The probability of a soil grain to pass through a potential path in a granular medium was examined depending on the constriction sizes of the interstitial space and their occurrences within the filter. Locke & Indraratna (2001) and Indraratna et al. (2007, 2015) also improved the retention criterion for non-uniform granular filter design by calculating the constriction size distribution instead of using directly the particle size distribution.

1.3.2 Microstucture of polydisperse granular assemblies (stress criterion)

For the initiation of suffusion, fine particles must be small enough to pass through the constrictions of the void network between coarser particles, but they must not completely fill the voids formed by the coarse particles. Intensive research has been devoted to the role of fine particles in the soil structure showing that the fines content, FC (the ratio of the mass of fines to the total soil mass), may influence significantly the microstructure of the soil. Consequently, the soil behavior depends on the range of fines content, which, according to some researchers, may explain the changes in the soil strength after suffusion. For example, some experimental studies have indicated that changes in the fines content may cause either a decrease or an increase in the soil shear strength. Skempton & Brogan (1994) proposed that the critical FC below which fines play a minor role in stress transfer is 24-29% depending on the relative density, with an upper limit (usually called threshold fines content, FC_{th}) of 35% above which fines completely separate the coarse particles from one another and the material becomes internally stable. Similarly, both, Polito (1999) performed cyclic triaxial tests and Naieni & Bazier (2004) carried out a series of undrained monotonic and dynamic triaxial compression tests and they found that, at a constant global void ratio, as FC increases up to 35%, the peak shear strength (and the residual shear strength) decreases. Beyond that threshold value, the peak shear strength (and the residual shear strength) increases (Figures 1.2a, and 1.2b).
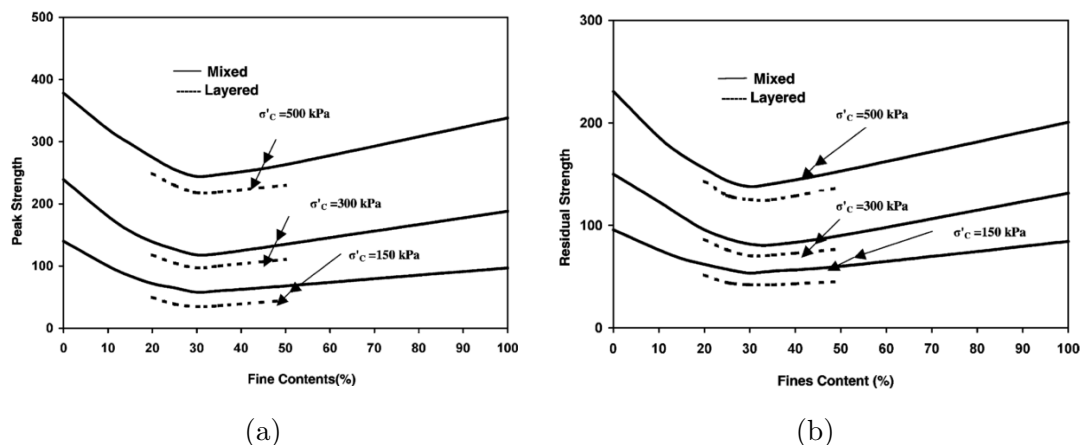
Figure 1.2: Peak and residual shear strengths of mixed and layered samples versus fines content (Naieni & Bazier (2004)).

Nowadays, more studies concentrate on the description of the fabric of polydisperse granular media to study the role of fine particles at the microscopic scale. This helps in understanding the internal stability of polydisperse granular assemblies. According to Vallejo (2001), the soil mechanical properties mainly depend on coarse particles when the percentage of coarse particles is greater than 70%, while fine particles dominate if the percentage of coarse particles is less than 40%. In between these limits, the macroscopic mechanical properties depend on both coarse and fine particles. However, a recent study done by Benahmed et al. (2015) on silty sand mixtures showed that fine particles affect the soil shear strength even for low fines content down to 5%. Thus, one should not neglect even small fractions of fine grains.

In fact, the threshold fines content, FC_{th} depends as well on the size ratio. FC_{th} decreases with the size ratio as shown in Figure 1.3. In other words, as the size ratio increases, more fine particles are needed to fill the void spaces between coarse particles, increasing, therefore, the threshold fines contact.
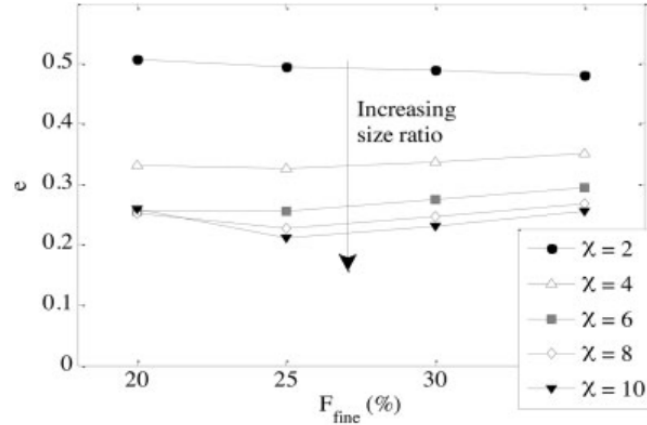
Figure 1.3: Variation of void ratio with the fines content, FC, and size ratio χ (Shire et al. (2015)).

Later, Voivret et al. (2009) investigated with a discrete numerical model the morphology and space-filling properties of polydisperse densely packed granular media. They found that two conditions are required to fill efficiently the pores: a broad size distribution which corresponds to higher size span (size span: $s = \frac{d_{max} - d_{min}}{d_{max} + d_{min}}$, where d_{min} and d_{min} are the smallest and largest diameters, respectively); and a large number of smaller particles. They concluded as well that the larger particles capture the strongest force chains, whereas small particles often miss them but provide support to the granular skeleton. This shows that the coarse grains have the main role in stress transfer in internally unstable soils.

This observation was recently confirmed by Shire & O'Sullivan (2013) using the discrete element method to analyze the relationship between the grain-scale fabric and the empirical criterion for assessing the internal stability as proposed by Kezdi (1979) for a series of idealized gap-graded soils with varying particle size distribution and fines content, FC, at a single relative density level. They studied the degree of interlocking of fine particles with neighboring particles with respect to their participation in the stress transfer in the granular skeleton. They found that the average number of inter-particle contacts per particle decreases as internal instability, with respect to Kezdi's criterion, increases as shown in Figure 1.4. This represents an increase in the proportion of loose, erodible fine particles. Therefore, the participation of a given particle in force chains decreases as internal instability increases. It is important to note that $(D'_{15}/d'_{85})_{max}$ has been usually used as an empirical geometric criterion. However, Shire & O'Sullivan (2013) has given this ratio a physical meaning by linking it to physical parameters.
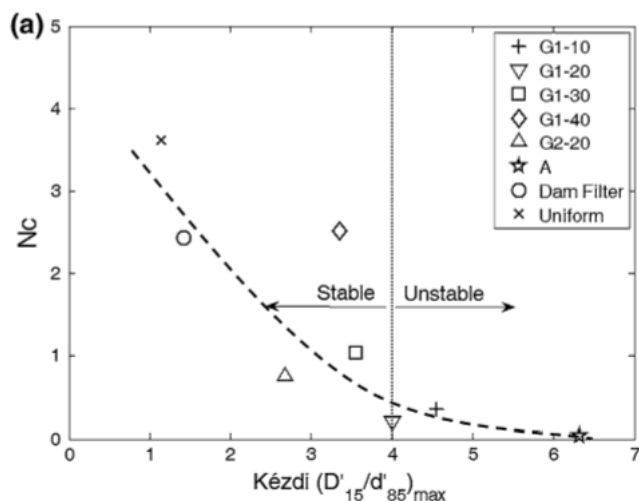
Figure 1.4: Variation in coordination number, N_c, with ratio $(D'_{15}/d'_{85})_{max}$ used in Kezdi's criterion (Shire & O'Sullivan (2013)).

The reduction in stress in the finer fraction can be quantified by the α-factor which is the ratio of the effective stress transferred by the finer fraction to the overburden effective stress (Skempton & Brogan (1994); Li (2008a); Shire et al. (2014)). Figure 1.5 shows the influence of FC and the relative density on α. It can be noticed that if $FC < 25\%$, the soil can be considered underfilled and the finer particles will sit loose in the voids. If fine particles can pass through the constrictions in the void network, there is a potential for suffusion. If $FC > 35\%$, the soil is overfilled, where the finer particles completely fill the voids and stress transfer is shared between coarse and fine grains. Overfilled soils can be considered internally stable. For transitional soils, α depends on the relative density, so an increase in the relative density significantly enhances the stress in the finer fraction and consequently enhances internal stability.

It can be concluded that the size ratio between coarse and fine particles, FC, and
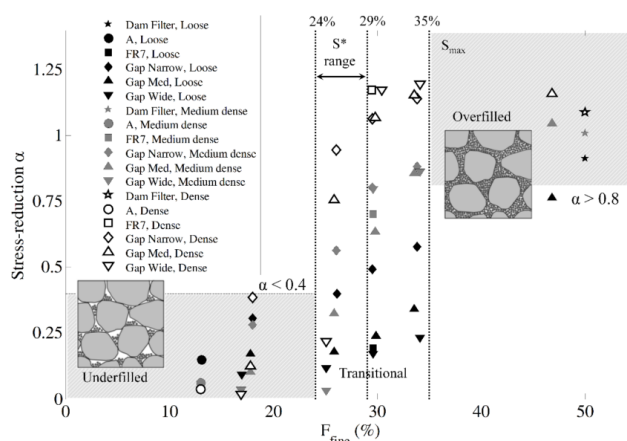
Figure 1.5: Variation of stress-reduction, α, with the fines content (Shire et al. (2014)).

the density of the soil are important parameters which should be coupled with geometric internal stability criterion to assess the potential of instability.

1.3.3   Effects of the hydraulic loading

In the previous sections, it was shown that the geometric and stress criteria help identify potentially erodible soils. However, the initiation of suffusion in potentially unstable soils is triggered if the hydrodynamic forces induced by the seepage flow on soil grains exceed a critical threshold. Therefore, even if soils satisfy a geometric criterion, sufficiently strong hydraulic loading is necessary to detach particles (Kovacs (1981); Terzaghi (1939); Skempton & Brogan (1994)).

In this section, the following points will be discussed:

- parameters related to the fluid phase affecting suffusion initiation;

- detection of suffusion initiation;

- factors affecting the critical hydraulic gradient;

Parameters related to the fluid phase affecting suffusion initiation

In laboratory investigations, seepage flow is maintained by assigning a constant water flow (Ke & Takahashi (2014a)) or a hydraulic pressure difference (D. Chang & Zhang (2011)). The critical threshold of these parameters represents the onset of suffusion. Unlike the critical hydraulic gradient, i_c, for soil stability as proposed by Terzaghi (1939) for cohesionless soils to determine a zero effective stress condition (always accompanied by the phenomenon of "heaving" where i_c is approximately equal to 1), the critical hydraulic gradient for internal erosion corresponds to the minimum hydraulic gradient at which the first sign of internal erosion appears when the imposed hydraulic gradient gradually increases.

Other approaches to characterize the suffusion initiation are based on:

- the average pore velocity (Perzlmier (2007)): this approach can be used to characterize the hydraulic solicitation to initiate suffusion. Moreover, it takes into account the spatial variability and the anisotropic characteristics of the hydraulic conductivity;

- the hydraulic shear stress (Reddi et al. (2000)): the evolution of the suffusion rate with respect to the hydraulic shear stress allows identifying a critical hydraulic shear stress at which suffusion initiaties;

- the fluid stream power (Marot et al. (2011, 2012)): in this approach, the energy dissipated by the fluid, when it flows within the porous medium is determined. Changes of hydraulic soil characteristics are implicitly taken into account through the flow power. Thus, the hydraulic loading and its evolution, as well as the soil response to this loading are completely coupled;

Detection of suffusion initiation

The initiation of suffusion can be evaluated from changes in the hydraulic gradient or the flow rate, the hydraulic conductivity and/or the observed eroded mass.

Skempton & Brogan (1994) developed an upward-flow permeameter with local head

measurements, and found the critical hydraulic gradient that triggers suffusion in cohesion-less soils. It was defined when a sudden increase in the outflow is noticed. The hydraulic gradient for internal erosion was found to be about one-fifth to one-third of the critical hydraulic gradient for soil stability against heave as defined by Terzaghi. Similarly, Shire et al. (2014) provided evidence to the hypothesis of Skempton & Brogan (1994) that internal instability can occur at lower hydraulic gradients than would be required for failure by heave or piping because finer particles may carry low stresses.

In addition, as fine particles migrate through the pore space, the hydraulic conductivity changes. A sudden increase in the hydraulic conductivity with the loss of fine particles can be noticed as shown in Figure 1.6a which is accompanied by a decrease in the hydraulic gradient (Figure 1.6b).
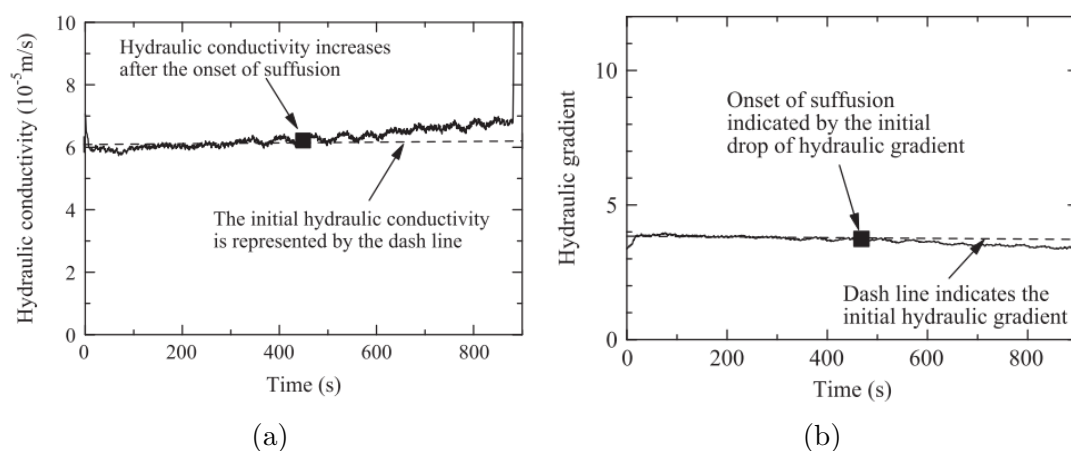
Figure 1.6: Variation of (a) the hydraulic conductivity and (b) the hydraulic gradient with time (Ke & Takahashi (2014a)).

Factors affecting the critical hydraulic gradient

Different factors may influence the critical hydraulic gradient initiating suffusion. These include: the initial soil's density, the fines content, the history of hydraulic loading and the mean effective stress.

Erosion tests on gap-graded non-cohesive soils with different densities show that specimens with a larger relative density require a higher critical hydraulic gradient for the initiation of suffusion as shown in Figure 1.7 from experimental tests done by Ke & Takahashi (2012b).
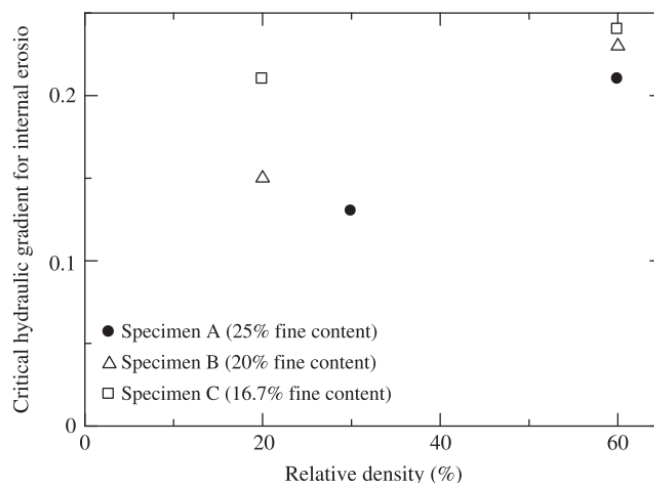
Figure 1.7: Relationship between relative density and critical hydraulic gradient (Ke & Takahashi (2012b)).

Furthermore, the lower the fines content, the larger the hydraulic gradient required to cause internal erosion as shown by Ke & Takahashi (2012b, 2014a) (Figure 1.8).
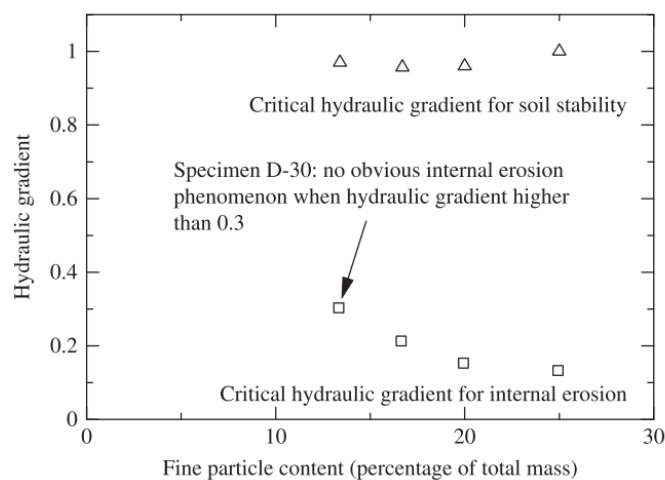
Figure 1.8: Relationship between relative density and the hydraulic gradient (Ke & Takahashi (2012b)).

In addition to that, the mean effective stress may influence the critical hydraulic gradient at which suffusion initiates (Li (2008a); Moffat & Fannin (2011); Moffat et al. (2011)). Li (2008a) found a linear relation between the critical hydraulic gradient and the mean effective stress as shown in Figure 1.9. As the mean effective stress increases, the soil stability is maintained up to higher values of the hydraulic gradient beyond which suffusion initiates.

Besides, one should not neglect the effect of the hydraulic loading. Sibille et al. (2015) performed a series of erosion tests on mixtures of glass beads with two different fines
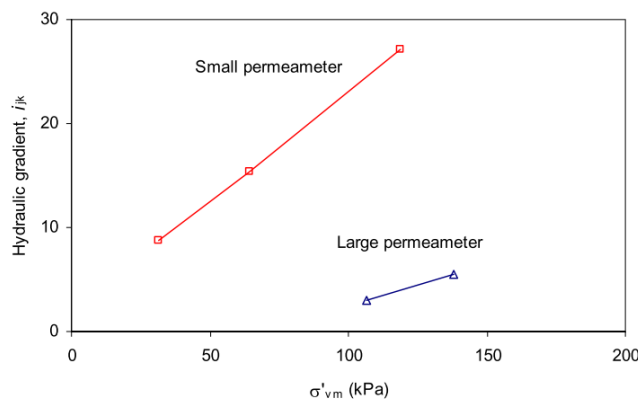
Figure 1.9: Relation between critical gradient and vertical effective stress (Li (2008a)).

contents (20% and 40%). The applied hydraulic gradient is increased by stages for different amplitudes and duration. It was observed that the initial content of fine particles and the history of hydraulic loading are important parameters in the suffusion initiation and development. In other terms, the cumulative eroded mass, the induced deformations and the evolution of the hydraulic properties change for different FC and for different hydraulic loadings.

1.4 Suffusion Development

In this section, the different phases of suffusion develpment are described. Thereafter, the volumetric deformation of soil samples during erosion is presented. Then, the effects of stress state on the suffusion process are addressed.

1.4.1 Different phases of suffusion development

Suffusion development can be characterized by analyzing the evolution of the erosion rate and/or the evolution of the hydraulic properties (such as the hydraulic conductivity and the hydraulic gradient). Figure 1.10 illustrates typical reported data of the progression of erosion in terms of the cumulative eroded mass and the evolution of the coefficient of permeability with time. Studies, such as Ke & Takahashi (2014a); D. Chang & Zhang (2011); Ke & Takahashi (2012b), show an increase in the hydraulic conductivity as a result of the erosion of large amounts of fine particles.

Suffusion, however, may be accompanied by the filtration of some detached particles causing a redistribution of the porosity. This may lead to clogging and consequently to a decrease in the hydraulic conductivity. The particle redeposition or internal clogging of specimens by transported grains is a significant factor in the suffusion of soils (Reddi et al. (2000); Marot et al. (2009); Sibille et al. (2015)). This was also noticed during erosion tests done by Ke & Takahashi (2014a,b) where a sharp increase in the hydraulic gradient have been observed at a certain moment followed by a dramatic drop as demonstrated in Figure 1.11 and which was attributed to a temporary clogging.

(a)   (b)
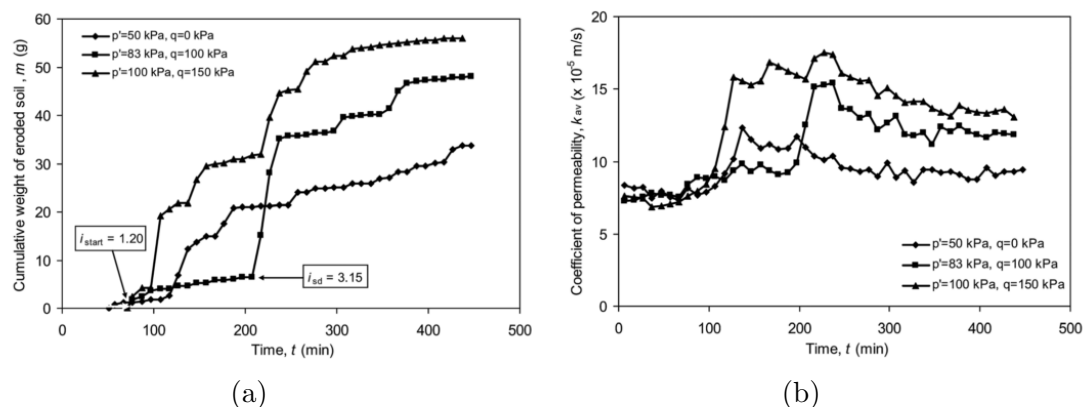
Figure 1.10: (a) Cumulative eroded soil and (b) variations in the coefficient of permeability during the internal erosion tests under different stress states (D. Chang & Zhang (2011)).
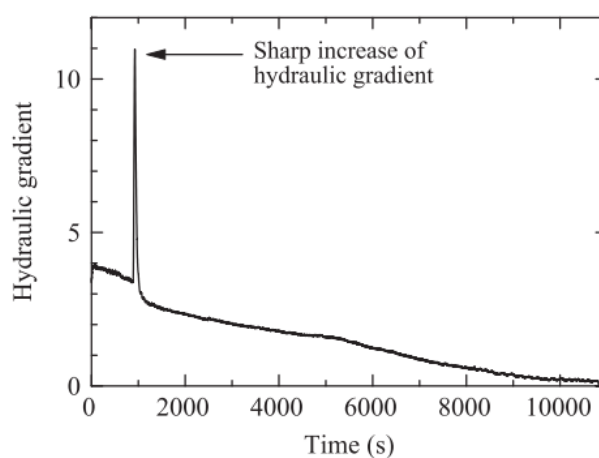
Figure 1.11: Hydraulic gradient within seepage test (Ke & Takahashi (2014a)).

Therefore, two successive phases can be distinguished during a suffusion process (D. Chang & Zhang (2011); D. Chang et al. (2012); Sibille et al. (2015)):

- In the first phase, a suffusion process is characterized by a progressive and diffuse migration of fine particles over a long period of time. This phase may be accompanied locally by the filtration of some transported particles resulting in a partial clogging of some constrictions. Consequently, an interstitial overpressure is generated in the blocked zones;

- The second phase is characterized by a strong migration over a short period of time. The induced overpressure at blocked constrictions causes blowout of fine particles and produces rapidly large settlement of the specimen;

Recent studies attempt to describe the mass of eroded particles (reaching the outlet of the specimen) during the suffusion process. Sibille et al. (2015), for example, proposed a simple phenomenological model which is able to capture the main features observed experimentally during suffusion tests composed of several hydraulic loading stages. This model requires at least a single multi-stage test to be calibrated. The mass erosion rate is

then expressed by the following equation:

$$\dot{m}_v = \alpha_{ref}\left(\frac{1}{\frac{\Delta E_v}{P_v t^*} + 1}\right)P_v^b \qquad (1.1)$$

where α_{ref} and b are parameters intrinsic to the tested material and represent its erodibility; P_v is the ratio of the flow power by the specimen volume; ΔE_v is the flow energy per unit volume; t^* is the characteristic time relative to the tested material.

However, with the progression of suffusion, eroded soil samples usually become heterogeneous. Figure 1.12 shows the particle size distribution of the top, middle and bottom sections of an eroded soil sample. It can be noticed that the top and middle sections lose more fine particles than the bottom one. Particles from the top migrate and are captured at the bottom of the soil sample. Hence these induced heterogeneities should be taken into account while describing eroded soil specimens.
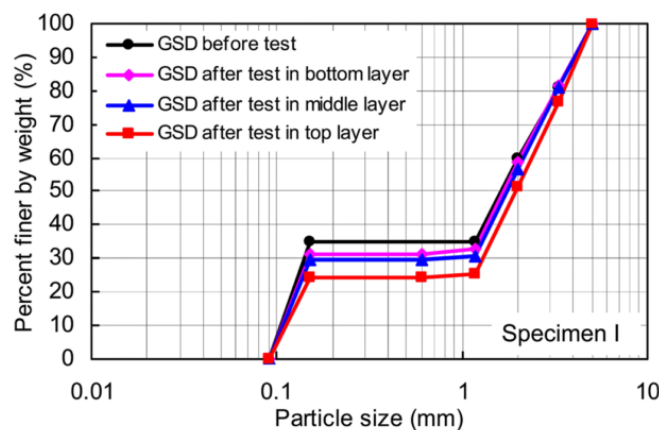
Figure 1.12: Particle size distribution of different sections of an eroded soil sample (D. Chang & Zhang (2011)).

1.4.2 Volumetric deformation of the soil during suffusion

Relatively rapid volumetric deformation of eroded soils is one of the characteristics of suffusion as described by Moffat et al. (2011). However, the soil deformation/settlement depends on different factors, such as: the soil gradation (Sibille et al. (2015)) and the initial fines content (Ke & Takahashi (2014a); Sibille et al. (2015)).

Figure 1.13 shows the evolution of the volumetric deformation during erosion tests under different effective confining pressures.

As can be noticed, the eroded soil compresses during erosion. D. Chang & Zhang (2013a) proposed that the soil deformation is related to the buckling of the strong force chains through the coarse particles due to the loss of fine particles that may provide lateral support for the granular skeleton. Furthermore, D. Chang & Zhang (2011) found that the erosion-induced deformation of the specimen also increases with the increase in the deviator stress. If suffusion initiates at a stress state with a stress ratio greater than or equal to that at the critical state, Muir Wood et al. (2010) and Scholtès et al. (2010)
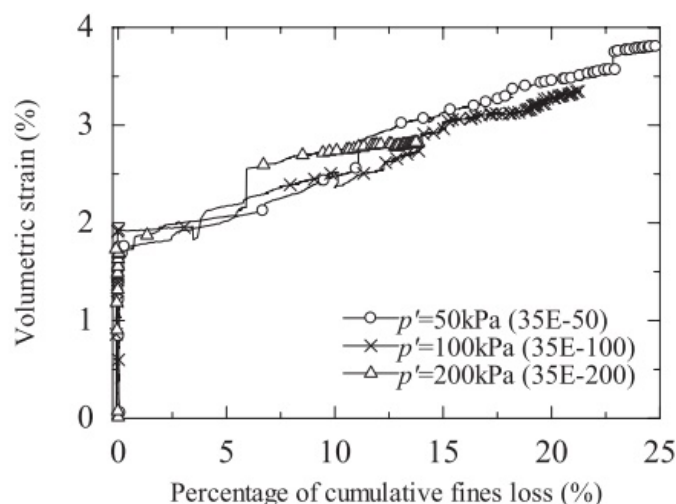
Figure 1.13: Volumetric strain versus percentage of cumulative fines loss under different effective confining pressures for specimens with 35% initial fines content (Ke & Takahashi (2014a)).

noticed, numerically, that the soil fails by developing very large deformations.

In addition to that, Ke & Takahashi (2014a) performed erosion tests on soils with different FC and found that the fines loss is larger for the specimens with larger initial fines content and correspondingly, the suffusion induced volumetric strain increases too (Figure 1.14).

Nevertheless, even if the soil compresses during erosion, the void ratio increases with the
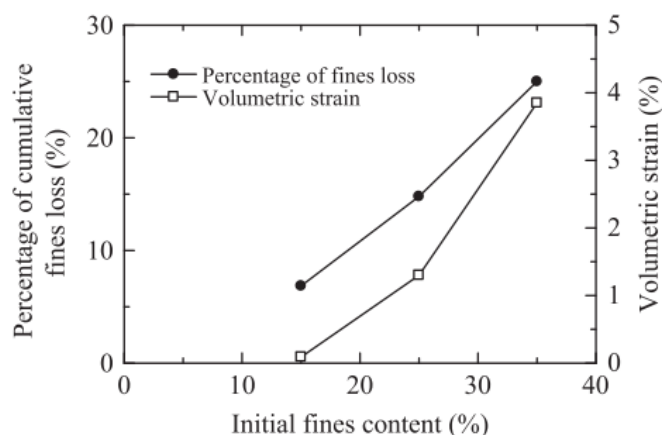
Figure 1.14: Percentage of cumulative fines loss and suffusion induced volumetric strain versus initial fines content under an effective confining pressure of 50 kPa (Ke & Takahashi (2014a)).

loss of fine particles. Thus, the creation of a more open microstructure dominates the effect of the compression of the soil. Figure 1.15 shows a commonly observed increase in

the void ratio during experiments.
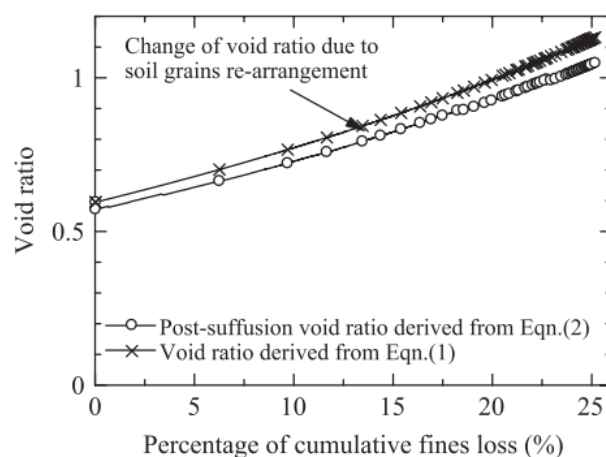
Figure 1.15: Void ratio versus percentage of cumulative fines loss under an effective confining pressure of 50 kPa (Ke & Takahashi (2014a)).

1.4.3   Effects of the stress state on suffusion development

The behavior of a soil is highly influenced by its stress state. Studies under isotropic stress conditions (see for instance Bendahmane et al. (2008); Ke & Takahashi (2014a)) showed that as the confining stress decreases, the maximum cumulative fines loss increases. Figure 1.16 shows the results obtained by Ke & Takahashi (2014a) who performed suffusion tests and concluded that the percentage of cumulative fines loss is the least in specimens under an effective confining pressure of 200 kPa and the largest in specimens under an effective confining pressure of 50 kPa (Figure 1.16).
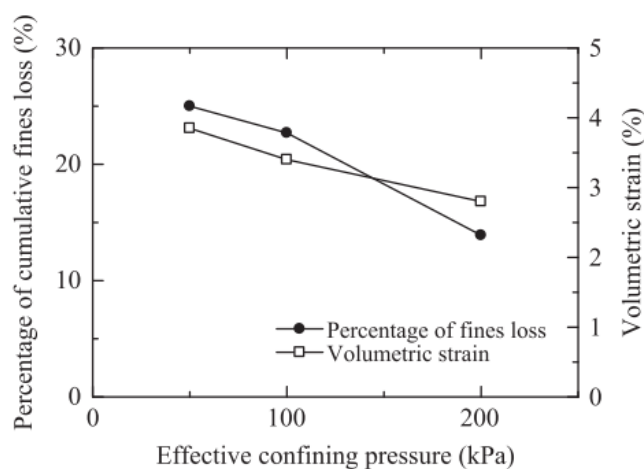
Figure 1.16: Normalized hydraulic conductivity versus effective confining pressure for specimens with 35% initial fines content (Ke & Takahashi (2014a)).

For anisotropic stress states, the maximum erosion rate, the total loss of fine particles, and the erosion-induced deformations increase with increasing the deviator stress (D. Chang & Zhang (2011); D. Chang et al. (2012)) as shown in Figures 1.10a and 1.17. Besides, D. Chang & Zhang (2013a) conducted laboratory suffusion tests on soil samples
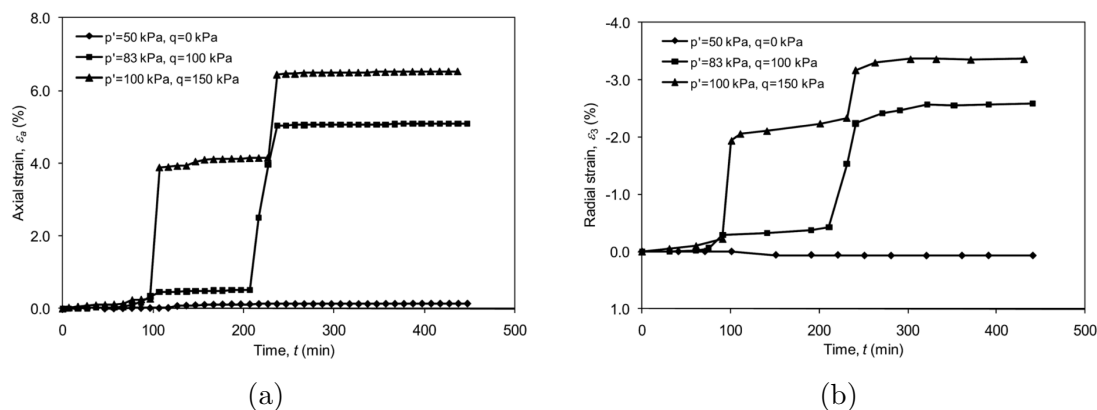
Figure 1.17: Deformation of the specimen during internal erosion testing under different stress states: (a) axial strain and (b) radial strain (D. Chang & Zhang (2011)).

under isotropic stress state, compression and extension stress states. The comparison of the erosion results showed that a soil under an extension stress state may lose more fine particles than under the other stress states.

1.5 Consequences of suffusion on the soil mechanical properties

With the erosion of large amounts of fine particles, the metastable structure might be formed which easily triggers the re-arrangement of soil grains into a stable packing. Consequently, a volumetric deformation and therefore, a change in the void ratio takes place and the mechanical properties of the soil may change significantly. Recent studies attempt to analyze the mechanical behavior of eroded soils. In this section, main conclusions from the literature are presented. Few experimental and numerical studies have been done to analyze the modifications in the shear strength of eroded soils. However, the conclusions are still controversial. Some researchers detected a decrease in the shear strength while others found that eroded soils may gain shear strength.

1.5.1 Characterization of post-erosion properties from laboratory mechanical tests

Several experimental studies have been done to characterize the post-erosion properties of soils. D. Chang & Zhang (2011) and D. Chang et al. (2012) performed drained triaxial compression tests on eroded soils. They noticed that after the loss of a significant amount of fine particles, the original dilatant stress-strain behavior becomes contractant and the peak stress decreases as shown in Figure 1.18.
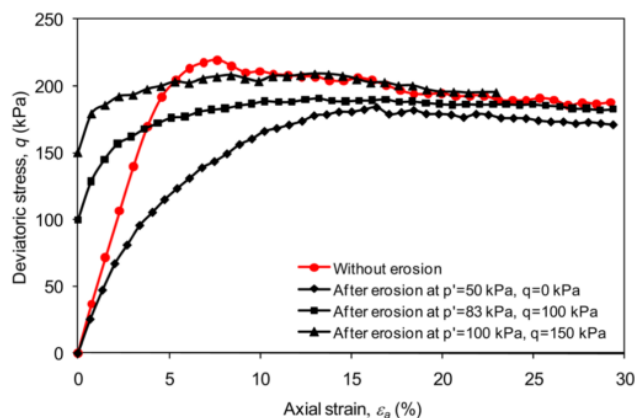
(a)
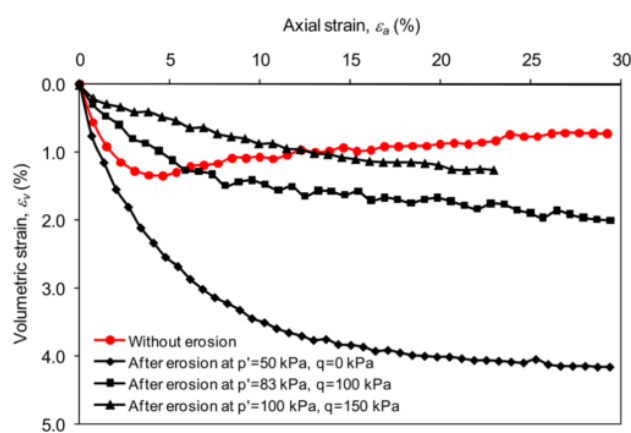
(b)

Figure 1.18: Drained triaxial compression tests performed on a soil without and with internal erosion under different initial stress conditions: (a) deviatoric stress versus axial strain and (b) volumetric strain versus axial strain (final hydraulic gradient=8.0) (D. Chang & Zhang (2011))

This may be explained by the increase in the global void ratio when fine particles are washed out and the mechanical behavior of the soil depends on its global void ratio. In addition, Ke & Takahashi (2012b,a) attributed the reduction of the soil strength to the loss of fine particles actively engaged in the mechanical transfer and the spatial re-arrangement of the soil particles which may adjust the force transfer. A non-linear relation between the shear strength of eroded soils and the applied hydraulic gradient was given as illustrated in Figure 1.19. At a given imposed hydraulic gradient, the shear strength decreases significantly.
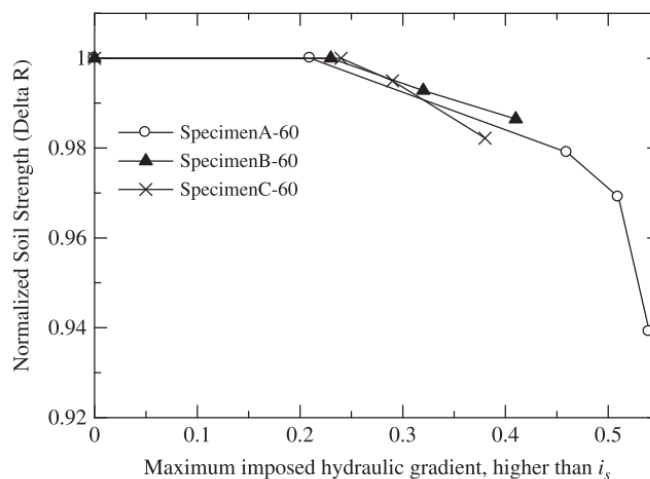
Figure 1.19: Relation between maximum imposed hydraulic gradient and normalized soil strength (Ke & Takahashi (2012b)).

On the other hand, some researchers showed an opposite mechanical behavior of the eroded soil. Ke & Takahashi (2014a) conducted drained triaxial compression tests on eroded soils and found that the deviator stress of eroded specimens is larger at the same small strain level compared to that of non-eroded specimens. However, at the same medium strain level, the specimens with suffusion show less deviator stress. Moreover, the eroded soil specimens show a larger initial stiffness at the same small strain level, whereas that value becomes less at the same medium strain level. Similarly, Ke & Takahashi (2014b) and Xiao & Shwiyhat (2012) performed undrained compression triaxial tests and showed also that the eroded soil specimens may gain shear strength after erosion as shown for example in Figure 1.20 of the experimental tests done by Ke & Takahashi (2014b).

Xiao & Shwiyhat (2012) attributed such behavior to the low degree of saturation. Whereas, Ke & Takahashi (2014b) suggested that such an inconsistency of the eroded soil behavior might be related to changes in the soil fabric. In fact, the eroded soil usually becomes heterogeneous at the end of suffusion and the fines concentration often presents a gradient in the main seepage direction. For instance, D. Chang & Zhang (2011), Ke & Takahashi (2014b) and Moffat et al. (2011) showed that after erosion, the fine fraction is different in the different layers of the soil sample. Therefore, the accumulation of fine particles at some zones might have provided reinforcement to the granular skeleton. Consequently, the peak deviator stress of the eroded specimen may become larger. However, to better understand the behavior of eroded soils, an investigation of the microstructure of the new arrangement of the soil grains might be necessary. Hence, a microscopic observation of the eroded soil fabric might better explain the mechanical behavior of eroded soils when interpretations of experimental results based on soil mechanics theories turn to be hardly applicable for heterogeneous soil samples.

(a) Relation of deviator stress and axial strain

(b) Relation of deviator stress and mean effective stress
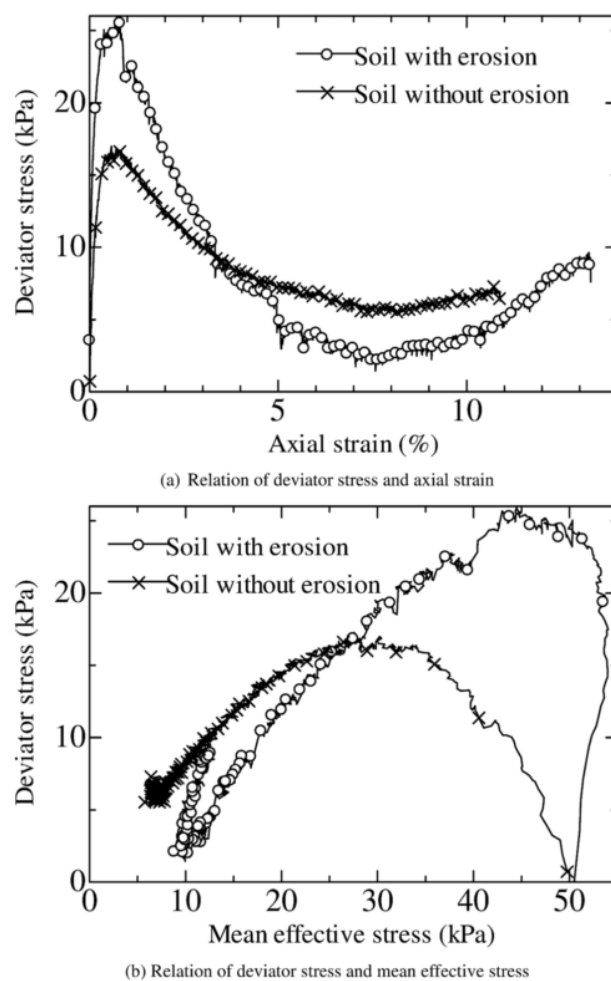
Figure 1.20: Undrained monotonic tests on the specimens with erosion and without erosion (Ke & Takahashi (2014b)).

1.5.2 Investigations of post-erosion properties from models

In addition to the experimental studies, few models could give comprehensively theoretical explanation about the modification in the soil shear strength after internal erosion, especially models based on the discrete element method where the microstructure of the soil can be investigated.

To describe the relation between the removal of soil particles and its consequences at the macroscopic scale, some numerical studies based on the discrete element method follow simplified procedures to remove particles from the granular assembly. Muir Wood & Maeda (2007)and Muir Wood et al. (2010) modeled the mechanical consequences of suffusion by a two-dimensional discrete element analysis. In their approach, the progress of suffusion was approximated by progressively removing the smallest grains from assemblies of circular discs at different stages of shearing. Simulations indicated that the particle removal causes the soil sample to compress. However, a more open microstructure with a higher specific volume is created. Moreover, as suffusion narrows the grading of the soil, the critical state line rises.

Similarly, Scholtès et al. (2010) considered the internal erosion as the progressive re-

moval of the less loaded finest grains. Both, a discrete element model and an analytical micromechanical model were compared to demonstrate the induced deformations and the changes in the soil properties during internal erosion. It was noticed that the soil shear strength was strongly influenced: the soil behaviour changed from dilatant to contractant when extracting the fine grains and eventually the internal friction angle decreases significantly. Figure 1.21 shows that the peak friction angle decreases from 24.2° for the non-eroded soil to 20.8° for the eroded soil specimen.
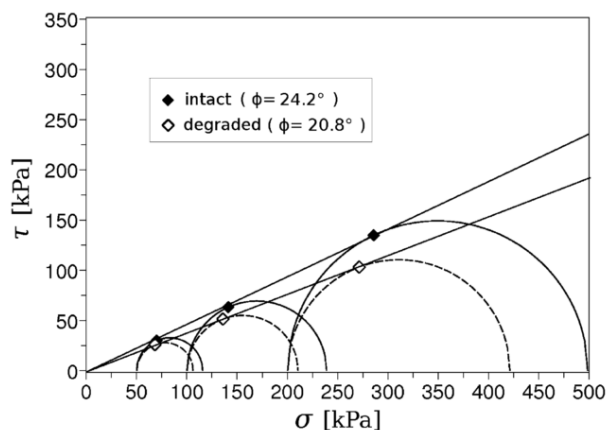
Figure 1.21: Mohr–Coulomb failure envelopes corresponding to the DEM numerical sample before and after particle extraction (Scholtès et al. (2010)).

In addition to that, Hicher (2012) defined, more recently, a micromechanical model to study the effects of particle removal on the behavior of granular materials. It was found that the removal of soil particles may cause diffuse failure in eroded soils. (A brief discription of all these models will be porovided in Chapter 3)

1.5.3   Void ratio definitions and density state of bidisperse soils

Besides all the studies found in the literature, the influence of suffusion on the mechanical properties of soils is still today an open question. Moreover, the defined numerical models do not take into account the effect of hydraulic loading and other important criteria. In addition to that, the interpretation of the results is mainly based on the global void ratio. However, one should take into account the different involvements of the fine and coarse fractions in the stress transfer as recognized by Kenney (1977) to better understand the mechanical behavior of the soil. Taking into account the possible interactions between coarse and fine grains, the inter-granular and inter-fine void ratios are introduced as primary indices for granular mixtures with low and high fines contents. Thus, new variables are proposed as an alternative to the global void ratio such that the soil matrix is considered as two submatrices: coarse-grain matrix and finer-grain matrix.

The microstructure of a granular mixture, composed of bidisperse particles, was described by Thevanayagam (2000). The granular mixture can be constituted in different ways, each leading to a different internal force chain network and consequently a different

stress-strain response during shearing which may explain the different conclusions about the mechanical behavior of eroded soils. Five categories of the microstructure can be distinguished as shown in Figure 1.22:
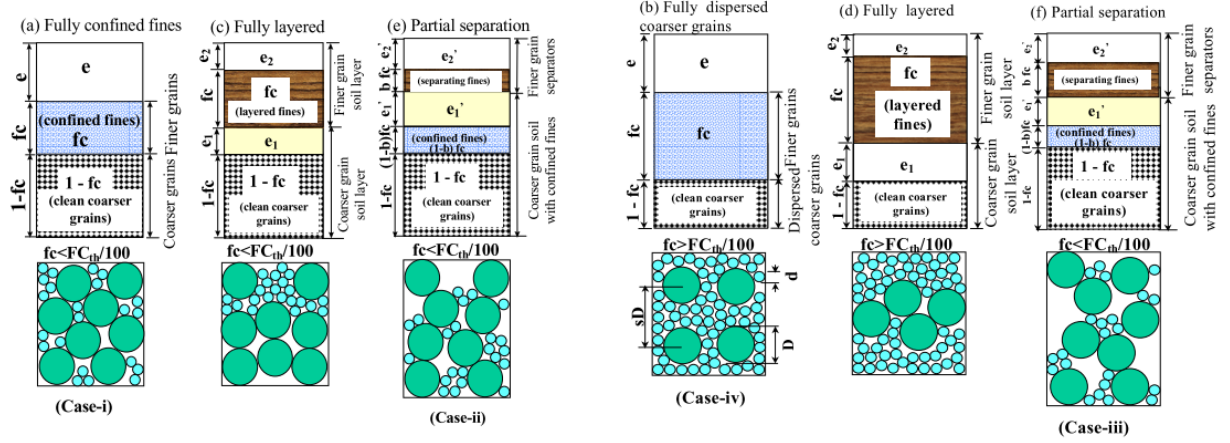
Figure 1.22: Microstructure and intergranular matrix phase diagram for bidisperse granular packings (Thevanayagam (2000)).

- The first category corresponds to the case when the finer grains are fully confined within the void spaces between coarser grains without supporting the granular skeleton. Therefore, fines are inactive or they play a secondary role in the transfer of inter-particle forces. They can be considered as a filler of the inter-granular voids. So the mechanical behavior is primiraly governed by the coarse particles and depends on the inter-granular void ratio defined as:

$$e_g = \frac{e + FC}{1 - FC} \tag{1.2}$$

where e is the global void ratio of the soil.

- The second and third categories correspond to two cases: if at a constant fines content, the position of fines is altered (i.e. their position is changed) or if more fines are added in a way that the global void ratio increases. Therefore, some fine particles may become active and are called "separating fines" while remaining fines stay "fillers". In this case, the coarse grain skeleton may be unstable without the separating fines. Consequently, fine particles supporting the coarse grains should be taken into account in active contacts. Therefore, an equivalent inter-granular void ratio is defined as:

$$e_{geq} = \frac{e + (1 + b)FC}{1 - (1 - b)FC} \tag{1.3}$$

where b is the fraction of active fines. The value of this parameter as well as its physical meaning remains a controversial topic. Different formulas to estimate this parameter have been proposed in the literature (see for instance Oda (1977); Rahman & Lo (2007); Bowling et al. (2009); T. Nguyen (2014); Dai & Yang (2013)).

- The fourth category is if FC increases sufficiently that fine particles start to make active contacts among themselves and the coarser grains begin to disperse in the finer grain matrix. This occurs when FC exceeds a threshold value, FC_{th}. Here, the coarse grains act as "reinforcing elements", but their effect is not negligible until they are separated sufficiently (i.e. when FC exceeds a limiting fines content, FC_l).

- The last category is when the coarser and finer grains form a layered system. In this case, when $FC>FC_l$, an interfine void ratio, e_f can be used:

$$e_f = \frac{e}{FC} \qquad (1.4)$$

When $FC_{th}<FC<FC_l$, neither e, e_g, nor e_f can represent active contacts alone. Thus an equivalent inter-fine void ratio is used:

$$(e_f)_{eq} = \frac{e}{FC - (1 - FC)/R_d^m} \qquad (1.5)$$

where $R_d=\frac{D_{max}}{D_{min}}$ and $0 < m < 1$, D_{max} and D_{min} are respectively the largest and smallest particles' diameters.

These contact indices help to predict the trends of stress-strain characteristics or liquefaction potential of silty or gravely soils relative to the host coarse matrix. Therefore, one can conclude that:

- when compared at the same e_g, an increase in FC increases the soil shear strength.

- when compared at constant e_f, an increase in FC decreases the soil shear strength.

- when compared at the same $(e_f)_{eq}$, an increase in FC slightly decreases the soil shear strength.

- when compared at the same global void ratio, the soil shear strength decreases with FC up to FC_{th}. Beyond that, the shear strength increases.

Recently, Benahmed et al. (2015) investigated experimentally the mechanical behavior of silty sand regarding instability phenomena using conventional triaxial tests under drained and undrained conditions. The results confirmed that if the global void ratio or the intergranular void ratio are used as the density parameters to define the critical state line, the latter will depend on the fines content. When using the global void ratio, the critical state line moved to a higher density as the fines content increased. Hence, the critical void ratio is lower than the initial value meaning that fine particles play a negative role in the soil strength resulting in a more contractant behavior. However, when using the intergranular void ratio, the critical state line moved slightly to a lower density and the fines content improved the shear strength of the soil. However, when using the equivalent intergranular void ratio, a unique critical state line is obtained. Thus, the equivalent inter-granular void ratio is a suitable parameter to characterize cohesionless soils with different fines content.

Therefore, the different density indices (i.e. global, inter-granular and equivalent inter-granular void ratios) should be considered to better interpret the mechanical behavior of soil samples.

1.6 Review of the main observations

Main conclusions from the literature review presented in this chapter concerning the phenomenon of internal erosion by suffusion are summarized hereafter:

- The suffusion phenomenon is characterized by two processes: the detachment and the migration of fine grains leaving behind the granular skeleton. The detachment process requires a sufficiently strong hydraulic loading capable of pulling off fine grains. The critical hydraulic loading parameter depends on the density of the soil, the fines content and the stress state. Once a particle is detached, the migration of this particle is controlled by the geometrical properties of the soil (i.e. the constriction sizes and the void network). Several empirical geometric methods have been suggested to assess the potential of erosion in internally unstable soils. Initially, the methods were based on the particle size distribution, PSD, which were found to be conservative. Nowadays, however, geometric criteria based on the constriction size distribution, CSD, are used to evaluate the suffusion potential;

- Intensive studies have been concerned by the role of fine particles in the soil structure and its macroscopic behavior. Studies found that the initiation of suffusion is possible if fine particles are small enough, as well as, if fine particles do not fill the voids between coarse particles. Different catogories based on the fines content, FC, have been proposed by Thevanayagam (2000). If the fines content is less than a threshold value, coarse particles capture the strong force chains while the fine particles may sit loose in the voids and may be transported by seepage flow if smaller than the constrictions between coarse grains. However, when $FC >> FC_{th}$, the soil is overfilled and is considered internally stable. However, if FC is around FC_{th}, the participation of fines in the force transfer depends on the density.

- Once the suffusion process takes place, different factors may influence its development. Soils subjected to higher effective confining pressure may suffer from less eroded material than at lower effective confining pressure. The hydraulic loading history is also important. The loading duration and the number of hydraulic loading stages seem to have an influence on suffusion development. Moreover, as the deviator stress increases, the erosion rate increases. However, it was noticed that the suffusion process may be accompanied by the filtration of some transported particles resulting in partial clogging with interstitial overpressure at these blocked zones which may eventually cause sudden blowout of fine particles and large settlement. At the end of suffusion tests, soil samples are no longer homogeneous and the fine fraction in different sections of the soil sample is different.

- Consequences of suffusion on the mechanical properties of soils can be characterized in terms of volumetric strain and shear strength. The post-suffusion soil is generally found to be looser after erosion because voids are created after the fines' departure and possible settlement of the sample is not enough to compensate this void creation. Although one would expect a decrease in the shear strength of eroded soil specimens, experimental studies showed contradictory conclusions. Some authors showed a decrease in the shear strength of eroded soils, while others showed that eroded soil specimens may gain shear strength. This necessitates a microstructural analysis of the eroded soil and a comparison with the initial non-eroded state. In fact, even if eroded soils become looser once analyzing the global void ratio, it would be

interesting to evaluate the inter-granular and equivalent inter-granular void ratios to better interpret the soil mechanical behavior. In other words, the increase in shear strength may be related to the decrease in the inter-granular void ratio after erosion. Furthermore, since the soil becomes heterogeneous after erosion, this may lead to inaccurate interpretations.

- Few numerical attempts based on the discrete element method are available in the literature, where soil particles are removed progressively based on their size and sometimes their degree of interlocking such that the least loaded particles among the fine particles are removed preferentially. However, the description of erosion in such methods lack other criteria that play a major role in the erosion of fine particles, such as the constriction sizes to allow particles to pass through or the driving fluid forces to cause the detachment of particles. Moreover, these models give so far only qualitative results. They use spherical particles which under-estimates the shear strength. Also, the particle size distribution used in these numerical studies is not representative of internally unstable soil (i.e. small size ratio and/or a very low fines content compared to the experimental ones).

Part II
DEM model and suffusion-like simulations

Chapter 2

Discrete Numerical Model

2.1 Introduction

This chapter introduces the discrete numerical model used in our study. In the discrete element method (DEM), the granular assembly is modeled as a set of independent entities, which interact with each other. This method can model the complex behavior of a granular medium with few parameters, unlike phenomenological models (requiring more parameters), and give access to the properties of the micro-structure of the granular assembly. Therefore, for studing the suffusion-induced modifications at the micro-scale, the DEM is chosen as the numerical tool in our simulations.

In what follows, a brief literature review of the discrete element method is first presented in Section 2.2. Concluding remarks will be addressed which will be taken into account in our defined model. Thereafter, the discrete numerical model used in this study is introduced in Section 2.3: the 3D granular assembly is modeled with spherical discrete elements. Previous studies from the literature showed that such simplified particles' shape leads to excessive rolling, limiting the mechanical resistance of the soil. Thus, contact rolling resistance is taken into consideration in this work to model the grain angularity and to better represent the macroscopic behavior of granular materials. The influence of elastic and plastic local parameters is also discussed in Section 2.3.2. Moreover, a procedure to obtain an initial density, ranging from loose to dense samples, is proposed. Finally, a calibration procedure based on all these considerations is defined in Section 5.2 and the defined numerical model is used to study the effect of fine particles on the microstructure of the soil and its mechanical behavior (Section 2.4.2).

2.2 A brief review on the discrete element method (DEM)

DEM is becoming a leading approach to compute the behavior of granular assemblies. It was first pioneered by Cundall & Strack (1979) and applied to problems in rock mechanics. This method is based on an explicit numerical scheme in which the interactions between independent particles are monitered at each contact and the motion of each particle is modeled. The particles are considered as rigid elements which can overlap at contact points possibly describing the deformation of individual particles.

2.2.1   DEM calculation process

The calculation process of DEM is quite simple. Each numerical cycle includes the application of Newton's second law and a force-displacement law at the contacts. Figure 2.1 illustrates the DEM calculation cycle. It involves two stages:

- Contact force calculation and detection of the list of interactions: Two spherical particles are in contact if the distance between their centers is smaller than the sum of their radii. Interaction laws are then applied locally for each contact in order to calculate the interaction forces (F_i) and moments (M_i).

- Calculation of the particles' position: Newton's second law is applied for each discrete element, to determine the resulting acceleration, which is then integrated to find the new element positions.
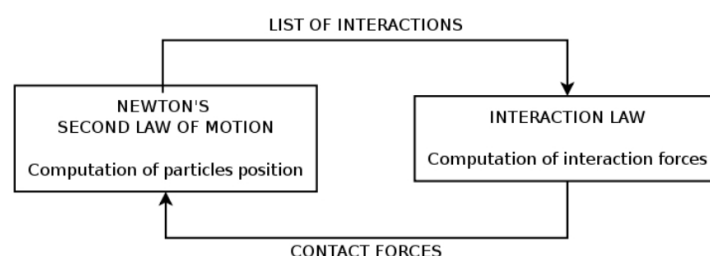
Figure 2.1: Computation cycle of a DEM model.

Once the new position for each particle is computed, the list of interactions is updated and new interaction forces are computed again. This calculation process is repeated until the simulation is achieved.

2.2.2   Interaction laws

The overall behavior of a material is simulated by attributing a simple interaction law at each contact. The contact model should describe how elements will behave when they come in contact with each other. One of the strengths of DEM is its capacity to reproduce complex mechanical behavior using few mechanical parameters. Therefore, the definition of a simple interaction law between particles is important in DEM models.

Different DEM models are found in the literature. One of the simplest models is defined by Cundall & Strack (1979) (see Figure 2.2). The contact between two spheres is modeled by normal and tangential springs characterized, respectively, by normal (K_n) and tangential (K_s) constant stiffnesses. In series with the tangential spring is put a slider of friction angle φ_c. This law corresponds to an elastic-perfectly plastic behavior.

Another commonly used contact model is the Hertz-Mindlin model based on a non-linear elastic relation between the normal and tangential contact forces (F_n and F_s, respectively) and the relative displacements at the contact taking into account the mechanical properties

(a)   (b)
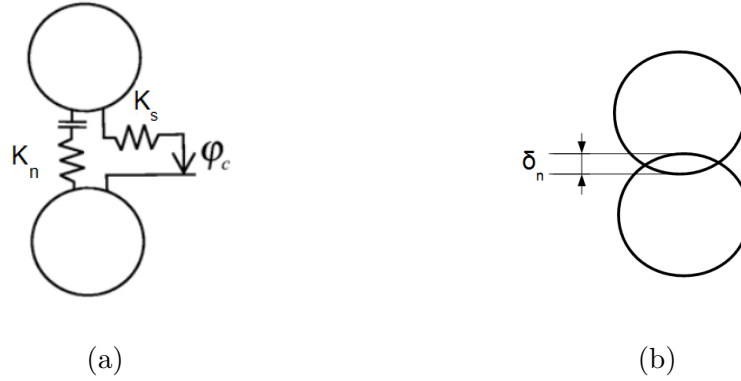
Figure 2.2: Interaction law used by Cundall & Strack (1979).

of the material (the shear modulus, G, and Poisson's ratio, ν_d):

$$K_n^* = \frac{dF_n}{d\delta_n} = \frac{G\sqrt{2R}}{1 - \nu_d}\sqrt{\delta_n} \tag{2.1}$$

$$K_s^* = \frac{dF_s}{dU_s} = \frac{(2(G^2 3(1 - \nu_d)R)^{\frac{1}{3}})}{2 - \nu_d}F_n^{\frac{1}{3}} \tag{2.2}$$

where R is the radius of the particle, G is the shear modulus, ν_d is the poissons ratio, U_s is the tangential relative displacement and δ_n is the interpenetration between two spheres (Figure 2.2).

These contact stiffnesses are updated at each iteration of the simulation. Consequently, this may be computationally expensive (Cundall & Strack (1979)).

Most studies based on the discrete element method use simplified particle shapes as disks (in 2D) (Ting et al. (1989)) or spheres (in 3D) (Thornton (2000)). Yet, such shapes lead to excessive rolling as compared to real granular materials (Iwashita & Oda (2000); Bardet (1994); Kozicki & Tejchman (2011)). Consequently, using simple circular (or spherical) shapes lead to lower shear strength compared to the experimental results. To overcome this setback, complex shapes as polygons (Szarf et al. (2011)) and polyhedrons (Lee et al. (2012)) can be used. But such shapes can be computationally expensive in detecting contacts and calculating forces and torques (Radjaï & Dubois (2011)). Another alternative solution is to use aggregates or clumps of disks or spheres (Salot et al. (2009)). However, this requires a larger number of spheres and the contribution of the non-convex surface of clumps becomes difficult to evaluate. In the conventional distinct element method, proposed by Cundall, circular (or spherical) particles interact at a contact point where rolling of particles can occur freely. However, real particles may interact at a contact surface or at multiple contact points instead of a single point. Thus, one solution is to fix the particle's rotation as proposed by Calvetti et al. (2003) or to take into account the transfer of a moment between elements in the local constitutive law as pioneered by Oda et al. (1982); Oda & Iwashita (2000); Iwashita & Oda (2000), or more recently by Estrada et al. (2013) to reflect the grain's angularity. In 3D, moment transfer laws can be defined with respect to both twisting (around the contact normal) and rolling (orthogonal to the contact normal) inter-particle relative rotation. The contact model proposed by Oda & Iwashita (2000) takes into account the rolling resistance at contact points. Hence it acts against relative

rotation arising from rolling. Therefore, in addition to the conventional contact model, a rolling elastic spring in series with a rolling slider are installed at each contact point (Figure 2.3). This model is used in this study. More details will be presented in section 2.3.

Previous studies investigated the influence of the contact rolling resistance properties
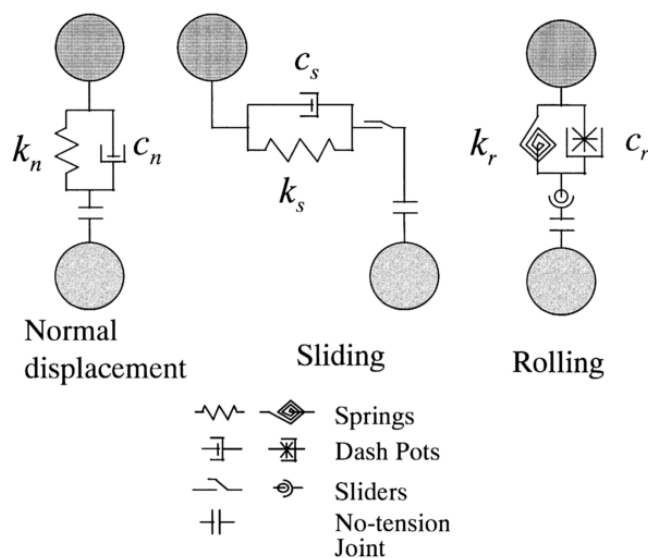
Figure 2.3: Interaction law used by Oda & Iwashita (2000) where a rolling resistance is added to the conventional interaction law of Cundall & Strack (1979).

(elastic rolling stiffness and plastic rolling moment) on the macroscopic behavior (Plassiard et al. (2009); Widuliński et al. (2009); Wang & Li (2014); Kozicki et al. (2013)). On one hand, studies showed that increasing the values of the rolling parameters causes an increase in the macroscopic internal friction angle, but has little influence on the dilatancy (Plassiard et al. (2009); Widuliński et al. (2009)) (see Figures 2.4 and 2.5). On
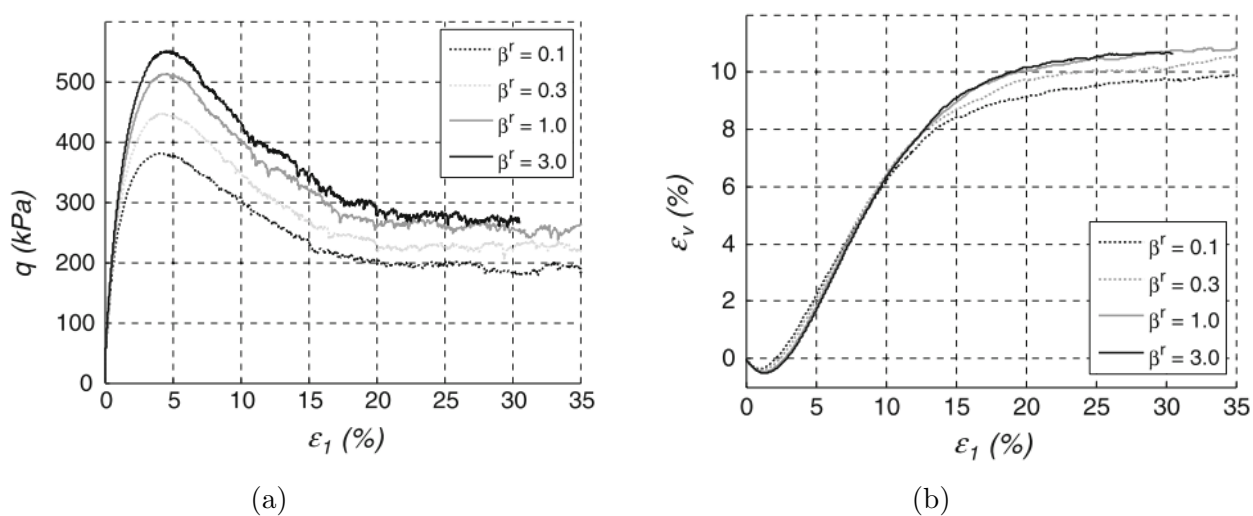
Figure 2.4: Triaxial compression for different values of rolling stiffness (β^r). (a) Deviator stress and (b) volumetric strain versus axial strain (Plassiard et al. (2009)).
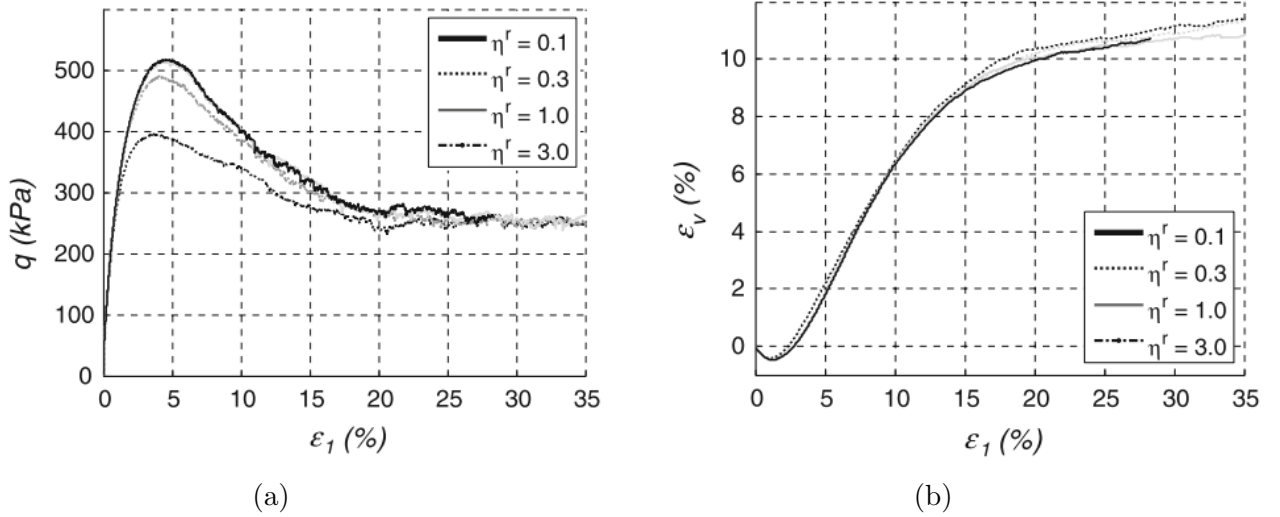
Figure 2.5: Triaxial compression for different values of plastic rolling moment (η^r). (a) Deviator stress and (b) volumetric strain versus axial strain (Plassiard et al. (2009)).

the other hand, Wang & Li (2014) showed that when the rolling stiffness is high enough, its influence on both the peak friction angle and the dilatancy angle becomes negligible. However, in all cases, it was suggested to calibrate the contact rolling stiffness (in addition to the plastic rolling moment) to match the macroscopic internal friction angle.

2.2.3 Stability condition

The DEM is usually based on an explicit time integration scheme implementing a central finite difference method. In other words, the scheme used for the numerical integration of the equations of motion implies a sufficiently fine discretization of time. At each iteration, a critical time step is calculated, Δt_{crit}, beyond which the integration scheme is no more stable. The critical time step is the minimum natural period of all particles.

The natural period of each particle, for all the degrees of freedom, supposed independent to each other is computed as follows:

In translation, the natural period is given as follows:

$$T_i^{trans} = \sqrt{\frac{m}{K_i^{trans}}} \tag{2.3}$$

and in rotation, the natural period is:

$$T_i^{rot} = \sqrt{\frac{J}{K_i^{rot}}} \tag{2.4}$$

where m is the mass of the particle, J is the moment of inertia, K_i^{trans} and K_i^{rot} are respectively the equivalent translational and rotational stiffnesses evaluated considering all the contacts of the particle in the direction i.

Then, the translational and the rotational critical time steps are given by:

$$\Delta t_{crit}^{trans} = \min \sqrt{\frac{m}{K_i^{trans}}} \quad and \quad \Delta t_{crit}^{rot} = \min \sqrt{\frac{J}{K_i^{rot}}} \tag{2.5}$$

The critical time step is chosen as the smallest critical timestep among Δt_{crit}^{trans} and Δt_{crit}^{rot}.

The consequences of the introduction of a rolling resistance (or even a twisting resistance) at contacts should also be taken into account in the stability of the model. This point has been discussed in Aboul Hosn et al. (2017) and the main conclusions about the role of normal, shear, rolling and twisting stiffnesses are reported here. These conclusions have been obtained considering the following assumptions:

1. all spheres are identical (same size and same inertia)

2. all contacts have the same stiffness values

3. the stiffness tensors are isotropic.

The small movements $\vec{u}$ and $\vec{\theta}$, in translation and in rotation, respectively, of a particle relative to an initially stable configuration are described by Aboul Hosn et al. (2017):

$$\ddot{\vec{u}} = -\frac{N_c K_n (1 + 2\alpha_s)}{M} \vec{u}, \tag{2.6}$$

$$\ddot{\vec{\theta}} = -\frac{N_c K_n (5\alpha_s + 5\alpha_r + 2.5\alpha_{tw})}{M} \vec{\theta} \tag{2.7}$$

where α_r and α_{tw} are respectively the rolling and twisting coefficients ($K_r = \alpha_r r^2 K_n$ and $K_{tw} = \alpha_{tw} r^2 K_n$), K_n is the normal stiffness, M is the mass of the particle, N_c is the number of contacts formed by the particle and α_s is the ratio between shear and normal stiffnesses. Numerators in the right hand sides of the uncoupled equations of motion 2.6 and 2.7 represent the global stiffnesses of the particle in translation and rotation respectively. The critical time step will be fixed by the highest global stiffness. So how the different kinds of contact stiffnesses can affect the order of magnitude of the timestep?

- if the normal stiffness is dominant ($\alpha_k \ll 1$ for all k), the stability condition is controlled by the translational motion (eq. (2.6));

- if α_s is not negligible, precisely as soon as $\alpha_s \geq 1/3$, the rotational motion governs the stability condition (eq. (2.7));

- if $\alpha_r \geq 1/3$ or $\alpha_{tw} \geq 2/3$ (even if α_s remains small), the rotational motion governs the stability condition;

- if $\alpha_k \approx 1$ for all k, the timestep imposed by the rotational motion is less than half of the one corresponding to translational motion

- if $\alpha_k > 1$ for at least one k, estimating the timestep from K_n alone leads to overestimate the maximum allowed timestep significantly.

When the numerical scheme is unstable due to the translational motion, particles are usually ejected away from the granular assembly after few timesteps. In most cases it cannot remain unnoticed by the user, so that mistakes on the timestep are immediately detected. On the other hand, the consequences of numerical instabilities for rotational modes may not be obvious at the macroscale. Only more detailed examinations may reveal spurious relative motion at some contacts and high angular velocities of few particles. It is, thus, highly required to use a robust and validated procedure for choosing the timestep in the general case. The numerical results may otherwise suffer from (apparently) unexplained bugs.

During simulations, elastic waves are generated in the medium. Energy should be dissipated in the system for these waves to stop and to reach a steady state. The dissipation is done in two ways: frictional sliding and damping. However, if at a given state of the granular assembly the interactions are purely elastic, the friction will not dissipate energy at all. Thus, the introduction of a damping may be necessary. Two forms of damping exist: viscous and non-viscous dampings.

On one hand, viscous damping may be introduced by adding normal and shear dashpots to each contact. They act in parallel to the existing contact model and the contact force is attenuated with a damping force. On the other hand, Cundall & Strack (1979) proposed using a non-viscous damping which acts independently to each particle to limit their oscillation. This type of damping dissipates energy in the whole system through damping of the equations of motion by adding a damping terms, F^a and M^a, to the force and moment tensors, respectively. These terms are given by:

$$F_i^a = -\lambda^a |F_i| sign(\dot{u}_i) \tag{2.8}$$

$$M_i^a = -\lambda^a |M_i| sign(\dot{\theta}_i) \quad \text{with} \quad \lambda^a \in [0,1] \tag{2.9}$$

where λ^a is the damping coefficient, $\dot{u}_i$ and $\dot{\theta}_i$ are, respectively, the translational and rotational velocities of particles in direction i.

2.2.4 Sample generation

Sample generation is a very important operation and the initial configuration (the initial density, granulometry, homogeneity and isotropy/anisotropy of the microstructure) strongly affects the macroscopic behavior. There are two kinds of methods to generate samples: geometric methods and dynamic methods.

Geometric methods are based on geometric functions applied to particles to generate granular packings. Different geometric algorithms were developed, for instance to generate sphere assemblies in cubical (Jodrey & Troy (1985)) or cylindrical (Mueller (2005)) containers. The advantage of using geometric methods rather than dynamic methods is to generate dense polydisperse packings at a lower computational cost.

Dynamic methods use Newton's second law of motion to determine the trajectory and the spheres' final positions of particles inside a container. A large variety of dynamic algorithms exists and they differ by the technique used. On one hand, particles may be deposited by gravity or by the action of external compaction load. They can be released

one by one in a box (Aparicio & Cocks (1995); Jodrey & Troy (2000)) or placed following a given mesh (Jerier et al. (2010)). However, this method leads to anisotopic distribution of the contact orientations where the preferential orientation is about 45 ° along the direction of the gravity (Chen et al. (1988)). Moreover, this method results in a looser top layer than the bottom one which means the granular assembly is not homogeneous. On the other hand, the dynamic method by compaction consists, first, of generating a random cloud of particles; second, performing a uniaxial compaction (Dutt et al. (2005)), or an isotropic compaction (Combe (2001)) or a compaction by the expansion of particles' radii (Chareyre (2003)). With this approach, packing properties can be quite easily controlled. In addition it is possible to generate isotropic packings with a high density. Nevertheless, a drawback of the dynamic algorithms is a relative high computational cost for packing preparation.

With the geometric algorithms, it is generally difficult to modify the final density of the packing. With the dynamic approach, however, the final density can be modified by changing the value of the inter-granular friction angle during compaction (see for instance Tong et al. (2012); Chareyre & Villard (2005)). The lower is the inter-granular friction angle, the denser the soil sample becomes. Current techniques used for generating specimens can hardly result in very loose samples. Jiang et al. (2003) proposed a method to produce samples with a wide range of initial densities. Their technique is named the Multi-layer with Undercompaction Method (UCM). It is based on dividing the soil sample into several layers. Then, each layer is compacted to a state looser than the final target value to reduce the effect of compaction energy transferred from compaction of successive layers. However, the lowest and the highest void ratios obtained are respectively, 0.265 and 0.34. Hence, a narrow range of densities can be achieved and a very loose soil is not yet modeled in DEM.

2.2.5   Boundary conditions

In order to subject a sample to a specified loading path, the boundary conditions are prescribed in terms of stress and/or strain, as it is the case in real laboratory experiments. Three different boundary conditions can be distinguished as shown in Figure 2.6.

| (a) | (b) | (c) |
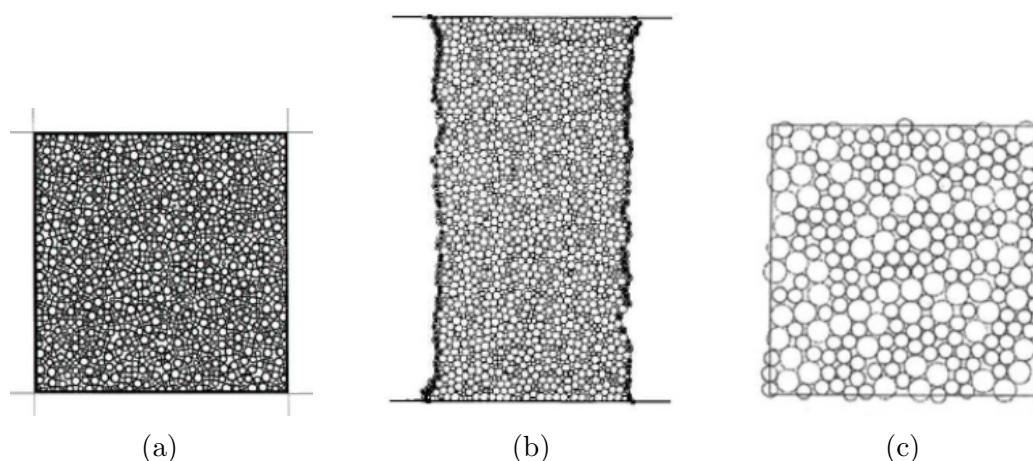
Figure 2.6: Types of boundary conditions: (a) rigid walls (b) flexible (c) periodic.

- Rigid walls (Figire 2.6a): the granular assembly is created in a deformable box with rigid walls. The position and orientation of these walls are controlled to either assign

a prescribed deformation or a prescribed stress (often via a closed-loop control). However, this type of boundaries strongly constrain the kinematic along the sample boundaries and may influence the initiation of the localization of the deformation and its development in shear bands. Moreover, another setback is related to the higher porosity as well as heterogeneities in terms of the number of contacts near the boundaries as shown in Figure 2.7 (Combe (2001)).
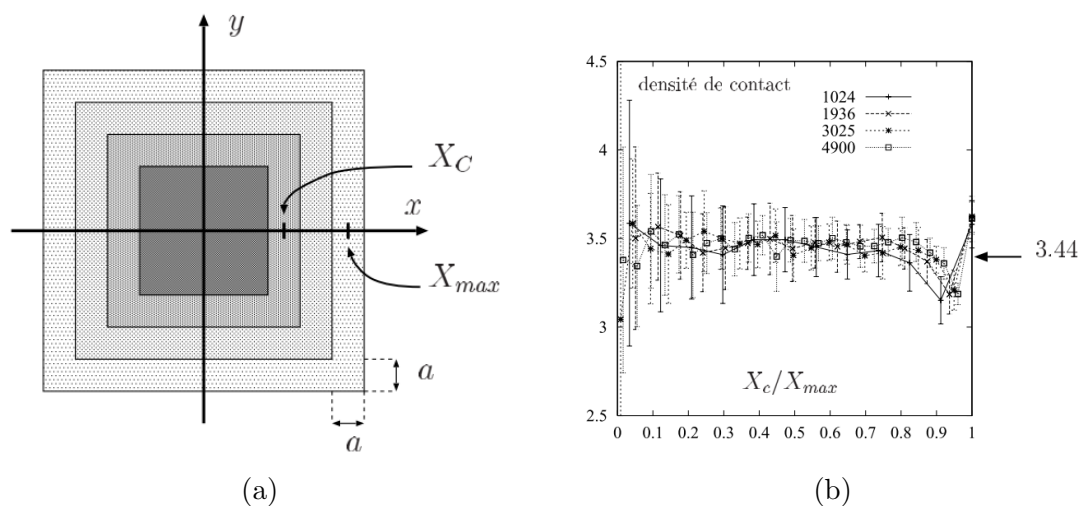
Figure 2.7: The coordination number as a function of the distance from the boundaries (Combe (2001)).

- Flexible membrane (Figure 2.6b): it has a similar effect to the one of the membranes generally used in the laboratory. It facilitates the localization of the deformation in shear bands, unlike rigid walls (Bardet (1994); Iwashita & Oda (2000)).

- Periodic boundaries (Figure 2.6c): the sample is part of a periodic space, such that it constitutes an elementary parallelepipedic-shaped cell. Periodic conditions mean as if the same grain arrangement is replicated periodically in space. In this way, the periodic boundary conditions extend the system to an infinite medium (Cundall (1988)). There is effectively no boundaries in this case and the loading conditions are defined directly by the macroscopic gradients of deformation. Such boundaries are capable of generating homogeneous samples overcoming, thereby, the effect of rigid walls; but shear bands, if any, have to satisfy the condition of periodicity.

2.2.6 Representative elementary volume

The representative elementary volume (REV) is the volume which gives a unique soil behavior independent from the heterogeneity it includes and which can be considered as a material point for an equivalent continuous medium. This definition implies that the macroscopic behavior of a sample is purely deterministic as long as the size of the studied sample is greater than the REV.

Calvetti et al. (1997) have done biaxial experimental tests on Schneebeli rollers and studied the dependence of the calculated microstrains on the size of the studied domain (or the number of rollers). To define a representative elementary surface (since it is a

2D test), they studied the evolution of the strain component with the surface used in each test as shown in Figure 2.8. It is noticed that, beyond a certain surface area, the results converge and are no more dependent on the size of the sample. In their test, the size of the REV was found to be ten times larger than that of the biggest roller diameter.

On the other hand, Chareyre (2003) proposed a definition of the REV based on
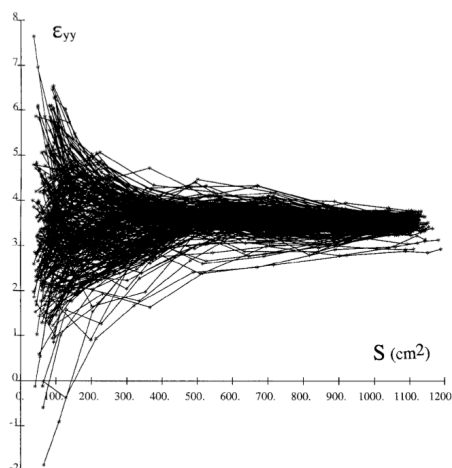
Figure 2.8: Dependence of the strain values on the surface area (Calvetti et al. (1997)).

the dispersion of the measured friction angle during the simulations of biaxial tests. Figure 2.9 shows that the representativeness is related to the number of particles used in the simulation. As the number of particles increase, the initial configuration of the packing becomes more homogeneous, leading to a higher reliability in the estimated macroscopic properties.

2.2.7 Concluding remarks from the literature review

From the brief review presented in this chapter, some concluding remarks are taken into account while developing a discrete numerical model to describe the mechanical properties of soil samples. The objective is to develop a model which gives quantitative and qualitative mechanical predictions; work on a wide particle size distribution; and define different initial soil's densities.

Previous studies have shown that the circular or spherical shapes of particles may influence significantly the shear strength of the discrete model due to the excessive rolling of such shapes. Therefore, some researchers modeled geomaterials using more realistic shapes (polyhedral shape for example) which requires more computational time while others added rolling resistance to the contact law. Thus, in our defined model, spherical particles will be used and rolling resistance will be taken into account in the contact law. Studies investigated the influence of the contact rolling resistance properties on the macroscopic behavior. The contact rolling stiffness, in addition to the plastic rolling moment, is generally calibrated to match the macroscopic internal friction angle. This leads to a surprising cross dependency of microscopic elastic parameters and macroscopic plastic ones. Therefore, one of the objectives of the next part of this chapter is to show that such a cross dependency can be avoided.
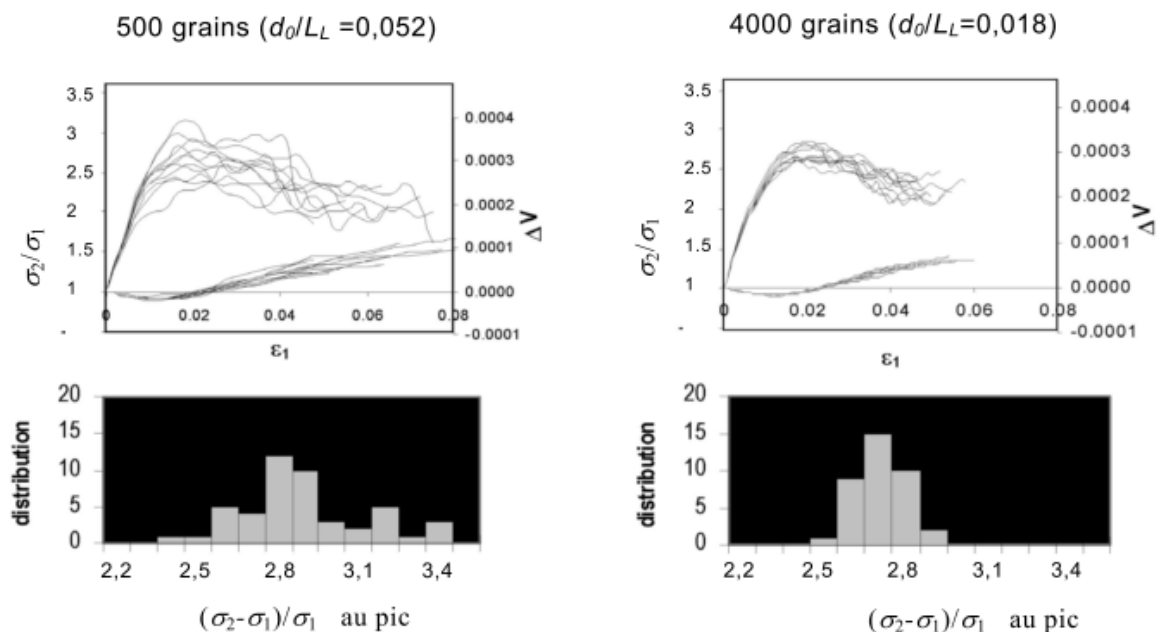
Figure 2.9: Dispersion of stress-strain curves for two samples of 500 and 4000 particles under biaxial test (Chareyre (2003)).

In addition to the particle's shape and the contact law, the mechanical behavior of a granular material is highly dependent on its initial density. The latter is often reached numerically by playing with the contact friction angle during the compaction phase which proves to be powerful in preparing medium dense to dense samples, but not very loose ones. Indeed, discrete numerical models of loose soils are quite rare in the literature. Hence, the second objective of this work is to address this issue by adding contact adhesion during the compaction phase of the numerical sample. In this way, we mimic the moist tamping technique used in the laboratory to reconstitute loose soil samples.

Before dealing with these objectives, the contact law including rolling resistance is presented in the next section. Then, a calibration procedure is proposed by comparing numerical simulations to experimental results of triaxial tests performed on Camargue sandy soil (T. Nguyen (2014); Benahmed et al. (2015)). Thereafter, the limitations of the defined model in reproducing the dependency of the volumetric strains on the mean pressure are discussed. Finally, an application of this model is presented where numerical simulations are performed to study the role of fine particles in the microstructure of soils. Soil samples with different grain size distributions are modeled. Then, the microstructure of the soil is analyzed for the purpose of investigating at which fines content, erosion of fine particles could start to influence significantly the integrity of the soil matrix.

2.3 Definition and characterization of the discrete numerical model

This section is dedicated to the definition and the characterization of the discrete numerical model implementing a rolling resistance at contacts. This part of the chapter corresponds to a work which has been published in the journal Granular Matter (Aboul Hosn et al. (2017)). Consequently, the presentation of the results and their interpretation, here, follow closely the content of this article.

2.3.1 Inter-particle contact law with rolling resistance

Let us consider two spheres in contact with radii R_1 and R_2. In the normal and tangential directions to the contact plane, the interaction law is very classical and characterized by constant normal and tangential (or shear) stiffnesses, K_n and K_s, respectively, and a contact friction angle, φ_c, such that:

$$\vec{F}_n = K_n \, \delta_n \, \vec{n} \tag{2.10}$$
$$\Delta \vec{F}_s = -K_s \, \Delta \vec{U}_s \quad \text{with} \quad ||\vec{F}_s|| \leq ||\vec{F}_n|| \tan \varphi_c \tag{2.11}$$

where $\vec{n}$ is the normal to the contact plane, δ_n, the overlapping distance between spheres, and $\vec{U}_s$, the relative tangential (or shear) displacement at the contact point. Only compressive normal forces are modeled, and the contact is lost as soon as the overlap, δ_n, vanishes.

The rolling resistance at the contact is defined by the rolling stiffness, K_r, and the coefficient of rolling friction, η_r (it is commonly called friction because of the mathematical form it takes although it does not directly involve the friction between two surfaces). Thus, the rolling moment, $\vec{M}_r$, acting against the relative rolling rotation of particles, $\vec{\theta}_r$, is expressed as:

$$\Delta \vec{M}_r = -K_r \, \Delta \vec{\theta}_r \quad \text{with} \quad ||\vec{M}_r|| \leq ||\vec{F}_n|| \, \eta_r \, \min(R_1, R_2) \tag{2.12}$$

$\Delta \vec{\theta}_r$ is computed as the tangential component of the incremental relative rotation, $\Delta \vec{\theta}$, of the contacting spheres. For spheres with incremental rotations, $\Delta \vec{\omega}_1$ and $\Delta \vec{\omega}_2$ respectively, $\Delta \vec{\theta} = \Delta \vec{\omega}_2 - \Delta \vec{\omega}_1$ and:

$$\Delta \vec{\theta}_r = \Delta \vec{\theta} - (\Delta \vec{\theta} . \vec{n}) \, \vec{n} \tag{2.13}$$

Note that Equation (2.12) defining the contact resistance to rolling is similar to Equation (2.11) representing the sliding resistance due to dry friction. Therefore, contact resistance to rolling can be interpreted as a rolling friction.

To avoid any dependency of macroscopic elastic properties on particle size, contact stiffnesses are defined from a stiffness modulus, E_c, and dimensionless shear and rolling coefficients, α_s and α_r, respectively:

$$K_n = 2 \, E_c \, \frac{R_1 \, R_2}{R_1 + R_2}; \quad K_s = \alpha_s \, K_n; \quad K_r = \alpha_r \, R_1 \, R_2 \, K_s. \tag{2.14}$$

Finally, adhesive normal and tangential forces, F_n^A and F_s^A, can be added to the contact law (used here during the sample compaction only) and defined from an adhesive stress σ_A such that:

$$F_n^A = F_s^A = \sigma_A \, [\min(R_1, R_2)]^2 \tag{2.15}$$

Then, the contact presents a resistance to a tensile normal force as long as:

$$\vec{F}_n \cdot \vec{n} > -F_n^A,\tag{2.16}$$

and a maximum shear force against sliding is given as:

$$||\vec{F}_s|| \leq ||\vec{F}_n|| \tan \varphi_c + F_s^A.\tag{2.17}$$

2.3.2 Local parameters and macroscopic constitutive behavior

Numerical triaxial compression tests were performed using YADE software (Šmilauer et al. (2015b)) to investigate the effects of some local mechanical parameters on the constitutive behavior of the model. It was made up of 10,000 spherical discrete particles whose radius is equal to 0.014 mm and 0.026 mm to avoid crystallization. Periodic boundary conditions were adopted.

The periodic cell was formed as a parallelepipedic block filled with a cloud of spheres (i.e. assembly of non-overlapping particles). The non-overlap constraint necessarily leads to rather loose clouds. Since this is only the starting point of the compaction, it has no consequences on the equilibrium state after compaction. Then, isotropic compaction was applied until reaching the required confining pressure, P_c. Finally, the triaxial compression was performed. During the compaction phase, the stress is controlled to reach a confining pressure of 80 kPa and a non-viscous damping of Cundall's type is applied to facilitate the convergence towards a quasi-static equilibrium. In the triaxial compression phase, the inertia number is chosen 1.65 $\times 10^{-4}$ to avoid inertial effects.

Moreover, no damping is considered in the triaxial phase. Typical simulated responses can be seen in Figures 2.12 and 2.14. Table 2.1 summarizes the parameters used for these studies.

	P_c (kPa)	E_c (kPa)	κ	α_s	φ_c (°)	α_r	η_r	σ_A (for compaction only) (kPa)
Case 1	80	$8\,10^2$-$8\,10^7$	50-5 10^5	0.8	30	-	-	-
Case 2	80	$3\,10^5$	1875	0.8	30	0.025-2.5	0.01-5	-
Case 3	80	$3\,10^5$	1875	0.8	5-40	1.25	0.1	-
Case 4	80	$3\,10^5$	1875	0.2	30	5	0.1	0-200

Table 2.1: Summary of the parameters used in each case of the parametric studies.

Elastic local parameters and plastic macroscopic properties

In this section, the influence of elastic local parameters, such as the normal and the rolling stiffnesses, on the macroscopic shear strength will be examined. Shear strength at failure is characterized by the peak friction angle, φ_p, reached at the peak of the deviator stress, q,

along a drained compression (constant effective confining stress), while, φ_0, characterizes the shear strength at the residual state (or the critical state).

We investigate first the effect of the normal contact stiffness represented via the dimensionless stiffness κ:

$$\kappa = \frac{E_c}{2P_c} \tag{2.18}$$

The response shown in Figure 2.10, where no rolling resistance was introduced (case 1 in Table 2.1), demonstrates that the peak friction angle, φ_p, decreases with the normal contact stiffness particularly for $\kappa < 50$. Similar results were obtained by Roux & Chevoir (2005) and Roux & Combe (2010). This is a remarkable disagreement with the experimental results on sand, in which the peak friction angle decreases for decreasing κ (i.e. for increasing the contact stiffness). This experimental trend may result simply from the dependency of the contact friction on the normal force (Suhr & Six (2016)). In numerical models, the contact friction coefficient is usually constant. Thus, the decreasing trend of the internal friction angle is explained by the decreasing number of contacts. Moreover, Figure 2.10 shows that for a higher dimensionless stiffness, where the overlap becomes negligible, there is still a scattering among the values of φ_p, but quite low (about $\pm 0.5°$ around the mean value). Thereby, for $\varphi_c = 30°$, plastic failure seems not significantly dependent of the contact normal stiffness for a value of κ greater than 50.

A more extended parametric study was performed concerning the parameters involved in
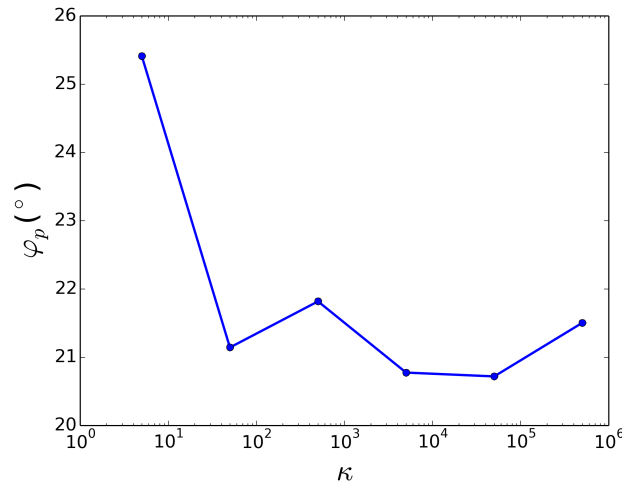
Figure 2.10: The influence of the dimensionless contact stiffness, κ, on the peak friction angle (case 1 in Table 2.1).

the contact resistance to rolling. The values of the parameters defined in Table 2.1, case 2, were chosen in order to test different pairs of α_r and η_r (note that for isotropic shape particles, η_r should be ≤ 1 (Iwashita & Oda (2000)); however, cases where $\eta_r > 1$ are investigated in this preliminary section). Macroscopic shear strength in terms of peak, φ_p, and residual, φ_0, friction angles is shown in Figure 2.11. Note that the residual friction angle is calculated from the average of stresses corresponding to $\epsilon_a > 25\%$. The results demonstrate that for a rolling stiffness, α_r, sufficiently high (here for $\alpha_r \geq 1.25$), the macroscopic plastic parameters reach constant values which depend only on η_r (Wang & Li (2014)).

Thus, if the contacts are sufficiently stiff, then the micro-elastic parameters, including
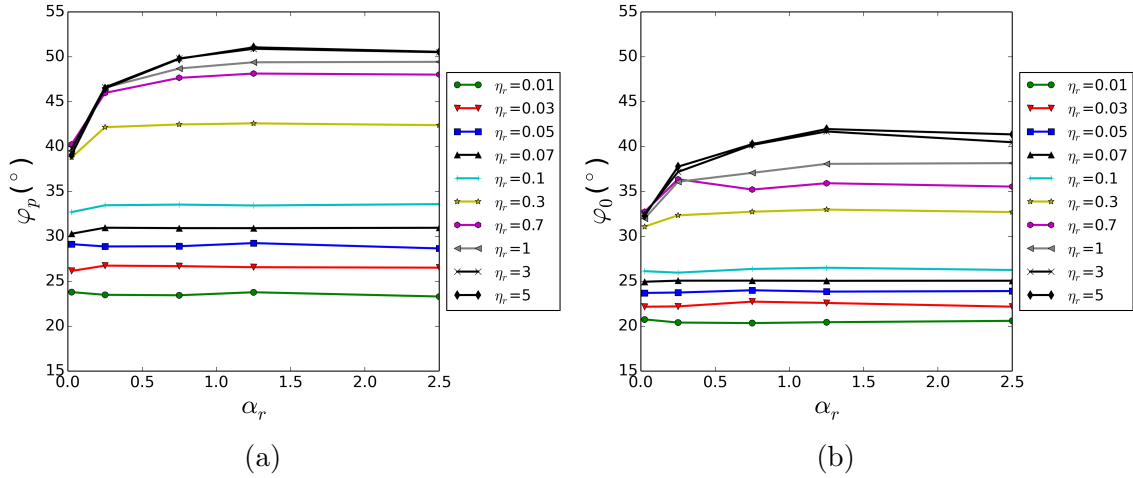
Figure 2.11: The variation of (a) peak friction angle, φ_p, and (b) residual friction angle, φ_0, with respect to α_r for different values of η_r (case 2 in Table 2.1).

rolling stiffness, have no influence on macro-plastic parameters. Approaching these normal and rolling stiff limits, should always be preferred to avoid cross dependencies between macroscopic plastic properties and elastic local parameters, in contrast with what was suggested by Plassiard et al. (2009) and Widuliński et al. (2009).

Plastic local parameters and plastic macroscopic properties

The influence of the plastic local parameters, η_r and φ_c, on the plastic macroscopic properties can be analyzed independently from the local elastic stiffnesses (as long as the elastic stiffnesses are close to the stiff limits). Therefore, E_c is set in the following to $3\,10^5$ kPa ($\kappa = 1875$) and α_r to 1.25. In addition, only cases for $\eta_r \leq 1$ are considered.

Figure 2.12 shows the variation of the stress ratio $\left(\frac{q}{p}\right)$ and porosity (n) versus axial deformation during a triaxial compression for different η_r values. As can be seen, both peak and residual shear strengths depend on η_r, as well as the dilatancy. The contact resistance to rolling increases with η_r, mimicking more and more angular particles, leading to higher peak and residual friction angles and to more dilatant behaviors. This is also shown in Figure 2.13 where the peak shear strength and the residual shear strength depend only on the rolling friction, η_r, for sufficiently high values of α_r (i.e. without the effect of an elastic parameter).

On the other hand, a series of triaxial compression tests were simulated with different values of the contact friction angle (Table 2.1, case 3). The response of the model is illustrated in Figure 2.14. It is shown that this parameter has a strong effect on the peak strength and dilatancy. However, for the initial porosity considered, only dilatant behaviors are observed, and purely contractant responses are not reproduced even for low values of φ_c. Finally, for $\varphi_c > 15°$, its influence on the residual shear strength becomes insignificant, as observed similarly by Huang et al. (2014).
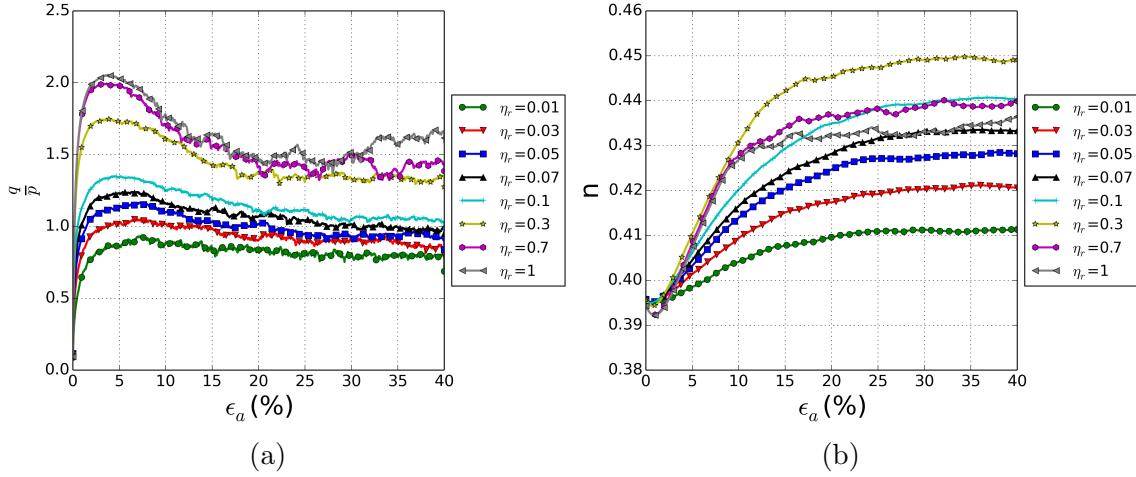
Figure 2.12: The variation of (a) the stress ratio and (b) porosity during triaxial drained compressions under different values of η_r (case 2 in Table 2.1 for $\alpha_r=1.25$).
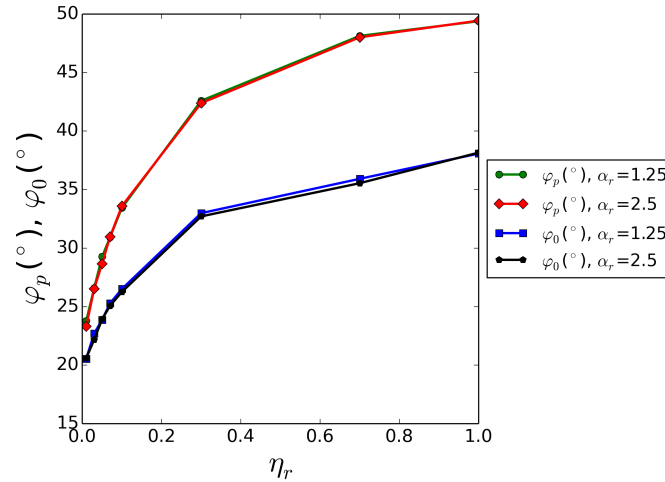
Figure 2.13: The variation of peak and residual friction angles with respect to η_r for different values of α_r (case 2 in Table 2.1 for $\alpha_r=1.25$ and 2.5).

Thus, for $\varphi_c > 15°$, the residual shear strength is governed only by η_r, whereas the peak strength can be fine tuned by φ_c for a fixed value of η_r. Volumetric strain cannot be adjusted with φ_c and/or η_r alone since, for instance, it was not possible to reach a contractant behavior during the parametric studies displayed in Figures 2.12 and 2.14. Nevertheless, the volumetric strain is also strongly dependent on the initial density, and a purely contractant behavior may be observed for loose or very loose granular materials. Consequently, a numerical preparation methodology allowing to reach a wide range of initial porosity of the model is presented in the next section.
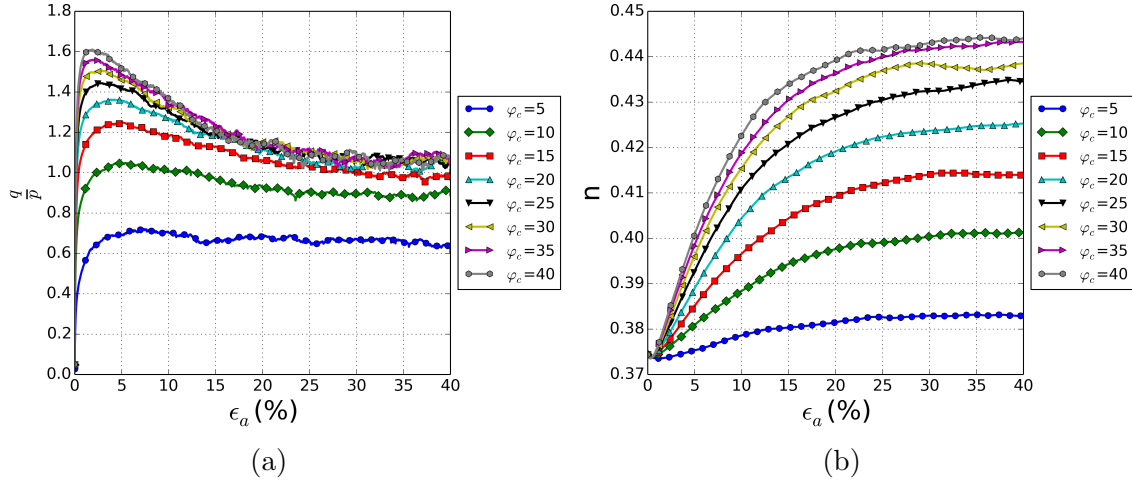
Figure 2.14: The variation of (a) the stress ratio and (b) porosity during triaxial compressions under different values of φ_c (case 3 in Table 2.1).

Preparation methodology for a large range of initial density

In the literature, several techniques to generate numerical discrete samples are suggested. They mainly include the isotropic-compression method (Cundall & Strack (1979)) and the particle expansion method (Plassiard et al. (2009); Wang & Li (2014)). Both methods can be combined with a progressive lubrication of contacts consisting in decreasing the inter-particle friction until reaching the target porosity (as proposed for instance in Chareyre et al. (2002) and Tong et al. (2012)). Such methods are efficient means to produce dense samples but they fail in repoducing very loose ones. However, little studies have been done on loose samples. Jiang et al. (2003) proposed the multi-layer with under-compaction method to produce looser soil samples, but a very loose soil was not achieved. We propose, thereafter, a new method for that purpose. It imitates numerically the experimental reconstitution technique of soil samples by the moist tamping method where a low moist content (about 2 to 3 %) introduces adhesion between particles allowing to reach even higher void ratios from the ones corresponding to the loosest state achieved by Jiang et al. (2003). Moreover, as explained in Gilabert et al. (2007), introducing adhesion in the model, in the presence of rolling resistance, stabilizes looser and less coordinated samples leading to a reduction in the solid fraction and coordination number.

The methodology comprises three steps as follows:

1. Random generation of a very loose cloud of non-overlapping particles;

2. Isotropic compaction until a target confining pressure is performed with the presence of an adhesive contact stress, σ_A (Eq. 2.15) and keeping the normal contact friction angle (i.e. the same value used later for compression tests), first at a high strain rate to save computational time, then slower when contacts start to percolate, until equilibrium is achieved (see Figure 2.15);

3. Removal of the contact adhesion ($\sigma_A = 0$) and waiting for a new equilibrium to be attained;

Figure 2.15 shows the evolution of the porosity and the unbalanced forces in each step. It can be seen that during the compaction process the porosity decreases until an equilibrium

state is reached. Equilibrium is assessed from the dimensenionless unbalanced force, U_f. It is computed as the ratio of the mean resultant particle force to the mean contact force. U_f tends to zero for a perfect static equilibrium and a value of $U_f = 10^{-3}$ was considered here as representative of a state sufficiently close to this limit (Figure 2.15). Notice that during the last step where contact adhesion is removed, the sample experiences a slight additional compaction (see Figure 2.15), as observed experimentally with the moist tamping technique during the saturation stage of the soil sample.

Following the proposed procedure, the accessible densities reached by this method
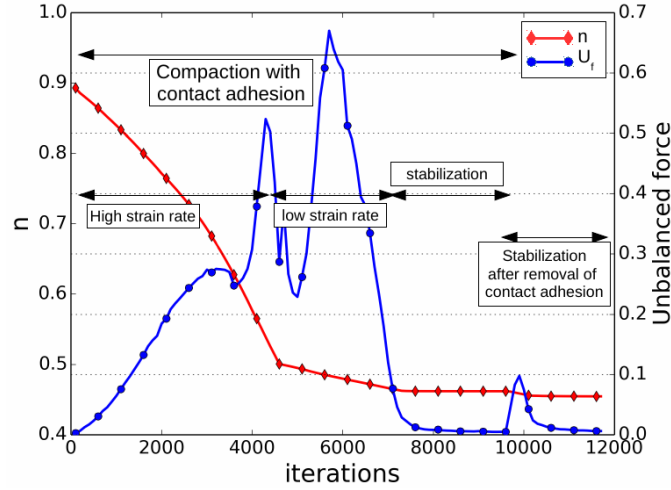
Figure 2.15: Evolution of the porosity and the dimensionless unbalanced force during the three steps of compaction.

are shown in Figure 2.16. It can be noticed that as the contact adhesion, σ_A, increases, the initial porosity after compaction increases too, and the sample shows more and more an obvious contractant behavior as shown in Figure 2.17. This happens up to a threshold adhesion value (here equal to $\sigma_A = 80$ kPa or $\frac{\sigma_A}{P_c}=1$), beyond which the numerical sample strongly collapses during the third step of the compaction method leading to lower porosities and more dilatant behavior (see the results for $\frac{\sigma_A}{P_c}=1.25$ and $\frac{\sigma_A}{P_c}=2.5$ in Figures 2.16 and 2.17).

Figure 2.17 shows the triaxial compression tests simulated from the accessible densities reached by this method. It can be observed that removing completely the adhesion during the compaction phase is not enough to reach dense samples presenting a strong dilatant behavior. For that, contacts need to be lubricated during the compaction phase by fixing a low friction angle, as described for instance in Tong et al. (2012), and illustrated in Figures 2.16 and 2.17 for a lower values of the contact friction angle during compaction. Hence, a large range of initial density can be reached by assigning during compaction either an artificial contact adhesion or a reduced contact friction.
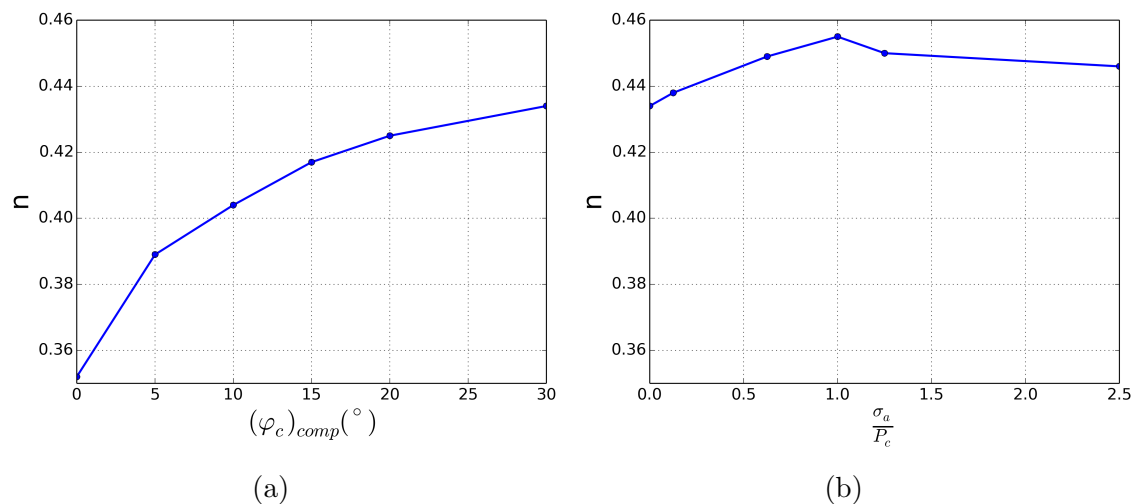
Figure 2.16: Range of porosity reached after compaction for: (a) reduction of contact friction angle, $(\phi_c)_{comp}$, during compaction, and (b) introduction of contact adhesion, σ_a, during compaction (with $(\phi_c)_{comp}$=30 °).
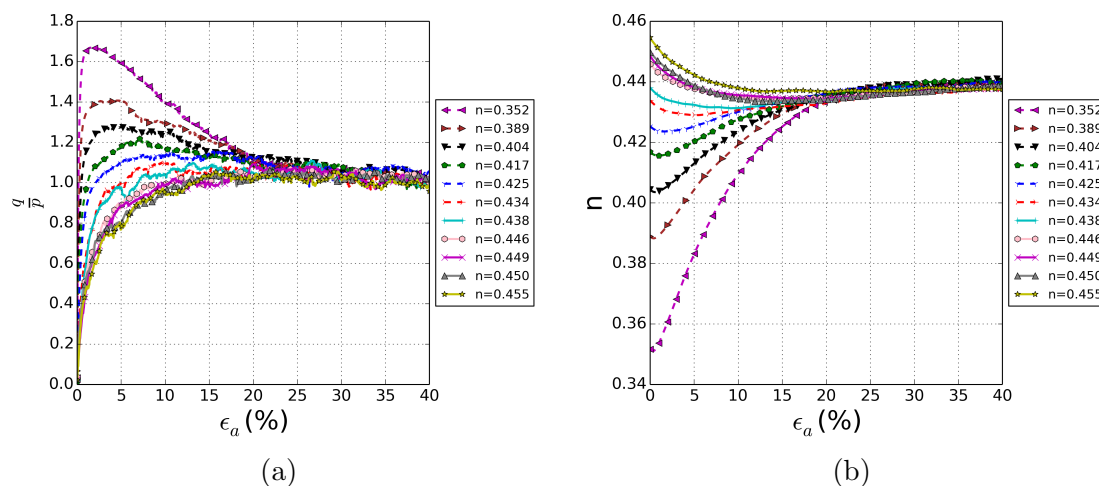
Figure 2.17: Effect of the introduction of adhesion, σ_A, or of the contact lubrication during compaction, on (a) the stress-strain response to a triaxial compression and (b) the porosity (case 4 in Table 2.1).

2.3.3 Modeling of the soil mechanical behaviour

In this section, a calibration procedure is defined and then applied to reproduce the experimental data obtained from drained triaxial compression tests with $P_c = 200$ kPa (i.e. constant effective confining stress). Moreover, to validate our model, it was tested with the data obtained from: drained triaxial compression tests with different confining pressures, undrained triaxial test (i.e. no volume change) as well as constant deviator stress test (constant q), done by T. Nguyen (2014).

Calibration process

After studying the influence of different parameters incorporated in our DEM model, a calibration procedure based on the simulated response to a triaxial compression was defined as follows:

1. As the residual shear strength is independent of the initial porosity and of the contact friction for $\varphi_c > 15°$, then η_r can be first calibrated by reproducing the experimental residual friction angle, while φ_c is set arbitrarily (let's say for instance 30° as a first approximation of the contact friction between two silica particles). For this step, the numerical sample may be compacted without the addition of contact adhesion or contact lubrication in order to start from a medium dense material;

2. Volumetric strain (i.e. dilatancy/contractancy) and peak stress (if any) are approached as close as possible by fine tuning the initial sample density. To get a looser material, adhesion is introduced during the compaction phase, while contacts are lubricated during the latter phase to reach a denser assembly, as described in the previous section;

3. Contact friction angle, φ_c, is calibrated (if necessary) to improve the reproduction of the volumetric strain and the peak stress. Knowing that a change of φ_c can affect the initial porosity reached after the compaction phase, it may be necessary to reiterate steps 2 and 3 until a satisfying calibration of both the initial porosity and φ_c is achieved.

Calibration of elastic parameters, contact elastic modulus, E_c, and shear factor, α_s, appears secondary to plastic parameters (as long as they are close to the stiff limit), with respect to their effects on the macroscopic mechanical behavior. They can be adjusted if necessary to better reproduce the macroscopic initial Young modulus and Poisson ratio as discussed in Plassiard et al. (2009). Rolling stiffness, α_r, is kept close to the rigid limit, not lower to avoid any impact on plastic macroscopic properties, but not higher to avoid possible reduction in the critical time step as discussed in section 2.2.3.

It is worth noting that this proposed calibration procedure stresses more on the rolling friction than on the contact friction angle. Indeed, one can expect the contact friction angle not to be very different for different granular soils since grains are generally made with similar constituents (silica and alumine), whereas particle shapes, reflected by the rolling friction, may change a lot and directly impact the soil mechanical behavior.

Validation on laboratory triaxial compression paths

The calibration procedure is applied to calibrate the numerical model on experimental data obtained from drained triaxial compression tests on a Camargue sandy soil. Laboratory triaxial compression results are presented in T. Nguyen (2014) and Benahmed et al. (2015). The triaxial tests were performed on very loose Camargue sand samples prepared with an initial (i.e. before isotropic compression) relative density of 20%. The particle size distribution of the numerical model partially follows the one of the sand as presented in Figure 2.18. It has been simplified by removing 3% of the largest particles and 3% of the smallest ones to limit the total number of discrete elements and so to reduce the computational cost.
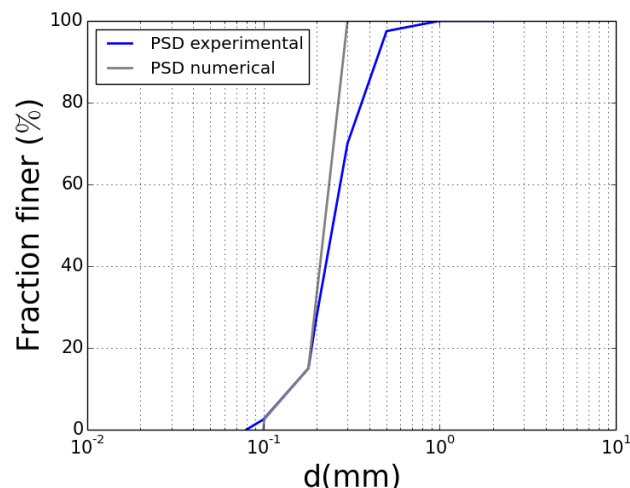
Figure 2.18: The gradation curve of the Camargue sand.

The model has been calibrated from a drained triaxial compression with a confining pressure, $P_c = 200$ kPa (Figure 2.19), leading to the parameters shown in Table 2.2.
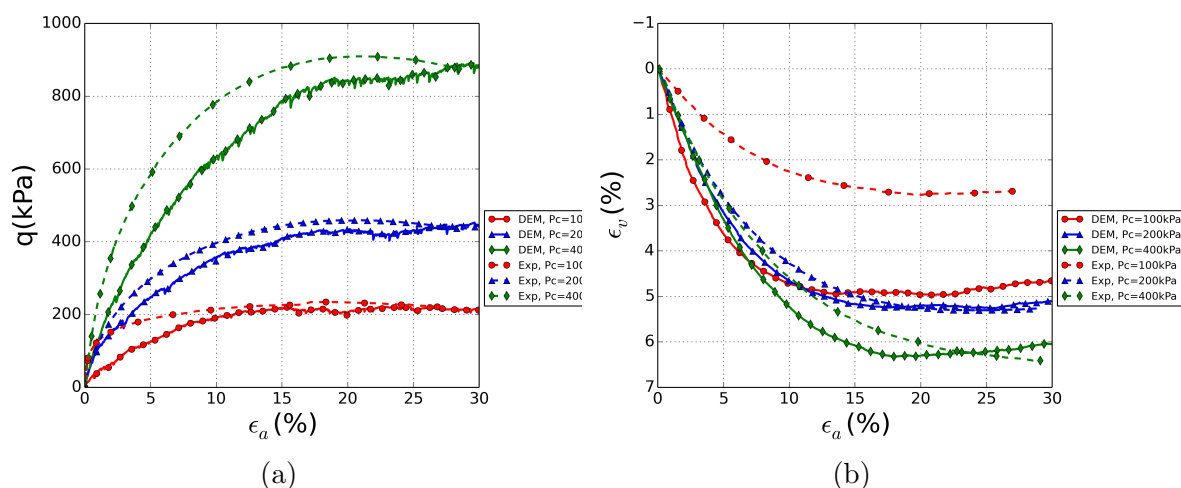
Figure 2.19: Comparison between experimental drained triaxial compression tests and DEM simulations on loose Camargue sand. (a) deviator stress, (b) volumetric strain.

E_c (kPa)	α_s	φ_c (°)	α_r	η_r	σ_A (for compaction only) (kPa)
$2\,10^5$	0.2	25	7.5	0.22	200

Table 2.2: Summary of the parameters calibrated on the loose Camargue sand.

When applied to compressions with different confining pressures than the one used for calibration (Figure 2.19), the model succeeded to describe the shear strength but

partially failed in reproducing quantitatively the dependence of the volumetric strain on the confining pressure. The important reduction of contractancy of the sand obtained experimentally for $P_c = 100$ kPa, with respect to $P_c = 200$ kPa and 400 kPa, is underestimated by the model.

Responses of the calibrated model and of the sand subjected to an undrained compression, after an initial isotropic compression, $P_c = 200$ kPa, are compared in Figure 2.20. The model exhibits sudden and total liquefaction at very low axial strain which was not the case experimentally for the sand, as if the ability of the numerical model to contract was more important than for the sandy sample. Responses were also compared to a constant deviator stress loading path performed after an initial drained compression. Stress and strain paths are displayed in Figure 2.21. The numerical model correctly describes the stress state at failure occurrence but predicts a much more contractant response than the experimental data. The constant shear drained path, such as the q-constant path, leads to a reduction of the mean pressure, p. Consequently, the overestimation of contractancy along these loading paths is in agreement with the results obtained from the drained compressions (Figure 2.19). In the latter case, we showed that the model underestimates the reduction of contractancy with the decrease of the mean pressure.
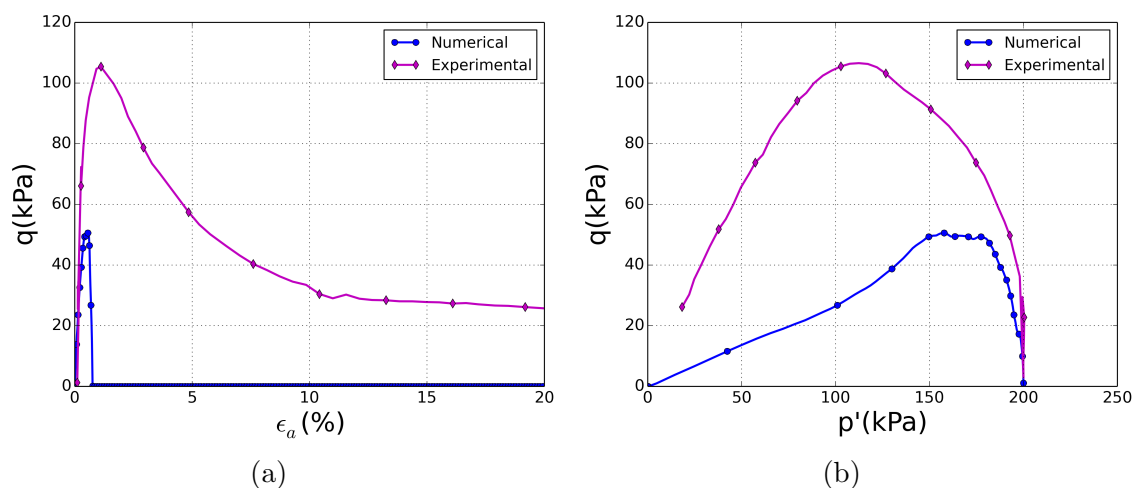
Figure 2.20: Comparison between experimental and numerical responses under undrained triaxial compression.

(a) (b)
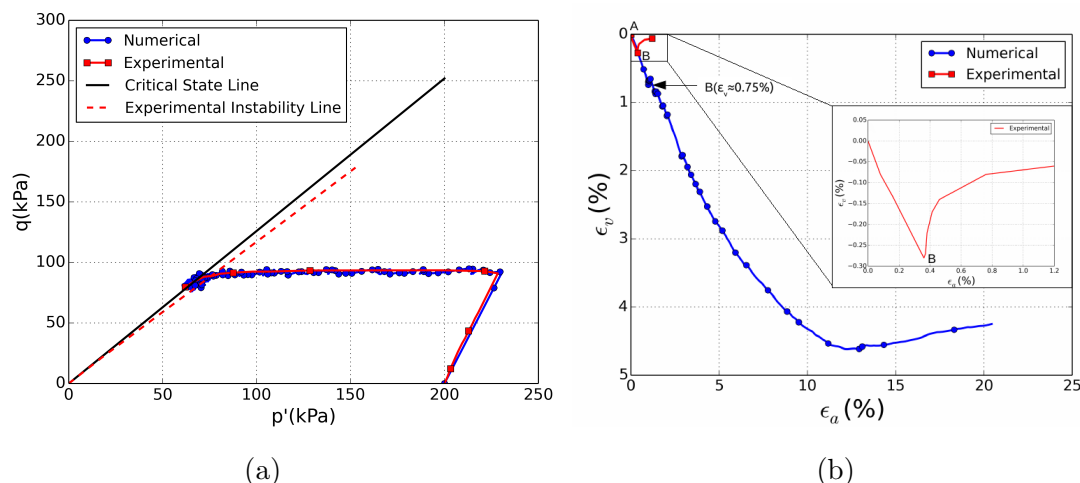
Figure 2.21: Comparison between experimental and numerical responses under constant deviator stress loading path just up to failure point.

2.3.4 Discussion

The observed difference of the dependency of the volumetric strain on the mean pressure can be related to different factors that differ between experimental and numerical tests:

1. Difference of the compressibility behavior induced by the isotropic compression: for the numerical sample, the relative variations of porosity after compaction when confining pressure is increased from $P_c =$100 kPa to 200 kPa, and up to $P_c =$400 kPa, are -0.09 % and -0.81 % respectively, whereas experimentally the sand sample presents a more important compressibility with relative porosity variations equal to -0.82 % and -2.22 % (always with respect to the state for $P_c =$100 kPa). This difference is particularly important in the range of confining pressure 100 kPa - 200 kPa where the relative reduction of porosity for the numerical model is about 9 times smaller than what is found experimentally. This may contribute to the discrepancy between numerical and experimental volumetric strains observed, especially for the compression at $P_c =$100 kPa;

2. Different particle shapes: this is related to the ability of angular or elongated particles to untangle. A reduction in the mean pressure, allowing more flexibility for angular or elongated particles to rotate, can promote their disentanglement, and thus a lower contractive behavior. In addition, even without any translational motion of particles, new contacts may be formed with elongated particles in rotation, limiting further compaction of the granular assembly. Such mechanisms are not reproduced with the numerical model made of spheres, even with the introduction of a contact resistance to rolling, and apparently, constitutes a limitation of the model;

2.4 Role of fine particles in a polydisperse granular soil

The main objective of this work is to study the effect of suffusion on the mechanical properties of the soil. During the suffusion process, the soil structure is modified and the

post-suffusion behavior may be strongly affected. Intensive research has been devoted to study the role of fine particles in the soil structure. Studies showed that the fines content, FC, may influence significantly the microstructure of the soil. The participation of particles of different sizes in the inter-particle contact force changes with FC (Thevanayagam (1998, 2000); Shire et al. (2015, 2014)). Moreover, the fines content has a significant influence on the shear strength and the onset of the mechanical instabilities in soils as well as on the position of the critical state line of silty sands as found by Benahmed et al. (2015) and Yin et al. (2014b). Therefore, the soil behavior seems to be dependent on the range of fines content, which may explain the changes in the soil strength after internal erosion. In this section, the previously defined model is applied to study the role of fine particles in the soil structure and how the mechanical behavior changes with the fines content. Knowing the role of fine particles allows us to understand at which fines content their erosion may start to influence the integrity of the soil matrix.

2.4.1 Calibration on a silty sand soil

To account for the effect of the loss of a fraction of fines, soils with different fines contents but similar inter-granular void ratio are considered. This results in assuming that fine particles can be lost without implying any volumetric deformation. The focus here is on the role of fine particles in the microscopic and macroscopic properties of the soil. For this purpose the mechanical parameters of the numerical model used here are calibrated from an experimental study on a natural silty sand which was collected in the adjacent zone of a breach of the Rhone embankment dike during the 2003 flood (Benahmed et al. (2015)). The problem that had occurred involved a soil in a relatively loose initial state that we search to describe.

The particle size distributions, resulting from a mixture of sand and silt, characterized by a fines content, FC (i.e. silt content) ranging from 0 to 15%, are displayed in Figure 2.22. They were simplified in our model to reduce the difference in diameter between large and small particles, else it will require a high number of particles and a high computational time.

We have chosen to calibrate the mechanical parameters in two steps. First the coarse
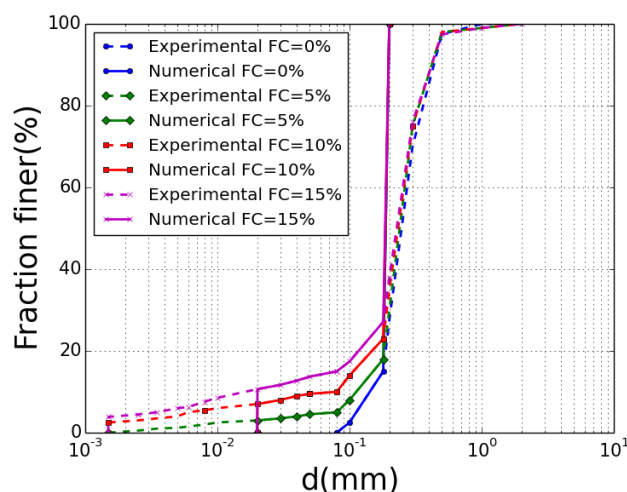
Figure 2.22: Particle size distributions for fines content, FC, ranging from 0 to 15%.

numerical fraction was calibrated on the properties of the pure sand alone. Second, the fine fraction of the model was calibrated on the porperties of the pure silt alone. Actually, the calibration on the pure sand has already been presented in Section 2.3.3. and we focus here on the calibration of the fine fraction on the pure silt. The model has been calibrated from a drained triaxial compression with a confining pressure, $P_c = 100$ kPa (Figure 2.23), leading to the parameters shown in Table 2.3.

Having calibrated the parameters for sand and silt separately, drained triaxial compres-

(a)   (b)
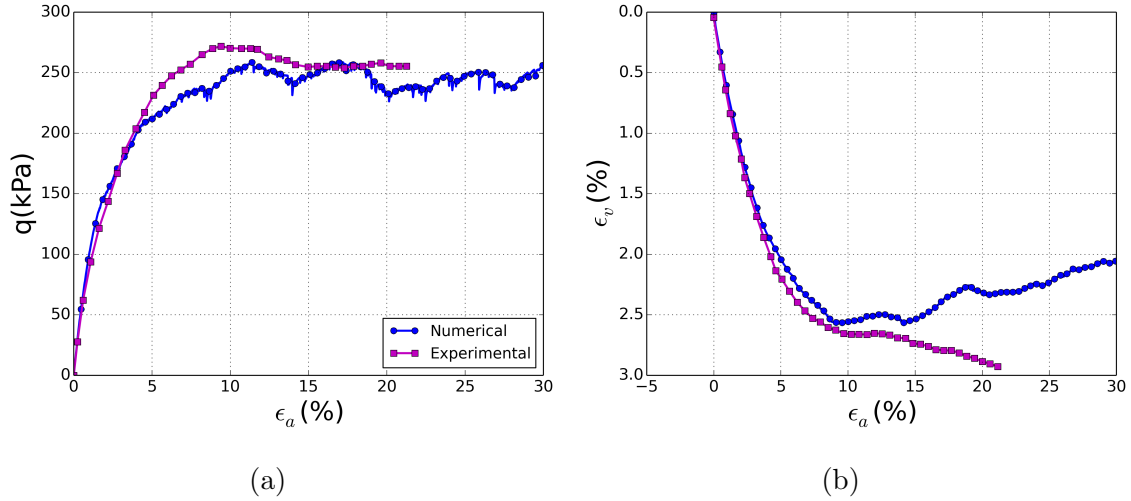
Figure 2.23: Comparison between experimental drained triaxial compression tests and DEM simulations on loose Camargue silt. (a) deviator stress, (b) volumetric strain.

E_c (kPa)	α_s	φ_c (°)	α_r	η_r	σ_A (for compaction only) (kPa)
$2\,10^5$	0.2	25	7.5	0.33	3

Table 2.3: Summary of the parameters calibrated on the loose Camargue silt.

sion tests were carried out on mixtures of sand and silt with different silt contents. For each fines content (FC=5, 10, 15 %), five different randomly generated soil samples are studied and the average of the results is then considered. Table 2.4 gives the values of the void ratio, the inter-granular void ratio and the equivalent inter-granular void ratio of each soil sample under an isotropic stress state of 200 kPa. The stress-strain curves obtained from triaxial compression tests on initially loose soil samples are illustrated in Figure 2.24. The effect of fines on the soil strength is reduced in the numerical model with respect to the experimental data. This can be related to the modification in the numerical gradations with respect to the experimental ones, but also to the difference between the angular shape of real particles and the spherical shape of numerical particles. In addition to that, the numerical model may have under-estimated the number of active fine particles compared to the experimental ones. Moreover, the initial void ratio of the numerical model is slightly different from the experimental soil samples. Nevertheless, the simulated responses to triaxial compression tests show that the numerical model presents

(a)	(b)
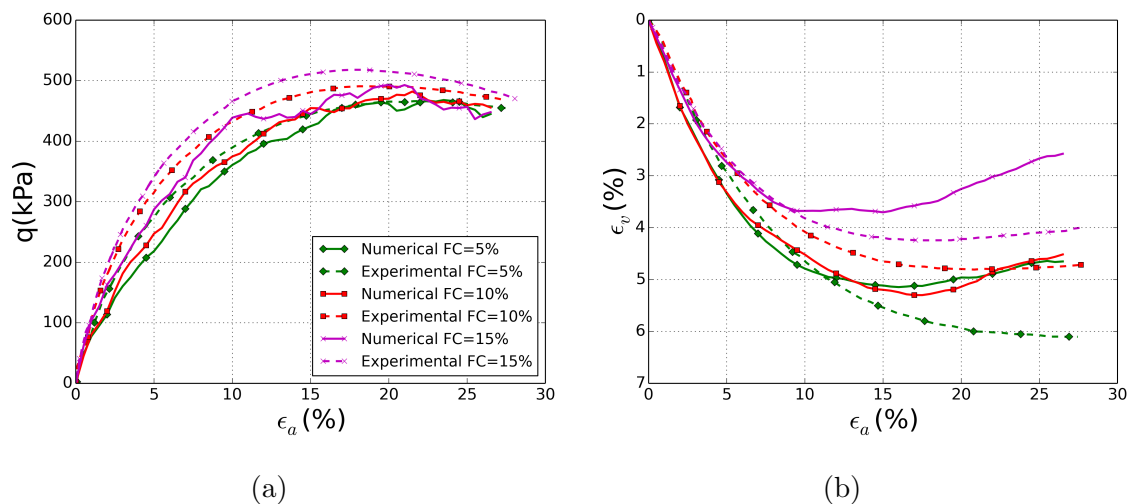
Figure 2.24: (a) Stress-strain response and (b) volumetric deformation of a loose silty sand subjected to a drained triaxial compression.

a realistic mechanical behavior close to the experimental data. Table 2.4 gives the peak and residual friction angles for each soil mixture. The numerical peak friction angle (the peak and residual friction angles are equal in the numerical model) increases very slightly from 31.9° at FC=5% to 32.1° at FC=10% and 32.7° at FC=15%. Hence, numerically, the shear strength is almost the same for all soil samples. In the experimental data, the peak friction angle increases slightly from 32.5° at FC=5% to 33.4° at FC=10% and 34.3° at FC=15%. Thus, experimentally, as FC increases up to 15 %, the soil shear strength increases. The residual friction angle is about 33° in all experimental soil samples. Therefore, it can be noticed that the influence of FC is lower for the model than in reality because the model may have under-estimated the number of active particles. Nevertheless, as FC increases, the soil becomes more dilatant as shown in Figure 2.24. When more fine particles fill the pore space, they provide lateral support to the coarse particles once sheared and prevent the buckling of force chains.

Generally, in order to understand at which FC fine particles start to play a significant effect in the microstructure, a micro-structural analysis of samples with a wider range of FC (0-100%) is presented in the following sections.

Soil sample	P_c (kPa)	FC (%)	e	e_g	e_{eq}	φ_p °	φ_0 °
Numerical-1 FC=5%	200	5	0.75	0.85	0.85	31.6	31.6
Numerical-2 FC=5%	200	5	0.79	0.86	0.86	31.4	31.4
Numerical-3 FC=5%	200	5	0.75	0.85	0.85	32.5	32.5
Numerical-4 FC=5%	200	5	0.75	0.84	0.84	31.7	31.7
Numerical-5 FC=5%	200	5	0.75	0.85	0.85	32.5	32.5
Numerical FC=5%	**200**	**5**	**0.76**	**0.85**	**0.85**	**31.9**	**31.9**
Experimental FC=5%	**200**	**5**	**1.088**	**1.198**	**-**	**32.5**	**32.2**
Numerical-1 FC=10%	200	10	0.67	0.86	0.86	31.4	31.4
Numerical-2 FC=10%	200	10	0.67	0.85	0.85	33.1	33.1
Numerical-3 FC=10%	200	10	0.67	0.84	0.84	32.2	32.2
Numerical-4 FC=10%	200	10	0.67	0.82	0.86	32.6	32.6
Numerical-5 FC=10%	200	10	0.67	0.86	0.86	31.4	31.4
Numerical FC=10%	**200**	**10**	**0.67**	**0.85**	**0.85**	**32.1**	**32.1**
Experimental FC=10%	**200**	**10**	**0.978**	**1.198**	**-**	**33.4**	**33.4**
Numerical-1 FC=15%	200	15	0.54	0.81	0.81	32.5	32.5
Numerical-2 FC=15%	200	15	0.56	0.85	0.85	32.3	32.3
Numerical-3 FC=15%	200	15	0.56	0.84	0.84	33.4	33.4
Numerical-4 FC=15%	200	15	0.54	0.82	0.82	33.3	32.3
Numerical-5 FC=15%	200	15	0.56	0.83	0.83	32.8	32.8
Numerical FC=15%	**200**	**15**	**0.55**	**0.83**	**0.83**	**32.7**	**32.7**
Experimental FC=15%	**200**	**15**	**0.868**	**1.198**	**-**	**34.3**	**33.2**

Table 2.4: Summary of the data of silty sand soil with different FC.

2.4.2   Dependence of the soil microstructure on fines content

The micro-structural analysis of the soil samples with different fines contents was done by studying different ways of considering the interstitial voids and floating fine particles. This results in different definitions of the void ratio: the global void ratio (e, calculated as done classically), the inter-granular void ratio (e_g, considering all fine particles as voids) and the equivalent inter-granular void ratio (e_{eq}, considering only inactive fine particles as voids). The distinction between active and inactive particles was done by checking the number of contacts of each particle. If the number of contacts is less than two, then the particles are considered inactive. The variation of these parameters with respect to FC is shown in Figure 2.25b for the granular assembly in a loose state (i.e. the state considered for the calibration in the previous section). In Figure 2.25a, the global void ratio, e, in the current loose state is compared with e_{min}, the void ratio reached for the densest state of the granular assembly (by setting to zero the contact friction angle during the compaction phase).

The global void ratio first decreases with the increase of FC, as more small particles
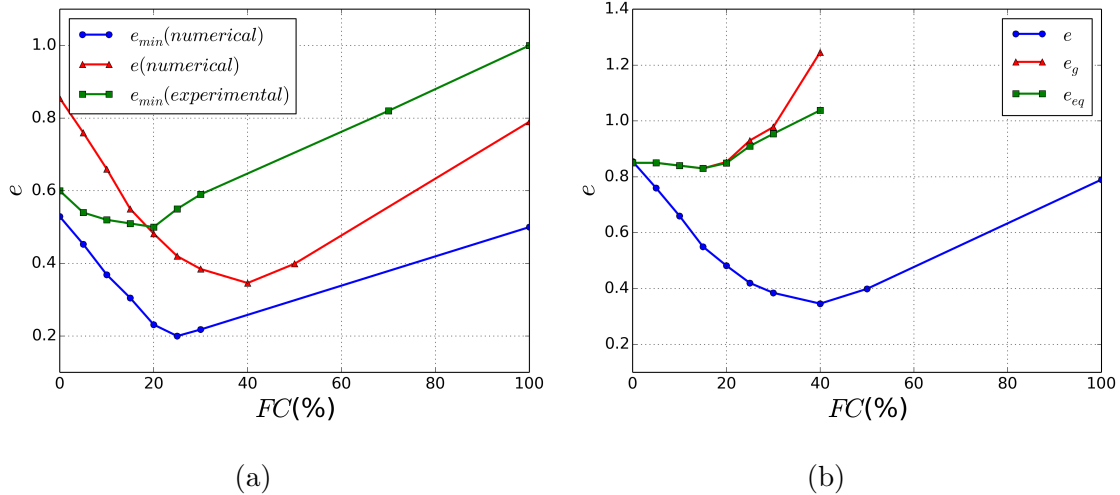
Figure 2.25: (a) Comparison of the global void ratio, e, reached with e_{min}, the void ratio at the densest state, (b) Comparison of e, e_g and e_{eq} in the current loose sample state.

fill the voids made by large particles (Thevanayagam (2000)), until reaching a threshold value at FC_{th}=40%. Beyond this threshold small particles start to separate large ones, increasing the global void ratio again. A similar behavior is noticed for the minimum void ratio (e_{min}), but with FC_{th}=25%. Therefore, we conclude that the threshold fines content beyond which the granular assembly becomes fines-dominated depends on the overall density and ranges between 25% and 40%.

Note that T. Nguyen (2014) found FC_{th}=20% based on the evolution of e_{min} with FC (cf. Figure 2.25a). This value is smaller than the one we obtained when studying the variation of e_{min}. This can be a result of the simplified gradation and the spherical grains' shape used in our model. In addition to that, the reason for the higher FC_{th} in the numerical soil samples may be related to the higher density of the silt particles in the voids.

Besides, another way to find the threshold fines content is using the diagram of Westman

& Hugill (1930) (Figures 2.26 and 2.27). Westman & Hugill (1930) proposed a diagram which can predict theoretically the total volume occupied by a binary mixture as a function of the solid volume of each size fraction considered alone. The horizontal axis in Figure 2.26 represents the composition of the material in terms of coarse and fine particles. The vertical axis represents the total volume occupied by the particles (solid + void volume). The point C corresponds to the case of coarse particles only ($FC=0\%$). Limit cases are now considered by assuming the coarse particles infinitely larger than the fine ones. Then if a small fraction of fine particles is added from this case, they will sit in the voids without any contribution to the total volume which is divided into the volume of coarse particles and the volume of the voids formed by the coarse skeleton. Then the total volume vanishes when the volume of coarse particles tends to zero. This trend is represented by the straight line CF_0 in Figure 2.27a. Point F corresponds to the soil with only fine particles ($FC=100\%$). If coarse particles are added, the volume of the soil will be divided into: volume of fine particles, volume of coarse particles and volume of voids formed by fines only. Then the total volume tends to the unit solid volume (made of coarse particles only) when the volume of fine particles vanishes. This is represented by the straight line FC_1 in Figure 2.27b (where $C_0C_1 = 1.00$). Combining the two lines CF_0 and FC_1 gives the theoretical curve of the total volume occupied by the mixture as a function of FC.

T. Nguyen (2014) also used this theoretical diagram to determine FC_{th} of the Ca-
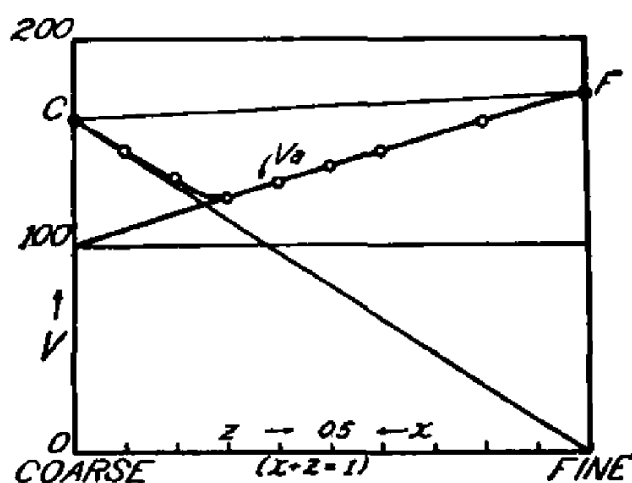
Figure 2.26: Diagram of Westman & Hugill (1930).

margue sandy soil (Figure 2.28). Using this method, FC_{th} was found around 23% which is close to the one obtained by studying the evolution of the minimum void ratio with FC ($FC_{th}=20\%$).

Similarly to T. Nguyen (2014), the theoretical diagram of Westman is given for the minimum and maximum densities for the numerical model in Figure 2.29. The intersection of the curves for the minimum density gives $FC_{th} \approx 25$ %. The maximum density gives $FC_{th}= 33\%$. In fact, another zone (hatched zone in Figure 2.29) can be defined from this diagram. If the coarse fraction has a maximum volume, while the fine fraction has a minimum volume, we would obtain a value of $FC_{th}=36.3\%$ which is close to 40%. Thus, a range of FC_{th} can be defined depending on the volume occupied by each soil fraction.
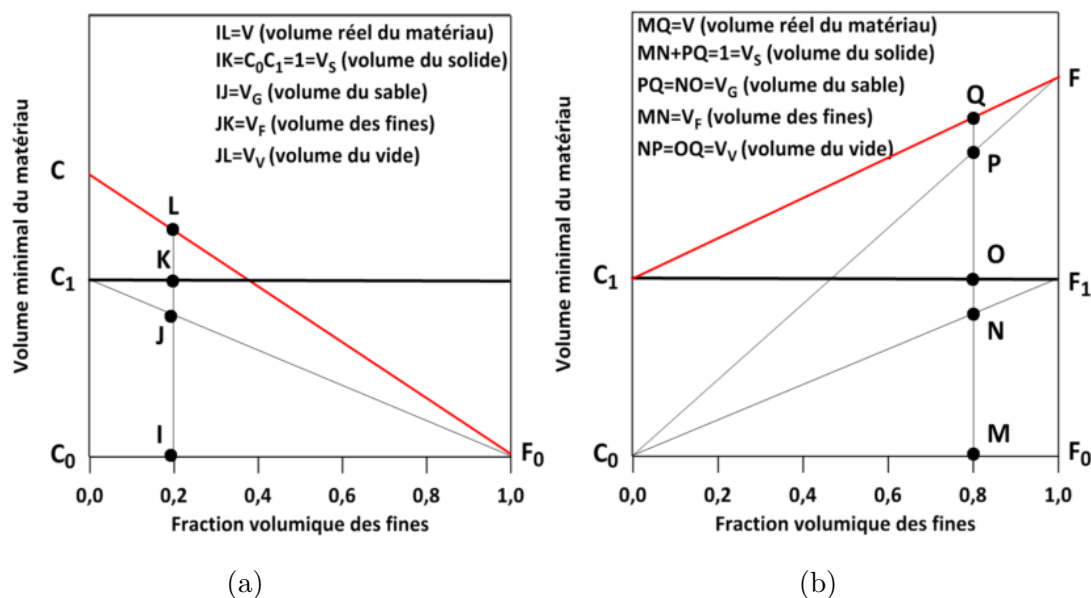
Figure 2.27: Representation of the diagram of Westman and Hugill (a) the case when the sand is dominant (b) the case when fines are dominant (T. Nguyen (2014)).
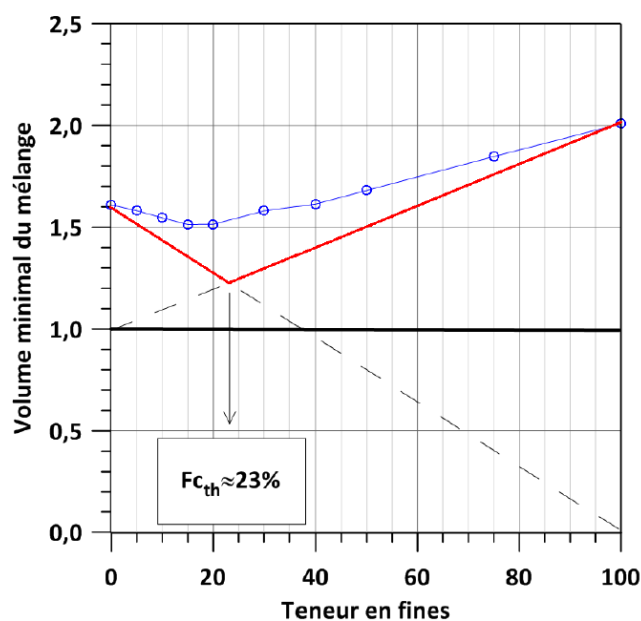
Figure 2.28: Theoretical diagram of Westman & Hugill (1930) for the experimental soil samples in T. Nguyen (2014).

In our model, we can imagine that the coarse skeleton is at a loose state, while the fine fraction is densely packed in the pore space between coarse particles which gives $FC_{th} \approx 40\%$.

As a conclusion, for a given density, FC_{th} depends separately on the specific volume of the coarse fraction and the fine fraction. In the experimental results, the specific volume of the fine fraction is more important than the specific volume of the coarse
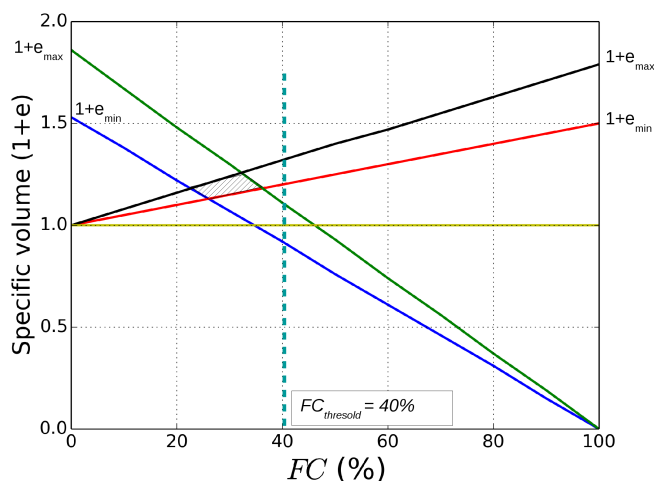
Figure 2.29: Theoretical diagram of Westman & Hugill (1930) for the numerical soil samples.

fraction leading (as shown by the diagram of Westman and Hugill) to FC_{th} lower than that in the numerical data where the specific volume of the fine and coarse fractions are similar (the numerical model is defined in such a way it is independent of the particle size). This is probably the main reason of the difference in FC_{th} between the experimental and numerical results.

Figure 2.25 also shows the variation of the inter-granular and equivalent inter-granular void ratios with FC. For $FC \leq 20\%$, both parameters are almost constant. At $FC > 20\%$, these void ratios start to increase although the global void ratio is still decreasing. This means that at $FC > 20\%$, a fraction of fine particles starts to separate large particles. In other words, a portion of small particles becomes active which may influence significantly the soil behavior.

In addition to that, the fraction of active particles can be represented through the parameter b which is the fraction of the volume of active fine particles to the total volume of fine particles. Figure 2.30 shows the variation of b with FC. It is clear that most particles are inactive until $FC=20\%$ where it can be noticed that some small particles start to be involved in the contact force network by forming two or more contacts with their neighbors.

Further investigations were done at the particles' scale to investigate whether FC_{th} in the case of maximum density, as defined above, effectively constitutes a threshold with respect to the constitution of the microstructure of the granular assembly or if other limits can be identified with respect to the role that the fine fraction plays in the contact force network. The relative number of contacts established between small particles (SS), large particles (LL) and between large and small particles (LS) are illustrated in Figure 2.31. The fraction of LL contacts decreases with FC and it almost vanishes for $FC > 40\%$ meaning that, beyond this point, all large particles have contacts with small particles only. In other words, large particles who had contacts with large particles establish new contacts with small ones as FC increases and are separated as well. Furthermore, Figure 2.31 shows that, as FC increases, large particles establish more contacts with small ones to reach a
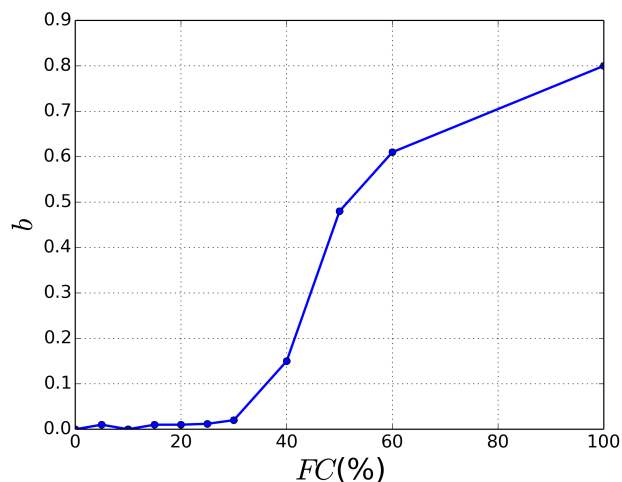
Figure 2.30: The variation of the parameter b with fines content.

maximum fraction of LS contacts at FC=30%. Beyond FC=30%, large particles become dispersed in the medium where fine particles start to form the major structure. This is proved by the SS contacts which increase significantly for FC>30% to eventually represent the majority of the contacts.

Consequently, a conclusion is that for FC greater than 20%, the microstructure is
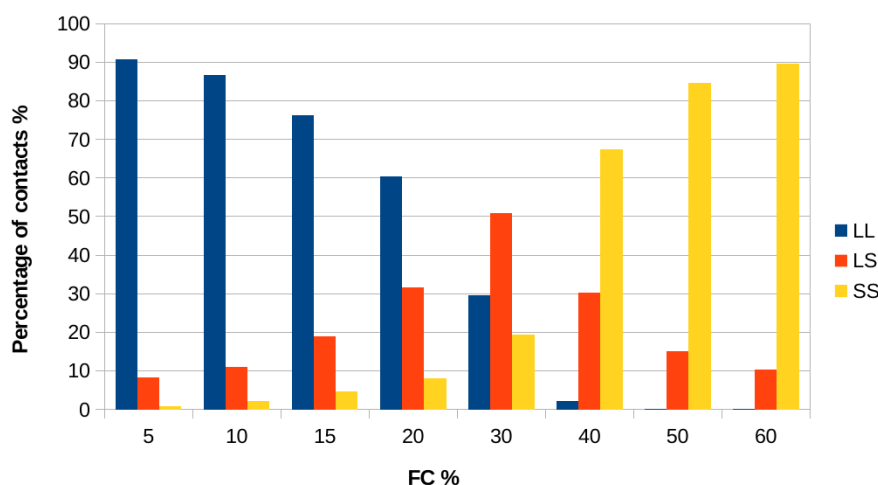
Figure 2.31: Percentage of contacts: LL(Large-Large particles), LS (Large-Small particles), and SS (Small-Small particles).

changing significantly. A portion of small particles starts to play an important role. For further interpretation, we checked among strong contacts which ones correspond to LS contacts. A strong contact is considered here as a contact carrying a force higher than the mean contact force in the system. Figure 2.32 summarizes the results.

It is noticed that for $FC \geq 20\%$, the ratio of the number of strong LS contacts to the total number of strong contacts increases significantly. Thus, more small particles separate large particles and contribute to the transfer of forces in the system. Therefore, a
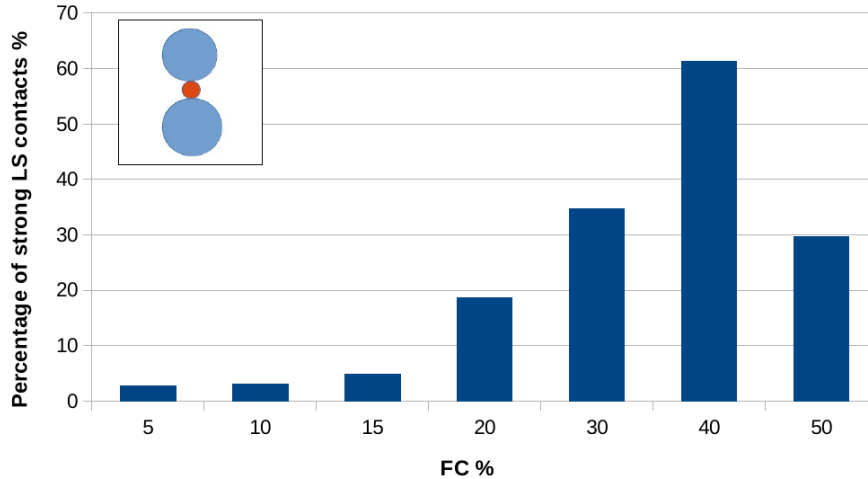
Figure 2.32: Percentage of the strong LS contacts.

configuration that may be expected in such a case can be as the one inserted in Figure 2.32.

As a conclusion, the microscopic analysis showed that fine particles start to be involved in the contact force network, and thus in the macroscopic shear strength of the granular assembly for a fines content lower than FC_{th}=40% and around $FC = 20\%$. We suggest to define this limit as the active fine limit FC_{active}. Note that FC_{active} is here different from FC_{th} for the granular assemblies we studied. However, FC_{active} may be equal to FC_{th} in other conditions (for other gradings, particle shape, density, ...). Thus if erosion of active fine particles occurs in our studied soil with initial $FC \geq 20\%$, one can expect a more important impact on the macroscopic mechanical properties of the soil than for lower initial fines content.

2.5   Conclusion

This chapter presented the DEM modeling of the mechanical behavior of granular soils by using spherical particles and contact rolling resistance. This model will be used to analyze the mechanical behavior and the microstructure of soils subjected to suffusion.

It was demonstrated that the macroscopic behavior of the granular assembly mainly depends on the model parameter fixing the plastic rolling moment at contacts. Other parameters as normal contact stiffness or contact friction angle prove to play a secondary role (bearing in mind that the contacts should be sufficiently stiff). This is consistent with the fact that the shear strength in cohesionless soils is more strongly related to the particle shape (presented here by the plastic rolling moment) than to the inter-particle friction angle, as shown previously by Estrada et al. (2013). Moreover, the macroscopic behavior depends on the initial density of the soil. Consequently, a new numerical method of compaction was proposed, involving either the introduction of inter-particle adhesion forces or the lubrication of contacts, to reach a wide range of initial density of granular assemblies, from very loose to very dense.

However, it was shown that even if our model succeeds in reproducing the experimental data, there are some limitations to be taken into account related to the description of the dependency of volumetric strains on the mean pressure. This is due to the difference in the relative variation of initial porosity after compaction between experimental and numerical tests as well as due to the different particles shape. Such marked differences may be partially due to the very loose state of the tested samples. In fact, a recent study on a dense Hostun sand showed a very good predictive ability of the model compared to the experimental data. Briefly, a comparison on drained axisymmetric compression paths is presented in Figure 2.33; further validations have been carried out on complex loading paths such as stress proportional loading paths and circular paths in the deviatoric stress plane. However, this study is not directly related to the scope of this PhD thesis. Consequently the results are not presented and discussed here but they can be found in Sibille et al. (2017).

Despite the limitations of this model, one should keep in mind the little number of parameters it involves. In total five parameters are involved, among which three elastic parameters are secondary if sufficiently close to the stiff limit, compared to a basic phenomenological elasto-plastic constitutive relation (without any hardening mechanisms) involving a minimum of four parameters (Young modulus, Poisson ratio, internal friction angle, and dilatancy angle). Moreover, the dependency of the dilatancy angle or the friction angle on the mean pressure for such elasto-plastic constitutive relation requires some additional empirical laws coming with additional parameters.

Finally, the model was applied to analyze polydisperse granular assemblies with differ-

(a)   (b)
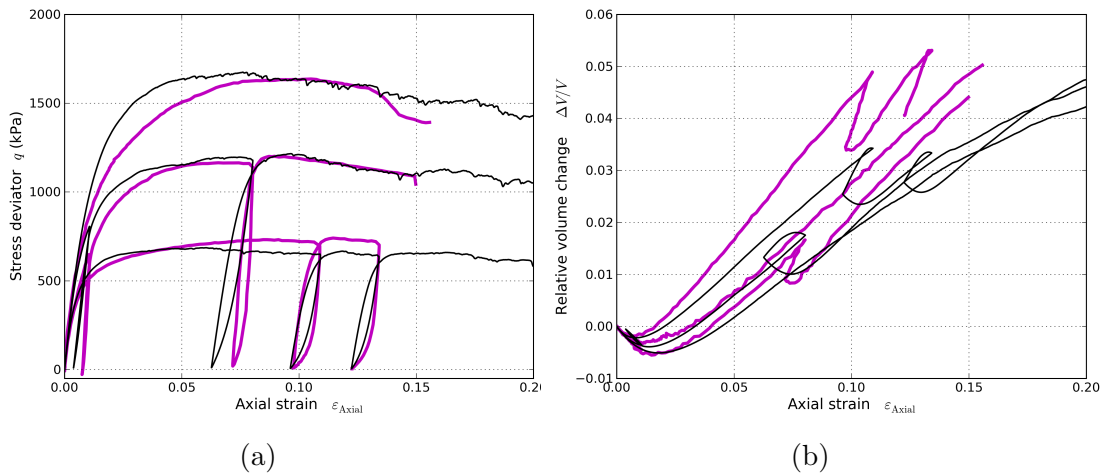
Figure 2.33: Comparison between experimental drained axisymmetric compression tests (thick magenta curves) and DEM simulations (thin black curves) on a dense Hostun sand under confining pressure of 200 kPa, 350 kPa and 500 kPa respectively. (a) deviator stress, (b) volumetric strain.

ent fines contents. Idealized samples with isotropic fabric and spherical particles were studied following the defined numerical model. Analysis of the microstructure of soils with different fines content is done by studying the impact on the void ratio -considering different definitions of the latter (e, e_g and e_{eq})- as well as the consequences on the contacts formed between particles. From such an analysis, an "active" fines content FC_{active} can

be distinguished from FC_{th}. Therefore, if erosion takes place for FC around FC_{active} and if active fine particles are eroded, the consequences on the macroscopic behavior should be particularly marked as fine particles are clearly involved in the strong contact force network, unlike the case of soil gradations with lower fines contents.

Chapter 3

A suffusion-like numerical model

3.1 Introduction

This chapter introduces the numerical extraction procedure followed in this study to mimic the suffusion process. Suffusion constitutes a strongly coupled fluid-solid interaction problem. Therefore, understanding the mechanical behavior of the soil, in the presence of seepage flow, requires a detailed description of the interactions between the two phases. Seepage flow through the porous medium exerts forces on soil particles leading to their displacement which in turn affects the fluid flow. Thus, only a fully coupled hydromechanical model is capable of describing such a complex process. Various numerical approaches have been adopted in the literature to describe the fluid flow through a granular packing and the mechanical interactions between the solid and the fluid phases. These coupled methods can be characterized by the scale at which the interactions and the fluid flow are described. A brief review of these approaches is presented in Section 3.3. However, using a complete hydromechanical coupling approach constitutes a difficult task which requires an important computational cost.

Recently, some studies proposed alternative simplified procedures to investigate the effect of the removal of fine particles on the mechanical behavior of the soil. These approaches attempt to define numerical or analytical models without any coupling with a fluid phase. The removal of particles in the numerical models is either based only on the size of the particles or, in addition to that, sometimes, the role of particles in the force transfer is also taken into account; hence, the least loaded particles among the smallest ones are removed. In the analyical models, the major parameter to be modified in the governing equations is the porosity which is assumed to increase with erosion. These approaches will be explained in Section 3.2.

Finally, this chapter presents an alternative and original approach which is a compromise between very simplified existing extraction procedures and complete hydromechanical coupling. It is based on a one-way fluid-solid coupling which allows taking into account both hydraulic and geometric criteria to describe the detachment and the migration of fine particles and keeping a reasonable computational cost. All details of the new approach and its evolution during this work will be discussed in Section 3.4. Moreover, the defined extraction procedure is applied on a narrow gradation (Section 3.5) to characterize the consequences of suffusion on the mechanical properties of the soil (Section 3.5). A micro-structural analysis of eroded soils is then considered in Section 3.6 to better understand

how the microstructure of the soil is modified after suffusion.

3.2 Brief review on mechanical models intergrating suffusion effect

In this section a brief review of existing numerical and analytical extraction procedures is addressed. The past few years had shown numerical progress to describe the initiation and the development of erosion as well as its influence on the hydraulic and the mechanical properties of the soil. These methods include:

- approaches based on analytical constitutive relations;

- simplified numerical extraction procedures to erode particles from a discrete model;

- fully-coupled hydro-mechanical approaches.

3.2.1 Approaches based on analytical constitutive relations

To predict the mechanical behavior of granular materials subjected to particle removal, analytical constitutive relations can be directly used to compute the induced deformations and to derive the stress-strain relationship (see for instance Muir Wood et al. (2010); Scholtès et al. (2010); Hicher (2012); Yin et al. (2014a)). The pertinent parameter modified to characterize the effect of suffusion in such models is the density of the soil. Since the erosion of fine particles leads to modifications in the pore space, the removal of a given fraction of particles is accounted for by relating the eroded mass to an increase in the void ratio as defined for example in the micro-mechanical model in Hicher (2012) and Scholtès et al. (2010). Hence, the void ratio can be seen as a loading parameter that would be controlled by the erosion law.

For each erosion step, an increase in the void ratio, representing the removal of fine particles is imposed. It results, through the constitutive relation, in a change of the mechanical properties (depending on the void ratio usually via a state parameter) and leading to a deformation response, and thus, a volumetric deformation, under a constant external stress loading. The latter volumetric deformation is considered in addition to the initially imposed increase in the void ratio to compute the final void ratio resulting from the erosion step. Then, the new mechanical properties of the soils resulting from the erosion process can be investigated by simulating conventional mechanical tests (as triaxial compression tests) with the considered constitutive relation and the final void ratio resulting from the erosion step as an input (C. Chang & Hicher (2005)).

However, suffusion leads also to a change in the soil gradation which may affect the critical state line. This can be taken into account in the models discussed here by establishing for instance a relation between the position of the critical state line and the fines content (Yin et al. (2014a)). Moreover, instead of using only the global void ratio, also the equivalent inter-granular void ratio was used. Finally, the model developed by Yin et al. (2014a) was validated by reproducing the behavior of eroded soils tested experimentally (Figure 3.1).
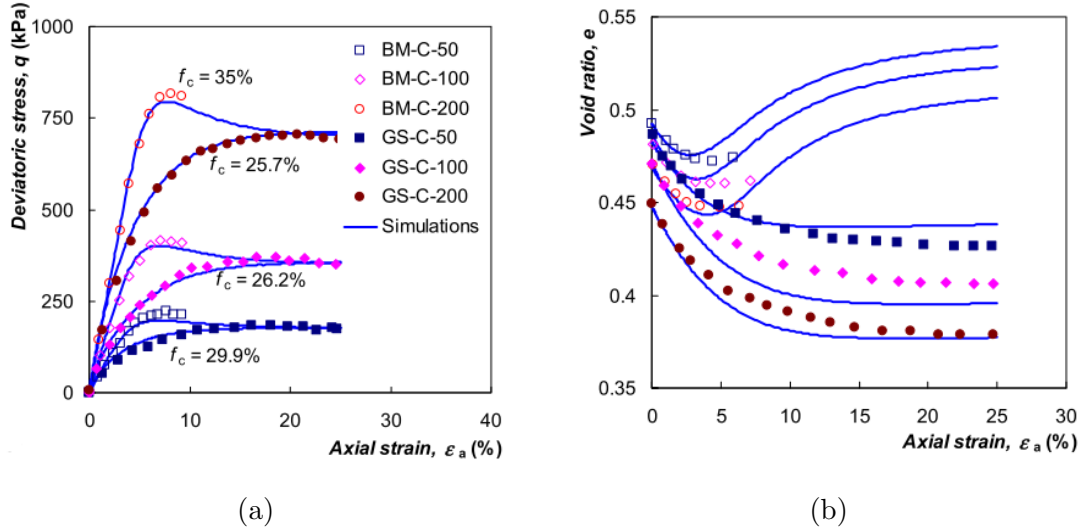
Figure 3.1: Comparison between experimental results and simulations before and after internal erosion (Yin et al. (2014a)).

3.2.2 Simplified numerical extraction procedures to erode particles from a discrete model

Effects on the soil due to the loss of a fraction of fine particles is investigated with numerical discrete models either by modeling soils with different grain size distributions and different initial fines content to study the soil instability or erosion potential in each case without performing any erosion process (Shire et al. (2014)); or by mimicking the suffusion process by defining a simple extraction procedure of potentially erodible particles. These approaches are being used by some researchers, instead of using a complete coupled approach, to reduce the computational time.

2D (Muir Wood et al. (2010); Maeda et al. (2012)) and 3D numerical discrete models (Scholtès et al. (2010)) have been proposed in the literature. The particle removal is done starting from an equilibrium state which can be reached after an isotropic compression or after shearing the sample up to a given stress deviator. Clogging or any constraint to the particle transport is neglected. Muir Wood et al. (2010) followed a very simple criterion to remove particles based on the particles size. Only the smallest discs constituting the numerical soil samples can be eroded. They are removed sequentially following their size order (first the smallest particle, second the second smallest particle, ... and so on). However, this criterion doesn't consider the stress state of the removed particles. Even if a given particle is the smallest, due to interlocking effects, it may be stable. Seepage flow will then erode other less loaded small particles (Shire et al. (2014); Li (2008b)). This condition was taken into account by Scholtès et al. (2010). The extraction process involves the removal of the less loaded smallest particles in the granular assembly. The degree of interlocking of each particle was defined by the mean stress computed at the particle scale from the inter-particle contact forces. Hence, particles with minimum mean stress among the fraction of particles considered as potentially erodible are the first to be removed.

Such simplified extraction procedures are numerically efficient as they do not require a

high computational time since the interstitial fluid dynamics and its interaction with the solid phase are not described. However, they lack important criteria that play a major role in the suffusion process, such as, the constriction sizes allowing particles to pass through or the hydraulic driving forces causing particles to detach. Therefore, in this chapter, an improvement of these extraction procedures is introduced.

3.2.3   Coupled-hydromechanical approaches

The transport of particles cannot be well described with the above simple transport models. The suffusion phenomenon constitutes a strongly coupled fluid-solid interaction problem. Thus, to understand the behavior of the soil subjected to suffusion, the complex interactions between the eroded particles, the coarse skeleton and the interstitial flow should be described. Such interactions require a fully coupled hydro-mechanical model. Few attempts are found lately for that purpose allowing the analysis of the particles detachment, their migration and the filtration processes during internal erosion by suffusion (Tejada et al. (2016)). However, due to the expensive computational cost, there are only few attempts in the literature using such discrete coupled models to describe the mechanical properties of a soil resulting from an erosion process (Wautier et al. (2017); Hama (2016))

3.3   Hydromechanical models based on DEM

In recent years, many efforts have been devoted to couple the discrete element method with fluid models able to describe flows through a porous medium. The different methods that have been developed differ in the scale at which the problem is observed and the modeling techniques adopted to describe the fluid-solid coupling. Therefore, the existing coupling approaches can be divided into three groups as shown in Figure 3.2:

- Group A: the fluid cell size is greater than the solid grain size (Figure 3.2a);

- Group B: the fluid cell size is smaller than the solid grain size (Figure 3.2b);

- Group C: the fluid cell size is similar to the solid grain size (Figure 3.2c).

3.3.1   Group A: The fluid cell size is greater than the solid grain size

This group considers models based on a continuum formulation of the fluid phase (kafui et al. (2002); El Shamy & Denissen (2010); Zeghal & El Shamy (2004)). A coarse-grid mesh is used for the fluid part of the problem. Each mesh represents a subdomain of the DEM model where the porosity and the velocity of the solid phase are averaged and introduced as field variables for the continuum formulation. Then, the fluid velocity and the momentum exchange between the phases at each node of the grid are determined based on empirical interaction laws and phenomenological assumptions such as Ergun's relation (Ergun (1952)) to evaluate the drag forces:

$$\bar{f}_i = (1-n)(150\frac{(1-n)}{n\bar{d}_p^2}\mu_f + 1.75\frac{\rho_f|\bar{v}_f - \bar{v}_p|}{\bar{d}_p})(\bar{v}_f - \bar{v}_p) \tag{3.1}$$

(a) | (b) | (c)
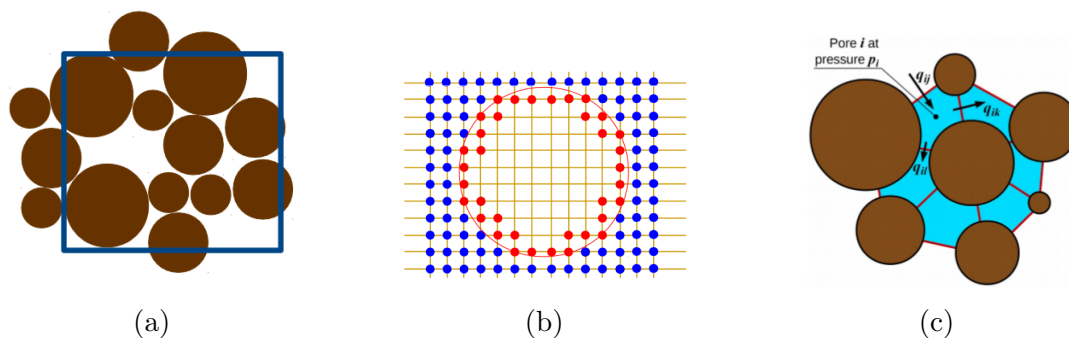
Figure 3.2: Scale of description for different fluid-solid coupling approaches: (a) Group A: the square element represents a typical fluid cell including several solid grains; (b) Group B: a small volume of LBM model; the fluid phase is represented by an ensemble of nodes separated in a regular lattice space (smaller than the circular solid grains in red); (c) Group C: a small volume of the PFV-method; the fluid space is represented by a network of connected pores between solid particles.

where, n is the porosity of the soil, $\bar{d}_p$ is the equivalent particle diameter, μ_f is the dynamic viscosity of the fluid, ρ_f is the density of the fluid, $\bar{v}_p$ is the average particle velocity, and $\bar{v}_f$ is the average fluid velocity.

The fluid flow through the porous medium is generally described using simplified semi-empirical models based on Darcy's law where the hydraulic gradient is related to the fluid velocity. Once the drag forces and the contact forces between particles are computed, the equations of motion are solved for each particle and new particles positions, velocities and contacts are calculated in each time step (see Figure 3.3).
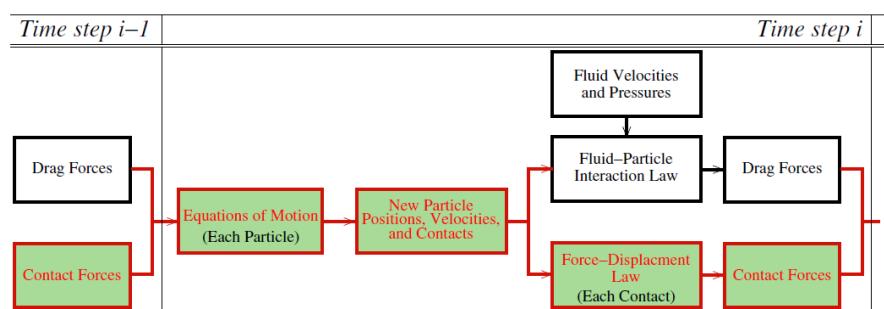
Figure 3.3: Algorithm of a proposed continuum-discrete hydromechanical model of saturated granular media (Zeghal & El Shamy (2004)).

One main advantage of using this method is the affordable CPU cost due to the small number of degrees of freedom associated to the fluid phase compared with those of the solid particles.

On the other hand, the drawbacks of this method are:

- it is not possible to describe accurately the effects of the fluid at the particles scale since the fluid variables are averaged at a large scale (coarse-grid cells) greater than

the average size of particles;

- continuum methods rely on simple phenomenological assumptions and empirical relations.

3.3.2   Group B: The fluid cell size is smaller than solid grain size

It was noticed from the previous group that considering the solid phase as a continuum porous medium to solve the fluid dynamics may not be suitable in some cases. The opposite alternative is to make each solid particle visible by the fluid phase and to describe fluid seepage and fluid/solid interactions at very fine scale, smaller than the typical size of solid particles. Therefore, DEM is either coupled, for instance, with a finite element method with a very fine discretization of the pore space to solve accuratly the Navier-Stokes problem (Glowinski et al. (2001)), or DEM is coupled with kinetic models, such as Lattice-Boltzmann method (Lominé et al. (2013)) or Smoothed Particle Hydrodynamics (Potapov et al. (2001)). The Lattice-Boltzmann method incorporates the essential physics of microscopic processes so that the macroscopic averaged properties obey the desired macroscopic equations. The smoothed Particle Hydrodynamics realizes a mesoscopic description of the fluid. Then, each element carries the information about all physical variables (velocity, pressure, mass,...) evaluated at its position. For all these coupled methods, typical fluid-grain interactions are generally governed by a no-slip condition at the fluid-solid interface.

An advantage of these coupling is that they do not rely on phenomenological assumptions as Group A. However, they may result in high computational time in 3D models limiting the problem, therefore, to small simulation domains.

3.3.3   Group C: The fluid cell size is similar to the solid grain size

This group corresponds to the pore network models which constitute a compromise for the description of the fluid phase between the high computational cost of Group B and the phenomenological assumptions of Group A (Chareyre et al. (2012); Catalano et al. (2014)). Such models are based on the representation of the void space as a network of connected pores and throats (Figure 3.2c). The properties of the throats are supposed to reflect the effect of local void geometry on the flow. This modeling technique reduces the number of unknowns compared to Group B models. It also reflects the effect of the local geometry of the pore space on the flow and it gives predictive estimates of the permeability.

This approach is, therefore, adopted in this work for the one-way coupling (Section 3.4) using the DEM-PFV (DEM-Pore Finite Volume) method. The reasons for choosing this method are:

- it is not based on empirical relations; Moreover, in the case of suffusion, we need to describe the fluid at the particle scale, unlike the hydromechanical models of group A.

- we are interested in describing soils with a realistic particle size distribution which require a high number of particles and consequently we need to limit the computational cost. Thus, we cannot consider the hydromechanical models of group B in our work.

In the PFV method, pore bodies are defined locally through a regular triangulation of the granular packing (i.e. the triangulation of the particle centers weighted by the particle radii). The void space being discretized by a tetrahedral mesh, each tetrahedron representing a pore (see Figure 3.4), a finite volume formulation of the Stokes flow between adjacent pores is made possible.
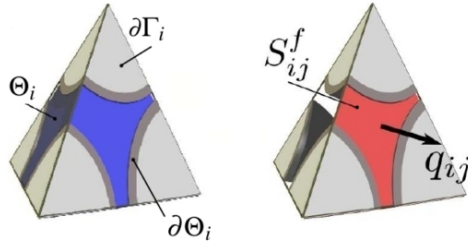
Figure 3.4: Tetrahedral element of the finite volume decomposition (Catalano et al. (2014)).

Dual to the triangulation, the Laguerre tessellation represents the connections/paths of the fluid between adjacent pores. Thereafter, viscous flow equations are upscaled at the pore level and approximated with a finite volume scheme. The flux q_{ij} between two connected pores, i and j, characterized by pressures p_i and p_j respectively, is related to the local pressure gradient and the pore-space geometry:

$$q_{ij} = g_{ij} \frac{p_i - p_j}{l_{ij}} \tag{3.2}$$

where g_{ij} is the hydraulic conductance of the throat between pores i and j, and l_{ij} the length of this throat. Note that, g_{ij} is directly computed from the hydraulic radius of the constriction without any fitting parameter.

The pressure field is obtained by solving a linear system composed of the continuity equations applied to the fluid phase in each pore. The latter implies that the rate of volume change of one pore is equal to the sum of the fluxes through the four facets of the tetrahedral pore element. Considering the pore i, the continuity equation writes:

$$\dot{V}_i^f = \sum_{j=1}^{j=4} q_{ij} = g_{ij} \frac{p_i - p_j}{l_{ij}} \tag{3.3}$$

where $\dot{V}_i^f$ is the volumetric strain rate of pore i deduced from the solid particle velocities at the four apexes of the tetrahedron i.

Finally, the forces exerted by the fluid on each particle can be derived from the pressure field and expressed as the contour integrals of the pressure p and of the viscous shear

stress $\boldsymbol{\tau}$. For a particle k with a boundary surface Γ_k, and by neglecting the effect of gravity, the fluid force $\vec{F}^k$ reads:

$$\vec{F}^k = \int_{\partial \Gamma_k} p\, \vec{n}\, ds + \int_{\partial \Gamma_k} \boldsymbol{\tau}\, \vec{n}\, ds \tag{3.4}$$

where $\vec{n}$ is the unit normal to the surface Γ_k.

Further details of the DEM-PFV coupling approach are found in Catalano et al. (2014).

3.4 Newly developed extraction procedure

A numerical extraction procedure is defined to mimic the suffusion process. To describe this phenomenon accurately, a fully coupled hydro-mechanical model is required. However, the typical time scale related to the transport of solid particles in the interstitial space under the action of a water seepage is quite large. It would require the simulation of a relatively long physical time resulting in an expensive computational cost. Therefore, a simplified extraction procedure, involving a one-way fluid-solid coupling is defined, keeping a reasonable computational cost. It is based on the association of the DEM and PFV method presented in the previous section.

As illustrated by the numerical scheme shown in Figure 3.5, the proposed method consists in splitting the suffusion process in two steps:

- the detachment of particles under the action of the water seepage;

- the transport of detached particles through the interstitial space;

These steps are considered sequentially from an equilibrium state of the granular assembly reached under a prescribed stress state, i.e. an isotropic compression up to a given confining pressure or a triaxial compression up to a given stress deviator. Equilibrium is assessed from a dimensenionless unbalanced force. It is computed as the ratio of the mean resultant particle force to the mean contact force and tends to zero for a perfect static equilibrium. A value of 10^{-3} was considered here as representative of a state sufficiently close to this limit.

Due to the periodic conditions used in our model, we needed to fix the coarse particles in the soil sample to avoid the translation of the periodic cell under the action of the fluid drag forces (similarly if gravity is added). Moreover, to assess the detachement and the transport of particles, a twin numerical model is produced before computing the fluid flow (see Figure 3.6). Fluid flow and hydrodynamic forces are computed in this twin discrete model, and once the eroded particles are identified we come back to the initial model where the position of particles have been kept unchanged (i.e. didn't move due to the fluid action); the particles from this initial model are removed, and the mechanical response is computed here. Figure 3.6 illustrates these modeling details followed in this work.

3.4.1 Particle detachment induced by water seepage

Prior to the detachment step, the seepage flow through the granular medium for a fixed global hydraulic gradient is resolved from a single iteration of the PFV method. As for the
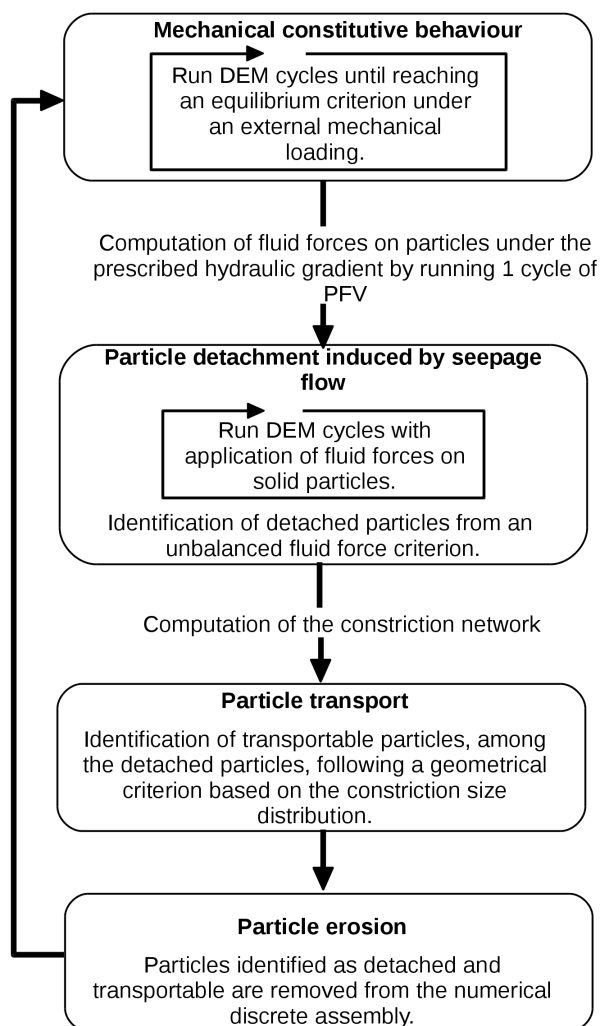
Figure 3.5: Dissociation of the detachment step and the transportation step in the simplified numerical description of suffusion.
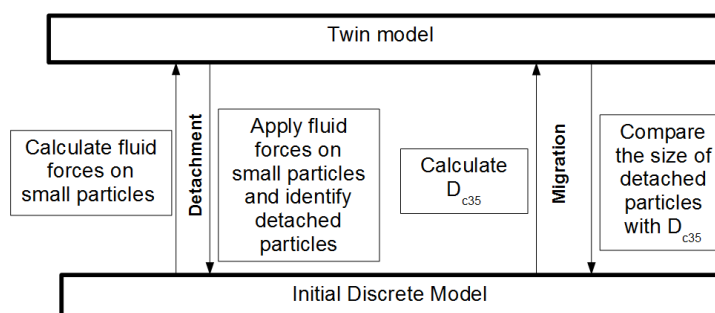
Figure 3.6: Scheme of the algorithm details for the detachment and transport steps.

solid phase, periodic limit conditions are considered for the interstitial water flow (Šmilauer et al. (2015a)). Then, fluid forces acting on each solid particle are computed and stored.

The detachment step consists in checking the equilibrium of solid particles under the combined action of inter-particle contact forces and fluid forces. A particle out of equilibrium is considered as detached. For this purpose, DEM cycles are iterated by applying permanently on solid particles the fluid forces previously stored. At this stage seepage flow and fluid forces are not updated by taking into account new particle positions and velocities, this is why we call it a one-way coupling. Nevertheless, this simplification is quite reasonable since the idea is not to give enough time for particles to be transported (i.e. particle displacements and velocities stay low) but to check for each particle if the fluid force can be balanced by the contact forces transmitted by neighboring particles in a configuration close to its initial equilibrium state. Formally, this is done by comparing the magnitude of the unbalanced force on the particle p subjected to a fluid force $\vec{F}_f^p$ and contact forces $\vec{F}_c^\alpha$ (where α spans over all the contacts involving the particle p):

$$F_{\text{unb}}^p = \left\| \sum_{\alpha \in p} \vec{F}_c^\alpha + \vec{F}_f^p \right\|, \tag{3.5}$$

with the mean magnitude of the contact forces, $\langle \|\vec{F}_c^\alpha\| \rangle$, and considered as stabilizing forces. Finally, a particle is considered as detached when:

$$F_{\text{unb}}^p > \lambda \, \langle \|\vec{F}_c^\alpha\| \rangle, \quad \text{for } \alpha \in p \tag{3.6}$$

where λ represents the threshold of the unbalanced force ratio below which a particle is considered at equilibrium.

Perfect equilibrium of the granular assembly is never reached with the DEM (it is reached only asymptotically) even without seepage forces. As one would not expect particle detachment when fluid forces are zero, λ in Equation 3.6 is chosen high enough so that no detached particles are detected in a granular assembly at equilibrium and without water seepage. However, it should be small enough to detect any particles out of equilibrium when a quasi-static state is sought under a hydraulic loading. Figure 3.7 presents the mass ratio, $\bar{M}_d = M_d/M_0$ (where M_d is the mass of detached particles and M_0 the initial mass of fine particles), of particles identified as detached in the absence of water seepage for the discrete model (as defined in Section 3.5.1) in a quasi-equilibrium state. For $\lambda \geq 0.1$, the mass of detached particles is negligible, therefore, the lower boundary $\lambda = 0.1$ is chosen as the threshold unbalanced force ratio for the next erosion simulations.

Finally, there is still the question of how many DEM cycles should be run once fluid forces are applied on solid particles. This number of cycles should necessarily be relatively small as only a one-way fluid-solid coupling is considered in this step. Fluid forces are not updated when the state (position, velocity) of solid particles is changing. Nevertheless, a sufficient number of cycles is needed to allow the existing contacts to deform and develop contact forces able to balance (or not) the fluid force. The number of detached particles according to the condition defined in Equation 3.6 is plotted in Figure 3.8 in terms of the number of DEM cycles run before checking this condition. Active and inactive detached particles, considered separately, are also represented in Figure 3.8. A particle with at least two contacts is considered active. The number of inactive detached particles is constant up to 1,000 DEM cycles. This is in agreement with the fact that the condition of Equation 3.6 holds, by definition, for all inactive particles which consequently should
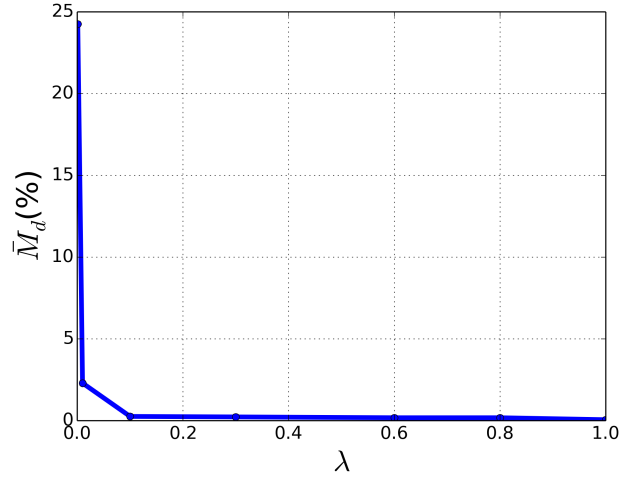
Figure 3.7: Mass ratio of particles identified as detached for different values of the threshold λ applied on the unbalanced force ratio for a nil hydraulic gradient (i.e. without water seepage simulated in the granular assembly).

be considered as detached whatever is the number of DEM cycles. Beyond 1,000 cycles, the number of inactive detached particles decreases, initially slowly, then drastically after 10,000 cycles. The partially-coupled model starts to deviate from the initially defined concept: inactive particles are transported under the action of the initial fluid force considered constant (whereas fluid force should vanish when the particle velocity tends to the fluid velocity) and pushed against some neighboring stable particles. Consequently, the designed model is valid for a maximum number of 1,000 DEM cycles. The same trend is observed for active particles from 10,000 cycles. Below this number of cycles, the number of the active detached particles results from the competition between particles being stabilized (when contact forces balance the fluid force) and those being destabilized (when contacts break under the action of the fluid force). As a conclusion, in this study, it is chosen to check detached particles after 1,000 iterations of the DEM cycle with the application of the fluid forces. This limitation may seem quite arbitrary with respect to the active particles, but this could be compensated by the repetition, for a given hydraulic loading, of the whole extraction procedure as detailed in Section 3.5.1.

Note that, in addition to the previously defined detachment criterion, two other criteria have been investigated in our work:

- criterion based on checking the evolution of the velocity of fine particles once subjected to fluid forces: following this criterion, two groups were distiguished (Figure 3.9):

   - Group 1: particles showing a continuous increase in velocity;
   - Group 2: particles showing initial increase of velocity under the effect of seepage flow, however, the variation of velocity kept fluctuating.

Particles of Group 1 can be considered detached. However, the setback of this criterion is when the velocity of fine particles keeps flucutating (Group 2). In this case, it is hard to differentiate between two cases:
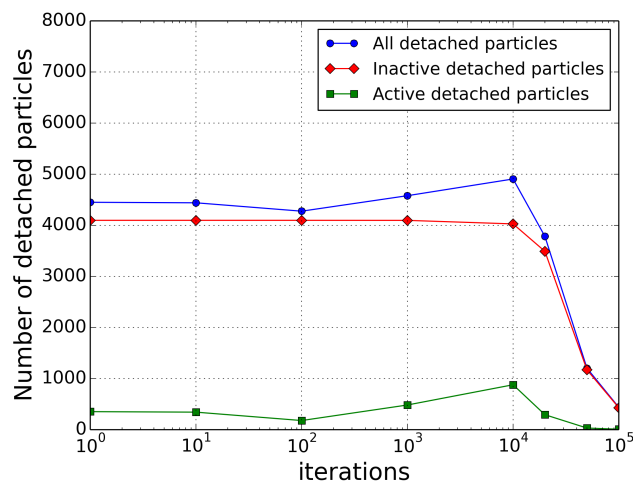
Figure 3.8: Number of detached particles for different DEM cycles.

- Non-detachable particles which remain blocked without breaking their contacts. The flucuations in this case may be related to the deformations of contacts without being destroyed;

- Detachable particles which are transported by seepage flow. Therefore, the velocity flucuations may be due to successive bouncing of one grain on another one encountered during its transportation through constrictions.

- criterion based on calculating the theoretical displacements of small particles under the effect of fluid forces alone: the procedure consists in comparing the numerical displacements with the theoretical ones; However, this criterion underestimates the total number of detached particles. Some few rattlers which are effectively detached may not be selected through this method. During the DEM cycles, some floating particles may hit each other and successively bounce. As a result, their displacement would be different from the calculated one and the detachment condition would not be satisfied where some floating particles may be considered as non-detachable particles. Therefore, such particles are deemed to be very close to their equilibrium state. However, if we study their equilibrium, we would notice that they are not stable.

In addition to that, it was difficult from the velocity and the displacement to define a detachment criterion independent of the hydraulic gradient. Therefore, these two approaches were discarded and the detachment criterion presented before is used in our work.

3.4.2   Particle transport through the interstitial space

The possibility of detached particles (as identified in the previous section) to be transported through the pore network is now checked. The migration of fine particles is controlled by the topology of the interstitial space. In other words, it depends on how the pores of different sizes are connected via constrictions. Thus, a detached particle should be able to cross a sufficient number of connected pores and constrictions to leave the soil matrix and be finally eroded. Simulating such a process with the fully coupled DEM-PFV
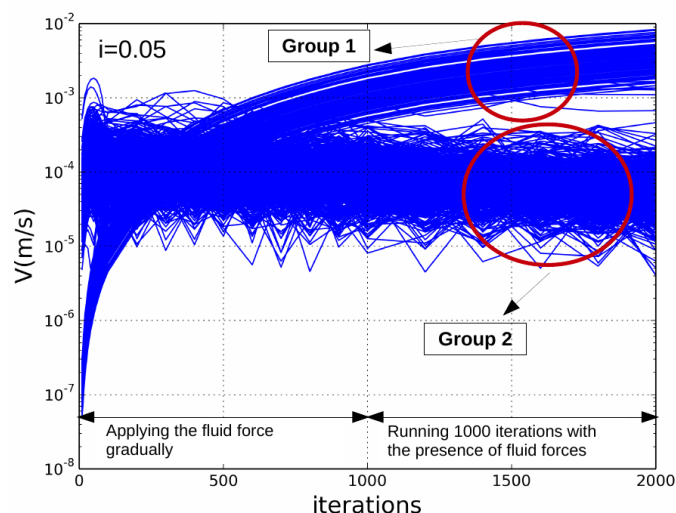
Figure 3.9: Velocity of small particles after the application of fluid forces.

method is possible (Tejada et al. (2016)) but requires a relatively high computational time. Moreover, this study does not aim to describe thoroughly the suffusion process in itself, but to investigate the effect of erosion, by the suffusion of fine particles, on the mechanical behavior of the soil. Hence, a simplified transport criterion is followed.

This criterion is based on the constriction size distribution, CSD, from the set of particles including the coarse ones and the non-detached finer particles as identified in the previous detachment step (i.e. all particles not detached by the water seepage). The computation of the CSD is a sub-product of the PFV method since it results from the regular triangulation of the granular packing and associating each tetrahedron with a pore. The constriction radius is identified at the interface between two tetrahedra as the radius of the inscribed circle between the three spheres intersecting the facet. A controlling constriction size is extracted from the CSD and the transport criterion consists in comparing the size of each detached particle to this controlling constriction size. The latter is chosen based on the suggestion of Raut & Indraratna (2008) in their filter criterion which corresponds to D_{c35} (the constriction size for which 35 % of the constrictions of the granular assembly are finer than this size). Then, a detached particle is considered as being transported through the interstitial space if its diameter is smaller than D_{c35}. It is important to note that D_{c35} is not a fundamental controlling constriction size; it is an empirical value proposed by Raut & Indraratna (2008).

Finally, a detached particle being transported is identified as an eroded particle and is erased from the granular assembly. DEM cycles are iterated again with the new particle configuration (i.e. without the eroded particles) and without any fluid forces. Due to the removal of some particles, the granular assembly may deform under the stress state maintained constant. The simulation is run until a new equilibrium state (if any) is reached. Such a process can be repeated to pursue the erosion development, or a drained triaxial compression test can be simulated to evaluate the new mechanical properties of the eroded soil.

3.5   Application of the extraction procedure on a simplified discrete model

3.5.1   Suffusion development and soil deformation

Suffusion simulation

Suffusion-like simulations were performed from an isotropic stress state (under a confining pressure of 100 kPa), following the numerical extraction procedure defined previously. The model parameters are given in Table 3.1. The relatively narrow particle size distribution displayed in Figure 3.10 was used in this first approach to limit the number of discrete elements (10,000 spherical particles were used) necessary to form a representative elementary volume (REV) and to keep a quite low computational cost. Note that, such

Number of particles	ρ_s	E_c	α_s	α_r	φ_c (compaction only)	φ_c (erosion and shearing)	η_r	ρ_w	μ
	$(\frac{Kg}{cm^3})$	(kPa)			(°)	(°)		$(\frac{Kg}{cm^3})$	(Pa.s)
$10,000$	2600	$2\,10^5$	0.2	7.5	15	30	0.22	1000	10^{-3}

Table 3.1: Summary of the parameters used in the discrete numerical model (ρ_s is the soil density, ρ_w is the water density, μ is the dynamic viscosity).
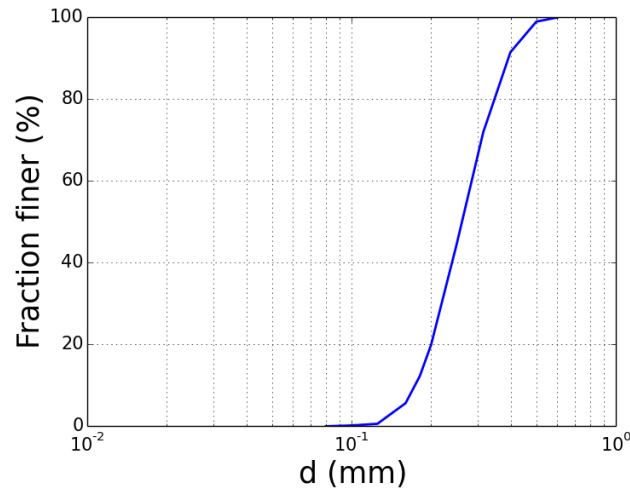
Figure 3.10: Initial particle size distribution of the granular assembly.

a particle size distribution represents an internally stable soil as considered in previous studies such as (Muir Wood et al. (2010); Scholtès et al. (2010)). Therefore, to be able to apply the previous erosion procedure, some simplifications are taken in what follows. These include:

- considering only the CSD of the coarse fraction of the granular assembly for the calculation of the controlling constriction size;

- assuming the fine fraction (i.e. the fraction of particles potentially erodible) is that corresponding to particles whose diameter is smaller than D_{50};

Despite these limitations, all the particles (fine and coarse) are taken into account to solve the interstitial flow and to compute the hydraulic forces on particles. The extraction algorithm in Figure 3.5 has been applied repeatedly for increasing values of the prescribed hydraulic gradient, i:

- for $i < 0.2$, the hydraulic gradient is increased by steps of 0.05;

- for $0.2 \leq i \leq 3$, an increment of 0.2 is applied;

- as i exceeds 3, the increment step increases to 0.5;

For a given hydraulic gradient, the extraction is repeated until no more particles are eroded. Figure 3.11 shows, for the hydraulic gradient $i = 6$, the relative masses of detached and eroded particles, $\bar{M}_d$ and $\bar{M}_e$ respectively (with $\bar{M}_e = \frac{M_e}{M_0}$, M_e is the mass of eroded particles and $\bar{M}_0$ is the initial mass of fine particles). The hydraulic loading process followed in the simulations immitates the experimental multi-stage procedure (D. Chang & Zhang (2011)) where the hydraulic gradient is increased by steps. In this way, we take into account the effect of the hydraulic loading history on the suffusion development (Sibille et al. (2015)).
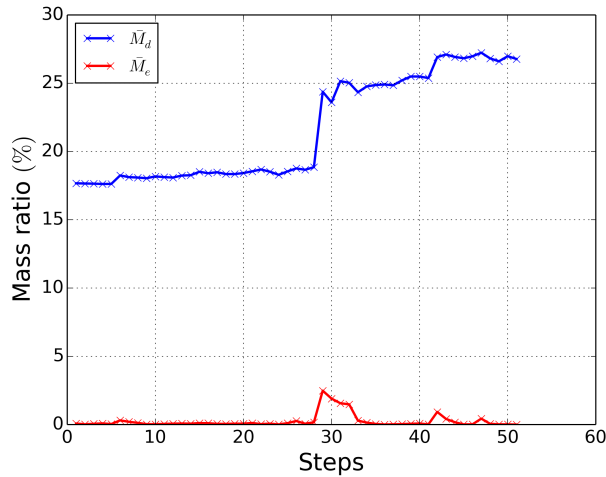
Figure 3.11: Relative masses of detached and eroded particles at each step of repetition of the extraction procedure until no more particles are eroded under the prescribed hydraulic gradient, $i = 6$.

Suffusion-like simulations are resumed in Figure 3.12 showing the cumulative eroded mass ratio for the prescribed hydraulic gradients. Here, the total mass of eroded particles M_e is distinguished from the eroded mass of active particles M_{ea} (i.e, particles participating in the inter-granular force transfer and involved in at least two contacts), with $M_{ea} \in M_e$. Then, eroded mass ratios $\bar{M}_e = M_e/M_0$ and $\bar{M}_{ea} = M_{ea}/M_0$ are respectively defined.

Under the initial isotropic stress state, rattlers (or non-active particles) of the fine fraction represents 38 % (by mass) of the total mass of fine particles. By definition, these rattlers are considered as detached for any non zero hydraulic gradient and their ability to be transported depends only on the transport criterion. That is why $\bar{M}_e$ is much higher than $\bar{M}_{ea}$ and a sufficiently strong hydraulic gradient (here about $i = 1.8$) is

necessary to destabilize active particles involved in the contact force network. Besides, for increasing values of the hydraulic gradient, new particles can become inactive (due to particle re-arrangements during the first step in Figure 3.5) and constriction sizes may globally increase (due to the previous erosion step) giving the opportunity for new inactive particles to be eroded. Finally, this results in a modified post-suffusion particle size distribution and constriction size distribution due to the selective erosion of particles as displayed in Figure 3.13.
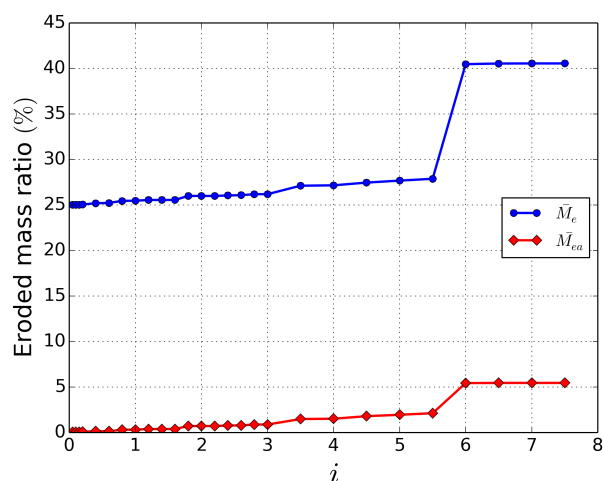
Figure 3.12: Simulated eroded mass for an increased by step of the prescribed hydraulic gradient, i.
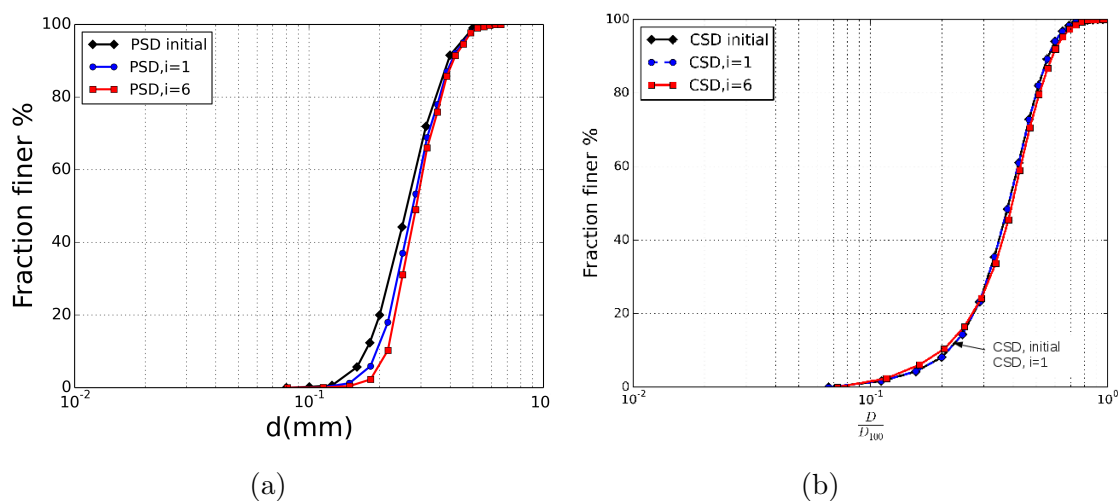
Figure 3.13: (a) Post-erosion Particle Size Distribution (PSD) and (b) Constriction Size Distribution (CSD).

Volumetric strain response

Mechanical response of the granular assembly during suffusion can be characterized in terms of volumetric strain. Under the external applied isotropic stress, the sample may compact only when active particles are eroded (since inactive particles do not participate

in the load bearing capacity of the assembly). Nevertheless, Figure 3.14 shows that the soil compaction is not concomitant with the erosion of active particles. For $\bar{M}_{ea} \geq 5.4$ %, the sample compresses significantly whereas below this threshold it presents negligible volumetric deformations, evidencing the negligible role in the contact force network of the active particles firstly eroded. However, as noticed from Figure 3.14, the porosity is always larger than the initial value even if the soil shows an eventual large contractive behavior. The creation of a more open micro-structure, induced by particle removal, is predominant over the sample compaction during suffusion, as shown by (Muir Wood et al. (2008); Muir Wood & Maeda (2007); Scholtès et al. (2010)). Although the eroded sample is always looser than the virgin one, the porosity change with erosion development is not monotonous here. For a high degree of erosion development (i.e. for $\bar{M}_{ea} \geq 5.4$ %) the eroded medium may become slightly denser. However, even if the soil becomes denser and gains some strength, the soil had already suffered from large settlements which may lead to serious drawbacks at the scale of hydraulic structures.
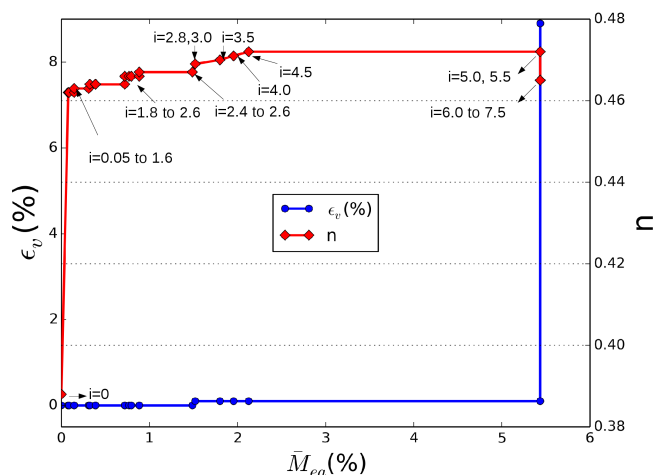
Figure 3.14: Contractive volumetric deformation of the granular assembly and evolution of the porosity with the erosion of active particles.

Laboratory experiments, aiming to characterize soil mechanical properties of soil samples eroded by suffusion, face a major issue related to the heterogeneous state of the sample after erosion. The fine concentration may present a gradient in the main seepage direction as shown in Ke & Takahashi (2014a) and D. Chang & Zhang (2011) (with a more important fine concentration in the downstream part of the sample). Moreover, the density itself may also be affected with possibly counterintuitive distributions as observed by Sibille et al. (2015) showing a looser state in the upstream part of the sample where the fine fraction is the lowest. However, interpretation of the triaxial compression tests performed to evaluate the post-erosion shear strength properties usually assumes a homogeneous state of the sample. The numerical erosion process defined here implicitly induced a homogeneous removal of eroded particles. For instance, the homogeneity of the granular assembly is checked in Figures 3.15 and 3.16 after it has been eroded for a hydraulic gradient up to $i = 3.5$. The soil sample is divided into 3 equal horizontal sections. Then, porosity and grain size distribution were computed in each section of the sample (bottom/downstream, middle, and top/upstream). Both porosity and gradation

are almost identical in all sections. Consequently, the modification of the microstructure of the numerical sample, being kept homogeneous, is indeed not directly representative of relatively large samples eroded in laboratory, but presents the advantage to get around this problem of interpretation of mechanical tests on heterogeneous samples. This constitutes an important basis for the next section about the post-erosion mechanical properties.
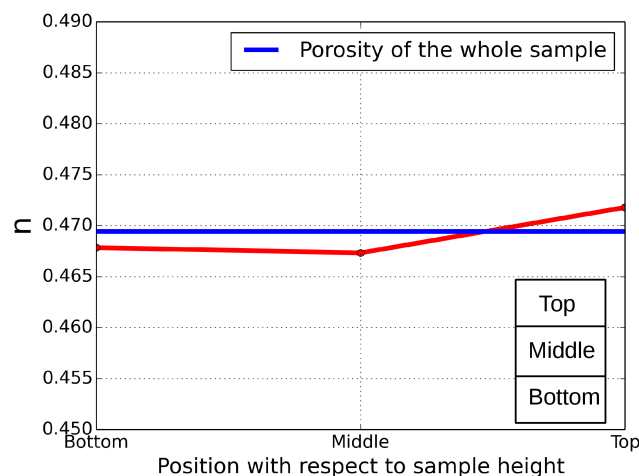
Figure 3.15: Local porosities at different sections of the eroded sample under a hydraulic gradient, $i = 3.5$.
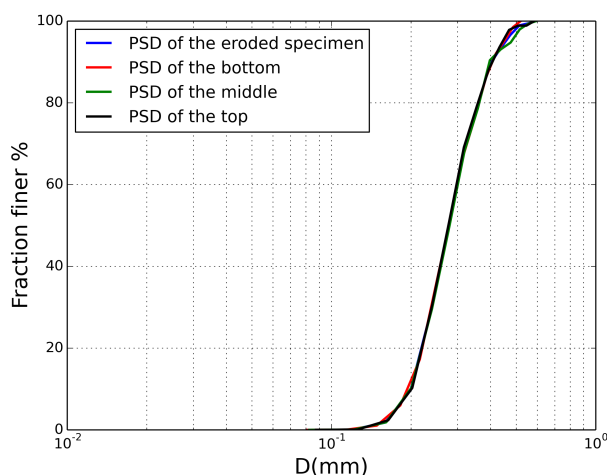
Figure 3.16: Local particle size distributions around different sections of the eroded sample under a hydraulic gradient, $i = 3.5$.

3.5.2 Effects of suffusion on the macroscopic constitutive behavior

Drained triaxial compressions have been simulated to highlight how such induced modifications in the microstructure, due to the removal of a fine fraction, affect the mechanical behavior of the soil. Results in terms of deviator stress ratio, $\frac{q}{p}$, and volumetric strains, ε_v,

are displayed in Figure 3.17 for the virgin sample (i.e. not eroded (NE)) and for the eroded ones at different degrees of erosion development. The eroded samples are characterized by the highest hydraulic gradient, i, reached before performing the triaxial compression; the corresponding eroded masses can be deduced from Figure 3.12.

Globally, the eroded samples present a reduced shear strength with respect to the
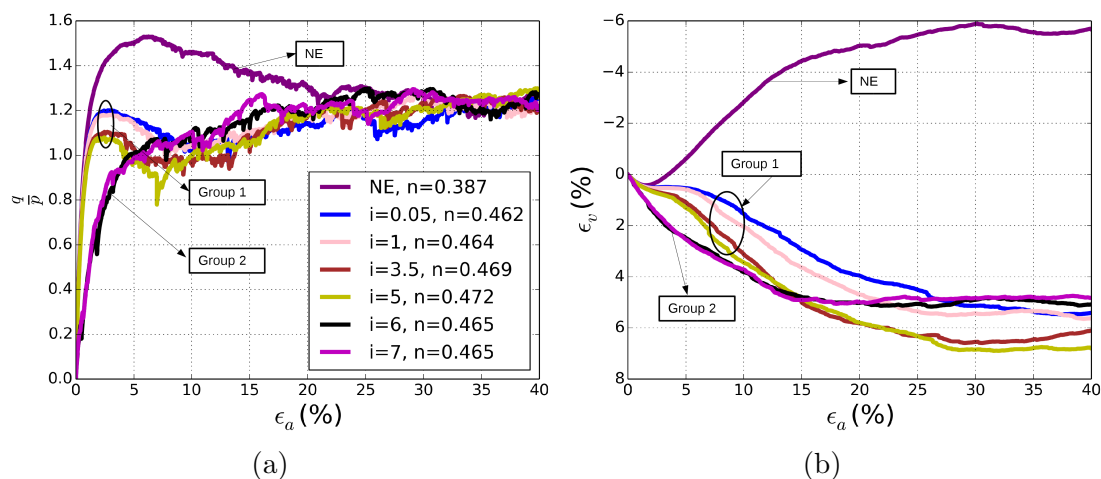
Figure 3.17: Simulated responses to drained triaxial compression tests of granular assemblies eroded at different hydraulic gradients.

virgin sample together with a significant change in the volumetric strains tendancy. Two distinct groups are clearly identifiable:

- Group 1: for a hydraulic gradient, $i < 6$, the eroded samples show a decrease in the shear strength with an atypical softening-hardening behavior (developing after an initial peak of $\frac{q}{p}$, from an axial strain of about 3%), and a volumetric reduction happening in two steps (a strong contractancy developing from $\varepsilon_a \approx 5\%$ after an initial moderate volume reduction), are also observed;

- Group 2: for higher hydraulic gradients, ($i \geq 6$), eroded soil samples show the most important shear strength reduction with a common contractive behavior typical for a loose material;

Despite the particular behavior of Group 1, that will be discussed further in this chapter, changes observed in the shear strength and volumetric deformation are consistent with the sample porosity reached after the erosion process. The porosity of samples of Groups 1 and 2 is more important (n between 0.462 and 0.472) than for the initial sample ($n = 0.387$) resulting in a contractant behavior for the eroded samples. However, some samples of Groups 1 and 2, respectively, with similar post-erosion porosities behave differently at low shear deformation. This may be related to the strong compaction and particles re-arrangement experienced during the extraction process in Group 2 (cf. Figure 3.14) as more active particles were eroded at higher hydraulic gradients.

The variation of the maximum friction angle with erosion development is presented in Figure 3.18 in terms of the eroded mass ratio of active particles, $\bar{M}_{ea}$. A non-linear relation is found, in good agreement with the post-erosion porosity following the same

trend (Figure 3.14). In other words, for the case studied here, the shear strength is greatly affected even for a low degree of development of erosion where the friction angle decreases by about 20 % (from 37.6° to about 30°).
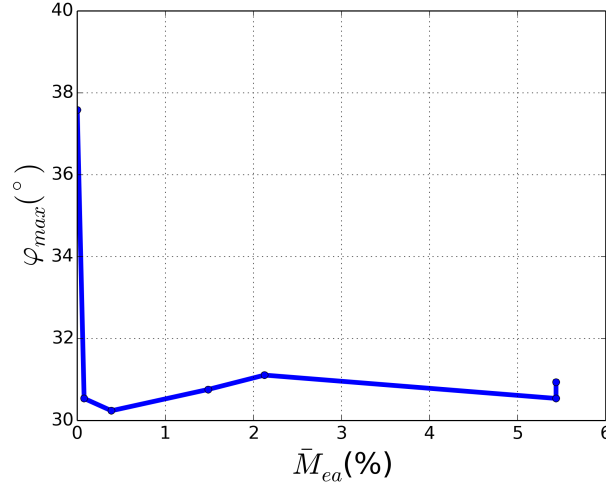
Figure 3.18: Maximum friction angle, $\varphi_{\max}$, in terms of eroded mass ratio of active particles, determined from simulations of triaxial compressions on eroded samples.

Another interesting point highlighted by these numerical results concerns the mechanical behavior of a soil when only inactive particles are eroded by suffusion. In this case, as inactive particles do not participate in the contact force network (and for the current mechanical state) and thus in the load bearing of the granular assembly, no deformation is induced by the suffusion and the original contact force network remains unchanged. However, does it affect the mechanical properties of the sample? Or, in other words, may the inactive particles in the initial state have a role in the load bearing capacity when the medium is sheared and deformed? Eroded samples belonging to Group 1, with $i < 1.8$, correspond to this case: the eroded mass of active particles is negligible whereas the inactive particles have been largely removed from the granular assembly ($\bar{M}_e \geq 25\%$). This is confirmed by the vanishing volumetric strain occuring during erosion for these samples. Nevertheless, as shown by Figures 3.17 and 3.18, these eroded samples present mechanical properties largely degraded with respect to the virgin sample, in particular with a reduction of the peak internal friction angle from 37.5° to about 30°. Therefore, although some particles are inactive in a given mechanical state, they may play a key role in subsequent states with respect to the macroscopic behavior of the granular assembly (even if this role, for each particle, may be very transient). It is not because no deformation (or settlement) is observed during the suffusion occurence that the soil mechanical properties have not been degraded by suffusion.

Finally, properties of eroded granular assemblies at the critical state are discussed in the last part of this section. Changes in the critical state may be of importance for many phenomenological constitutive relations relying on the definition of such a state. It can be deduced from the Figure 3.17 that the mobilized friction angle at large strains is unchanged (with $q/p \approx 1.2$) whatever is the hydraulic gradient and the degree of erosion development. For the numerical model used, and for a given particle grading, shear

strength at large deformations depends almost only on the inter-particle rolling friction (reflecting the angularity of the particle shapes) as shown for instance in Aboul Hosn et al. (2017). As the rolling friction, η_r, is here identical for all the particles (the eroded and non-eroded ones), the removal of a part of the particles does not affect the overall strength due to this resistance to rolling introduced at the contact level. Besides, the change in the gradation of the particle sizes due to the selective erosion of particles (Figure 3.13) is apparently not sufficiently marked in this case to have an influence on the shear strength at the critical state.

However, even if it is not very significant, this change in the gradation clearly affects the porosity reached at the critical state as shown in Figure 3.19. As the finest particles, possibly filling the voids between coarser particles, are removed, the porosity increased at the critical state. Unlike the post-erosion internal friction angle (Figure 3.18) depending on the initial (post-erosion) density, the relation between the porosity at critical state and the eroded mass is monotonous since it relies on the change of the grading (and obviously not on the initial configuration of the granular packing) also changing monotonously with the erosion development (Figure 3.13).
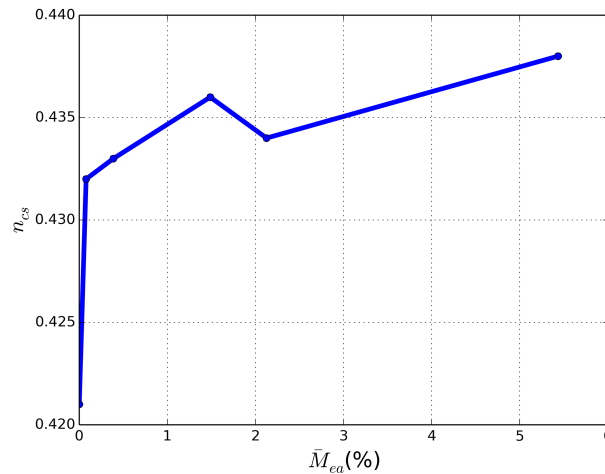
Figure 3.19: Porosity at critical state, n_{cs}, in terms of eroded mass ratio of active particles, determined from simulations of triaxial compressions on eroded samples.

3.6   Microstructure changes induced by suffusion

In order to better understand how the microstructure of the soil is modified during erosion and to explain the particular behavior of eroded soils of Group 1, the probability density function, P, of the normal contact forces is calculated for each soil sample. Furthermore the mechanical coordination number Z_m is also computed for each specimen. According to Thornton & Antony (1998), Z_m is defined as:

$$Z_m = \frac{2N_c - N_1}{N_p - N_0 - N1} \tag{3.7}$$

where N_c is the total number of contacts, N_1 is the number of particles with one contact, N_0 is the number of particles with zero contact, and N_p is the total number of

particles. Probability density of contact forces, P, and mechanical coordination number are displayed in Figure 3.20 for each eroded and non-eroded specimen. An additional granular assembly denoted LS is also considered in this figure. LS is a granular assembly reconstituted in a loose state by using the PSD of the specimens of Group 1 (i=0.05). The objective is to try to constitute a reference loose sample, possibly as loose as those of Group 1, but without subjecting it to the erosion process (contrary to those of Group 1). The methodology proposed in Aboul Hosn et al. (2017) to create initially very loose samples, by numerically imitating the moist tamping technique by adding inter-particle adhesion forces during the compaction phase, has been followed. However, the highest porosity we managed to reach for LS at the isotropic state is n=0.444 which is lower than the porosity of specimens of Groups 1 and 2. Hence, if specimens of Group 1 are
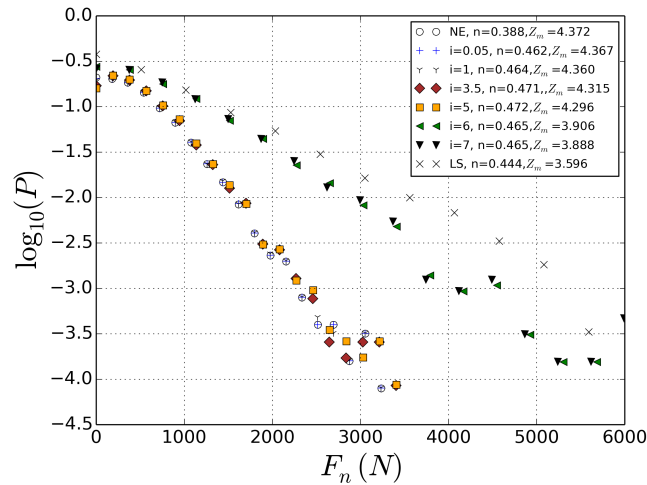
Figure 3.20: Probability density functions of normal contact forces at the isotropic state for the eroded specimens up to a hydraulic gradient, i, and for the non-eroded, initially dense (NE) and loose (LS) specimens.

discarded in a first time, then specimen NE on one hand, and specimens of Group 2 (i=6 and 7), and LS on the other hand, constitute two distinct groups clearly identifiable in Figure 3.20. Force distributions are different for the dense specimen, NE, and the loose one (LS) and distributions of Group 2 (behaving as a loose material) are close to the latter. However, it is interesting to note that specimens of Group 1 (i=0.05 to 5) do not follow this expected trend and constitute a very particular case. Although they are very loose, the erosion process has lead to unique granular assemblies characterized by very similar coordination numbers and quasi-identical contact force distributions to the ones of the initially dense specimen, NE. Specimen LS shows it is not possible to reconstruct at low initial density, without the erosion process, such a microstructure typical of a dense sample.

In addition, Figure 3.21 shows the response to a drained triaxial compression of the reconstituted loose sample compared with the other soil specimens. With contact force distributions and mechanical coordination numbers similar to the non-eroded granular assembly (NE) at isotropic state, specimens of Group 1 show a kind of transitional volumetric trend. It is characterized by an apparently slightly dilatant behavior with a peak stress after the initial contractancy with similar stiffness to NE specimen; However, as the shearing increases, the hidden loose character appears again by exhibiting a large contractant behavior (more important than for LS specimen) in accordance with the

higher initial porosity.

Finally, as the LS specimen is looser than the NE specimen it is characterized by a lower initial stiffness as shown in Figure 3.21. This is not the case for specimens of Group 1 where the initial stiffness stay quasi-unchanged with respect to the non-eroded one. However, specimens of Group 2 which deform during erosion (reflecting a modification of their microstructure), show lower stiffness similar to the loose specimen LS.

All these observations illustrate that suffusion may result in atypical soil microstructures

(a)   (b)
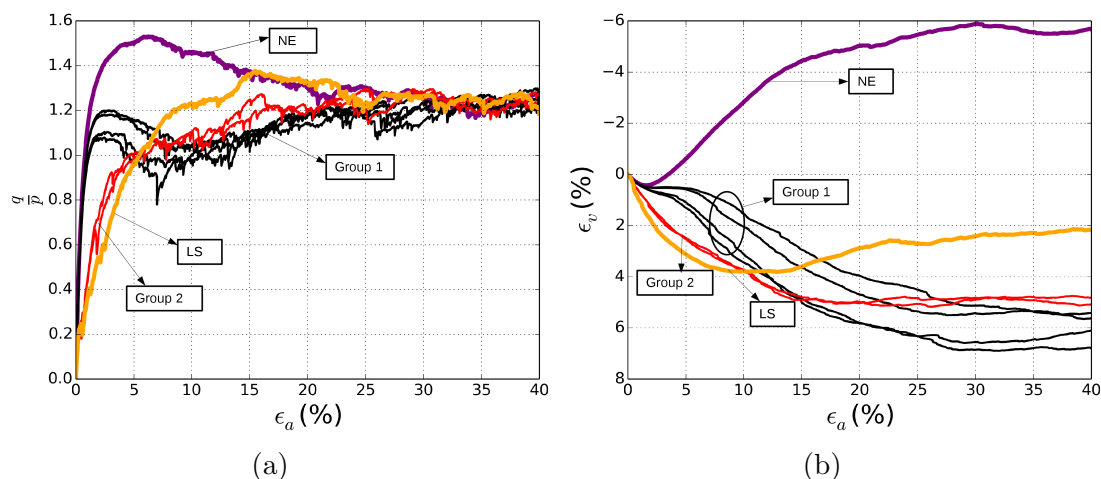
Figure 3.21: Comparison of the response of an initially loose sample (LS) to a drained triaxial compression to other granular assemblies eroded at different hydraulic gradients.

and macroscopic behaviors, particularly when erosion concerns only inactive particles without accompanying effects on the coarse matrix integrity.

3.7   Conclusion

A numerical approach has been presented in this chapter to describe the erosion of soil by suffusion. A simplified extraction procedure is defined based on the discrete element method with a one-way fluid-solid coupling. By taking into account the hydraulic loading, to determine the detachment of the solid particles, and the constrictions of the interstitial space, the definition of this extraction procedure constitutes new advances while limiting the computational cost.

The simulations of the erosion tests show that depending on the role and the amount of the eroded particles, two different post erosion mechanical behaviors may be concluded. On one hand, if mainly inactive particles are removed, the soil structure presents almost no deformation during erosion, maintaining the same probability density of contact forces and mechanical coordination number as the non-eroded soil. However, if sheared, this soil may suffer from a sudden collapse revealing its hidden loose character induced by the voids left at the place of the eroded particles. On the other hand, if more active particles are eroded, the granular assembly loses its equilibrium during the erosion process and the soil deforms with a global volume reduction to reach another equilibrium state. Once

sheared, the soil presents a contractant behavior with a more reduced shear strength with respect to the non-eroded soil. In all cases, the erosion process leads to the creation of more porous materials. However, a comparison with a granular assembly generated in an initial loose state showed that the post-erosion mechanical behavior cannot be only described by an increase in porosity. It results in atypical microstructures and macroscopic behaviors, particularly when only inactive particles have been eroded.

In this chapter, a simplified gradation (narrow PSD) has been used to limit the computational time. Consequently, the conclusions given here about the resulting mechanical responses may rely on this simplified gradation. However, in Chapter 5 a wider PSD, similar to those used experimentally and which is internally unstable, will be considered. For such a PSD, the numerical granular assembly should include at least several hundreds of thousands of particles to constitute a representative elementary volume.

Part III
Consequences of suffusion on the mechanical behavior of an internally unstable soil

Chapter 4

Experimental investigation of suffusion

4.1 Introduction

This chapter presents the experimental approach followed in this work to investigate the initiation and development of internal erosion and the consecutive effects on the soil mechanical properties. First, a brief literature review of the existing erosion apparatus is introduced. Then, the experimental procedure followed in this study is presented, including: the newly developed apparatus in IRSTEA (namely the suffusion permeameter), the testing material, the specimen preparation and the testing program. Thereafter, the experimental results of suffusion tests are discussed in terms of variations in the erosion rate, hydraulic gradient and hydraulic conductivity during erosion as well as the deformation at the end of the test. Finally, the influence of suffusion on the mechanical properties of the soil is investigated through drained/undrained monotonic triaxial compression tests.

It is worth noting that the development of the suffusion permeameter and of the technique to carry out mechanical tests on eroded soil samples have been performed in the framework of the ongoing PhD of Cong Doan Nguyen at IRSTEA and were not under the scope of the present research work. Consequently, the description of the experimental device and of the test procedures are voluntarily limited in this thesis. More detailed descriptions and presentations will be available in the forthcoming Phd thesis of C.D. Nguyen and the related publications. Finally, the experimental campaign presented in this Chapter has been carried out jointly with C.D. Nguyen.

4.2 Review of existing erosion apparatus

Numerous laboratory testing apparatus and methods have been designed and used in the literature to evaluate the initiation and development of suffusion as well as to describe the mechanical behavior of eroded soils. Two types of erosion apparatus are distinguished: rigid-wall permeameter and flexible-wall permeameter. Schematic examples of these permeameters used in the literature are shown in Figures 4.1 and 4.2.

4.2.1   Rigid wall permeameter

Early studies on internal instability have been carried out using rigid-wall permeameters. The susceptibilty of soils to internal erosion was investigated based on the eroded mass and modifications in the particle size distribution at the end of the test (Kenney & Lau (1985)). Later, rigid-wall permeameters included improved seepage control systems. Upward or downward seepage flow can be applied. The seepage flow is usually done under a constant water head (Moffat & Fannin (2006); Li (2008a); Crawford-Flett (2014); Israr & Rujikiatkamjorn (2016); Sibille et al. (2015)), and a multi-stage hydraulic loading is followed. The constant hydraulic head is either done manually by means of a head-control using an inlet and outlet tanks (Li (2008a); Wan & Fell (2004); Sail et al. (2011)) or an automated system such as for instance the one used by (Crawford-Flett (2014)) for testing at a hydraulic gradient greater than 1 and where the inlet flow was controlled by pressurization of a diaphragm tank. The hydraulic conditions are monitored using either piezometers (Ke & Takahashi (2012b); Wan & Fell (2004)) or pressure transducers (Moffat & Fannin (2006); Sail et al. (2011)).

Recently, rigid-wall permeameters are fitted with an axial loading system (Moffat & Fannin (2006); Li (2008a); Sail et al. (2011)). The axial load is applied to the test specimen by a rod and loading plate. Some apparatus are designed to apply cyclic and static loading, such as the loading system used by Israr & Rujikiatkamjorn (2016) where a servo-controlled hydraulic actuator is designed to apply high magnitude static and cyclic loads at higher frequencies through a flexible loading platen. The measurement of the axial effective stress is done by a submersible load sensor on the top of the specimen (Sibille et al. (2015); Sail et al. (2011); Li (2008a)) or by load cells placed in the middle and the bottom of the specimens to monitor effective stress variations (Israr & Rujikiatkamjorn (2016)). Moffat & Fannin (2006) calculated the vertical effective stress on the top surface of the test specimen from axial force in the loading rod. However, stress inhomogeneities may occur due to the effects of skin friction from the cell walls. Therefore, Li (2008a) and Israr & Rujikiatkamjorn (2016) proposed to divide the soil into n sub-layers. An equilibrium equation for each sub-layer is established allowing the estimation of the effective stress in each layer.
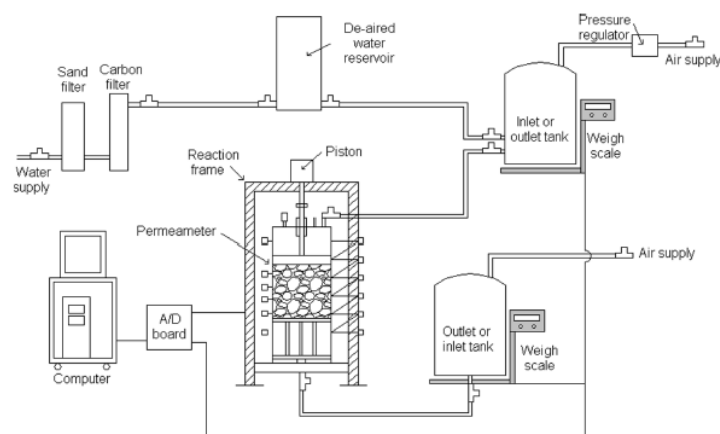
Figure 4.1: Schematic of rigid-wall permeameter developed by Moffat & Fannin (2006).

The variation in effluent flow rates were deduced by different ways. Li (2008a) and Israr & Rujikiatkamjorn (2016) measured the outflow at different intervals using a measuring graduated cylinder for a given period of time. Israr & Rujikiatkamjorn (2016) measured the turbidity using a portable turbidity meter. On the other hand, Sail et al. (2011) designed a collecting system which allows collecting and measuring the mass of eroded soil in a continuous manner. However, using such a system, it wasn't possible to maintain a constant hydraulic gradient in the sample. Therefore, they used an effluent tank with an overflow outlet to control the downstream hydraulic head and a rotating sampling system containing 9 beakers for collecting the eroded particles carried with the effluent.

Induced axial deformations due to erosion can be quantified using a linear variable differential transducer (LVDT) (Moffat & Fannin (2006); Sail et al. (2011)). Another method is followed by Crawford-Flett (2014) where the specimen length was monitored graphically, with reference to a series of grid-references fixed to the outside of the permeameter. Visual records of top surface elevation were obtained throughout the test, using photographs taken around the entire perimeter of the specimen at the beginning and the end of each seepage stage and also using continuous time-lapse video recording at a single location of the permeameter wall. Then, the change in the average length of the specimen was obtained at the specimen's perimeter throughout the test.

Since erosion leads to modifications in the soil's density, some apparatus provide measurments of the density along longitudinal profiles of the specimen. Sail et al. (2011) and Sibille et al. (2015) used for example a gammadensitometric system.

Besides, a setback of rigid-wall permeameters is related to the preferential flows through the wall-specimen interface. To avoid this problem, it is usually advised to avoid smooth cell walls; Kenney & Lau (1985) used a compressible rubber layer against the inside wall to prevent the formation of leakage channels at these boundaries. Moreover, using such apparatus, it is difficult to study the mechanical strength of eroded soils due to difficulties in retrieving undisturbed samples after erosion tests. One way to overcome this setback, is to use an in-situ testing technique such as the cone penetration tests used by Ke & Takahashi (2012b).

4.2.2   Flexible wall permeameter

In order to reduce parasitic flows between a soil sample and a rigid cell wall, flexible soil permeameters are developed (See for example Figure 4.2). These permeameters also offer the potential for more control over stresses that act on the soil specimen. Flexible-wall permeameters are often created from a modified triaxial apparatus giving, therefore, the possibility to perform mechanical tests (i.e. triaxial compressions) directly on the eroded soil samples (i.e. the erosion apparatus and the mechanical loading appartus are a single and unique apparatus). Sanchez et al. (1983) were the first to develop an internal erosion test within a modified triaxial apparatus to evaluate the erosion of embankment core materials. Later, several triaxial erosion tests were developed by Bendahmane et al. (2008); Moffat & Fannin (2006); Marot et al. (2009); Ke & Takahashi (2014a); D. Chang & Zhang (2011); Xiao & Shwiyhat (2012) allowing an independent control of the hydraulic gradient and stress state for investigating the initiation and development of internal erosion, and the stress-strain behavior of eroded soils.

Upward (Slangen (2015)) or downward (Marot et al. (2009); Ke & Takahashi (2014a);
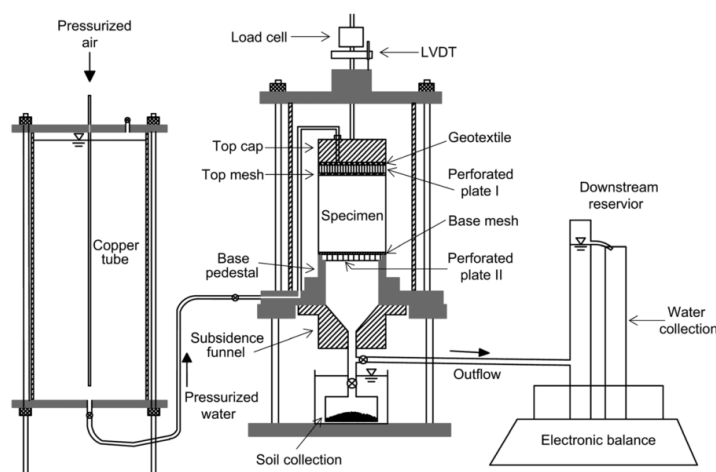
Figure 4.2: Schematic of flexible-wall permeameter developed by D. Chang & Zhang (2011).

Xiao & Shwiyhat (2012)) seepage-flow can be performed. Seepage flow can be done by either applying a constant hydraulic gradient (D. Chang & Zhang (2011)) or constant flow rate (Ke & Takahashi (2014a)). The hydraulic gradient, flow rate, eroded mass and the deformation of the tested specimen are then monitored.

Flexible-wall permeameters may allow erosion tests at different stress states. In fact, soils within embankment dams or levees are usually subjected to complex stress states. Thus, the final stress state can be approached in flexible-wall permeameter by setting a stress path through a control loading system.

The eroded mass can be either collected manually over an increment of time in a detachable container in the case of cohesionless soils (D. Chang & Zhang (2011); Slangen (2015)), or the cumulative eroded mass is recorded automatically by the load cell inside the sedimentation tank (Marot et al. (2009); Ke & Takahashi (2014a)). For cohesive soils a turbidimeter can be connected to the outflow hose to measure the rate of erosion of the fine particles (D. Chang & Zhang (2011)).

Due to the loss of fine particles during suffusion, the soil structure changes and the soil specimen can deform simultaneously. Different ways are followed to calculate the volumetric deformation. D. Chang & Zhang (2011) used a linear variable differential transducer (LVDT) to measure the total vertical displacement of the specimen. The lateral deformation during the erosion process was measured by using a photographic method (White (2002)). Ke & Takahashi (2014a) used three pairs of clip gauges with the capacity of 62mm to measure the radial deformation and the axial strain was measured by LVDT. Xiao & Shwiyhat (2012) used a volume change unit (VCU) to monitor the total movement of the confinement water into and out of the triaxial cell, thereby monitoring the total volume change of the specimen. Slangen (2015) developed a double-walled triaxial cell, which is assembled in a large water bath; this arrangement enables measurement of the volume change of the cell's fluid, from which the volume change of specimen is

deduced, independent of changes in the cell pressure.

Besides all the advantages of using flexible-wall permeameter, a setback of this apparatus is related to the difficulty in maintaining a high saturation (Xiao & Shwiyhat (2012)) or a constant confinement during erosion.

4.3   Experimental erosion procedure

In this section, the experimental erosion procedure, adopted in this study, is introduced. The material used is first presented. Then, a description of the suffusion permeameter and the testing program are provided.

4.3.1   Materials used

Since gap-graded soils are deficient in certain grain classes, studies showed that they are more prone to suffusion (Skempton & Brogan (1994)). They may be a result of defects in construction or substandard procedures of soil mixing leading to a gap in certain grain sizes. Therefore, a gap-graded soil was chosen in our suffusion experiments.

Experiments are done using mixtures of coarse and fine silica Hostun sands, (HN 1/2.5 and HN34, respectively). The siliceous sand used here is mainly composed of quartz, categorized as an angular to sub-angular material with a specific gravity, ρ=2.65 g/cm^3. Figure 4.3 presents the particle size distribution of the used sand with a uniformity coefficient $C_u = 8.1$, and an effective diameter, $D_{50} = 1.55$ mm.

 The potential of internal stability is assessed following the methods proposed by Istomina (1957); Kezdi (1979); Kovacs (1981); Kenney & Lau (1985); Burenkova (1993); Wan & Fell (2008); Li & Fannin (2008), which indicated that the studied soil is potentially unstable and vulnerable to suffusion.

The study of soil mixtures requires the estimation of the variation of the maximum and minimum void ratio with the amount of fines content. The variation of the maximum and the minimum void ratios for the host soil (sand HN 1/2.5) and soil mixtures of different fines contents is illustrated in Figure 4.4. Both French and Japanese standard procedures to obtain reliable values were used to find these parameters (T. Nguyen (2014)). The maximum void ratio was determined by depositing carefully with a spoon, at a null drop height (to obtain very loose conditions), layers of the dry soil mixture (40 g each) in a mold. Once the mold is full, its surface is then flattened and the mass of the soil in the mold is weighed to calculate the maximum void ratio. On the other hand, the minimum void ratio is calculated by compacting each layer of the soil in the mold using a hammer and a heavy wait. Once the mold is full, the soil is weighed and the minimum void ratio is calculated. Figure 4.4 shows that the minimum values of e_{min} and e_{max} are reached around FC=35 %. This value is called the threshold fines content, FC_{th}, which refers to the maximum amount of fines that can be contained in the void by keeping the skeleton of the host sand unchanged (Thevanayagam (2000)). The latter governs the mechanical behavior of the soil as long as the fines content does not exceed the threshold value.

Soil samples with a fines content of 25% are considered in this study with minimum and
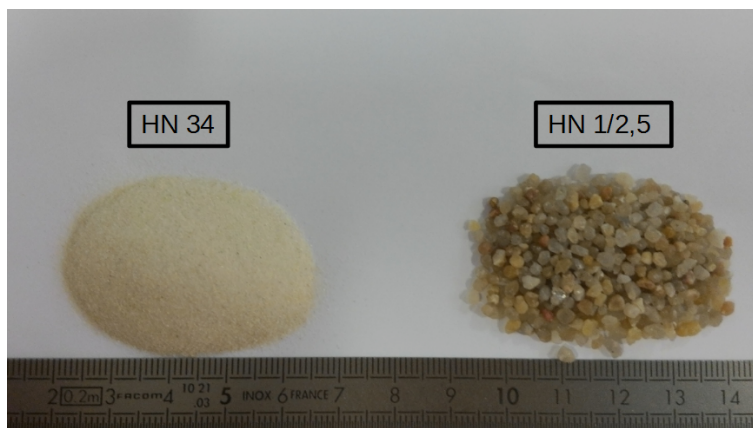
(a)
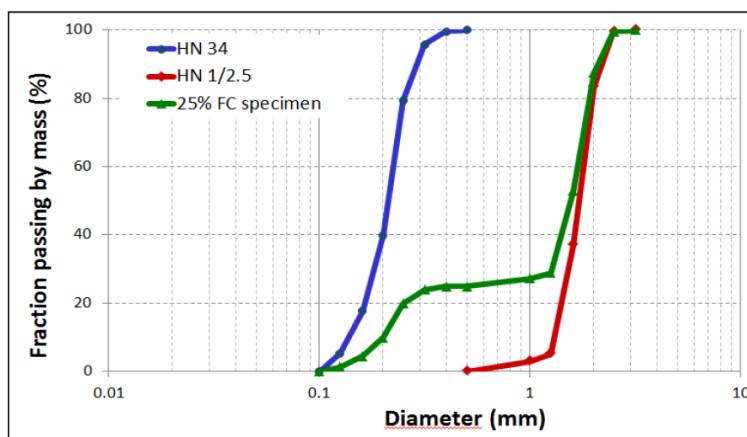
(b)

Figure 4.3: (a) Photograph of the two fractions of Hostun sand used in this study and (b) the particle size distribution.

maximum void ratios of 0.38 and 0.63, respectively.
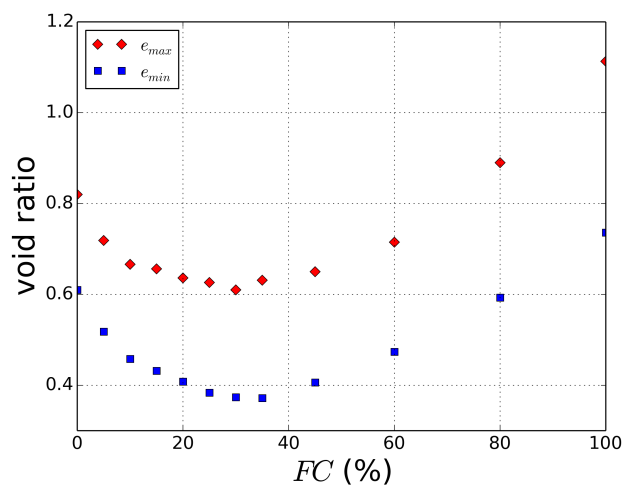
Figure 4.4: The variation of e_{min} and e_{max} with fines content, FC.

4.3.2 Suffusion permeameter and test procedure

Suffusion tests were carried out using a newly developed suffusion permeameter made up of a cylindrical Plexiglass cell, 140 mm in height and 70 mm in internal diameter, to fit the pedestal triaxial cell. The permeameter is connected to a water supply system and a fines collector. The general configuration of the permeameter is illustrated in Figure 4.5. The initial version of this apparatus used in this study could investigate the hydraulic characteristics of soils, the settlement by visualisation and measurement, and the appearance of preferential paths (if they exist) during the suffusion process. More detailed descriptions and presentations will be available in the forthcoming Phd thesis of C.D. Nguyen and the related publications.

The seepage control system is a recirculation circuit based on a multi-stage flow-
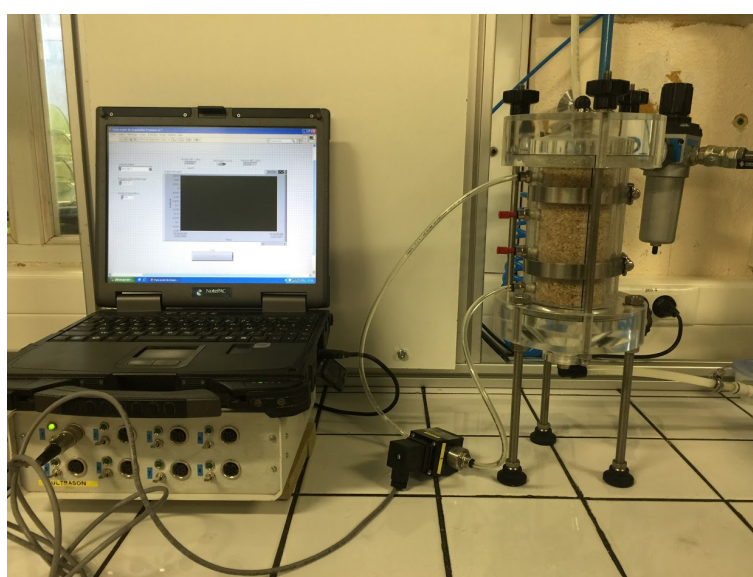
(a)
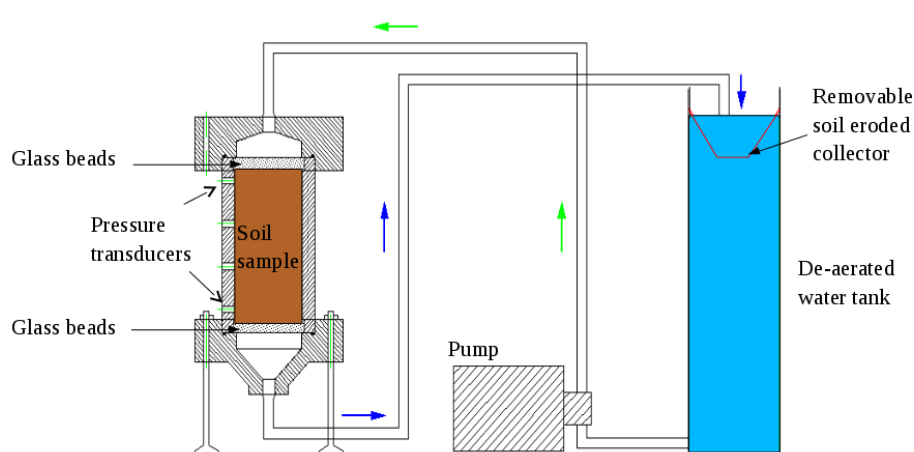
(b)

Figure 4.5: (a) Picture of the suffusion permeameter and data acquisition; (b) Sketch of the seepage test assembly.

rate control. The control unit is composed of a rotary pump for pumping water through

the specimen and a low capacity differential pressure transducer (LCDPT) for measuring the pressure drop from the top to the bottom of the tested specimens.

A series of suffusion tests was conducted following a multi-stage procedure. Each test usually takes about 8 hrs. The detailed procedure is as follows:

- The moist tamping method to prepare the specimens is used in this study to minimize the potential segregation of different grain sizes. Once the desired density is fixed, the predetermined amount of dry soil mixture is divided into seven equal parts. Each part is mixed uniformly with de-aired water (water content, w=2.5 %), placed into the suffusion cell with a spoon and then compacted by a hand graduated tamper at a fixed height of 20 mm to achieve the target density. To avoid any preferential seepage flow paths along the soil-wall interface of the rigid-wall permeameter, a rough plastic sheet is placed in the inner wall of the cell prior to the soil sample reconstitution.

- Two layers of glass beads, each fitted between two grids, are put at the bottom and the top of the soil specimen. The top layer serves to break up the incoming flow and to ensure a uniform water flow on the specimen. Whereas, the bottom layer of glass beads serves as a filter which can allow only fine eroded particles to pass.

- Before starting the suffusion tests, the soil sample is saturated by flushing CO_2 first, followed by de-aired water in an upward direction at a very low flow rate to prevent the heave phenomenon.

- Thereafter, the soil sample is subjected to the erosion test by flushing water in the downward direction. In this test, the flow rate is increased by steps. The corresponding hydraulic gradient, i, for each flow rate is determined from the pressure gradient measured by a low capacity differential pressure transducer connected to the upper and lower parts of the suffusion cell. Similarly, the eroded mass which is collected in a detachable container is recovered and weighed at the end of this step. The flow rate is increased by steps to take into account the effect of hydraulic loading history on the suffusion development (Sibille et al. (2015)). Note that, except for the saturation stage, the flow rate is increased to a fixed value large enough to trigger the erosion of fine particles for each step, and then is kept constant until no more eroded fine particles are observed. The test is then stopped when reaching the maximum laminar flow velocity. The increasing flow rate process is illustrated in Figure 4.6.

- Once the internal erosion process is done, the mechanical behavior of the eroded soil is investigated by performing triaxial compression tests (see Section 4.5).
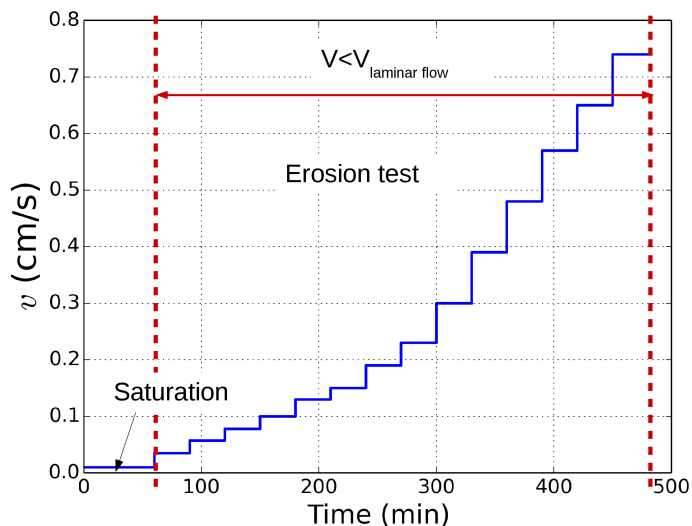
Figure 4.6: Illustration of the hydraulic loading during an internal erosion test.

4.3.3 Erosion testing program

A series of suffusion tests was conducted. Each test is described with reference to measurements of the hydraulic gradient, hydraulic conductivity, eroded mass, final volume change, and final density, as well as the global void ratio, the inter-granular void ratio and the final fines content to take into account the modifications in the soil microstructure. The objectives of these tests include:

- the study of the effect of flow rate on erosion;

- the study of the effect of the density on the erosion process;

- the assessment of the repeatability of the erosion tests;

Table 4.1 shows a summary of the test program.

Soil sample	FC %	Id	e_0	Not eroded(N) or Eroded(E)	V_{max} (cm/s)	Triaxial compression test
NS-0.2-CD	25	0.2	0.58	N	-	Drained
ES-0.2-CD	25	0.2	0.58	E	0.74	Drained
NS-0.4-CD	25	0.4	0.53	N	-	Drained
NS-0.4-CD-R (repeatability)	25	0.4	0.53	N	-	Drained
NS-0.4-CD-F (Frozen)	25	0.4	0.53	N	-	Drained
NS-0.4-CD-RF (Repeatability frozen)	25	0.4	0.53	N	-	Drained
ES-0.4-CD-L	25	0.4	0.53	E	0.1	Drained
ES-0.4-CD-M	25	0.4	0.53	E	0.3	Drained
ES-0.4-CD-H	25	0.4	0.53	E	0.74	Drained
NS-0.6-CD	25	0.6	0.48	N	-	Drained
ES-0.6-CD	25	0.6	0.48	E	0.74	Drained
NS-0.2-CU	25	0.2	0.58	N	-	Undrained
ES-0.2-CU	25	0.2	0.58	E	0.74	Undrained
NS-0.4-CU	25	0.4	0.53	N	-	Undrained
ES-0.4-CU	25	0.4	0.53	E	0.74	Undrained
NS-0.6-CU	25	0.6	0.48	N	-	Undrained
ES-0.6-CU	25	0.6	0.48	E	0.74	Undrained

Table 4.1: Summary of the test program.

4.4   Investigation of the erosion mechanism

4.4.1   Repeatability of suffusion tests

A series of suffusion tests was carried out to study the repeatability of the results; or in other words to check if specimens reconstituted under the same initial conditions behave in a similar manner once subjected to the same seepage flow conditions.

For that purpose, two soil samples were reconstitued at an initial relative density of 20 % (ES-0.2-CD and ES-0.2-CU), three samples at an initial relative density of 40 % (ES-0.4-CD-H, ES-0.4-CD-R and ES-0.4-CU) and two samples at an initial relative density of 60 % (ES-0.6-CD and ES-0.6-CU). Figures 4.7, 4.8 and 4.9 present the variations in the hydraulic properties and the cumulative eroded mass, in terms of Darcy's flow velocity, in the suffusion tests on soils of different initial densities. In addition to that, Table 4.2 gives the characteristics of each soil sample before and after suffusion.

Soil sample	Q_{max} $(\frac{ml}{min})$	V_{max} $(\frac{cm}{s})$	Before suffusion				After suffusion						Δe_g
			FC_0 (%)	Id_0	e_0	e_{g0}	M_e (%)	FC_f (%)	Id_f	ϵ_v (%)	e_{er}	e_{ger}	
ES-0.2-CD	1700	0.74	25	0.2	0.58	1.10	33.42	18.16	0.15	6.57	0.61	0.97	-0.13
ES-0.2-CU	1700	0.74	25	0.2	0.58	1.10	52.05	13.87	0.02	8.86	0.65	0.91	-0.19
ES-0.4-CD-L	250	0.10	25	0.4	0.53	1.04	4.00	24.24	0.39	0.64	0.54	1.03	-0.01
ES-0.4-CD-M	700	0.30	25	0.4	0.53	1.04	20.61	20.92	0.18	1.21	0.59	1.01	-0.03
ES-0.4-CD-H	1700	0.74	25	0.4	0.53	1.04	40.65	16.52	0.20	5.71	0.61	0.93	-0.11
ES-0.4-CD-R	1700	0.74	25	0.4	0.53	1.04	38.83	16.94	0.07	3.57	0.63	0.96	-0.08
ES-0.4-CU	1700	0.74	25	0.4	0.53	1.04	47.70	14.85	≈ 0	4.64	0.66	0.95	-0.09
ES-0.6-CD	1700	0.74	25	0.6	0.48	0.97	37.21	17.31	0.15	1.21	0.61	0.95	-0.02
ES-0.6-CU	1700	0.74	25	0.6	0.48	0.97	40.42	16.57	0.15	1.86	0.62	0.94	-0.03

Table 4.2: Summary of the suffusion test results. (e_0=initial void ratio; e_{er}=final void ratio; $\Delta e_g = e_{ger} - e_{g0}$)

It can be noticed that the repeatability of the suffusion tests for the reconstituted soil samples at the same density is globally quite good from one test to another, especially regarding the eroded mass, except for the density of 20%. The latter case can be explained by the fact that for low densities, the macro-pores of the structure are more pronounced and the induced local heterogeneity could significantly differ from one specimen to another when the reconstitution method by moist tamping is used. These differences cause the specimens to behave differently when subjected to suffusion tests.

In the case of ES-0.2-CU (Figure 4.7), the eroded mass (52.05%) is higher than that of ES-0.2-CD (33.42%) which leads to lower final density (Id_f =0.02) even if the volumetric deformation, ϵ_v, at the end of suffusion is higher in this case (8.86 %) compared to that of ES-0.2-CD (6.57 %). Besides, this resulted in a higher permeability in ES-0.2-CU. In fact, the observed fluctuations in the hydraulic gradient in ES-0.2-CD indicate that the soil sample suffered from consecutive events of clogging of constrictions resulting in a decrease in the eroded mass, unlike ES-0.2-CU. The large deformations in ES-0.2-CU has led to a slightly denser soil skeleton characterized by a lower inter-granular void ratio, e_{ger}, given in Table 4.2.
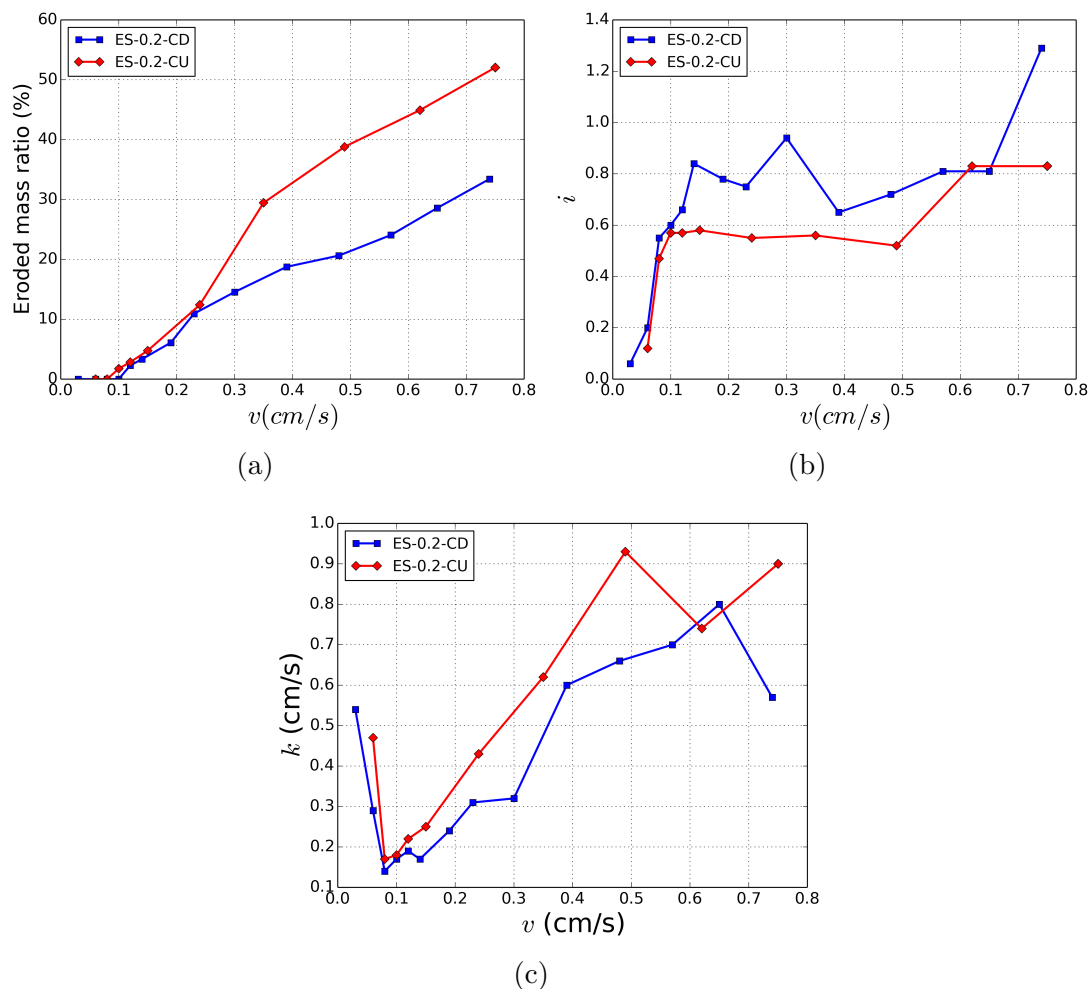
Figure 4.7: Comparison of the variation in (a) the eroded mass, M_e, (b) the hydraulic gradient, i, and (c) the hydraulic conductivity, k, with the flow velocity, v, for ES-0.2-CD and ES-0.2-CU.

In the case of Id=0.4, Figure 4.8 shows that the three samples have almost similar hydraulic properties, except ES-0.4-CU which had higher hydraulic conductivity attributed to the higher eroded mass (47.7%) as well as, probably, to a difference in the inter-granular void ratio compared to other samples, ES-0.4-CD-H (M_e=40.65%) and ES-0.4-CD-R (M_e=38.83%). Samples that lost more particles show slightly more volumetric deformations and a slightly denser soil skeleton (lower e_{ger}).

As the initial relative density increases to 60 % (Figure 4.9), ES-0.6-CD and ES-0.6-CU show similar eroded mass. The hydraulic properties, however, differ from one test to another. This may be related to the different pore network in the two samples. Moreover, the volumetric deformations are almost identical; ϵ_v=1.21 % in ES-0.6-CD and ϵ_v=1.86 % in ES-0.6-CU. Hence, suffusion tests at higher initial densities show better repeatability of the results.

(a)

(b)

(c)
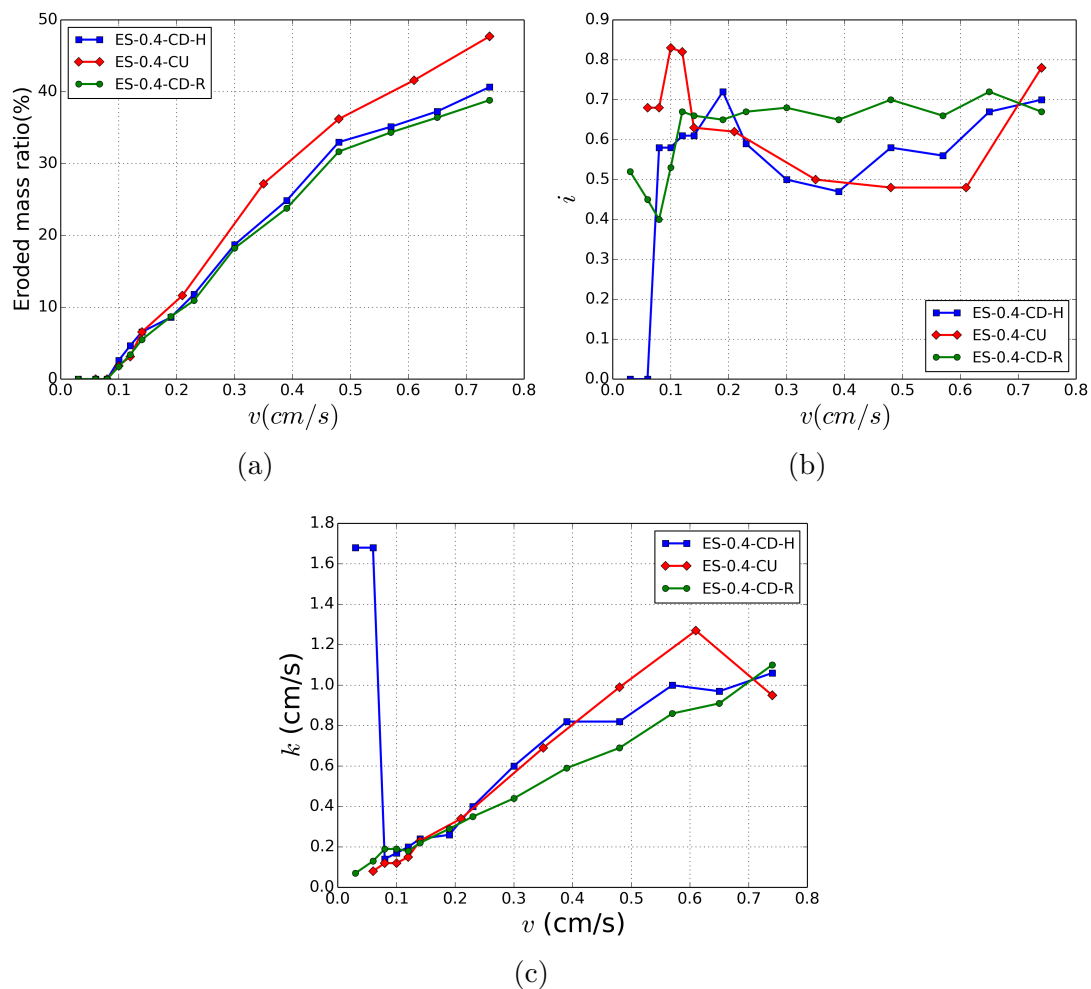
Figure 4.8: Comparison of the variation in (a) the eroded mass, M_e, (b) the hydraulic gradient, i and (c) the hydraulic conductivity, k, with the flow velocity, v, for ES-0.4-CD-H, ES-0.4-CD-R and ES-0.4-CU.
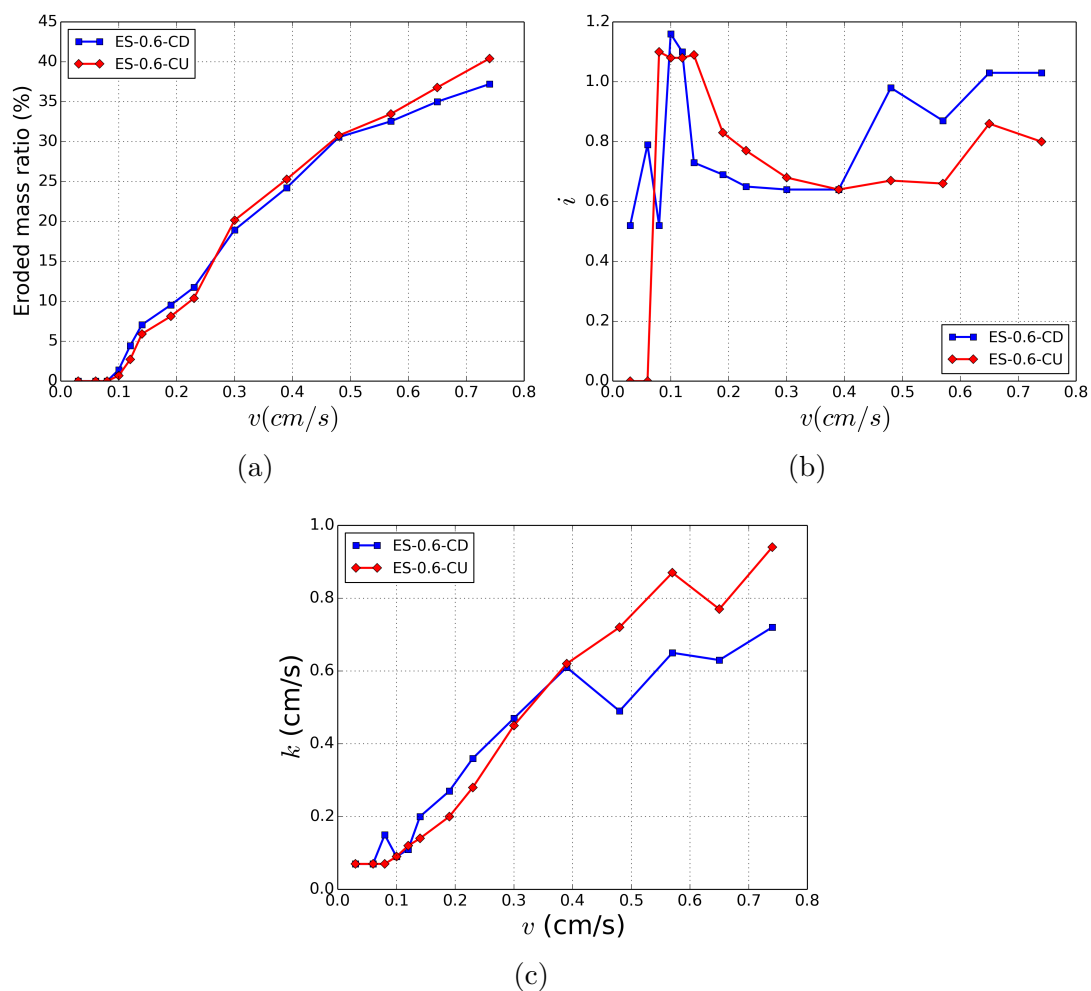
Figure 4.9: Comparison of the variation in (a) the eroded mass, M_e, (b) the hydraulic gradient, i and (c) the hydraulic conductivity, k, with the flow velocity, v, for ES-0.6-CD and ES-0.6-CU.

In conclusion, these erosion tests imply a rather good repeatability of the suffusion experiments, particularly for medium dense states (ES-0.4 and ES-0.6). In fact, when using the moist tamping technique, the heterogeneity linked to the deposition mode decreases with the increase in the density which confirms why at higher densities the discrepancies in the erosion results decrease.

4.4.2   Effect of the flow rate on suffusion

Three soil samples prepared at the same initial density (Id=0.4) were subjected to suffusion tests under different flow rates (Table 4.1).

Table 4.2 shows the data before and after suffusion tests for each soil specimen (ES-0.4-CD-L, ES-0.4-CD-M and ES-0.4-CD-H) which were subjected to flow rates of 250ml/min, 700 ml/min, and 1700 ml/min, respectively.

At the end of the erosion tests, 4% of the total mass of fine particles was eroded in ES-0.4-CD-L. This value increased to 20.61% in ES-0.4-CD-M as the flow rate increases and reached 40.65% in ES-0.4-CD-H (Figure 4.10a). Therefore, a monotonic increase in the eroded mass with the flow velocity was found as shown in Figure 4.11a. As a result, the fines content, FC, that is left after erosion is 24.24%, 20.92% and 16.52% in ES-0.4-CD-L, ES-0.4-CD-M and ES-0.4-CD-H, respectively.

The onset of internal erosion is evaluated primarily from changes in the hydraulic gradient (i), the hydraulic conductivity and the eroded mass. The transported particles can be either trapped causing a decrease in the hydraulic conductivity; or washed out leading to its increase. Such phenomena are detected from measurements of the variation of the local hydraulic gradient between ports on the wall of the permeameter.

Variations in the hydraulic gradient (i) and hydraulic conductivity (k) are illustrated in Figures 4.10b and 4.10c. At low velocity (v), the hydraulic gradient is almost negligible. When the flow velocity exceeds 0.06cm/s in ES-0.4-CD-H and 0.03 cm/s in ES-0.4-CD-M and ES-0.4-CD-L, a sudden increase in the hydraulic gradient is observed accompanied by a sudden decrease in the hydraulic conductivity. It is worth noting here, that no eroded mass was collected at this stage. Therefore, such a sharp increase in the hydraulic gradient may be attributed to the clogging of some constrictions by the transported fine particles. In other words, erosion might have occurred inside the sample, but particles were not washed out. With further increase of the flow rate, the hydraulic gradient increases very slightly. Some fine grains were collected at this stage resulting in an increase in the hydraulic conductivity. This indicates that the trapped particles were dislodged and transported outside the sample; However, the erosion is not predominant. As the flow velocity increases, the hydraulic properties keep changing as a result of the co-existance of erosion-clogging processes.

Moreover, in response to the loss of fine particles and the loss of equilibrium of the granular skeleton, when active fine particles leave the force chains, the soil specimen may deform. ES-0.4-CD-L lost a small percentage of fine particles resulting in little volumetric deformation at the end of suffusion (almost negligible, 0.535 %) and the density index didn't change significantly (Id=0.39) which is still close to its initial value (Id=0.4).
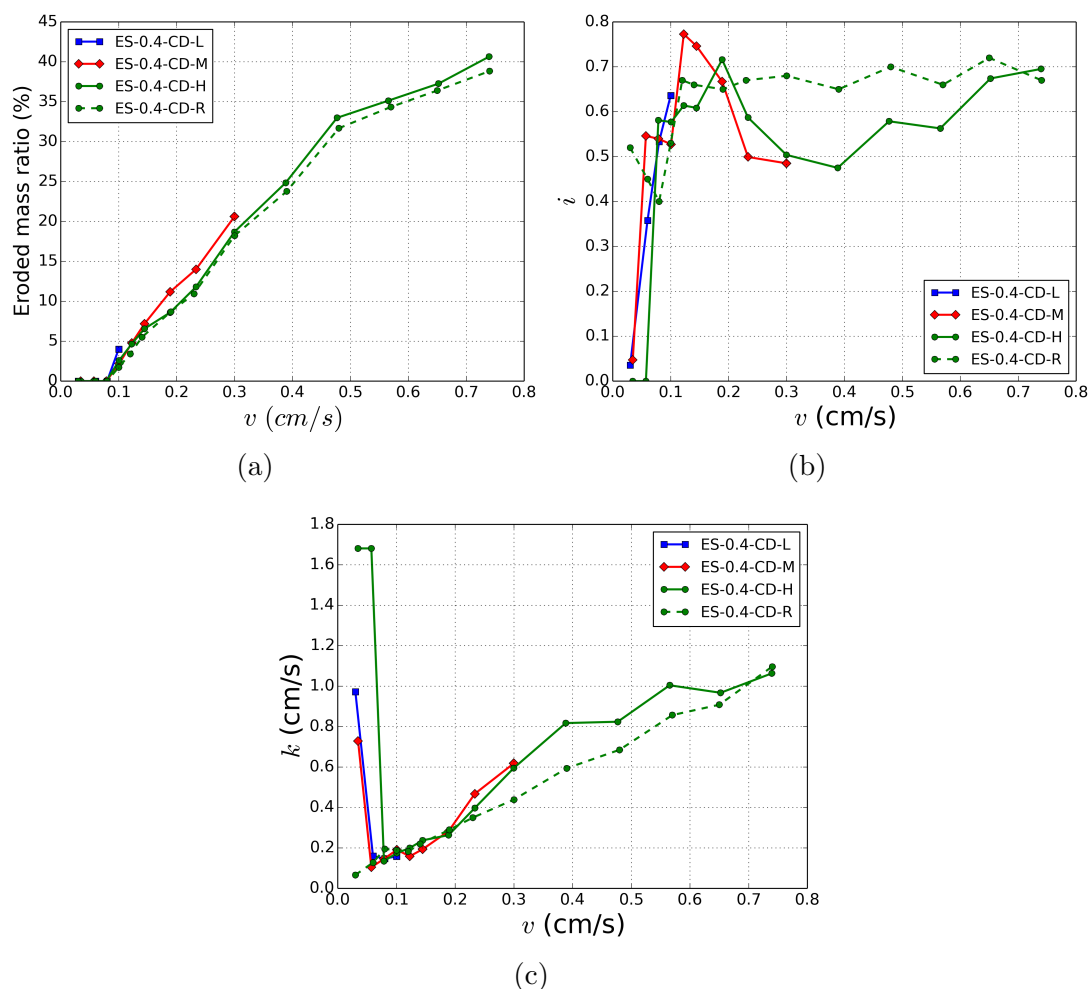
Figure 4.10: The variation of (a) the eroded mass, M_e (b) the hydraulic gradient, i and (c) the hydraulic conductivity, k, with the flow velocity, v.

However, as the flow velocity increases, eroding more fine particles (20.61 % and 40.65 %), the soil specimens loose equilibrium and soil particles re-arrange themselves to reach a new equilibrium state. Consequently, the soil compacts more at higher flow velocities as the eroded mass increases (Figure 4.11c). Although the soil shows large settlement, Figure 4.11b shows that as Darcy's flow velocity increases, the density index decreases; In other words, the creation of a more open microstructure dominates the compression of the soil during erosion. Hence, the decrease in the soil density seems to be a characteristic property of eroded soil samples (Ke & Takahashi (2014a); D. Chang & Zhang (2011); Muir Wood et al. (2010); Scholtès et al. (2010)).

Further investigations were done by checking the variation in the inter-granular void ratio, e_g, as an attempt to characterize the modifications in the microstructure and the soil behavior since the granular skeleton is mainly involved, especially when the fines content is lower than FC_{th} (see Chapter 2, Section 2.4.2). The variation of the inter-granular void ratio, e_g, is given by $\Delta e_g = e_{g0} - e_{ger}$. The following data was found: $\Delta e_g = -0.01$ for ES-0.4-CD-L, -0.03 for ES-0.4-CD-M, and -0.11 for ES-0.4-CD-H. Samples subjected to the lowest flow rates with little eroded mass (ES-0.4-CD-L) had the lowest decrease in e_g. However, the stability of the soil skeleton is highly affected when more fine particles are

(a)

(b)

(c)
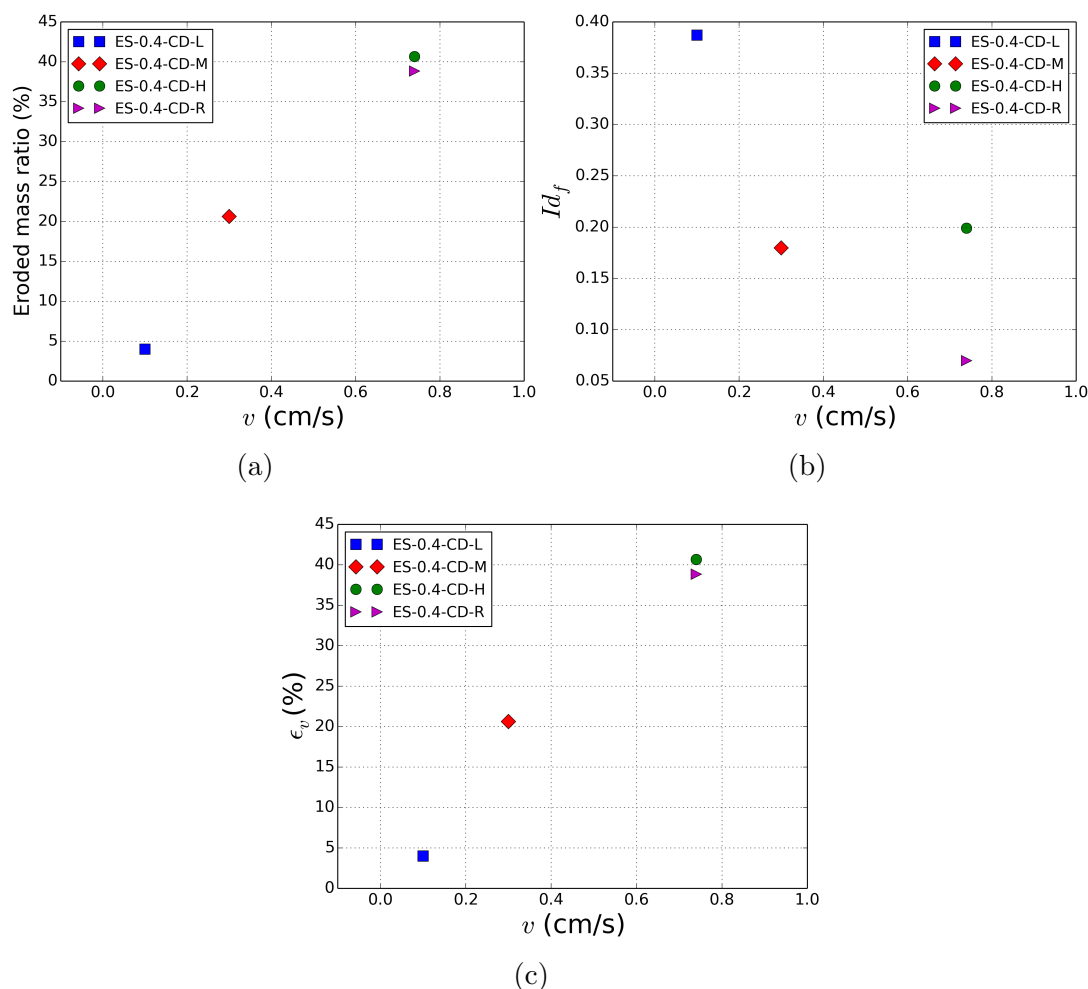
Figure 4.11: The variation of (a) the final eroded mass, M_e (b) the final density index, Id_f and (c) the volumetric deformation, ϵ_v with the flow velocity, v.

eroded (ES-0.4-CD-M, ES-0.4-CD-H), resulting in particles' re-arrangement and a larger decrease in e_g (resulting in a denser soil skeleton).

4.4.3 Effects of the density on suffusion

Three soil samples with three different densities (Id=0.2, 0.4, 0.6) are used to investigate the effect of the initial density on the suffusion process. Table 4.2 gives the data of each soil sample before and after erosion.

The evolution of the hydraulic properties and the eroded mass in each case are demonstrated in Figure 4.12. The curves show similiar tendencies. With the increase in Darcy's flow velocity, the eroded mass increases. However, one can notice a slight gradual decrease of the eroded mass rate during the erosion process. Besides, the rate of eroded mass is much higher for the ES-0.2-CU and ES-0.4-CU for $v >0.3$ cm/s. The rate of erosion depends on the modifications induced by suffusion in the pore space. As constictions get partially clogged, the hydraulic gradient increases and the hydraulic conductivity and erosion rate decreases. On the other hand, when blocked particles are free to migrate again in the pore space, the hydraulic gradient decreases, increasing therefore the hydraulic

conductivity and the erosion rate. Furthermore, we can observe that when the soil is dense (Id=0.6), a higher hydraulic gradient is developed just before the initiation of erosion which may be attributed to the smaller constrictions at a higher density that can be blocked easier than in the case of lower densities.

Figure 4.13a shows the relation between the eroded mass at the end of the test

(a)

(b)

(c)
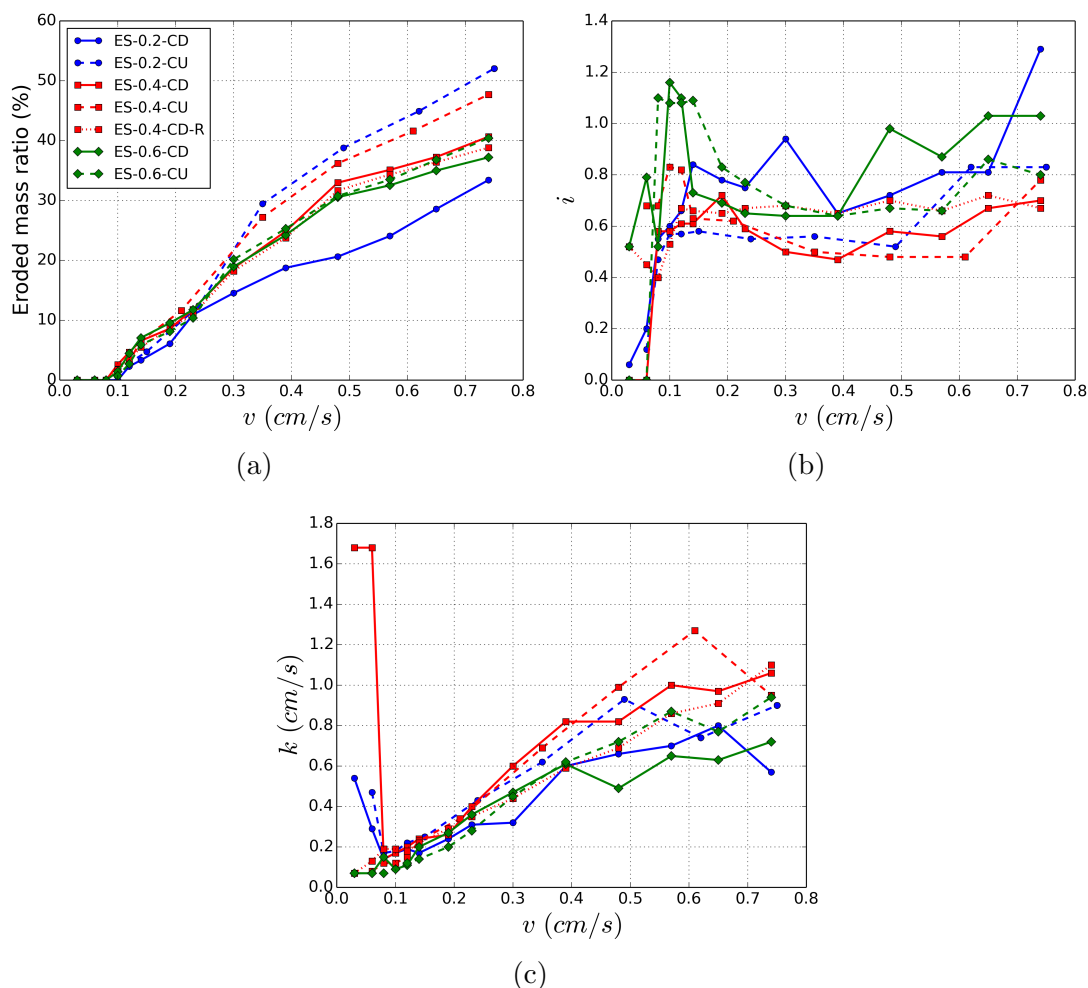
Figure 4.12: The variation of (a) the eroded mass, M_e, (b) the hydraulic gradient, i and (c) the hydraulic conductivity, k, with the flow velocity, v, for three different inital densities (Id = 0.2; 0.4 and 0.6).

(v=0.74 cm/s) and the soils initial density. One would expect that the looser soil specimens, ES-0.2-CD and ES-0.2-CU, may lose more fine particles than denser specimens since in a loose soil, fine particles may find larger voids to occupy without participating greatly in the stress transfer and more pores to circulate or to be transported freely. So, fine particles may be more prone to erosion at looser states. It is clear that as the initial density increases, less fine particles are eroded. At low initial density, Id=0.2, ES-0.2-CU lost 52.05 %. At Id=0.4, ES-0.4-CD-H lost 40.65 %, ES-0.4-CD-R lost 38.83 % and ES-0.4-CU lost 47.70 %. At Id=0.6, ES-0.6-CD lost 37.21 % and ES-0.6-CU lost 40.42 %. An exception is the particular case of ES-0.2-CD where the eroded mass (33.42%) was lower than in the other samples. It can be noticed that during the erosion test, the hydraulic conductivity in ES-0.2-CD was lower than that in the other soil samples as shown in Figure 4.12. This implies

that ES-0.2-CD suffered from more clogging events which prohibitted further migration of fine particles. As explained previously (see Section 4.4.1), this may be attributed to the effect of the heterogeneities induced by erosion which differs from one sample to another. Such heterogeneities are due to the inherent anisotropies linked to the initial soil deposition.

In addition to that, Figure 4.13b shows the relation between the settlement after erosion and the initial density of the soil. As the initial density increases, the soil settlement decreases (ϵ_v=6.57% and 8.86 % for ES-0.2-CD and ES-0.2-CU); this value decreases to 5.71%, 3.57% and 4.64% in ES-0.4-CD-H, ES-0.4-CD-R and ES-0.4-CU respectively and to 1.21% and 1.86% for ES-0.6-CD and ES-0.6-CU respectively. In fact, for lower initial density, the soil skeleton is looser. This is confirmed by the initially high inter-granular void ratio (see Table 4.2). Thus, as fine particles, which may contribute to the soil stability (or strength), leave the soil sample, a looser soil skeleton may lose equilibrium. In other words, force chains buckle due to the loss of support by fine grains. Therefore, particles will re-arrange themselves to reach a new equilibrium state resulting in higher soil settlement in looser soil samples which lost more fine particles. Besides, Table 4.2 also gives the values of Δe_g for the three eroded samples at the end of the suffusion tests. As can be noticed, Δe_g is negligible in ES-0.6-CD and ES-0.6-CU (Δe_g=-0.02 and -0.03, respectively). This means that for the same fines content, denser samples deform less significantly compared to the other soil specimens. Nevertheless, these prelimenary results should be completed by further experiments to support our conclusions.
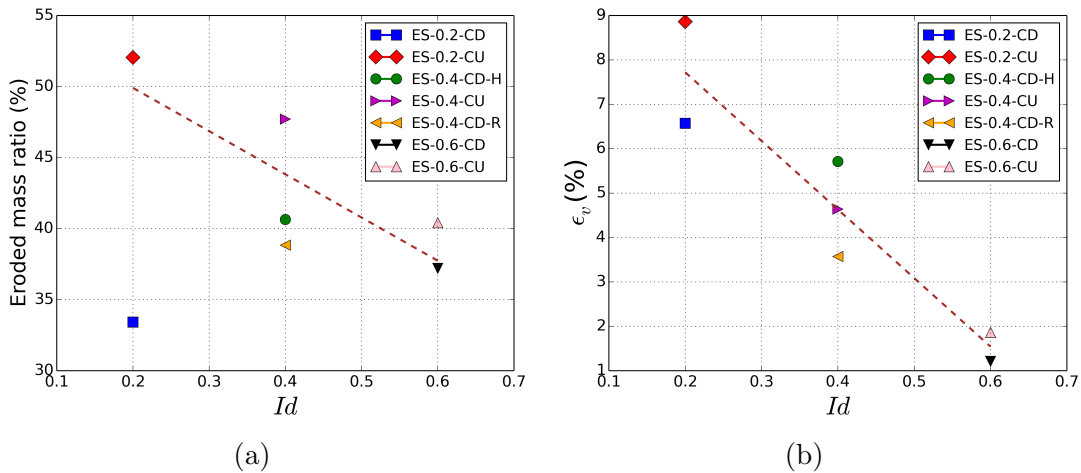
Figure 4.13: The variation of (a) the final eroded mass, M_e, (b) the volumetric deformation, ϵ_v, with the density index, Id.

4.5 Mechanical behavior of soils

In the present case, the soil specimens, after being eroded in the suffusion permeameter, have to be handled to be transferred to a conventional triaxial cell to characterize their mechanical behavior. Therefore, one of the main challenges, here, is to handle the eroded specimens without disturbing their microstructure resulting from the erosion process. In the literature, methods to recover undisturbed samples of cohesionless soil have been proposed by several researchers for micro-structural studies and strength determination (Hvorslev (1949); Frost (1989); Schneider et al. (1989)). The general procedure

Figure 4.14: Frozen eroded specimen prepared for triaxial compression test.

employed in most studies is to first stabilize the soil, then extract the sample and finally remove the stabilizing agent for further tests. Reversible stabilization methods include biopolymers agar and agarose, Elmer's glue, and freezing. However, these were used on natural soils or reconstituted ones, but to our knowledge, not on eroded soils.

In our study, an adjusted procedure of eroded soil samples is adopted. Once the erosion test is finished, soil samples are de-saturated at very low rate, recovered by keeping it in the suffusion cell and frozen over the night in a freezer (approximately 12 hours) to preserve the microstructure. After this freezing stage, the frozen soil specimens are removed from the erosion cell, put in the triaxial apparatus (Figure 4.14) and confined at 50 kPa to prevent their collapse.

After 4 hours (the time needed for the frozen soil to thaw), monotonic triaxial compression tests are carried out. A fully computer controlled triaxial system from Wykeham Farrance is used. The axial load is monitored by an internal submersible load transducer while the axial displacement is measured by LVDT mounted on the top platen. The volume variation of the sample is measured by an automatic volume change device. Soil specimens are confined at 100 kPa, and then saturated by flushing CO_2 under a pressure of 20 kPa for 30 minutes, followed by de-aired water of about three times the specimen's volume. Back pressures up to 400 kPa is applied to ensure full saturation of the specimens and to obtain a Skempton coefficient, B, higher than 0.96. The specimens are then sheared at a constant strain rate of 1 % per minute.

The objectives in this section are:

1. verify that the freeze/thaw process has no influence on the mechanical behavior of the soil;

2. perform drained and undrained triaxial compression tests on eroded and non-eroded soil samples to investigate the effect of suffusion on the mechanical properties of the

soil.

4.5.1 Drained behavior of non-eroded and eroded soils

This section presents the results of the drained triaxial compression tests which are summarized in Tables 4.3 and 4.4; The peak and residual friction angles, φ_p and φ_0, as well as the maximum dilatancy angle, ψ_{max}, are given for each soil sample.

Soil sample	FC %	e_0	e_{g0}	e_c	e_{gc}	φ_p (°)	φ_0 (°)	ψ_{max} (°)
NS-0.2-CD	25	0.58	1.11	0.57	1.09	30.8	29.7	1.47
NS-0.4-CD	25	0.53	1.04	0.53	1.04	31.4	29.2	1.90
NS-0.4-CD-R	25	0.53	1.04	0.49	0.99	31.4	29.2	1.90
NS-0.4-CD-F	25	0.53	1.04	0.56	1.08	31.4	29.2	2.40
NS-0.4-CD-RF	25	0.53	1.04	0.58	1.11	31.4	29.2	1.41
NS-0.6-CD	25	0.48	0.97	0.48	0.97	31.9	29.3	1.89

Table 4.3: Summary of the drained triaxial compression results on non-eroded soil samples. (e_c: void ratio after consolidation; e_{gc}: inter-granular void ratio after consolidation)

Soil sample	M_e (%)	FC_f (%)	Id_f	ϵ_v (%)	e_{er}	e_{ger}	$e_{er\text{-}c}$	$e_{ger\text{-}c}$	φ_p (°)	φ_0 (°)	ψ_{max} (°)
ES-0.2-CD	33.42	18.16	0.15	6.57	0.61	0.97	0.61	0.97	30.8	28.9	1.22
ES-0.4-CD-L	4	24.24	0.39	0.64	0.54	1.03	0.54	1.03	31.3	28.8	2.33
ES-0.4-CD-M	20.61	20.92	0.18	1.21	0.59	1.01	0.63	1.06	29.1	27.4	2.08
ES-0.4-CD-H	40.65	16.52	0.20	5.71	0.61	0.93	0.61	0.93	28.1	26.7	2.34
ES-0.4-CD-R	38.83	16.94	0.07	3.57	0.63	0.96	0.63	0.96	30.2	27.9	2.92
ES-0.6-CD	37.21	17.31	0.15	1.21	0.61	0.95	0.63	0.97	29.9	27.8	2.44

Table 4.4: Summary of the drained triaxial compression results on eroded soil samples. (e_{er} =void ratio after erosion; e_{ger} =inter-granular void ratio after erosion; $e_{er\text{-}c}$ =void ratio after consolidation; $e_{ger\text{-}c}$ =inter-granular void ratio after consolidation;)

Effects of freeze/thaw on the mechanical behavior of soil

Following the procedure of freezing the eroded soil to retrieve it while preserving the resulting microstructure, an essential step is to further verify that there is no significant impact of this procedure on the mechanical behavior of the soil. For that purpose, a comparison is done by performing drained triaxial compression tests on two sets of soil samples:

- unfrozen soil specimens (NS-0.4-CD, NS-0.4-CD-R);

- soil specimens frozen then thawed before the triaxial compression test (NS-0.4-CD-F, NS-0.4-CD-RF);

Figure 4.15 illustrates the responses of frozen and unfrozen soil samples to drained triaxial compression tests together with repeatability tests. It was observed that all samples, frozen and unfrozen, show a similar mechanical behavior. The stress deviator is fairly

the same and there is a negligible effect on the volumetric deformation up to 12-13 % of axial strain. Beyond that, the observed slight difference is attributed to the appearance of heterogeneous deformations. The peak and the residual friction angles are, respectively, φ_p=31.4° and φ_0=29.2° (Table 4.3). The maximum dilatancy angle, ψ_{max}, varies very slightly; ψ_{max} is 1.90° for NS-0.4-CD and NS-0.4-CD-R, 1.41 ° for NS-0.4-CD-F and 2.40 ° for NS-0.4-CD-RF. Hence, the freeze/thaw method seems to preserve the microstructure of soil specimens without important secondary effects.
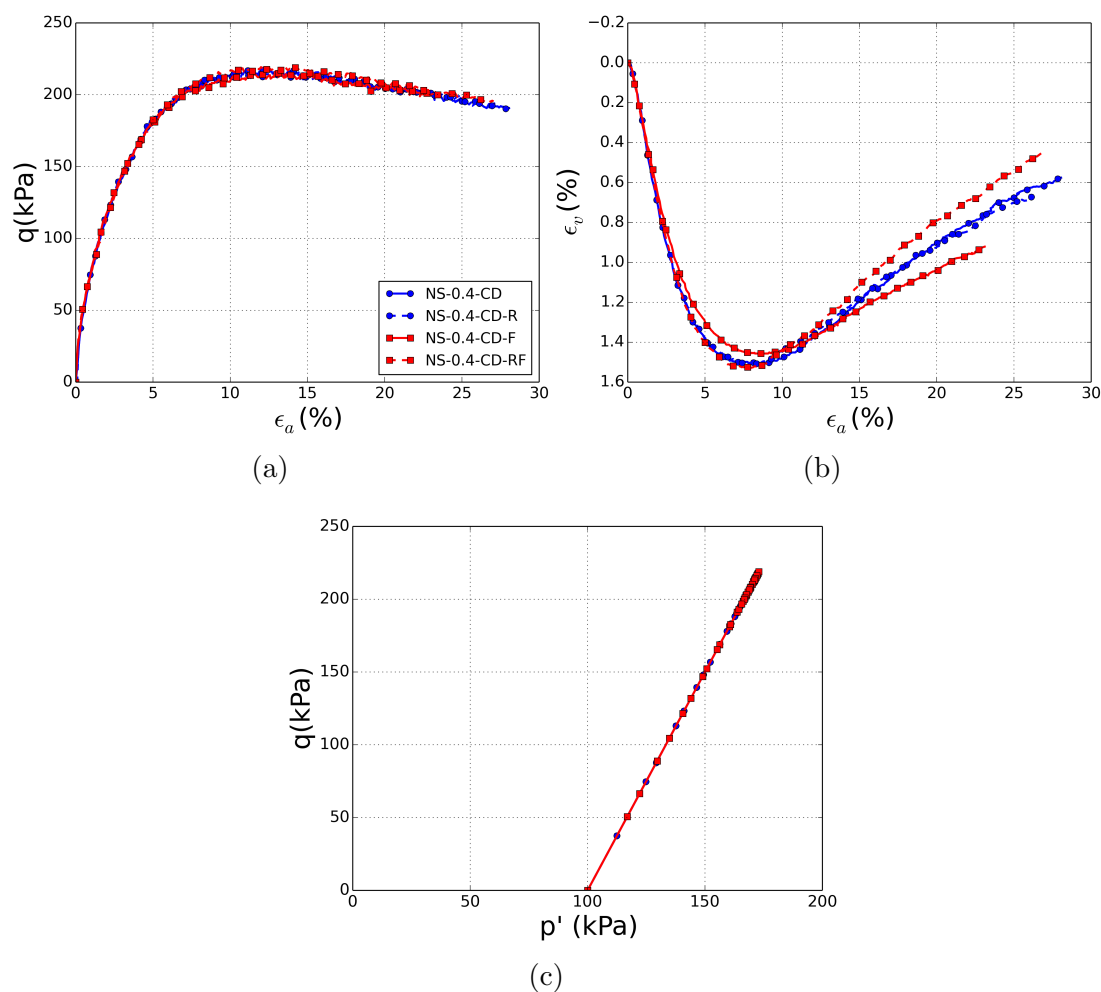
Figure 4.15: Effect of freeze/thaw on the mechanical response to drained triaxial compression tests. (a) Deviator stress versus axial strain; (b) Volumetric strain versus axial strain (c) Deviator stress versus mean effective stress.

Repeatibility of the whole erosion process and the mechanical behavior of soil

In Section 4.4.1, two soil samples, were prepared at the same initial state with an initial density index, Id=0.4, and were subjected to suffusion tests. It was shown that ES-0.4-CD-R lost similar mass of fines (38.83%) as ES-0.4-CD-H (40.65%). However, the repeatability test shows a lower volumetric deformation at the end of suffusion (ϵ_v=5.71% in ES-0.4-CD-H and 3.57 % in ES-0.4-CD-R). Moreover, ES-0.4-CD-R becomes looser than ES-0.4-CD-H. The suffusion results seem quite repeatable. In order to check if the whole process of erosion and drained triaxial tests is repeatable as well, drained triaxial compression tests were

carried out after erosion (see Figure 4.16). However, due to the different microstructures in each case (i.e. slightly different void ratios, fines content,..), the comparison is qualitative, but serves to validate the effect of suffusion on the mechanical properties of the soil.

Although the soil skeleton becomes denser after erosion (i.e. the inter-granular void ratio decreased), both soil specimens showed a decrease in the peak and residual shear strengths (Table 4.4). The peak friction angle decreased from 31.4 ° to 28.1 ° in ES-0.4-CD-H and to 30.2 ° in ES-0.4-CD-R. The residual friction angle decreased from 29.2 ° to 26.7 ° in ES-0.4-CD-H and to 27.9 ° in ES-0.4-CD-R. Therefore, it can be concluded that the suffusion leads here to a reduction of the shear strength with an apparent nil or very slight increase in the dilatancy. Thus, for a given density, the repeatability results are quite good showing same qualitative behavior.
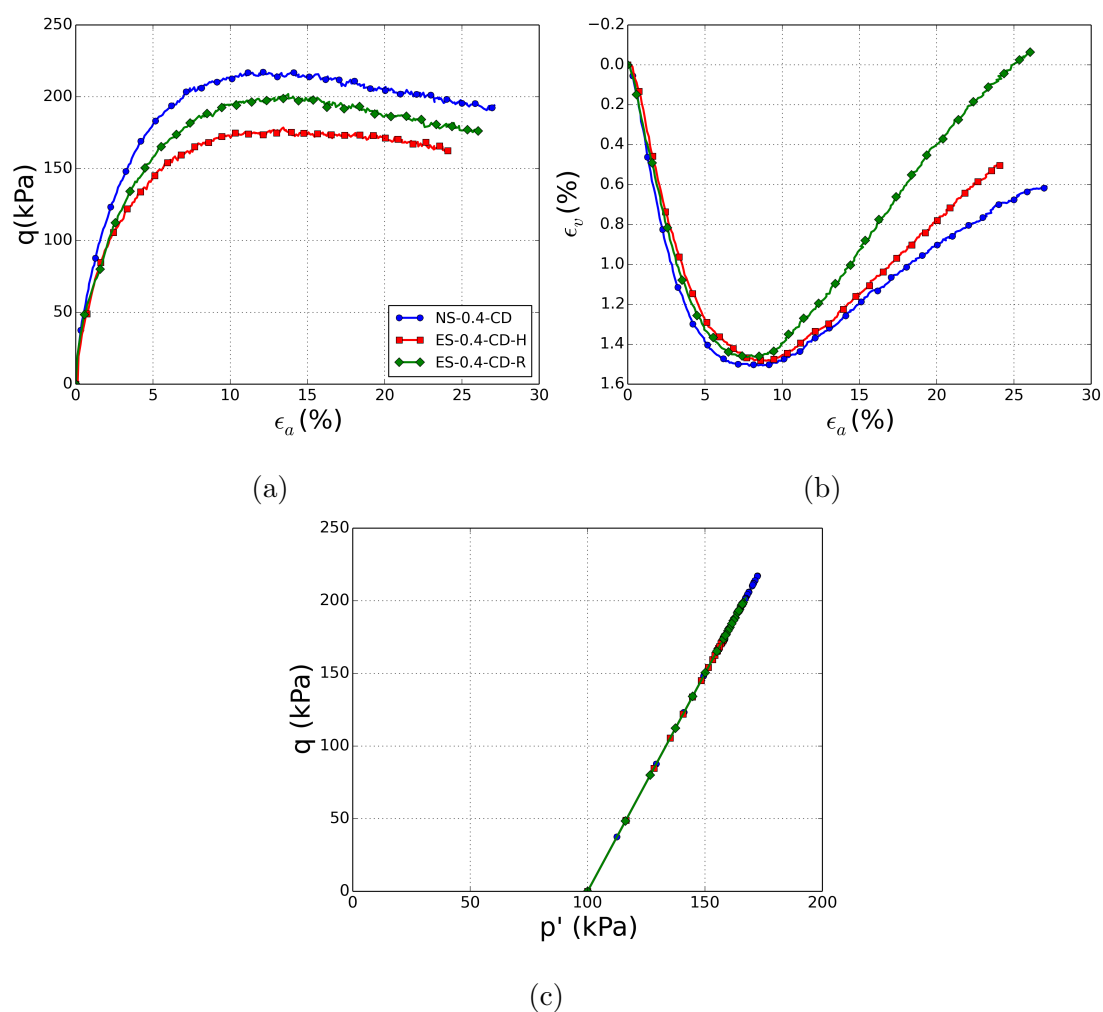
Figure 4.16: Comparison of the responses to drained triaxial compression tests of NS-0.4-CD, ES-0.4-CD-H and ES-0.4-CD-R. (a) Deviator stress versus axial strain; (b) Volumetric strain versus axial strain (c) Deviator stress versus mean effective stress.

Drained response of non-eroded soils at different initial densities

Drained triaxial compression tests were carried out to study the mechanical behavior of three non-eroded soil samples reconstituted at different initial densities (Id=0.2, 0.4, 0.6)

and confined at 100 kPa. Figure 4.17 illustrates the mechanical response of the three samples (NS-0.2-CD, NS-0.4-CD, NS-0.6-CD). The observed behavior is similar to the one of medium-dense sand, with a contractant phase, followed by a dilatant one. The evolution of the stress deviator shows that the shear strength increases as the initial density increases, which is in accordance with the conventional observations on the effect of density on the shear strength. The peak friction angle, φ_p, is 30.8° in NS-0.2-CD; it increases slightly to 31.4° in NS-0.4-CD and 31.9° in NS-0.6-CD (see Table 4.3). Furthermore, denser soil samples show a slightly more dilatant behavior; the maximum dilatancy angle, ψ_{max} is 1.47 ° for NS-0.2-CD and 1.9 ° for NS-0.4-CD and NS-0.6-CD.

Figure 4.18a illustrates the characteristic state points in q-p' plane of the soil sam-
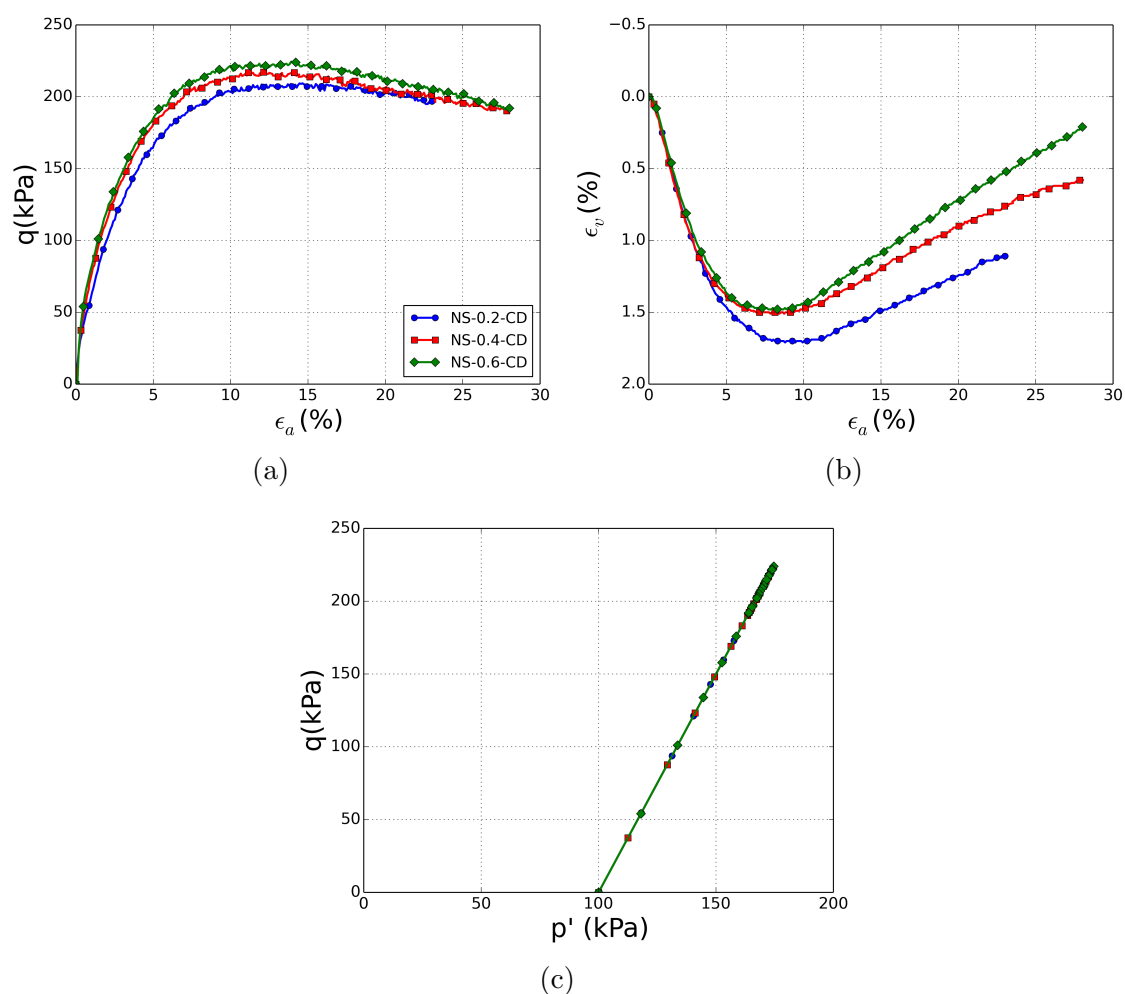
Figure 4.17: Responses to drained triaxial compression tests of soil samples reconstituted at different initial densities. (a) Deviator stress versus axial strain; (b) Volumetric strain versus axial strain (c) Deviator stress versus mean effective stress.

ples reconstituted at different initial densities. The characteristic state corresponds to the point at which the behavior of the soil changes from contractant to dilatant one. According to Luong (1982), this state occurs at the point where the volume change is null. The characteristic state line of the three tested non-eroded soil is unique, giving a friction angle around 30.7°.

Concerning the critical state, up to an axial strain of 28%, the soil did not reach
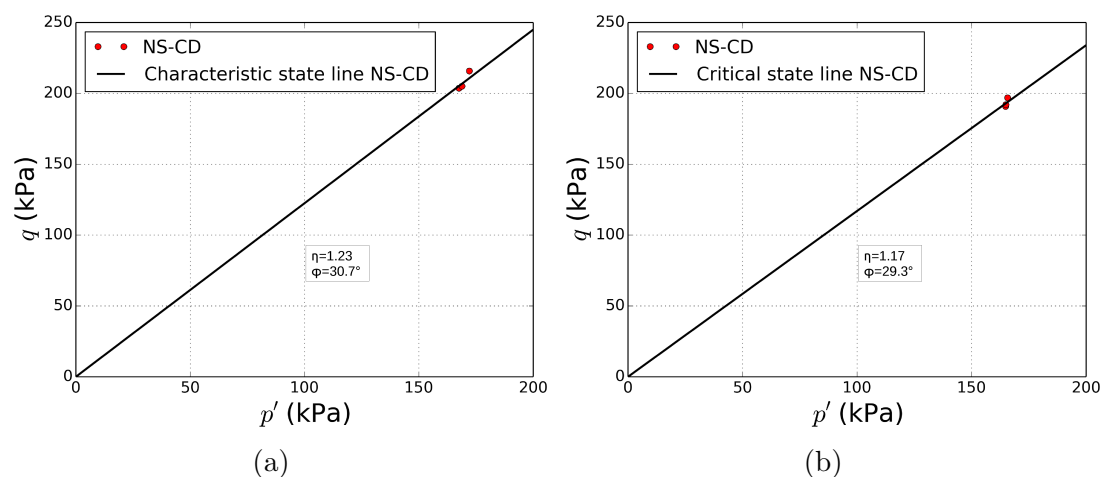
Figure 4.18: (a) Characteristic state line and (b) critical state line of non-eroded soil samples.

a constant volumetric strain; hence, a critical state was not reached in these experiments. Nevertheless, the critical state points of all the non-eroded samples collapse to the same critical state line passing through the origin, irrespectively of the soil's initial density (Figure 4.18b). The internal friction angle at the critical state is about 29.7° for NS-0.2-CD, 29.2° for NS-0.4-CD and 29.3° for NS-0.6-CD.

Drained response of eroded soils at different initial densities

To study the mechanical behavior of eroded soils at different initial densities, eroded soil samples in Section 4.4.3 were subjected to drained triaxial compression test. Figure 4.19 shows the response of the eroded soil samples. All the three samples exhibit the same tendency of the mechanical response in terms of deviator stress and volumetric strain characterized by contractant-dilatant behavior which usually corresponds to the behavior of medium dense sand. However, ES-0.2-CD and ES-0.6-CD show the highest peak shear strength and dilatancy although these samples have lower post-suffusion density index and higher inter-granular void ratio compared to ES-0.4-CD-H. This implies that the final density index and inter-granular void ratio (after erosion) are not the only parameters governing the mechanical behavior of eroded soils. The resulting fines content should be considered as well.

 ES-0.2-CD has suffered from high deformations during suffusion, inducing a decrease of the inter-granular void ratio and leading to a denser granular skeleton (the latter was still slightly looser than ES-0.4-CD-H). Nevertheless, this sample lost fewer fine particles. Thus, the resulting gain in strength may be attributed to a combined effect of the final fines content and the inter-granular void ratio.

The same conclusion could be drawn for the ES-0.6-CD. Despite the resulting low density (Id=0.15), induced by the suffusion process and loss of fine particles (compared to the initial one, Id=0.6), the granular skeleton has not been affected as demonstrated by the low settlement and the slight variation in the inter-granular void ratio during erosion.
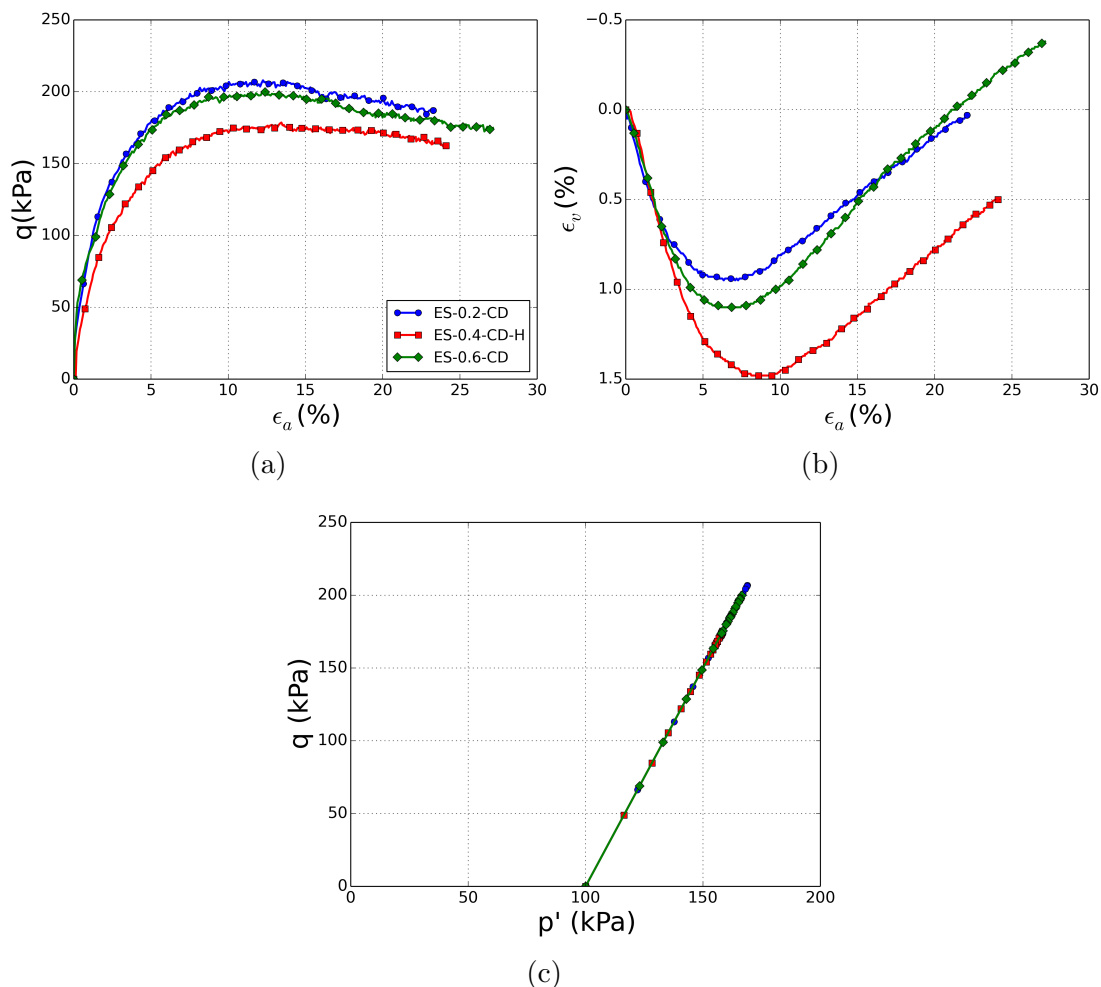
Figure 4.19: Responses to drained triaxial compression tests of eroded soils reconstituted at different initial densities. (a) Deviator stress versus axial strain; (b) Volumetric strain versus axial strain (c) Deviator stress versus mean effective stress.

However, it is worth noting that the final value reached by ES-0.4-CD in terms of inter-granular void ratio is slightly smaller and should have induced higher strength, which is not the case. This may be explained by the higher loss of fine particles compared to ES-0.6-CD.

Thus, the mechanical behavior seems to be governed by both, the coarse skeleton, responsible for the stress transfer and represented by the inter-granular void ratio, and by the fine particles which may play an important role in stress transfer as well to some extent. The final density alone is not a suitable parameter to interpret such experiments on this type of materials.

Figure 4.20a presents the characteristic state points of eroded samples in q-p' plane. Conversely to the non-eroded soils, the characteristic state line of eroded soils seems to be declined into different lines implying that erosion creates different materials with relation to final fines content and grain size distribution.

From Figure 4.20b, the same tendency is observed concerning the critical state line. In other words, eroded soils seem presenting different critical state lines characterizing
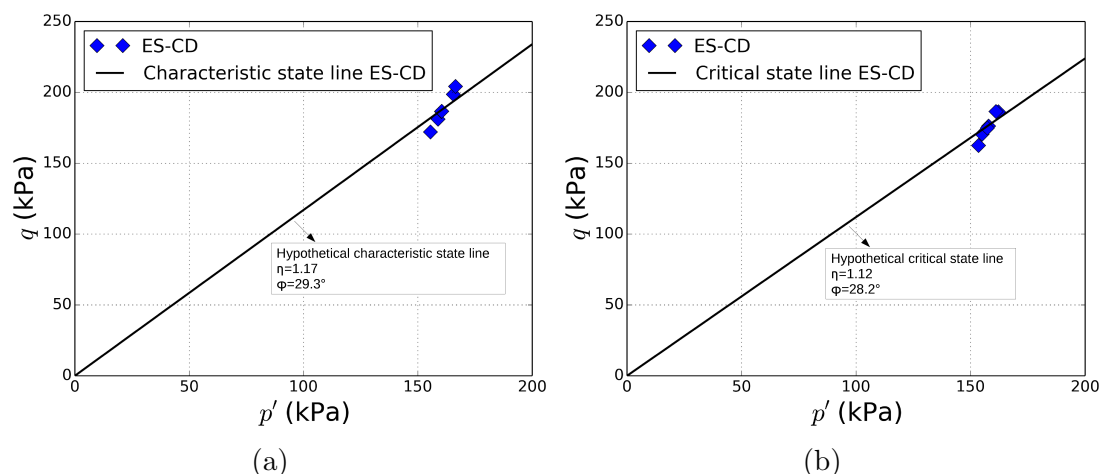
Figure 4.20: (a) A hypothetical characteristic state line and (b) a hypothetical critical state line of eroded soil samples.

different materials after erosion as explained above. This type of results has already been reported in several researches dealing with the behavior of granular soils with different fines content. Nevertheless, precautions have to be taken to conclude because, on one hand, the critical state has not been reached in all the samples; on the other hand, it is often observed that the critical state line in q-p' plane is unique irrespectively of fines contents, especially when the coarse granular material and the fine particles have the same characteristics (grains shape, mineralogy, etc...).

Drained response of eroded soils at different flow rates

Soil samples prepared at an initial relative density of 40% were eroded (Section 4.4.2) and then compressed under drained conditions. Responses of eroded soil samples (ES-0.4CD-L, ES-0.4-CD-M and ES-0.4-CD-H) eroded up to different maximum flow rates (250, 700 and 1700 ml/min) are shown in Figure 4.21. Also Table 4.4 gives the data of each soil sample after suffusion.

All the eroded soil samples exhibit similar stress-strain behavior but with a decrease in shear strength as the flow rate increases. This decrease is related to the loose state of the samples at the end of erosion knowing that the mechanical behavior of the soil is controlled by its density. The peak friction angle decreases from 31.3 ° for ES-0.4-CD-L test to 29.1 ° for ES-0.4-CD-M and to 28.1 ° for ES-0.4-CD-H. The latter shows slightly lower friction angle despite slightly higher final density compared to ES-0.4-CD-M. This may be attributed to its final fines content which is much lower than the threshold value (25 %) compared to the other samples.

The friction angle at the residual state also decreased from 29.2° for ES-0.4-CD-L to 27.4° for ES-0.4-CD-M and to 26.7° for ES-0.4-CD-H. Notice that the latter shows slightly lower friction angle at the peak and residual state despite a slightly higher final density and a smaller inter-granular void ratio, e_{ger}, compared to ES-0.4-CD-L and ES-0.4-CD-M, which means that the granular skeleton is denser in such case. One may expect a higher strength, however, with the loss of fine particles (final fines content lower than the threshold value

(a)

(b)

(c)
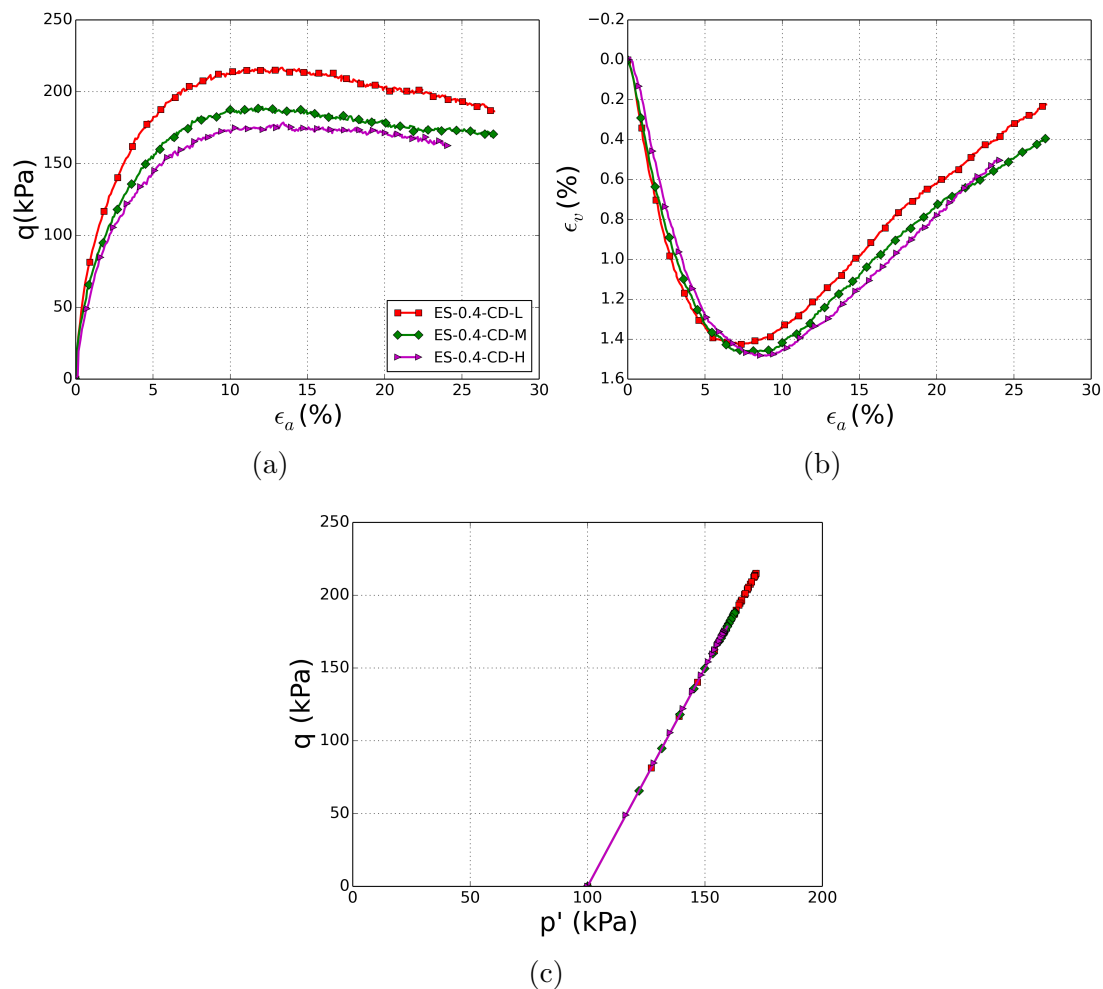
Figure 4.21: Responses to drained triaxial tests of soils subjected to different flow rates. (a) Deviator stress versus axial strain; (b) Volumetric strain versus axial strain (c) Deviator stress versus mean effective stress.

(25%)), and the increase in the global void ratio, the soil skeleton lost the support of the finer fraction which results in a lower shear strength. The relation between the eroded mass and the peak and residual friction angles is shown in Figure 4.22 and appears to be monotonic.
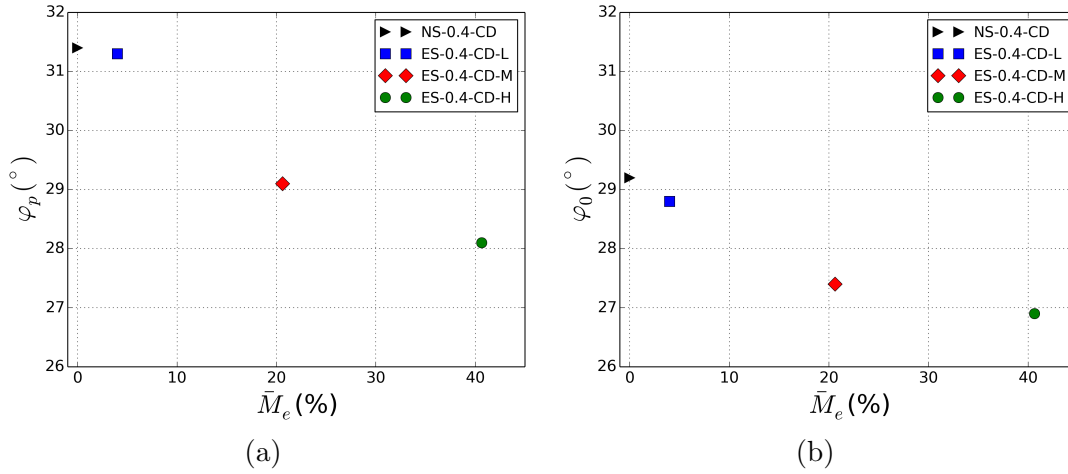
Figure 4.22: The variation of (a) the peak friction angle, φ_p, and (b) the residual friction angle, φ_0, with the eroded mass ($\bar{M}_e$).

Comparison of drained response of non-eroded and eroded soils

From Figures 4.23, 4.24 and 4.25, it can be observed that eroded soil samples exhibit similar tendency of stress-strain behavior as the non-eroded soil. However, quantitatively, the shear strength and the volumetric strains are different for the same density.

In the case of NS-0.2-CD and ES-0.2-CD (Figure 4.23), the deviator stress is fairly the same indicating that the shear strength was not highly affected, though, the density index decreased for the eroded sample. The peak friction angle is the same before and after erosion (30.8 °) and the residual friction angle decreased slightly from 29.7 ° to 28.9 ° which is negligible. In section 4.4.3, Figure 4.12 shows that the hydraulic conductivity in ES-0.2-CD decreased strongly at the end of erosion. This may be a consequence of clogging of some constrictions by fine particles rendering the behavior of ES-0.2-CD original compared to the other specimens. Hence, the conservation in the shear strength for ES-0.2-CD may be attributed to the fact that blockage of small particles (resulting in the decrease in permeability) may have created reinforced zones responsible for stress transfer. Besides, the decrease in inter-granular void ratio may have created new contact forces with the blocked fine particles which then contribute in stress transfer. Regarding the volumetric strains, one can expect to get the same deformations for both samples, eroded and non-eroded, as they have similar shear strength. However, it is observed that ES-0.2-CD seems less contractant than NS-0.2-CD. This may be attributed to the denser coarse fraction. Nevertheless, the variation in the dilatancy angle is negligible (ψ_{max}=1.47 ° for NS-0.2-CD and 1.22 ° for ES-0.2-CD).

 ES-0.4-CD-H showed a decrease in the shear strength compared to NS-0.4-CD (Figure 4.24). The peak friction angle decreases from 31.4 ° to 28.1 ° and the residual friction angle decreases from 29.2 ° to 26.7 °. The granular skeleton has been modified during erosion, confirmed by the high settlement and lower inter-granular void ratio, e_{ger}. Although the granular skeleton becomes denser, the soil lost lots of fine particles. Therefore, the force chains lack the support from fine particles to resist the applied shear forces in a way similar to the non-eroded soil specimen. The denser coarse skeleton, together with a global looser soil has led to lower shear strength. Conversely, volumetric deformations of both

(a)   (b)

(c)
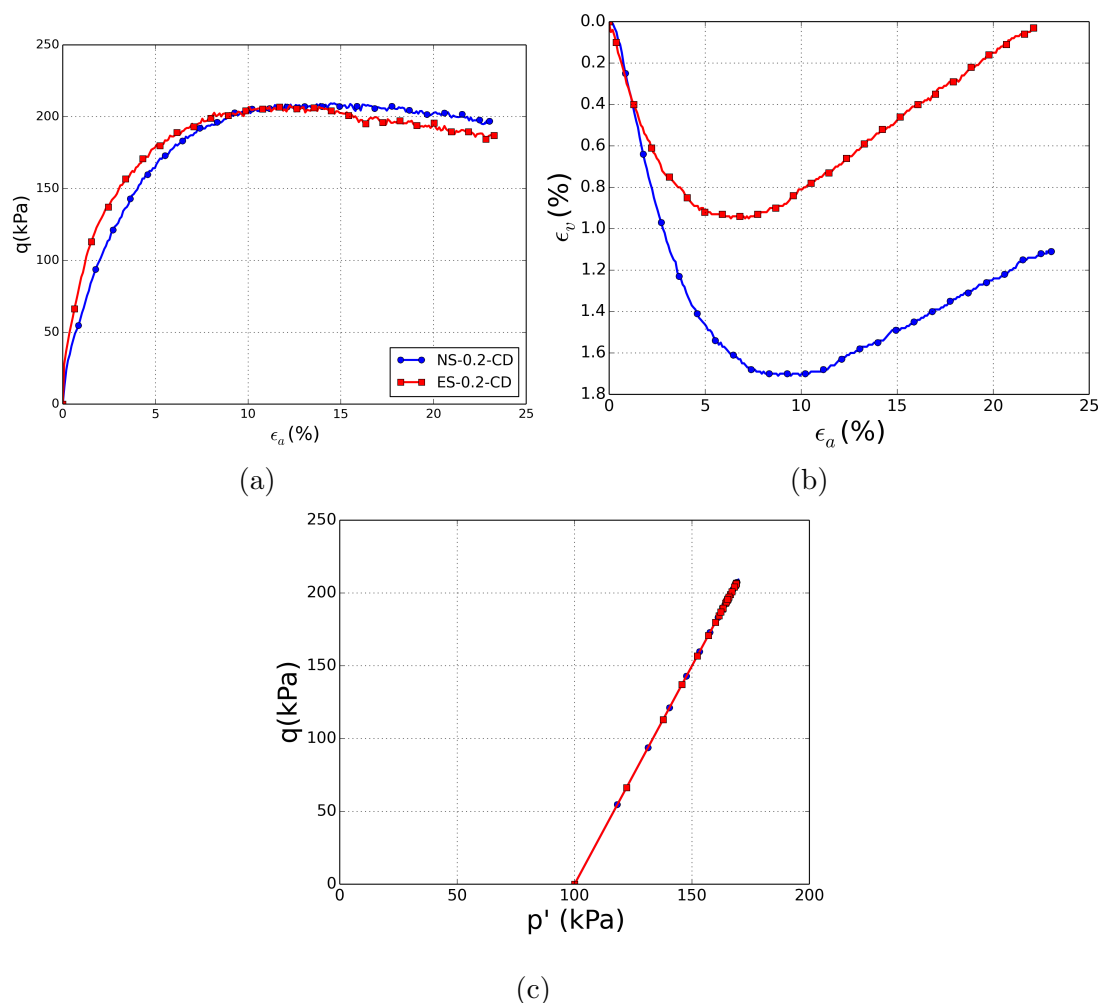
Figure 4.23: Comparison of the responses to drained triaxial compression tests of the non-eroded (NS-0.2-CD) and eroded (ES-0.2-CD) samples at an initial density Id = 0.2 (a) Deviator stress versus axial strain; (b) Volumetric strain versus axial strain (c) Deviator stress versus mean effective stress.

materials, eroded and non-eroded, can be considered similar. The denser coarse skeleton and the global loose state of the material may have led to such a coincidence of volumetric deformations of eroded soil samples with different granulometry and microstructure. In fact, ES-0.4-CD-H shows similar contractant behavior as that of the soil before erosion. The dilatancy angle changed slightly from 1.90 ° for NS-0.4-CD to 2.34 ° for ES-0.4-CD-H.

One should point out that the sample ES-0.4-CD-L, which was subjected to a low flow rate, showed the same behavior as the non-eroded soil. This is related to the little modifications induced in this case where the density index, void ratio, inter-granular void ratio and fines content did not change significantly after erosion. Hence, the soil did not show high deformations and preserved the same mechanical properties as the non-eroded soil. ES-0.4-CD-L developed similar shear strength as the non-eroded soil (φ_p =31.3 °, φ_0 =28.8 °).

In the case of ES-0.6-CD, it can be seen from Figure 4.25 that the eroded sample suffered from slight decrease in the shear strength even if the granular skeleton has not been affected
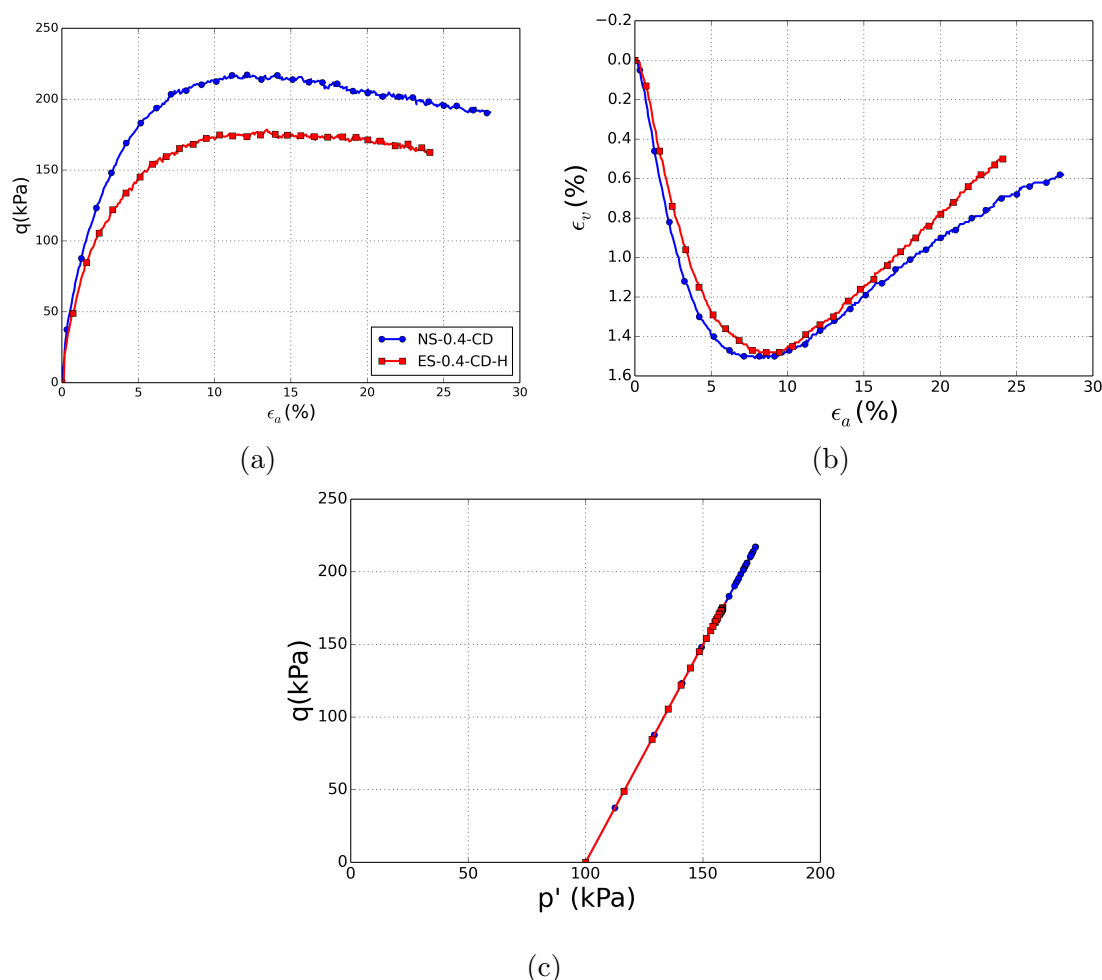
Figure 4.24: Comparison of the responses to drained triaxial compression tests of the non-eroded (NS-0.4-CD) and eroded (ES-0.4-CD-H and ES-0.4-CD-R) samples at an initial density Id = 0.4. (a) Deviator stress versus axial strain; (b) Volumetric strain versus axial strain (c) Deviator stress versus mean effective stress.

by suffusion and the inter-granular void ratio has not been changed significantly. The peak friction angle decreased from 31.9 ° to 29.9 ° and the residual friction angle decreased from 29.3 ° to 27.8 °. Thus, the observed decrease in strength may be attributed to the loss of fine particles. This implies that for denser coarse skeleton (beyond a certain density of coarse granular assembly), the fine particles play an important role in the stress transfer, and a decrease in fines content, leading to a higher void ratio, weakens more the force chains. In terms of volumetric strains, the loss of fine particles led to a less contractant behavior of the eroded sample and the dilatancy angle increased slightly from 1.89 ° to 2.44 °.

Figure 4.26a illustrates the characteristic state line of non-eroded and eroded soils. It can be seen that the "hypothetical" different characteristic state lines of eroded soils appear to be located below the one corresponding to the non-eroded soils. Thus, the transition from contractant to dilatant behavior occurs in this case at a characteristic friction angle lower than that of the non-eroded soils.

From Figure 4.26b, the "hypothetical" different critical state lines of eroded soil seems

(a)

(b)

(c)
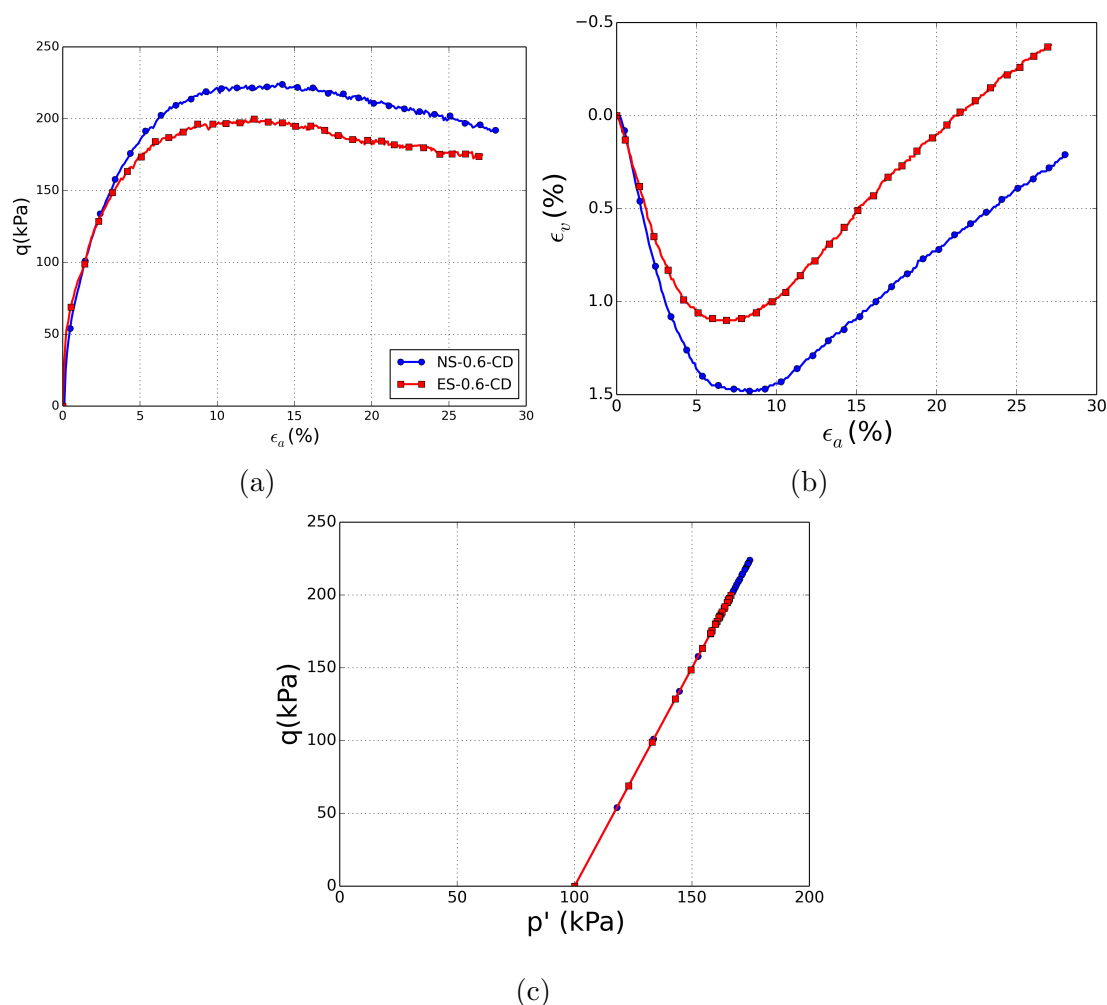
Figure 4.25: Comparison of the responses to drained triaxial compression of the non-eroded (NS-0.6-CD) and eroded (ES-0.6-CD) samples at an initial density Id = 0.6. (a) Deviator stress versus axial strain; (b) Volumetric strain versus axial strain (c) Deviator stress versus mean effective stress.

also to be situated below that of the non-eroded soil. Hence, the failure of eroded soils may occur at a lower friction angle (28.2 ° instead of 29.3 °).

Finally, it can be concluded that in case of eroded samples, generally, the mechanical characteristics change with the erosion process and the modification of the state parameters in terms of void ratios and fines content. The shear strength decreases after erosion, except in the case of ES-0.2-CD where the shear strength was not affected. Moreover, volumetric deformations become more dilatant, which may be attributed to the decrease in the inter-granular void ratio and to the less compressible material due to the loss of fine particles. Furthermore, the fact that the eroded soil becomes highly heterogeneous should be taken into account. The eroded soil may be composed of different zones with different properties. Some zones may have higher strength than other zones which may lead to original behavior once sheared, such as decrease, increase or even maintaining the shear strength of the soil with a more dilative volumetric deformations even if the shear strength decreases.
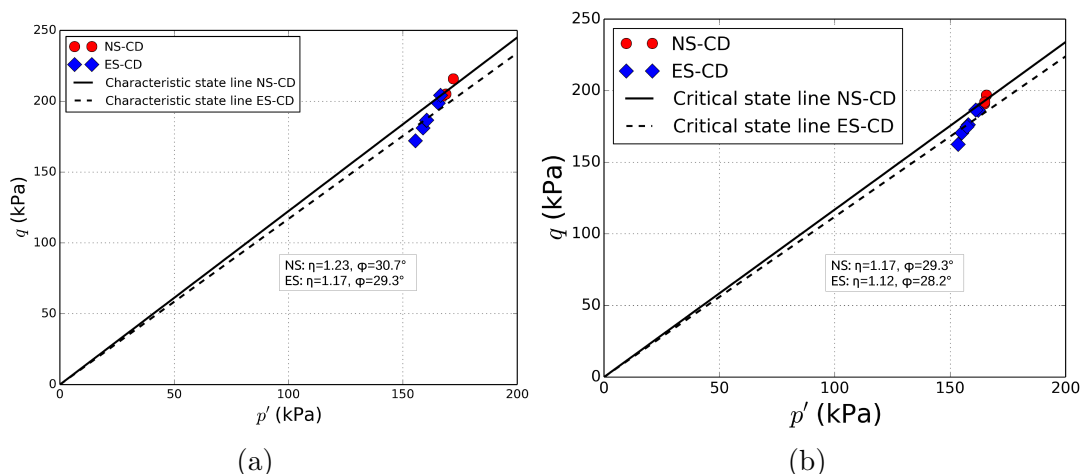
Figure 4.26: (a) Characteristic state line and (b) critical state line of eroded and non-eroded soil samples.

4.5.2 Undrained behavior of non-eroded and eroded soils

This section presents the results of the undrained triaxial compression tests which are summarized in Tables 4.5 and 4.6.

Sample name	FC %	e_0	e_{g0}	e_c	e_{gc}	φ_{FL} (°)	φ_{PT} (°)
NS-0.2-CU	25	0.58	1.10	0.58	1.10	29.8	29.2
NS-0.4-CU	25	0.53	1.04	0.53	1.04	29.03	30.3
NS-0.6-CU	25	0.48	0.97	0.49	0.99	30.3	30.9

Table 4.5: Summary of the undrained triaxial compression results on non-eroded soil samples; (φ_{FL} is the friction angle at failure and φ_{PT} is the friction angle at the phase transformation point).

Soil sample	M_e (%)	FC_f (%)	Id_f	ϵ_v (%)	e_{er}	e_{ger}	e_{er-c}	e_{ger-c}	φ_{FL} (°)	φ_{PT} (°)
ES-0.2-CU	52.05	13.78	0.02	8.86	0.65	0.91	0.65	0.91	28.2	30.8
ES-0.4-CU	47.7	14.85	≈ 0	4.64	0.66	0.95	0.65	0.94	28.2	27.5
ES-0.6-CU	40.42	16.57	0.15	1.86	0.62	0.94	0.62	0.94	28.6	29.4

Table 4.6: Summary of the undrained triaxial compression results on eroded soil samples.

Undrained response of non-eroded soils

Three soil samples, namely NS-0.2-CU, NS-0.4-CU, and NS-0.6-CU are reconstituted at an initial relative density of 20 %, 40 % and 60 %. Thereafter, undrained triaxial compression tests were carried out. Figure 4.27 illustrates the mechanical behavior obtained on the three non-eroded soil samples. A typical mechanical response for medium-dense sands, characterized by a contractant behavior as a first step followed by dilatant behavior (strain hardeining), was observed in the three tests. However, the peak strength increases with

the increase in density. The lowest shear resistance was obtained for the loosest sample, NS-0.2-CU. It is important to point out that no marked strain softening was observed and, consequently, no instability line can be defined in the sense of Lade instability criterion (Lade (1992)). The excess pore water pressure (ΔU) in these tests shows a rapid increase in the beginning of loading until reaching a maximum value, less than the confining pressure (100 kPa) corresponding to the contractant phase, followed by an important decrease beyond an axial strain of 5 % when the dilatancy takes place. In the q-p' plane, the mean effective stress curves move to the left towards the origin of the axes (initial contractant phase), then they orient to the right (increase in the mean effective stress with the appearance of dilatant behavior).

The transition point from a contractant behavior to a dilatant one is called the phase transformation point according to Ishihara et al. (1975). This phase is defined at the point where the effective stress path changes its direction in the q-p' plane. Moreover, according to Lade & Ibsen (1997), the phase transformation state observed in undrained tests is similar to the characteristic state observed in a drained test. Hence the two states should be identical. For the undrained test, the phase transformation state can be determined

(a)   (b)

(c)
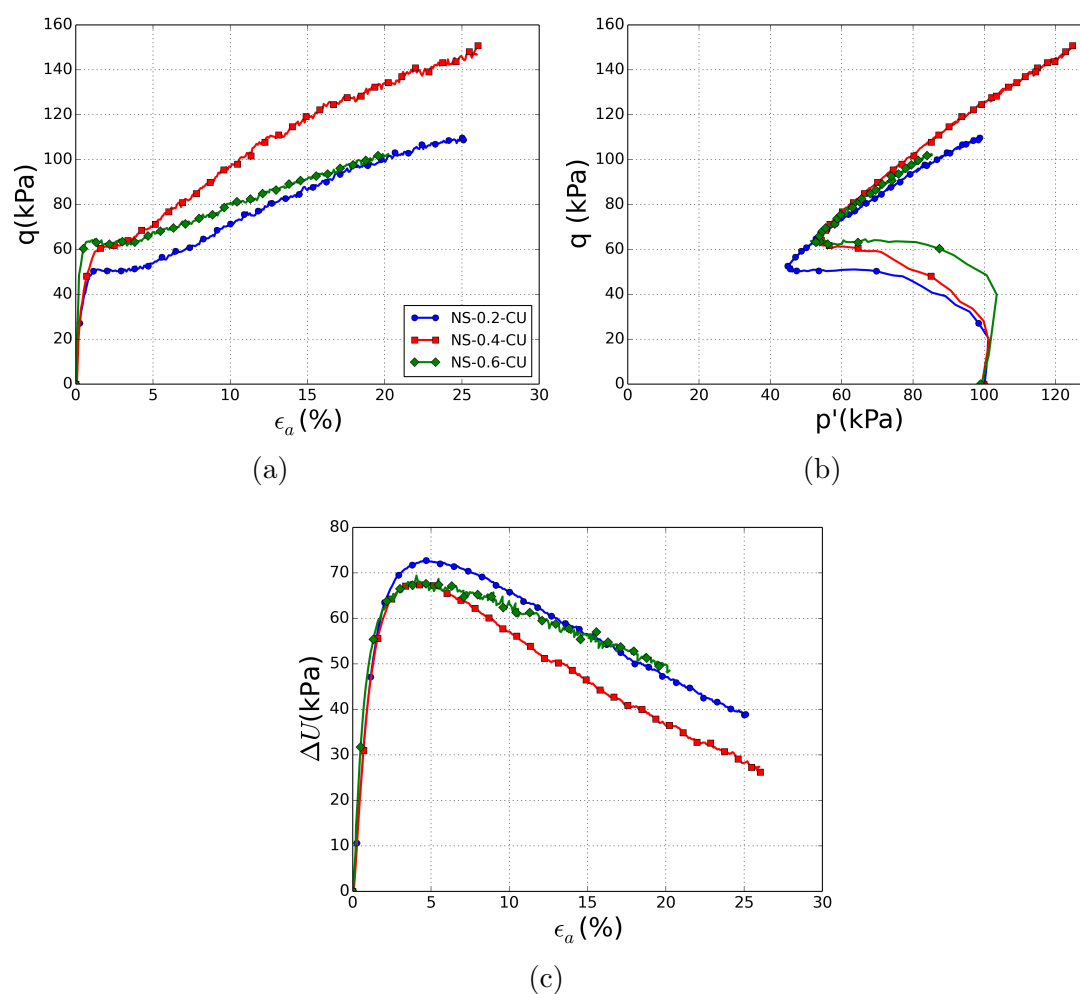
Figure 4.27: Responses to undrained triaxial compression tests of soil samples reconstituted at different initial densities (Id = 0.2; 0.4; 0.6) (a) Deviator stress vs. axial strain; (b) Deviator stress vs. mean effective stress; (c) Pore water pressure vs. axial strain.

either at the minimum value of the mean effective stress in q-p' plane or at the maximum value of the excess pore water pressure. The phase transformation angle in our experiment is 29.2 ° for NS-0.2-CU, 30.3 ° for NS-0.4-CU and 30.9 ° for NS-0.6-CU. The phase transformation points for each relative density as well as the corresponding characteristic state obtained from the drained tests were reported in Figure 4.28a. It can be seen that all points are linked by a common straight line, implying that the characteristic state/phase transformation angle is almost the same for the three specimens, irrespective of the initial density, whose value is around 30.2 °.

Furthermore, in order to determine the friction angle at failure, all points corresponding
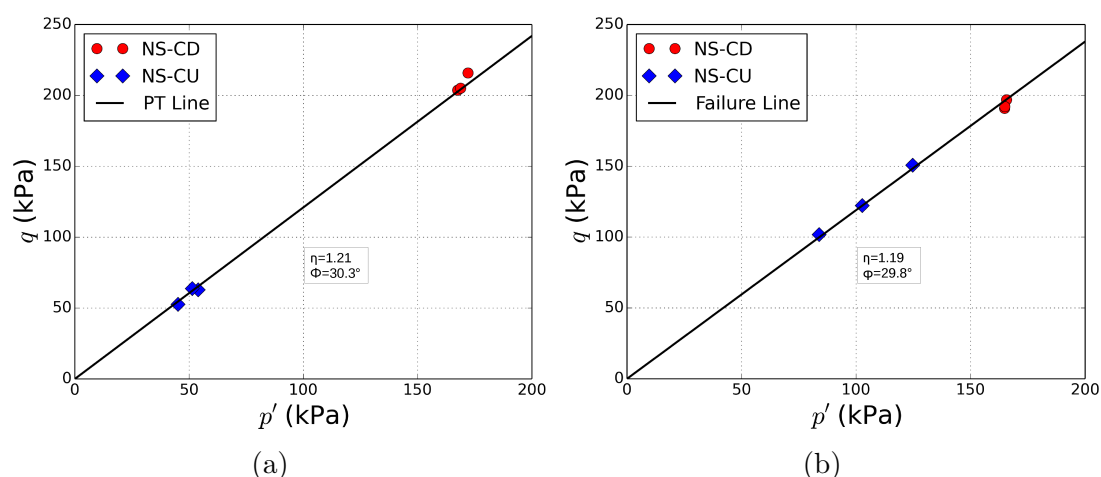
Figure 4.28: (a) Phase transformation line and (b) failure line of non-eroded soil samples.

to the critical state obtained from the different densities were reported in q-p' plane. Notice that these points were taken at the final stable state which forms a straight line passing by the origin in q-p' path. It is clear that all samples have similar failure lines as shown in Figure 4.28b. Moreover, the points obtained at the critical state from the drained tests were also reported on Figure 4.28b for comparison. It is found that the failure line of undrained tests fits well these points. Hence, the drained and undrained sheared samples exhibit the same critical state irrespective of the density and type of loading, which is in accordance with the critical state theory.

Undrained response of eroded soils at different densities

To investigate the mechanical behavior of eroded soil, soil samples prepared at different initial densities (Id=0.2, 0.4, 0.6) were first eroded and then subjected to undrained triaxial compression tests. Results are plotted on Figure 4.29 in terms of stress-strain curves, effective stress path and excess pore water pressure versus axial strain. As observed previously, for the undrained behavior of the non-eroded soil, a typical mechanical response for medium-dense sand, contractant behavior followed by dilatant one, was exhibited by the three eroded samples. Quantitatively, the deviator stress shows that the shear strength is slightly higher for ES-0.4-CU and ES-0.6-CU than that of ES-0.2-CU, although the latter has the same density as ES-0.4-CU. Again, the initial density is not the suitable parameter in such comparison. The explanation of this tendency should take into account the combined effect of the fines content and inter-granular void ratio, as pre-

sented in Section 4.5.1. In fact, ES-0.2-CU has the lower inter-granular void ratio, hence a denser skeleton, but its fines content is much lower than that of ES-0.4-CU and ES-0.6-CU.

The phase transformation points were reported on Figure 4.30a. It is interesting to note

(a)

(b)

(c)
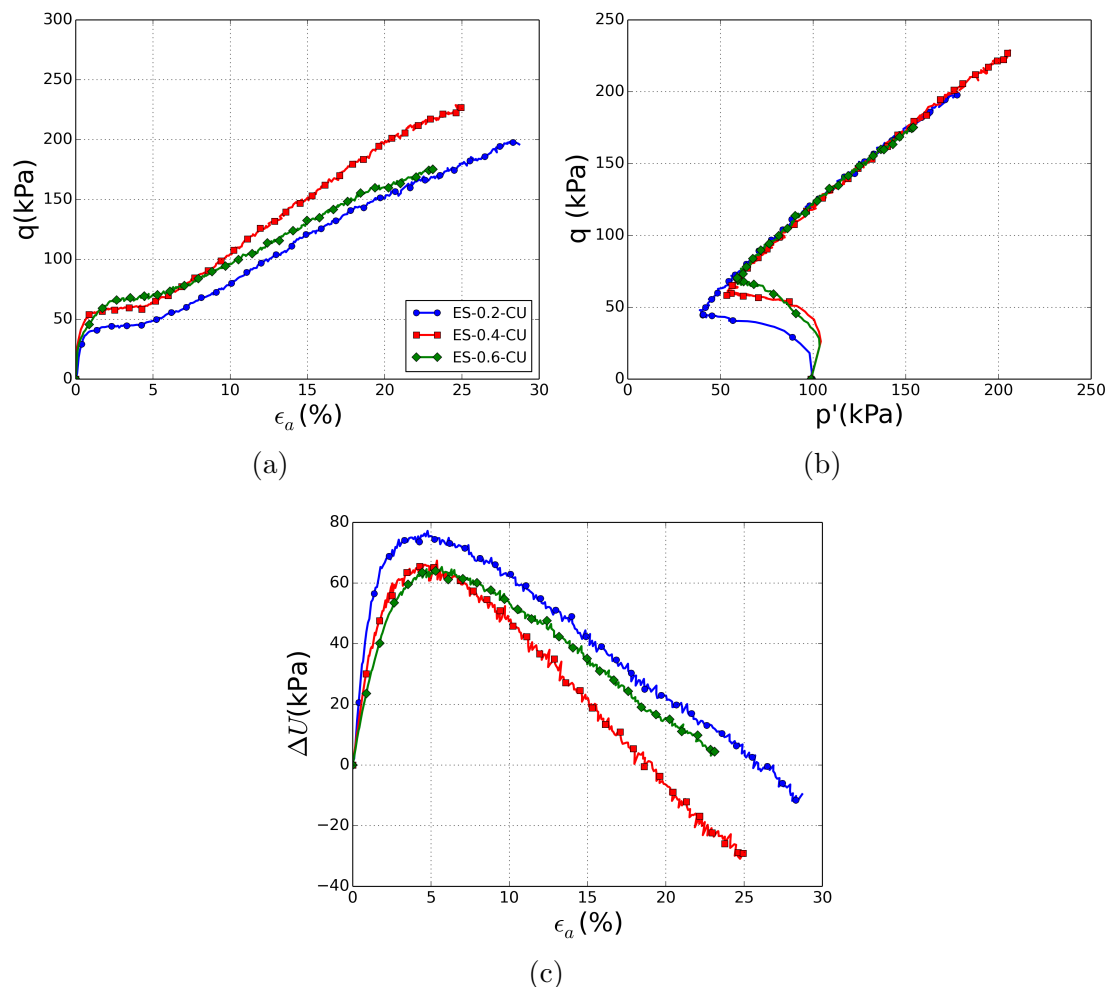
Figure 4.29: Responses to undrained triaxial compression tests of eroded soils at different initial densities. (a) Deviator stress vs. axial strain; (b) Deviator stress vs. mean effective stress; (c) Pore water pressure vs. axial strain.

that a unique phase transformation line is obtained. Regarding the critical state line presented in Figure 4.30b, it can be observed that this one is unique, which could be surprising because the erosion, by changing the fines content of soil, creates a new material with a new mechanical characteristics as demonstrated by several studies. However, as postulated in the drained section, the critical state line is usually unique in q-p' plane irrespectively of fines contents, especially when the coarse and fine particles have the same characteristics (grains shape, mineralogy, etc...). Consequently, this point, however, needs more investigations such as determining the critical state line in e-logp' plane (Which is not possible here due to the lack of data).
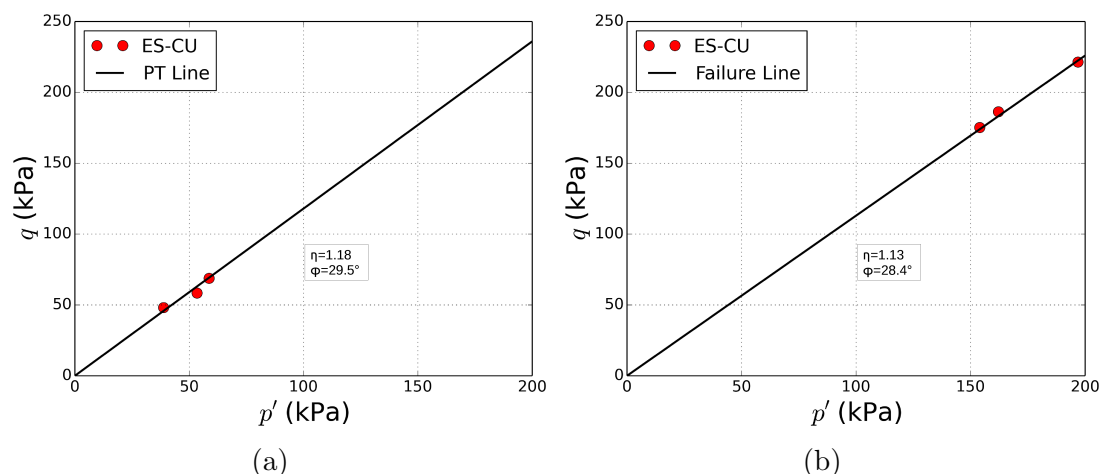
Figure 4.30: (a) Phase transformation line and (b) failure line of eroded soil samples.

Comparison of undrained response of non-eroded and eroded soil

Figures 4.31, 4.32 and 4.33 show that eroded soil samples have the same stress-strain response as the non-eroded ones, i.e. contractant-dilatant behavior. Although the inter-granular void ratio becomes smaller giving a denser coarse skeleton after erosion, the eroded samples have lower shear strength at small and medium strains. This is due to the significant loss of fine particles, which was not compensated by a decrease in the inter-granular void ratio. The non-eroded samples have a higher inter-granular void ratio, meaning a looser soil skeleton. However, their fines content which approximates the threshold makes the fine particles participating much more in stress transfer and soil strength. Beyond an axial strain of about 5 %, eroded soil samples exhibit higher shear strength with a rapid decrease in the excess pore water pressure. This is attributed to the dilatancy development which is more important than in the case of non-eroded soil. One should note the analogy between the evolution of the excess pore water pressure under undrained conditions and the volumetric strains under drained ones.

From the phase transformation lines presented on Figure 4.34a, it can be seen that these lines are almost the same for the eroded and non-eroded soils. Regarding the critical state line, Figure 4.34b shows that both eroded and non-eroded samples have a unique critical state line but not the same one. In fact, the critical state line of eroded soils is located below the non-eroded one and the critical friction angle is about 28.4 °, slightly lower than that of the non-eroded one which is 29.3 °.
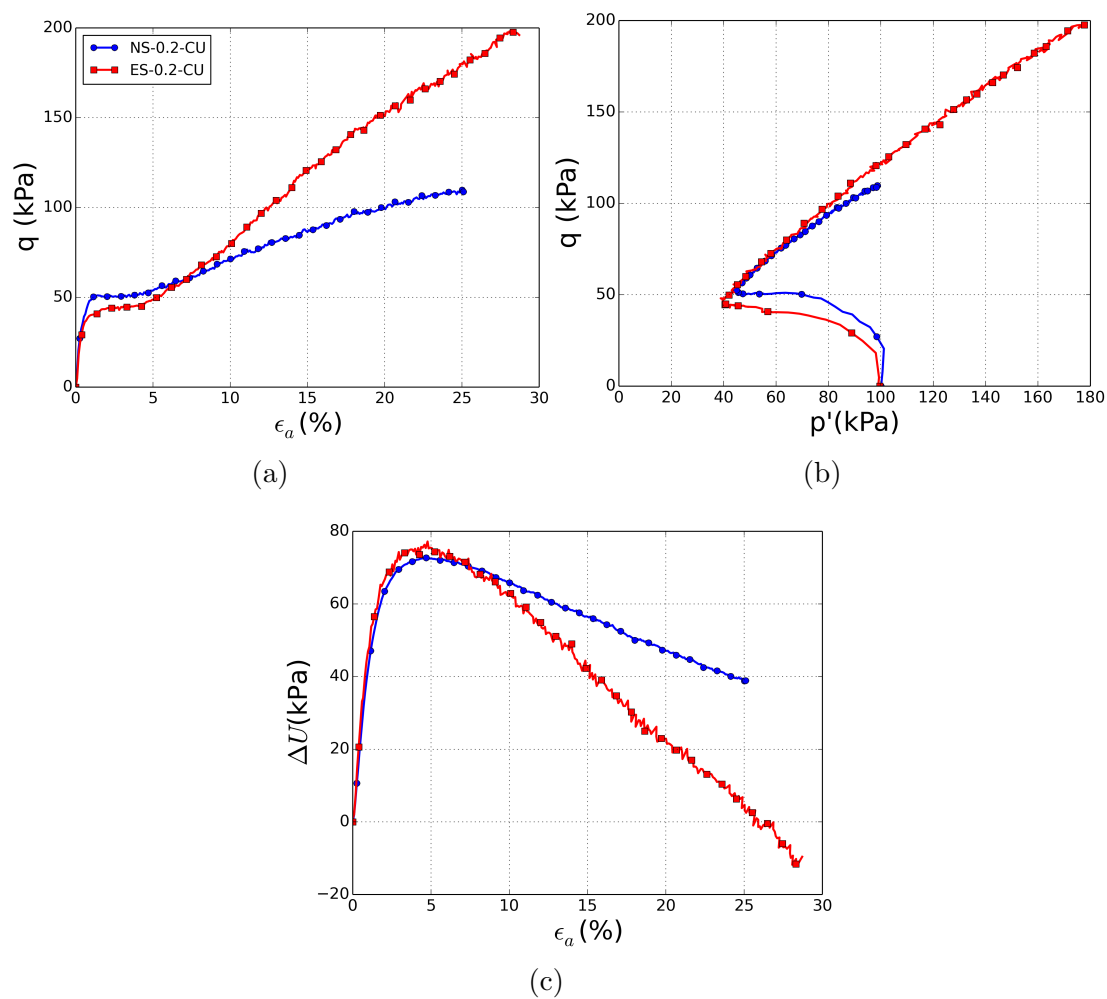
Figure 4.31: Comparison of the responses to undrained triaxial compression tests of the non-eroded (NS-0.2-CU) and eroded (ES-0.2-CU) samples at an initial density Id = 0.2 (a) Deviator stress vs. axial strain; (b) Deviator stress vs. mean effective stress; (c) Pore water pressure vs. axial strain.
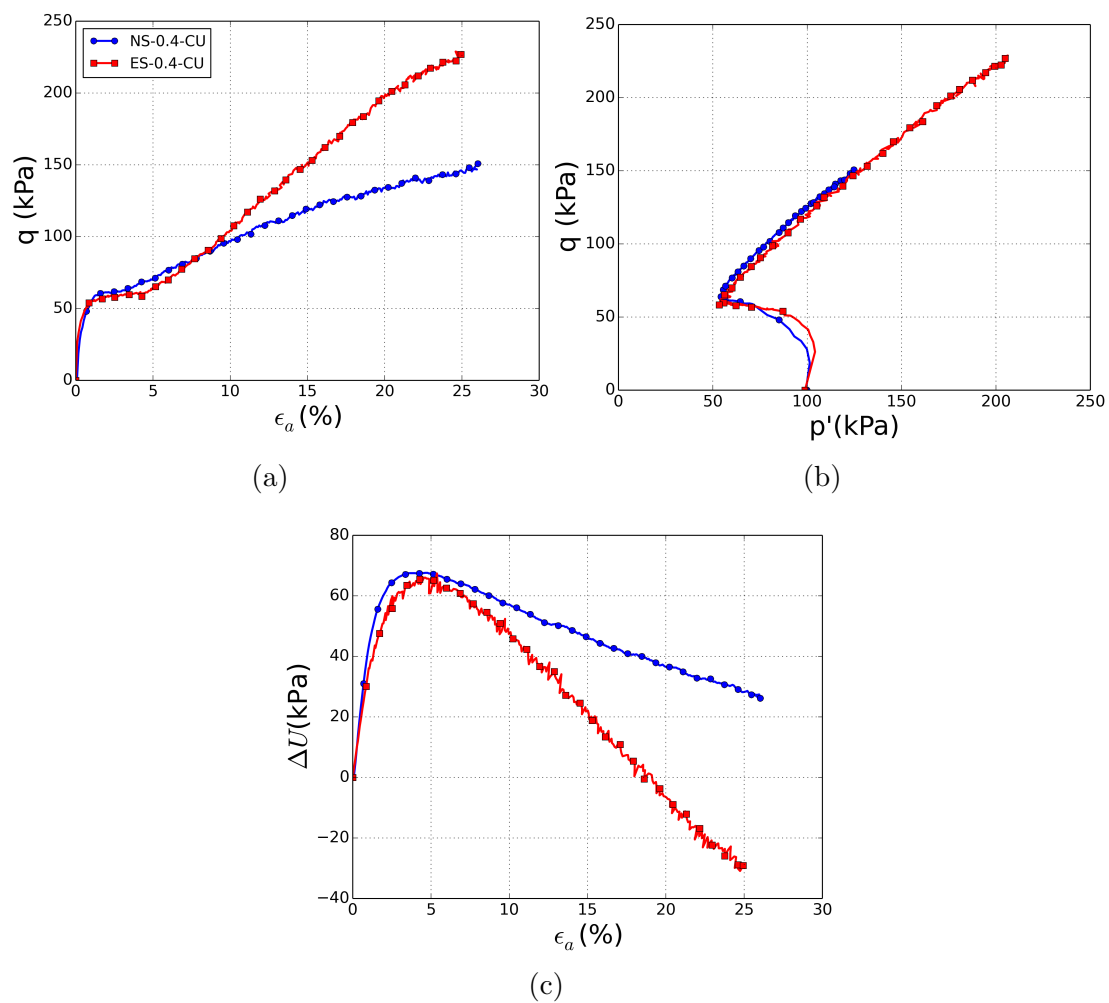
Figure 4.32: Comparison of the responses to undrained triaxial compression tests of the non-eroded (NS-0.4-CU) and eroded (ES-0.4-CU) samples at an initial density Id = 0.4 (a) Deviator stress vs. axial strain; (b) Deviator stress vs. mean effective stress; (c) Pore water pressure vs. axial strain.

(a)   (b)

(c)
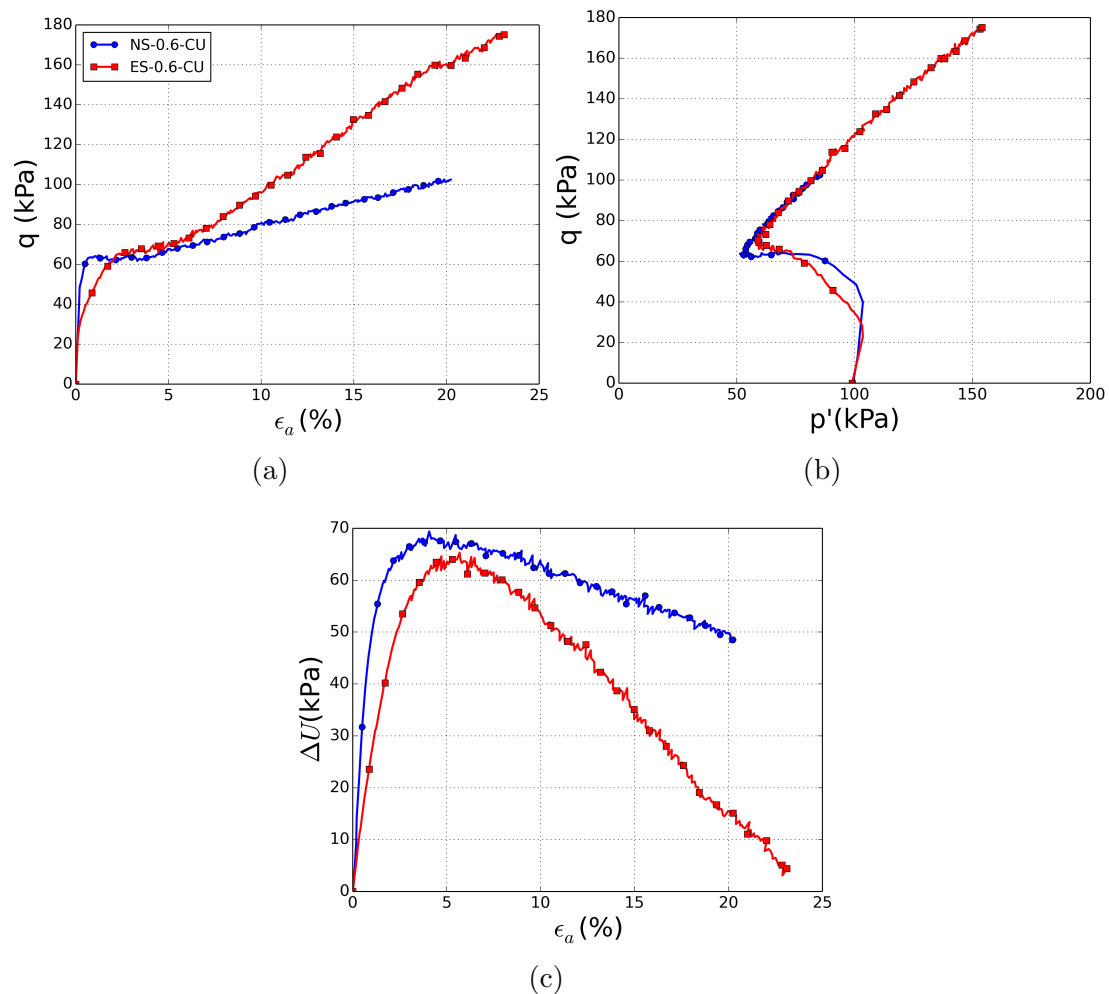
Figure 4.33: Comparison of the responses to undrained triaxial compression tests of the non-eroded (NS-0.6-CU) and eroded (ES-0.6-CU) samples at an initial density Id = 0.6 (a) Deviator stress vs. axial strain; (b) Deviator stress vs. mean effective stress; (c) Pore water pressure vs. axial strain.

(a)   (b)
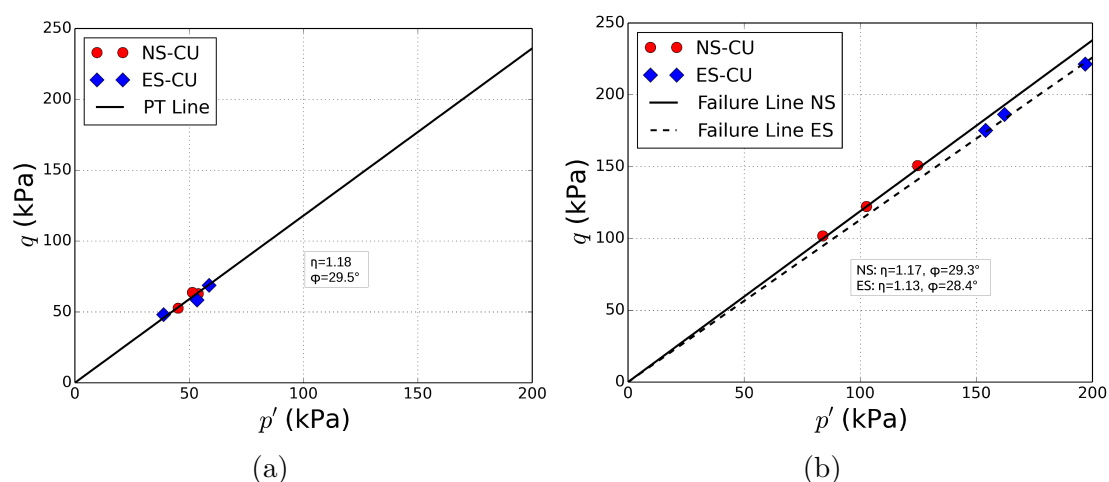
Figure 4.34: (a) Phase transformation line and (b) failure line of eroded and non-eroded soil samples.

4.5.3 Synthesis on shear strength and critical state analysis

Shear strength

From the previous experimental data and analysis of the mechanical behavior of non-eroded and eroded soils subjected to drained and undrained triaxial compression tests, an approach to predict the mechanical response of eroded soils is proposed below.

Comparison of the shear strength of the non-eroded soils and the eroded ones is expressed in terms of the difference between the stress ratio at the peak, $\Delta\eta_p$ ($\eta_p = \frac{q_p}{p'_p}$, where q_p and p'_p are respectively the peak stress deviator and the corresponding mean effective pressure). The evolution of $\Delta\eta_p$ versus the difference of the void volumetric variation between the eroded samples and the non-eroded ones, δ, is plotted in Figure 4.35.

δ is defined as follows:
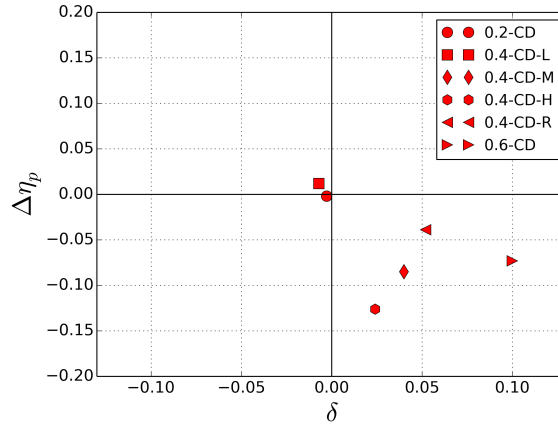
Figure 4.35: The evolution of $\Delta\eta_p$ versus the difference of the void volumetric variation between the eroded and the non-eroded soil samples.

$$\delta = \frac{V_{vES} - V_{vNS}}{V_g} \tag{4.1}$$

where V_{vES} and V_{vNS} are the volumes of the voids of eroded and non-eroded samples respectively and V_g is the volume of coarse grains.

The expressions of the void ratio (e), the inter-granular void ratio (e_g) and fines are:

$$e = \frac{V_v}{V_s} = \frac{V_v}{V_g + V_f} \tag{4.2}$$

$$e_g = \frac{V_v + V_f}{V_g} \tag{4.3}$$

$$FC = \frac{V_f}{V_g + V_f} \tag{4.4}$$

where V_v is the volume of voids and V_f is the volume of fines.

Hence,

$$\frac{V_f}{V_g} = \frac{FC}{1 - FC} \tag{4.5}$$

$$e_g = \frac{e + FC}{1 - FC} \tag{4.6}$$

The erosion is associated to the wash out of the fine particles; i.e. the decrease in the fines content. V_g is assumed to be constant as the erosion of the coarse particles is prevented.

$$V_v = eV_s = e(V_g + V_f) = \frac{eV_g}{1 - FC} \tag{4.7}$$

By dividing V_v by V_g, the following dimensionless expression is obtained:

$$\frac{V_v}{V_g} = \frac{e}{1 - FC} \tag{4.8}$$

Consequently,

$$\delta = (\frac{e}{1 - FC})_{ES} - (\frac{e}{1 - FC})_{NS} \tag{4.9}$$

When δ is greater than 0, this means that the effect of the erosion process is dominant leading to an increase in porosity induced by the departure of fines, which is not compensated by the settlement; the mechanical response of the soil in this case may be strongly affected by the induced loosest state. The shear strength of the eroded soils is lower than that of non-eroded soil as demonstrated by the negative stress ratio at the peak, $\Delta\eta_p$, illustrated in Figure 4.35.

When δ is close to or smaller than 0, this means that the settlement due to erosion predominates and induces an increase in the soil skeleton's density. In this case, the shear strength of the eroded samples is almost preserved and the soil will behave like the non-eroded one.

The main interest in determining the parameter "δ" relies on the fact that it assesses whether the eroded soil will be more resistant or not compared to the non-eroded soil.

It is worth to note that the undrained tests are not presented in Figure 4.35. Indeed, it was difficult to conclude in this case as the results were contradictory. This might be due to the uncertainty in determining the stress ratio at the peak strength as practically none of the undrained samples exhibit a real or distinguishable peak. This point needs more investigations and experimental data. However, it is interesting to note that in undrained conditions, erosion appears to have less effect on shear strength in small and medium deformations. Up to 5% of axial strains (Figures 4.31 to 4.33), there is no large difference observed between eroded and non-eroded mechanical behavior.

Critical state analysis

To consider the mechanical behavior of non-eroded and eroded soils within the critical state framework, the critical state points of both eroded and non-eroded soil samples subjected to drained and undrained triaxial compression tests are plotted in $e - \log p'$ and $e_g - \log p'$ planes (Figure 4.36).

Although the data is not sufficient to draw the complete critical state lines, an interesting trend can be concluded. Figure 4.36a shows that the critical state points in $e - \log p'$
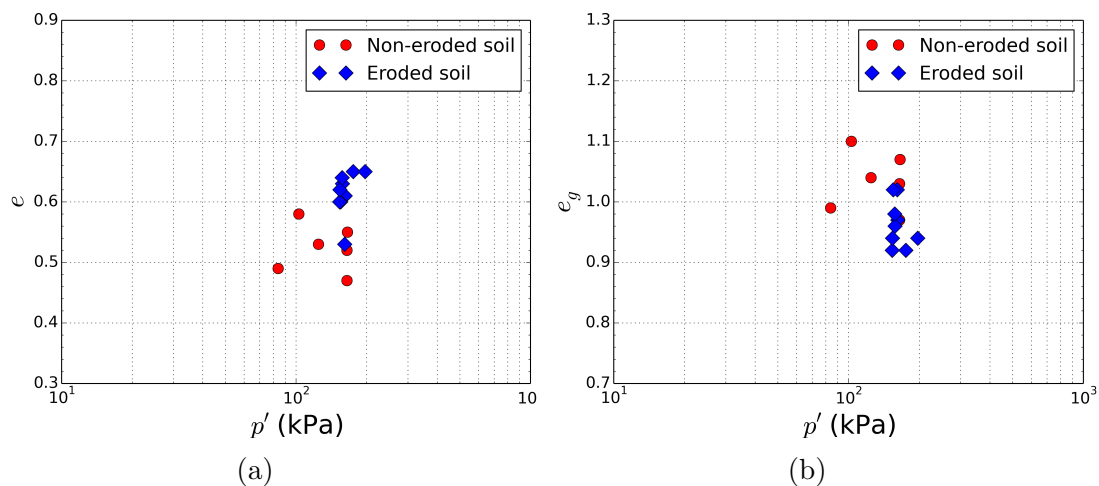
Figure 4.36: Evolution of the critical state points in (a) $e - log(p')$ plane and (b) $e_g - log(p')$ plane.

plane of eroded samples are located above that of the non-eroded ones. This means that the expected critical state lines of eroded soils would move upwards to a lower density, implying that for a given void ratio, the shear resistance at the critical state increases with the increase of erosion and the wash out of the fine particles.

Whereas, Figure 4.36b shows that in $e_g - \log p'$ plane, the critical state points of eroded samples are situated below that of non-eroded ones. In this case, the expected critical state lines would move downwards after erosion to a higher density. Since the internal friction angle at the critical state changed only slightly, the translation of the critical state line downwards implies that for a given inter-granular void ratio, the shear resistance at the critical state line decreases with the erosion of fine particles; i.e. the decrease of fines content. This trend has been also found by other researchers, such as for instance T. Nguyen (2014). However, in these studies, soil samples reconstituted with different fines contents were analyzed; i.e. without any erosion process. Thus, it seems interesting that similar conclusions were found concerning the effect of fines content on the critical state line performing suffusion tests leading to a loss of fine particles.

4.6 Conclusion

A new suffusion apparatus developed at IRSTEA has been used to investigate the seepage-induced internal instability in cohesionless soils. A novel feature of this apparatus is the freezing procedure followed to preserve the microstructure of the eroded soil which allows separate erosion and triaxial tests. Gap-graded mixtures reconstituted from different fractions of Hostun sand representing fine and coarse fractions with a fines content of 25 % were used in our experiments.

The testing program has been developed to: validate the apparatus; assess the effect of different flow velocities and the initial density on the degree of erosion; and generate data to investigate the influence of suffusion on hydraulic and mechanical properties of the soil.

The most important contributions of this research are summarized as follows:

- *Experimental techniques:*

  - The new permeameter makes it possible to recover the sample after erosion without disturbing it;

  - freezing the soil, after de-saturating it at very low rate up to a low water content, preserves the microstructure of soil specimens without any modifications in the mechanical behavior of the soil;

  - The suffusion results are consistent with each other with a very good repeatability;

- *Suffusion development:*

  - The eroded mass and the volumetric deformation increase with the flow velocity;

  - As the initial density increases, the settlement during suffusion decreases. Thus, the soil compaction during suffusion is more pronounced for the loosest samples; this is explained by the fact that the loose soil has a more metastable microstructure;

  - The final density depends on the variation of the voids volume, induced by the loss of fine particles and by settlement, before and after suffusion: when this variation is greater than zero, the density decreases as the erosion process is predominant; the loss of fines is not compensated by the settlement. Conversely, when the voids variation is smaller than zero, the soil skeleton density increases due to the predominance of the settlement. It is worth noting that the first case concerns the dense soil while the second case is observed in the loose soil.

- *Consequences of suffusion on the mechanical behavior of the soil:*

  - Although the eroded soils show lower shear strength at peak and residual state, surprisingly, they exhibit a less contractant behavior that cannot be explained only by the change in density or void ratio which go against the gain in dilatancy. Combined effect of the global void ratio, inter-granular void ratio and fines content should be considered, as well as the geometric rearrangement of the soil particles which require further investigations such as the use of visualization techniques; In fact, it appears that suffusion induces heterogeneities which may lead to decrease, increase or even conservation of the shear strength of eroded soils depending on the induced micro-structural modifications;

  - When the change of the void volume is positive, the shear strength of the eroded soils appears to be lower than that of the non-eroded soils as demonstrated by the negative change in the stress ratio at the peak presented in Figure 4.35. It is interesting to note that the dense soil exhibits the more increase in the voids volume (less compaction) leading to a significant decrease of its shear strength even if its initial density was high. It should be pointed out that the voids volume is related to the variation of the void ratio, inter-granular void ratio and fines content implying that the combined effect of these parameters is considered.

– The decrease of the voids volume after erosion (negative) allows the eroded soil to preserve its mechanical properties. This tendency is observed for the loose samples which have more ability to compact during erosion process.

– The loss of shear strength for the eroded soils seems to be more important under drained triaxial conditions. When sheared under undrained loading, the mechanical shear strength of eroded soils appears not to be influenced significantly by erosion, particularly at small and medium deformations.

– There is no effect of erosion on the phase transformation of eroded and non-eroded soils under undrained conditions; both have the same phase transformation line. However, a slight difference was observed for the eroded soils under drained shearing regarding the characteristic line.

– The critical state line in $e - \log p'$ (hence the crtical friction angle) of non-eroded soil samples in drained and undrained conditions is the same. Similarly, eroded soil samples exhibit the same critical state line in drained and undrained conditions. However, the critical state line of eroded soils compared to the non-eroded ones is slightly lower.

– Although the data are not sufficient to express the complete critical state lines in $e - \log p'$ and $e_g - \log p'$ planes, an interesting trend was found regarding the critical state of eroded and non-eroded soils. The location of the critical state points of eroded smaples above that of non-eroded ones in $e - \log p'$ implies that the shear resistance at the critical state for a given void ratio increases with the increase of erosion and the loss of the fine particles. Whereas, in $e_g - \log p'$ plane, the critical state points of eroded samples are situated below that of the non-eroded ones indicating that for a given inter-granular void ratio, the shear resistance at the critical state decreases with erosion of fine particles; i.e. the decrease of the fines content. These results are in agreement with studies done on samples reconstituted with different fines contents.

Chapter 5

Numerical description of suffusion and its consequences on the soil mechanical behavior

5.1 Introduction

In the preceding chapters, two approaches have been defined to investigate the initiation and development of suffusion and to analyze the effect of this phenomenon on the mechanical behavior of the soil. Chapter 3 was dedicated to the definition of a numerical extraction procedure and its application on a narrow gradation. Chapter 4 presented the experimental approach based on an original permeameter. The experimental study provided some data that can be used to calibrate and validate the numerical model. Therefore, in this chapter, the previously defined numerical extraction procedure will be applied on a wider gradation similar to that used experimentally.

Section 5.2 of this chapter presents the calibration process of the numerical model to describe the experimental results. Then, in Section 5.3, the numerical extraction procedure is applied on a grain size distribution similar to that used experimentally. A combined analysis of the suffusion results is given by comparing both the experimental and the numerical data. Thereafter, two propositions are presented in Section 5.4 in order to investigate some possible causes of discrepancy between the numerical and the experimental data: the definition of a heterogeneous extraction procedure; and the attribution of different mechanical properties to the fine and the coarse grain fractions, respectively. In addition to that, the effect of the initial density on the suffusion development and therefore on the mechanical behavior of the soil is investigated as well in Section 5.4. Finally, Section 5.5 concludes the main outcomes of this chapter.

5.2 Calibration of the numerical model

Before starting the erosion process, the numerical model is calibrated to reproduce the mechanical behavior of the virgin soil (i.e. the non-eroded soil) as characterized experimentally. In this section, the material used for the numerical soil samples is given and a representative elementary volume is defined. Then, the calibration of the mechanical response of the soil to a drained triaxial compression test is presented.

5.2.1   Material used

An objective of this work is to simulate the mechanical behavior of a soil with a wide particle size distribution, similar to those used experimentally. In Chapter 3, a narrow gradation was used to assess the numerical extraction procedure. Similarly, in other numerical studies (see for instance Muir Wood et al. (2010); Scholtès et al. (2010)), narrow gradations or gradations with a low fines content were used, which are far from internally unstable soils tested in the laboratory. However, to study numerically the suffusion problem, it is essential to use a numerical soil similar to internally unstable ones.

In Chapter 4, different fractions of Hostun sand were used to reconstitute internally unstable soil samples. The resulting particle size distribution corresponds to a gradation whose $\frac{D_{max}}{D_{min}} = 25$ with a fines content of 25 % (D_{max} and D_{min} are respectively the biggest and the smallest diameters of the PSD). This gradation, however, requires a high number of discrete elements which results in a very high computational time. Therefore, a simplified particle size distribution is defined, PSD-Simplified, where the PSD is modified by removing particles whose diameter is larger than 2 mm and those whose diameter is smaller than 0.3 mm. Thus, $\frac{D_{max}}{D_{min}}$ decreases to 6.67. To make sure that this modification does not have a significant effect on the results, the real gradation, PSD-Real, is also used to model one of the soil samples. The results using each gradation are then compared. This comparison serves to study the effect of the particle size distribution on the suffusion outcomes. Both gradations are presented in Figure 5.1.
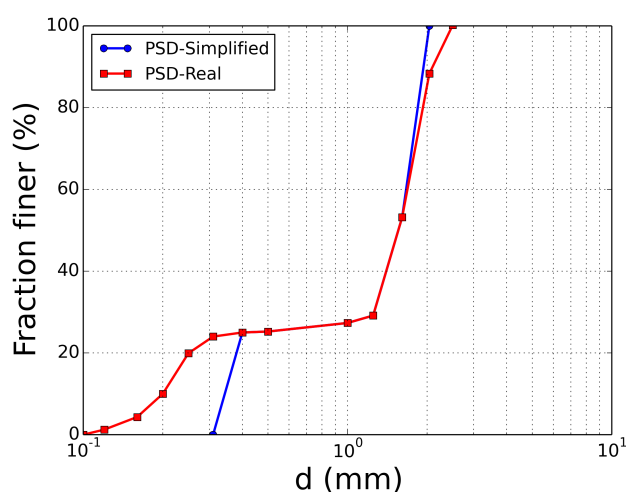
Figure 5.1: Real and modified particle size distribution from different size fractions of Hostun sand.

5.2.2   Choice of a representative elementary volume and calibration of the numerical model

Two particle size distributions are used in this chapter. In each case, a representative elementary volume should be defined. In what follows different REVs are used in the case of PSD-Simplified. Either 50,000 or 100,000 or 200,000 spheres are used. In the case of 50,000 and 100,000 spheres, different randomly generated granular assemblies will be considered and the average of the results will also be considered:

- in the case of 50,000 spheres, four samples are generated: DEM-NS50-1 to DEM-NS50-4; and the average response is named DEM-NS50-A.

- in the case of 100,000 spheres, three samples are generated: DEM-NS100-1 to DEM-NS100-3; and the average response is named DEM-NS100-A.

- for the granular assembly of 200,000 spheres, only one randomly generated assembly is considered, DEM-NS200, due to limitations related to the expensive computational cost.

- finally a sample with 200,000 spheres involving the real gradation has also been considered, it is named DEM-NS200-PSD_Real.

All soil samples have a fine fraction of 25 %. Under a confining pressure of 100 kPa, the ratio of the total number of rattlers to the total number of fine particles is 95 % for the simplified PSD and 99 % for the real PSD.

The discrete models with the different reconstituted soil samples have been calibrated from a triaxial compression test (NS-0.4-CD) performed on a soil sample with an initial relative density of 40 % and with a confining pressure $P_c = 100\ kPa$. The parameters identified by this calibration are given in Table 5.1 (chosen identical for both fine and coarse particles as there was no experimental characterization done separately). Figures 5.2 and 5.3 show the responses of the two calibrated samples using 50,000 and 100,000 particles respectively, compared to the experimental results. Using 50,000 spheres leads to more scattered results than 100,000 spheres. Nevertheless, the average response is very close to the experimental data. Figure 5.4 sums up all the simulation results (including those with 200,000 particles with the simplified and real PSD) compared to the experimental one.

The calibration showed that all soil samples of different number of particles using the case
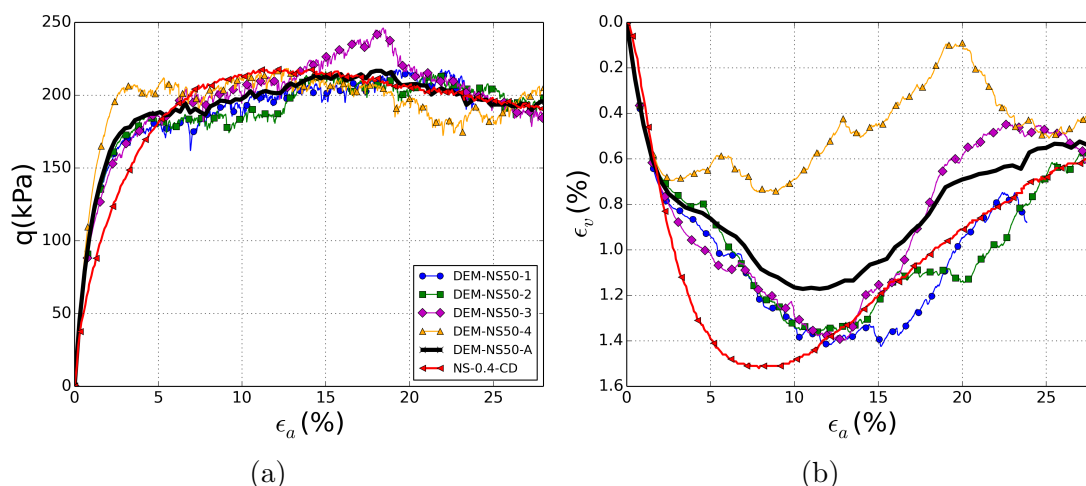
Figure 5.2: Comparison between the experimental drained triaxial compression test and DEM simulations of different granular packings with 50,000 spheres.

of PSD-Simplified or PSD-Real show a similar stress-strain response as the experimental results. The resulting residual friction angle (φ_0) is very close to the experimental one (29.2 °). However, the experimental results show a small peak in the stress-strain curve
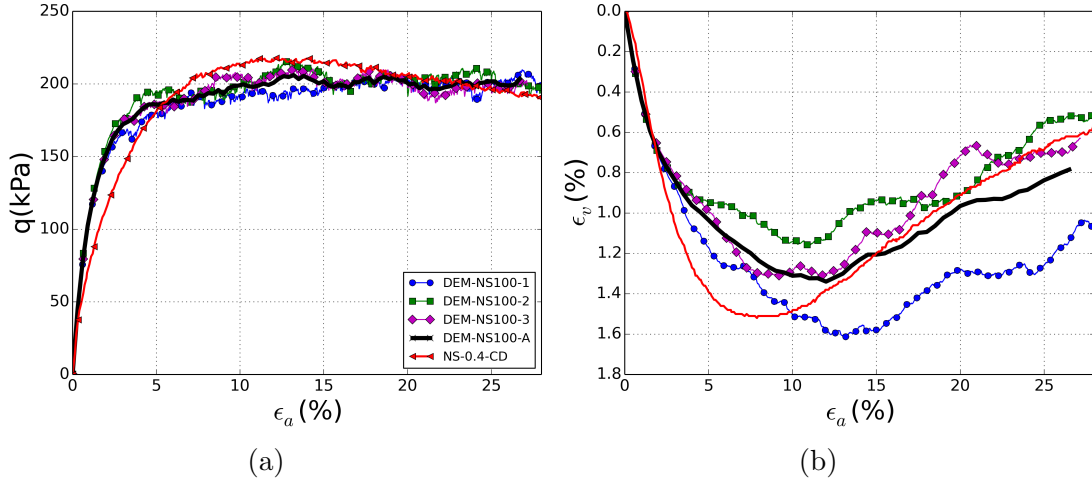
Figure 5.3: Comparison between the experimental drained triaxial compression test and DEM simulations of different granular packings with 100,000 spheres.
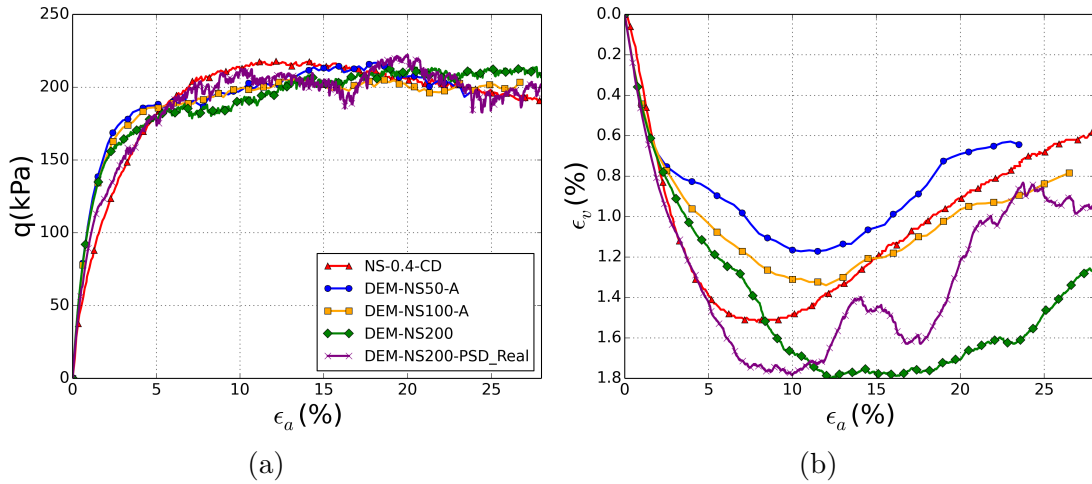
Figure 5.4: Comparison between experimental drained triaxial compression test and DEM simulations of different granular assemblies.

E_c (kPa)	α_s	φ_c during compaction (°)	φ_c after compaction (°)	α_r	η_r
$2\ 10^8$	0.2	18	30	7.5	0.2

Table 5.1: Summary of the calibrated parameters.

which is not obtained numerically. Table 5.2 gives the data of all soil samples confined at 100 kPa. All samples generated using the simplified gradation, have a similar void ratio (≈ 0.45). However, the soil sample generated using the real PSD has even a smaller void ratio (0.37). In all cases, the experimental soil sample is slightly looser (e_0=0.53) than the numerical ones, but as seen in Chapter 2, there is no particular reason, according to the followed calibration process, that the numerical void ratio is identical to the "real" one.

The volumetric deformations are also shown in Figure 5.4. The data is more scat-

Sample name	e	e_g	e_{eq}	φ_p (°)	φ_0 (°)
DEM-NS50-1	0.45	0.92	0.89	30.71	30.71
DEM-NS50-2	0.45	0.94	0.91	31.04	28.92
DEM-NS50-3	0.45	0.94	0.91	33.17	28.76
DEM-NS50-4	0.45	0.93	0.90	31.01	29.31
DEM-NS50-A	**0.45**	**0.93**	**0.90**	**31.34**	**29.38**
DEM-NS100-1	0.45	0.94	0.91	29.41	29.41
DEM-NS100-2	0.45	0.93	0.90	30.25	30.25
DEM-NS100-3	0.45	0.93	0.90	29.86	29.86
DEM-NS100-A	**0.45**	**0.93**	**0.90**	**29.96**	**29.96**
DEM-NS200	**0.45**	**0.94**	**0.90**	**30.85**	**30.85**
DEM-NS200-PSD_Real	**0.37**	**0.81**	**0.82**	**29.55**	**29.55**
NS-0.4-CD	**0.53**	**1.04**	**-**	**31.4**	**29.2**

Table 5.2: Summary of the non-eroded soil properties (note that φ_p and φ_0 are respectively the peak and the residual friction angles).

tered from one simulation to another. However, the same tendency is reproduced in all cases. Therefore, using the simplified gradation, results show that soil samples prepared using 50,000, 100,000 or 200,000 spheres exhibit similar behavior. Hence, a representative elementary volume of 100,000 spheres is considered in what follows. It is a compromise between a large number of particles in the case of 200,000 spheres and a large scattering in data in case of 50,000 spheres. Therefore, the numerical extraction procedure will be applied on DEM-NS100-A (considering the three randomly generated packings) and DEM-NS200-PSD_Real.

5.3 Numerical description of suffusion and its induced mechanical effects

Having calibrated the numerical parameters to reproduce the experimental results of a drained triaxial compression test, this section presents the results of the suffusion-like simulations compared to the experimental data. The effect of suffusion on the mechanical properties of the soil is then highlighted by simulating drained triaxial compression tests on eroded soil samples.

The numerical extraction procedure is done in a way to mimic the experimental test. Experimental suffusion tests were done without initial confinement. The soil sample was reconstituted in a plexiglass cylindrical cell. The walls, though, may have exerted

small confining pressure on the soil. Hence, numerically, the soil sample is first confined up to a low confining pressure of 5 kPa. Then, suffusion-like simulations start from that equilibrium isotropic state. Thereafter, similar to the experimental procedure, the soil sample is confined up to 100 kPa and drained triaxial compression tests are carried out.

Table 5.3 gives the properties of each soil sample confined at 5 kPa just before erosion. Notice that, DEM-NS100-A has a slightly smaller void ratio (0.46) than the experimental one (0.53). DEM-NS200-PSD_Real has even a smaller void ratio of 0.41. Moreover, numerically the inter-granular void ratio is also smaller than the experimental one. Thus, numerical soil samples are slightly denser. The equivalent inter-granular void ratio, e_{eq}, is also calculated in the numerical soil samples. Table 5.3 shows that $e_{eq} \approx e_g$. In fact, almost all fine particles are rattlers (97.28 % of the fines in DEM-NS100-A and 99.67 % in DEM-NS200-PSD_Real under a confining pressure of 5 kPa) which explains why $e_{eq} \approx e_g$. We recall that e_g is calculated by considering all fine particless as voids and e_{eq} is calculated by considering only inactive fine particles as voids (as defined in Chaper 2, Section 2.4.2).

Soil sample	P_c (kPa)	% of small rattlers	FC_0 (%)	e_0	e_{g0}	e_{eq0}
DEM-NS100-1	5	97.41	25	0.47	0.97	0.95
DEM-NS100-2	5	97.23	25	0.47	0.96	0.94
DEM-NS100-3	5	97.19	25	0.45	0.94	0.93
DEM-NS100-A	**5**	**97.28**	**25**	**0.46**	**0.96**	**0.94**
DEM-NS200-PSD_Real	**5**	**99.67**	**25**	**0.41**	**0.88**	**0.88**
NS-0.4-CD	**-**	**-**	**25**	**0.53**	**1.04**	**-**

Table 5.3: Characteristics of soil samples confined at 5 kPa before the initiation of suffusion.

5.3.1 Validation of the extraction procedure and modification of the transport criterion

The numerical extraction procedure was first applied on sample DEM-NS100-1. Almost all fine particles are rattlers in the numerical model (about 97 % of all small particles). According to the detachment criterion, these particles are well detected as detached. Thus, the only condition in their erosion is the transport criterion. Let us recall the transport condition: detached particles should be smaller than D_{c35} (the constriction size for which 35 % of the constrictions of the granular assembly are finer than this size). Figure 5.5 presents the eroded mass in the numerical soil sample versus Darcy's velocity, compared to the experimenal one. Note that, in the numerical erosion tests, the hydraulic gradient is controlled unlike the experimental test based on a flow-rate control system. Nevertheless, after applying numerically the hydraulic gradient, the pore flow velocity is calculated and Darcy's velocity is concluded. As the filtration of the fine transported particles, and thus clogging of the pore space, is not described by the model, the gradual increase by steps of the hydraulic gradient results also in a monotonous increase of the flow rate as imposed experimentally.

In the numerical sample, all fine particles were eroded ($\bar{M}_e = 100\%$, where $\bar{M}_e$ is
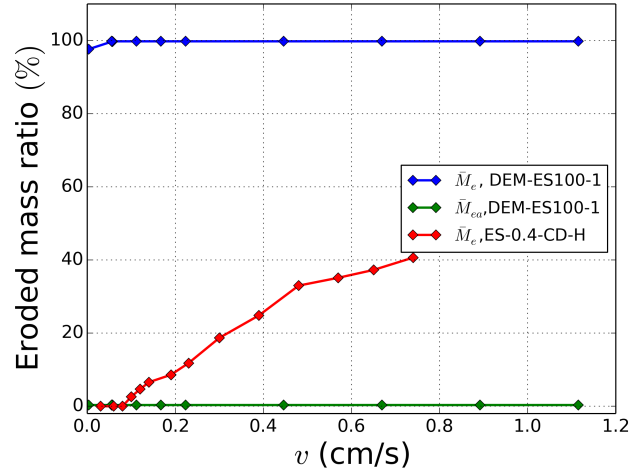
Figure 5.5: Mass of eroded particles in DEM-ES100-1 in terms of Darcy's velocity, v, of the interstitial flow.

the mass of eroded particles divided by the total mass of fine particles). However, experimentally, only 40.65% of the mass of fine particles was collected at the end of the suffusion test (i.e. at a maximum Darcy's velocity, $V_{max} = 0.74$ cm/s). Therefore, the transport criterion, used so far in this work, over-estimates the ability of detached particles to be transported. Notice also that all eroded particles were removed at a very low flow velocity (≈ 0.01 cm/s). In fact, rattlers will be detached once subjected to any small flow velocity as they are effectively detached even before erosion. The only way to limit the erosion of fine particles is to modify the transport criterion. This modification is presented in the next paragraph.

It is important to highlight that an important process possibly taking place during suffusion is the filtration of transported particles passing through constrictions. This may be a result of a particle whose size is greater than the constriction size; or it may be related to the collective migration of fine particles possibly resulting in a collective blockage at some constrictions. Such processes may limit the suffusion development and may result in less eroded fine particles. Our model does not describe accurately such a process. Figure 5.5 shows how far is our model from the experimental results. Therefore, to approach the experimental data, the transport of fine particles should be limited. This is done by comparing the size of detached particles to xD_{c35} instead of D_{c35}, where x is any positive real number. For $0 < x < 1$, x could stand for the collective passing of fine particles through a given constriction. Effectively, detached particles may not move one after another in the pore space, but may move together. Therefore, if several particles arrive together in front of a constriction with a typical size D_{c35}, the size of a given particle should not be compared to D_{c35} (to know whether it can pass or not the constriction), but to a fraction of D_{c35} depending on the number of particles present in front of the constriction. In what follows, x has been calibrated to fit the eroded mass collected experimentally at the end of the test.

5.3.2   Simulation of erosion

Three numerical samples, DEM-NS100-1, DEM-NS100-2 and DEM-NS100-3, were subjected to suffusion. Also, soil sample DEM-NS200-PSD_Real was eroded. Then drained triaxial compression tests were performed with a confining pressure of 100 kPa.

As mentioned previously, a new variable, x, is defined which limits the transport of particles. This parameter is calibrated to obtain numerically a similar percentage of the eroded mass to the one measured experimentally at the end of the suffusion test (i.e. $\bar{M}_e =$40.65 % for $V_{max} =$0.74 cm/s). The calibration process using the simplified gradation results in $x = 0.68$; for the real PSD, $x = 0.35$. Table 5.4 gives the sample properties before and after erosion. DEM-ES100-A is the average response of the three soil samples: DEM-NS100-1, DEM-NS100-2 and DEM-NS100-3.

An average of 34.77 % of fine paricles was eroded while using the simplified PSD

| Soil sample | Before suffusion | | | | After suffusion | | | | | | | $\Delta e_g/e_{g0}$ (%) | $\Delta e/e_0$ (%) |
	FC_0 (%)	e_0	e_{g0}	e_{eq0}	M_e (%)	FC_f (%)	ϵ_v (%)	ϵ_a (%)	e_{er}	e_{ger}	e_{eqer}		
DEM-ES100-1	25	0.47	0.97	0.95	40.21	16.79	2.1	0.9	0.61	0.93	0.92	-4.12	29.79
DEM-ES100-2	25	0.47	0.96	0.94	34.64	18.05	1.7	0.6	0.58	0.92	0.91	-3.13	25.40
DEM-ES100-3	25	0.45	0.94	0.93	29.47	19.19	1.5	0.6	0.55	0.92	0.91	-3.19	22.22
DEM-ES100-A	**25**	**0.46**	**0.96**	**0.94**	**34.77**	**18.01**	**1.8**	**0.7**	**0.58**	**0.92**	**0.91**	**-3.48**	**25.80**
DEM-ES200-PSD_Real	**25**	**0.41**	**0.88**	**0.88**	**36.30**	**17.66**	**0.0**	**0.0**	**0.54**	**0.88**	**0.88**	**0.0**	**31.71**
ES-0.4-CD-H	**25**	**0.53**	**1.04**	**-**	**40.65**	**16.52**	**5.7**	**5.7**	**0.61**	**0.93**	**-**	**-10.58**	**15.09**

Table 5.4: Summary of the soil properties before and after erosion. ($\Delta e_g/e_{g0}$ and $\Delta e/e_0$ represent, respectively, the relative change in the inter-granular and global void ratios induced by the erosion process)

and 36.30 % while using the real PSD. However, the evolution of the eroded mass is different from the experimental one (see Figures 5.6a and 5.6b). Numerically, more fine particles were removed at lower flow velocities whereas the erosion process is more gradual in the experiment. Nevertheless, if x is reduced to erode less particles at low flow velocities, the final eroded mass will be under-estimated. Experimentally, some eroded particles may be still migrating within the pore network before leaving the soil sample; or particles may get blocked temporarily throughout their migration. However, numerically such a process is not considered, a particle identified as detached and able to migrate is immediately removed. In addition to that, most fine particles are rattlers, hence, this may have resulted in a very high erosion at low flow velocities. Regardless that, the main focus in this work is to study the effect of the loss of fine particles and not to describe all details of the suffusion development (this is a compromise in order to keep a numerical model with a reasonable computational cost).

Concerning the simplified PSD, Figure 5.7b shows an increase in the void ratio even
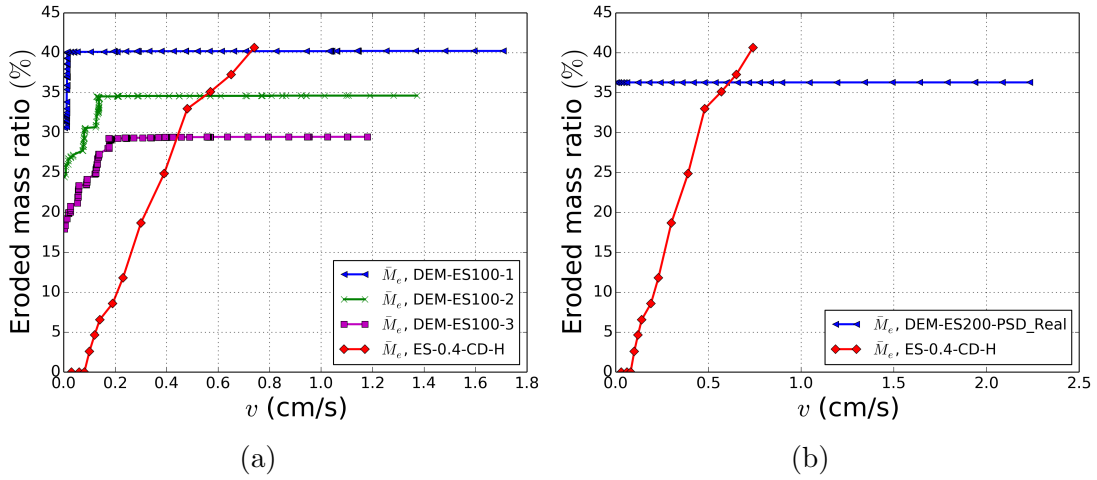
Figure 5.6: Eroded mass with the increase in flow velocity, v, for (a) soil samples prepared using gradation PSD-Simplified and (b) soil samples prepared using gradation PSD-Real.

though the soil globally contracts during the extraction process as shown in Figure 5.7a. However, the increase in the global void ratio is overestimated in the numerical model compared to the experimental one ($\Delta e/e0 = 25.80$ % for the model and 15.09 % for the experiment). This is due to the lower compaction in the numerical samples. In fact, the soil mainly deforms when active particles are removed. Table 5.5 gives the active eroded mass in each soil sample. Notice that the active eroded mass is very small numerically, about 0.31 % in DEM-ES100-A resulting in a volumetric deformation of 1.8 % which is smaller than the experimental volumetric deformation (5.7 %). Consequently, the densification of the coarse fraction is underestimated in the model ($\Delta e_g/e_{g0} = -3.48$ % for the model and -10.58 % for the experiment).

Soil sample	$\bar{M}_e$ (%)	$\bar{M}_{ea}$ (%)
DEM-ES100-1	40.21	0.26
DEM-ES100-2	34.64	0.34
DEM-ES100-3	29.47	0.33
DEM-ES100-A	**34.77**	**0.31**
DEM-ES200-PSD_Real	**36.30**	**0.003**

Table 5.5: Percentages of total eroded and active eroded mass in each soil sample.

Concerning the real PSD, the soil sample did not deform during erosion (Figure 5.8a). Hence the coarse skeleton was not affected by the removal of fine partilces ($\Delta e_g/e_{g0} \approx 0$ %). This is due to the fact that almost no active particles are eroded in this case ($\bar{M}_{ea} = 0.003$ % as given in Table 5.5). This results in a higher change of the global void ratio ($\Delta e/e_0 = 31.71\%$) than the experimental one. Thus, the densification of the coarse granular skeleton during erosion is more important in the experimental test than the numerical samples. Therefore,

it was found that the numerical model succeeds qualitatively in reproducing the experimental data, however, quantitatively the results are different. Numerical soil samples showed a lower global volumetric reduction representing a lower densification of the coarse granular skeleton and resulting in more important increase in the overall porosity.

In addition to that, the hydraulic conductivity in the numerical soil increases as the global void ratio increases (Figures 5.7c and 5.8b). The erosion of fine particles creates a more open microstructure which increases the permeability of the soil. The model, however, underestimates this increase, possibly due to the creation of preferential flow paths in the experimental test. But, it is also important to recall that there is not any fitting parameter in the model to predict the hydraulic conductivity. In this context, the prediction of the hydraulic conductiviy (at least the initial value) is quite satisfactory.

In order to explain the difference between the numerical and the experimental re-

(a)   (b)

(c)
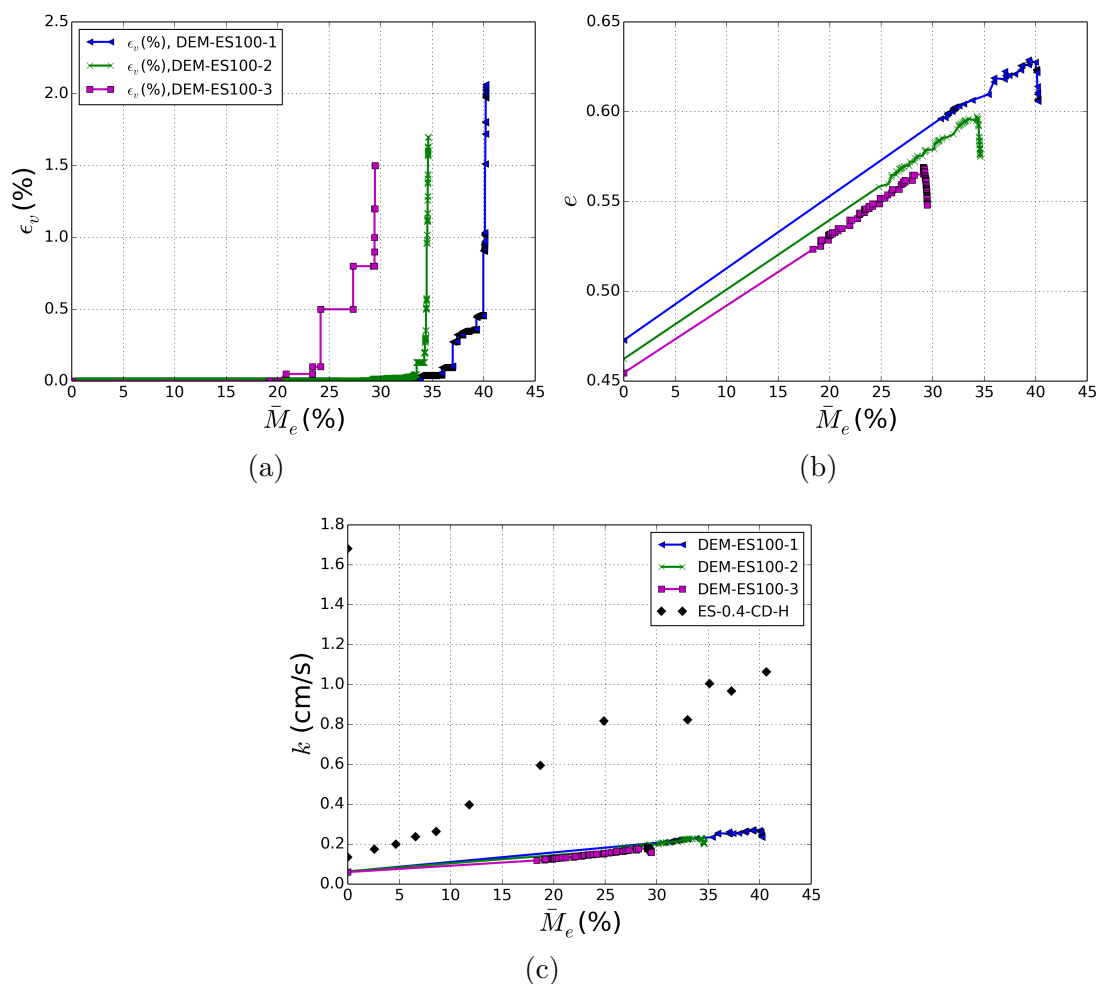
Figure 5.7: The variation in the (a) volumetric deformation, (b) global void ratio and (c) hydraulic conductivity with the eroded mass for gradation PSD-Simplified.

sults, it is important to recall the results obtained in Chapter 2, Section 2.4.2 about the effect of fine particles in the microstructure. In that study, the threshold fines content, FC_{th}, of the numerical model was calculated and compared with the experimental one. It was found that the numerical FC_{th} (for the considered gradation) was larger than the

(a)   (b)
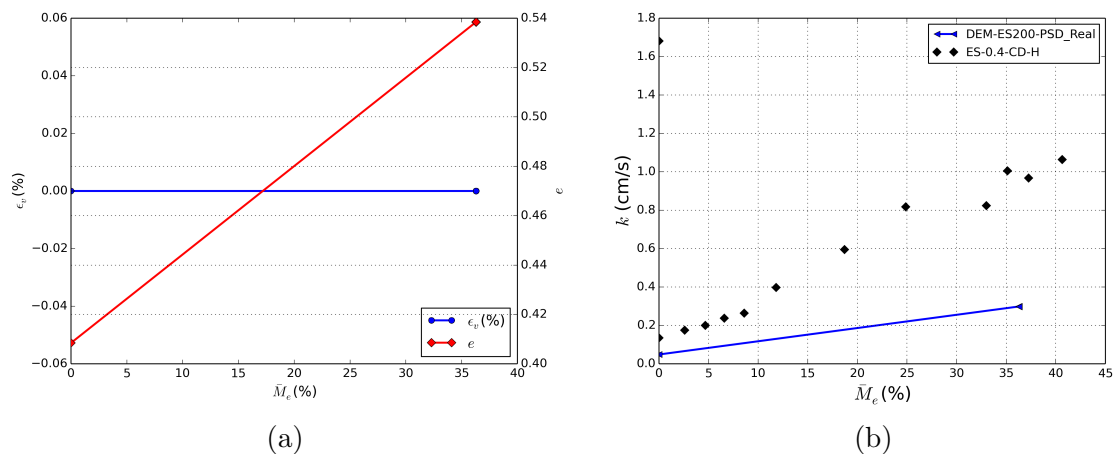
Figure 5.8: The variation in the (a) volumetric deformation and void ratio and (b) hydraulic conductivity with the eroded mass for gradation PSD-Real.

experimental one. Hence, in this chapter, the numerical soil may also have FC_{th} higher than the experimental value (35 %). Therefore, several soil samples with the simplified PSD were reconstituted with different fines content, FC. Then, the evolution of the void ratio with FC was studied showing that FC_{th} for the numerical granular assembly is 40 % (Figure 5.9). This difference in FC_{th} illustrates that, for a given fines content (here $FC = 25$ %), the initial microstructures of the numerical assemblies and the experimental soil samples are probably different. In others words, as experimentally the gap between the considered FC and FC_{th} is smaller than the numerical one, the active fine particles may represent a higher fraction than in the numerical case. Therefore, for a given total eroded mass, the fraction of the active particles among the eroded particles is probably more important experimentally influencing significantly the soil matrix integrity; unlike the numerical samples where almost all fine particles are rattlers. As a conclusion, the model may not reproduce accurately the microstructure of the real sample (this is indeed not straightforward when spherical particles are used instead of the real angular particles) resulting in a different configuration of the fines (mainly rattlers in the numerical model) and thus a different response to erosion processes. Nevertheless, using the simplified PSD seems to give slightly closer results to the experiment.
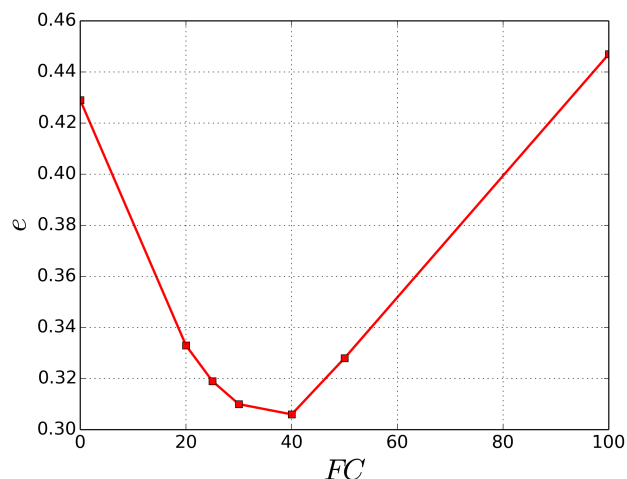
Figure 5.9: The variation of the global void ratio, e, with the fines content, FC, for the simplified PSD.

5.3.3   Characterization of the mechanical properties

Suffusion-like simulations were then followed by drained triaxial compression tests to study the effect of suffusion on the mechanical properties of the soil. In this way we followed the experimental procedure. As mentioned previously, the confining pressure is first increased to 100 kPa and then drained triaxial compression tests are carried out. During the increase in the confining pressure, the soil may suffer from additional deformation. Table 5.6 shows that the numerical soil deforms slightly during this phase (ϵ_v=1.3%, ϵ_a=0.4% in DEM-ES100-A and ϵ_v=1.7%, ϵ_a=0.6% in DEM-ES200-PSD_Real). The void ratio also decreases slightly from 0.58 to 0.56 in DEM-ES100-A and from 0.54 to 0.52 in DEM-ES200-PSD_Real. Hence the soil becomes slightly denser in this phase. However, for the experimental results, the soil sample is thawed in the triaxial cell before the saturation and the consolidation steps, but the deformation of the soil was not monitored during thawing. Thus, there is no clear experimental data about the possible changes in the density during this phase.

Figures 5.10 and 5.11 show the responses of the eroded soil samples during the drained

Soil sample	P_c=5kPa			P_c=100kPa				
	e_{er}	e_{ger}	e_{eqer}	ϵ_v (%)	ϵ_a (%)	e'_{er}	e'_{ger}	e'_{eqer}
DEM-ES100-1	0.61	0.93	0.92	1.3	0.5	0.59	0.90	0.89
DEM-ES100-2	0.58	0.92	0.91	1.4	0.4	0.56	0.90	0.88
DEM-ES100-3	0.55	0.92	0.91	1.3	0.4	0.54	0.89	0.88
DEM-ES100-A	**0.58**	**0.92**	**0.91**	**1.3**	**0.4**	**0.56**	**0.90**	**0.88**
DEM-ES200-PSD_Real	**0.54**	**0.88**	**0.88**	**1.7**	**0.6**	**0.52**	**0.85**	**0.84**

Table 5.6: Response of the eroded soil samples due to the increase in the confining pressure from 5 kPa to 100 kPa.

triaxial compression tests. The average response of the three soil samples reconstituted using PSD-Simplified (DEM-ES100-A) as well as the response of DEM-ES200-PSD_Real are compared to the experimental data. Results of both numerical samples, with simplified and real PSD, are similar. Globally, the numerical eroded samples behave as a looser sample with respect to the non-eroded ones (despite there was a slight densification of the coarse skeleton represented by a decrease in the inter-granular void ratio, e_g). Thus, the eroded soil shows a lower initial stiffness, a softer behavior in the hardening phase and a more important initial contractancy (even if the material stays slightly dilatant at large strains). The increase in the global void ratio seems to govern the mechanical response more than the inter-granular void ratio (densification of the coarse skeleton). Concerning the critical state, the eroded numerical samples reach the same stress deviator as the non eroded ones at this state. However, Figures 5.10c and 5.11c show the evolution of the void ratio during the triaxial compression test and it is noticed that at the critical state, the void ratio of eroded soils is higher than that of the non-eroded one. As shown previously in Chapter 3, the change in the gradation may have resulted in a similar shear stress at the critical state, as fine particles are almost not involved in the contact force network, but impacts the porosity at this state.

Comparing these results with the experimental results, it is noticed that the model succeeds in describing the loss in the soil rigidity (i.e. initial rigidity and in the hardening regime). However, the loss of the shear strength (at peak stress and also apparently at large deformations) obtained experimentally is not correctly described by the model (Table 5.7). The model presents a higher contractancy than the experiment for the eroded case. However, the model conserves at large strains a dilatancy very close to the experimental one. The dilatancy angle, ψ_{max} is given in Table 5.7 which shows that it slightly increases after erosion as is the case experimentally. Futhermore, the shift in the void ratio between the eroded and the non-eroded responses as presented in Figures 5.10c and 5.11c is quite well described in the model, more particularly at the critical state (we recall that absolute values of experimental and numerical void ratios should not be compared directly, cf. Chapter 2, Section 2.3. It is important to note that the critical state in the experiment is not perfectly reached. Thus, we refer here to the maximum axial deformation applied to the soil sample.

Moreover, it is important to highlight different possible sources of discrepancies

Soil sample	Before suffusion			After suffusion		
	φ_p (°)	φ_0 (°)	ψ_{max} (°)	φ_p (°)	φ_0 (°)	ψ_{max} (°)
DEM-ES100-1	29.41	29.41	1.16	30.77	30.77	2.15
DEM-ES100-2	30.25	30.25	1.34	31.68	29.85	2.90
DEM-ES100-3	29.86	29.86	2.53	30.55	30.55	2.26
DEM-ES100-A	**29.96**	**29.96**	**1.68**	**30.50**	**30.50**	**2.26**
DEM-ES200-PSD_Real	**29.55**	**29.55**	**1.67**	**30.58**	**30.58**	**2.10**
ES-0.4-CD-H	**31.4**	**29.2**	**1.90**	**27.8**	**26.7**	**2.34**

Table 5.7: Peak and residual friction angles and dilatancy angles before and after suffusion.

(a) (b)

(c)
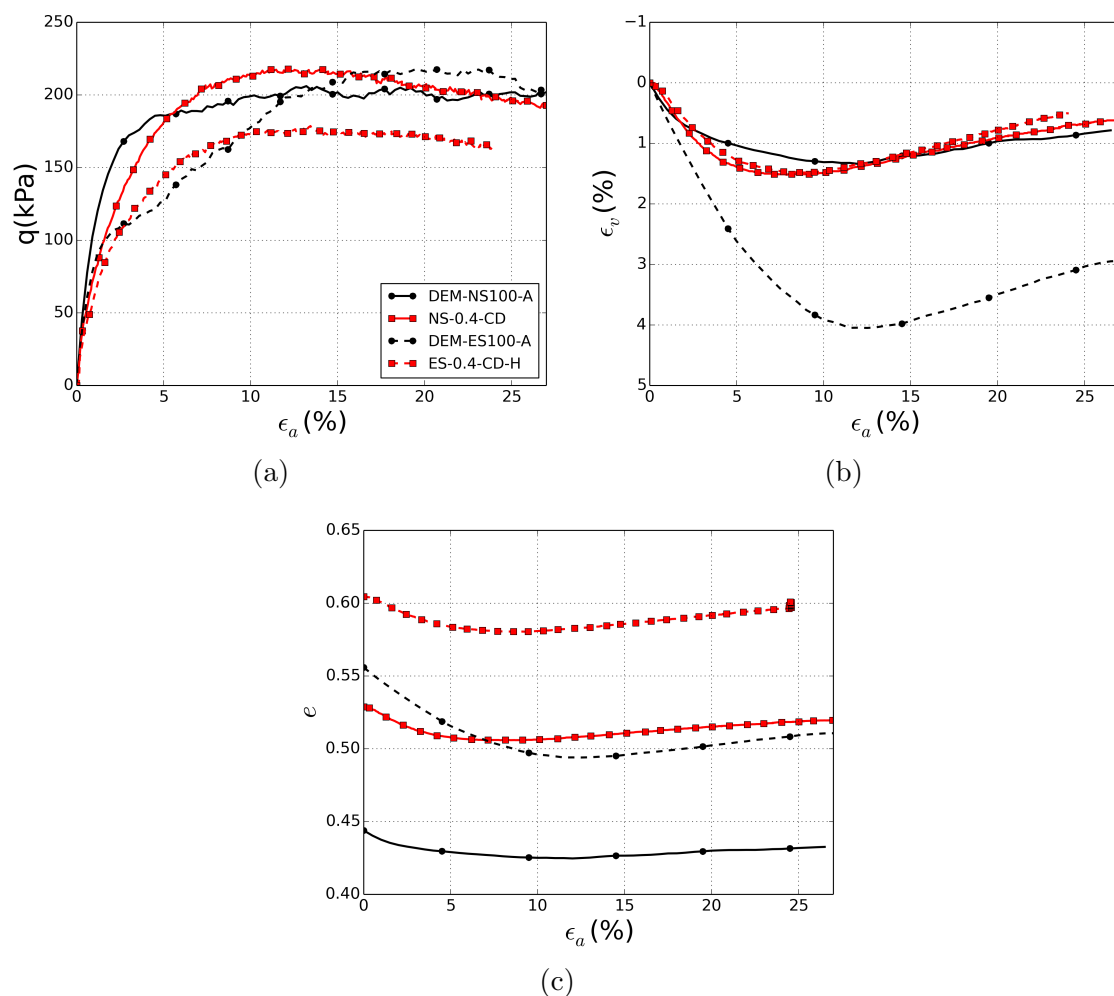
Figure 5.10: Comparison between experimental and DEM soil response (using gradation PSD-Simplified) to drained triaxial compression test before and after erosion. (In the legend, NS means non-eroded soil, ES means eroded soil).

between the numerical and the experimental tests. The numerical extraction procedure results in a homogeneous eroded soil (see Chapter 3) unlike experiments which result in a heterogeneous soil sample. Thus, the calculation of the density indices (void ratio, inter-granular void ratio...) is not totally representative of the different states of density present in a heterogeneous soil. Another assumption is related to the role of the eroded particles (i.e. active or inactive). Since very few active particles were removed from the models, even if this removal caused deformations, the re-arranged structure maintained a microstructure with a similar strength to the non-eroded soil. To support this idea, the probability density function, P, of the normal contact forces, F_N, is drawn for the different gradations before and after erosion. Figures 5.12a and 5.12b show that the probability density function after erosion shows that the force distribution is slightly different corresponding to a slightly looser soil which explains the decrease in initial rigidity and the larger initial contractancy. However, this difference is not very important which confirms that the soil microstructure did not change significantly after suffusion.
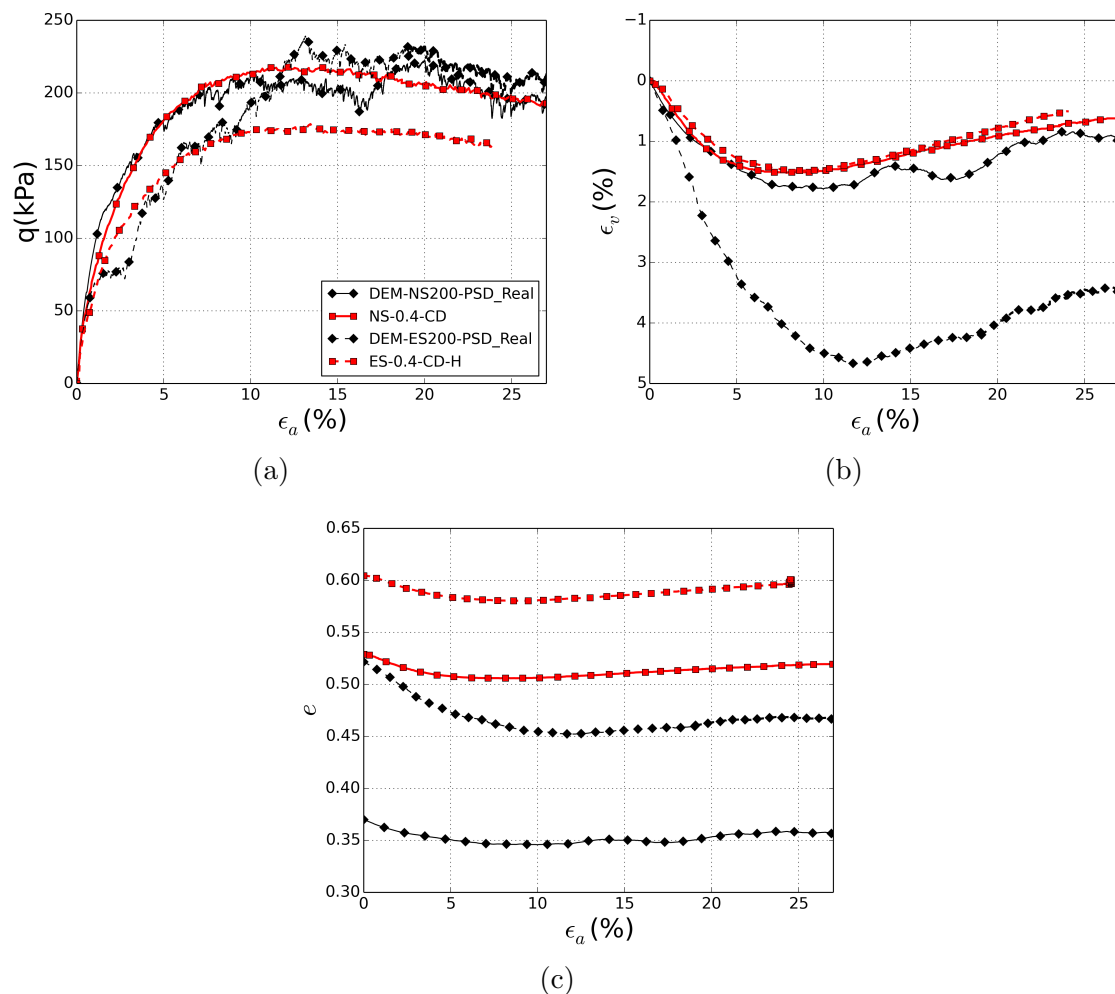
Figure 5.11: Comparison between experimental and DEM soil response (using gradation PSD-Real) to drained triaxial compression test before and after erosion. (In the legend, NS means non-eroded soil, ES means eroded soil).
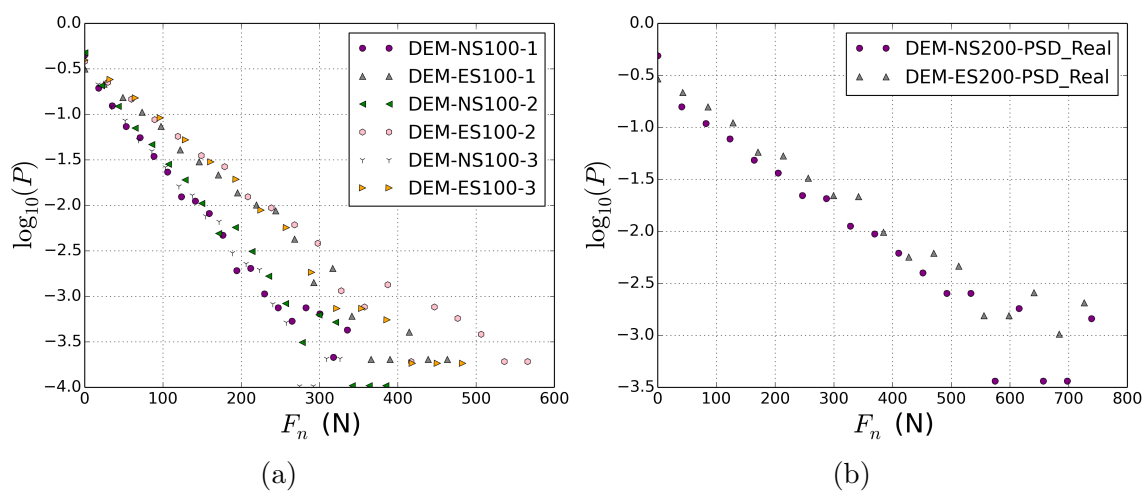
Figure 5.12: Probability density function of normal forces of eroded and non-eroded soil samples prepared using (a) PSD-Simplified, (b) PSD-Real.

5.4   Parametric study

So far, the defined extraction procedure followed in this work results in a homogeneous eroded soil sample unlike the experimental ones. Moreover, in all the previous sections, both fine and coarse particles have the same properties (i.e; same contact friction, rolling friction,...). In addition to that, Chapter 4 showed that the density of the soil can influence the suffusion development and can lead to higher degradation of the mechanical properties for denser soils. Therefore, in this section we address these three issues:

- Heterogeneous erosion process: during experiments, the wall effect of rigid-wall permeameters cannot be ignored; more particles are eroded near the wall where the porosity is higher. In addition to that, usually after erosion, particles from the lower part of the soil sample are eroded and particles from the upper part migrate to the bottom of the sample. As a result, erosion leads to a heterogeneous sample with zones of different PSDs and densities. These two cases are modeled in the following sections;

- Different rolling resistance of fine and coarse particles: if smaller soil particles are less spherical than the coarser ones, their resistance to rolling can be different than that of big particles. When fine particles are removed, the shear strength of the soil may then decrease. This concept is adopted by considering a higher rolling friction for the smaller particles in the soil sample;

- Influence of the initial density on the degradation of the mechanical properties induced by erosion: suffusion and mechanical characterization are simulated on a very dense sample to investigate if a similar behavior, as in Chapter 4, is obtained;

5.4.1   Case of heterogeneous erosion processes

In an attempt to mimic more accurately the experimental erosion development, this section presents two scenarios:

- Scenario # 1: From the experimental results, it was noticed that the erosion in the different parts of the soil samples is different. Figure 5.13 shows the PSD of the top and bottom sections of an experimental eroded soil sample. As can be noticed, the top part of the sample lost more fine grains than the bottom part. To model this type of erosion, we consider the removal of about 40 % by mass of the fines only from the upper part. It is as if particles from the bottom part leave the sample, but then new particles migrate from the top to the bottom which compensate the loss in the lower part.

- Scenario # 2: Figure 5.14 shows the distribution of fine particles in the vertical section of an eroded soil sample. This image has been obtained from an X-ray tomograpgy performed jointly with IRSTEA and 3SR Laboratory (C. Nguyen et al. (2017)). The image highlights the wall effect during erosion. More particles were eroded near the wall. Therefore, although we do not use rigid walls in our model, another simulation is done to mimic such an erosion process by removing only the fine particles near the lateral boundaries. Figure 5.15 shows the hatched zones where particle extraction took place in our model.
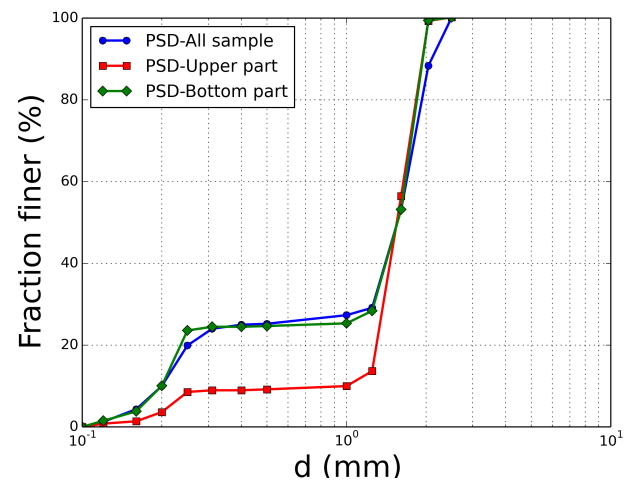
Figure 5.13: Grain size distribution curves of the experimental post-suffusion specimen.
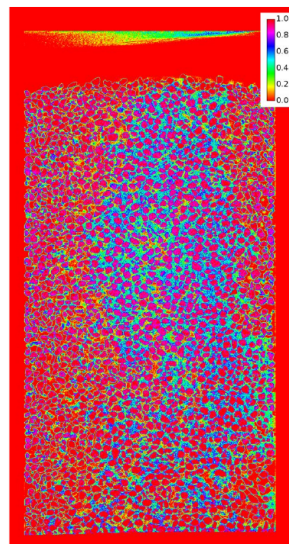
Figure 5.14: Distribution of fines in a vertical section of an eroded soil sample. The color scale represents the volumetric fraction of fines in the inter-granular voids (the coarse grains are displayed in red). Image reconstituted from an X-ray tomography (C. Nguyen et al. (2017)).
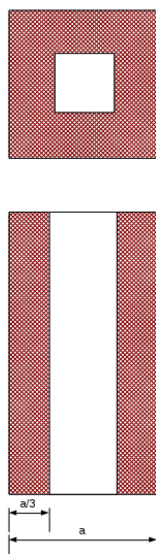
Figure 5.15: Hatched zones of the numerical soil sample where particle extraction is limited to (Scenario #2).

Although this is a very simplified way to model the heterogeneities induced by suffusion, it can give an idea of their effect on the induced mechanical response. In other words, is it true that the reason for the differences between experimental and numerical results is due to the induced heterogeneities during laboratory tests?

The three soil samples with the simplified PSD prepared before with a confining pressure of 5 kPa were used to remove particles following the previously defined scenarios. The calibration of x needs to be updated and it gives a value of 0.75 for scenario # 1 and 0.7 for scenario # 2.

Table 5.8 gives the soil properties before and after erosion in each case. An average mass of 36.61% is removed in scenario # 1 (Figure 5.16a) and 40.57 % in scenario # 2 (Figure 5.16b). Volumetric deformations, changes in void ratio and hydraulic conductivity are displayed in Figures 5.17 and 5.18 for scenarios # 1 and # 2 respectively. Although the sample compaction is still underestimated by the model both scenarios of heterogeneous erosion tend to make the response of the model during the suffusion phase closer to the experimental response. The volumetric deformation of the average responses is now equal to 2.7 % for scenario # 1 and 2.5 % for scenario # 2 (whereas it was of 1.8 % for the "homogeneous" erosion) compared to an experimental volume reduction of 5.7 %. Consequently the computed relative variation of the inter-granular void ratio is also closer to the experimental one: $\Delta e_g / e_{g0} = -5.57$ % and -4.86 %, for scenarios # 1 and # 2, respectively (whereas it was -3.48 % previously) compared to the experimental data, -10.58 %. Changes in the hydraulic conductivity are presented in Figures 5.17c and 5.18c for scenarios # 1 and # 2 respectively. Scenario # 2 leads to a higher final hydraulic conductivity than scenario # 1 because of the non eroded bottom layer in scenario # 1, orthogonal to the main flow direction and limiting the global apparent hydraulic conductivity. However, there is no significant improvement in the prediction of the change of the hydraulic conductivity even in the case of scenario # 2.

After erosion, the soil is then confined up to 100 kPa. During this phase, the

Soil sample	Before suffusion				After suffusion									
	FC_0 (%)	e_0	e_{g0}	e_{eq0}	M_e (%)	FC_f (%)	ϵ_v (%)	ϵ_a (%)	e_{er}	e_{ger}	e_{eqer}	$\Delta e_g/e_{g0}$ (%)	$\Delta e/e_0$ (%)
DEM-ES100-h1-1	25	0.47	0.97	0.95	36.75	17.60	2.6	2.1	0.58	0.92	0.91	-5.15	23.40
DEM-ES100-h1-2	25	0.47	0.96	0.94	36.61	17.59	2.8	2.1	0.57	0.90	0.89	-6.25	21.28
DEM-ES100-h1-3	25	0.45	0.94	0.93	36.48	17.57	2.7	2.0	0.56	0.89	0.89	-5.32	24.44
DEM-ES100-h1-A	**25**	**0.46**	**0.96**	**0.94**	**36.61**	**17.59**	**2.7**	**2.1**	**0.57**	**0.90**	**0.90**	**-5.57**	**23.04**
DEM-ES100-h2-1	25	0.47	0.97	0.95	43.49	16.01	2.9	1.4	0.61	0.91	0.91	-6.19	29.79
DEM-ES100-h2-2	25	0.47	0.96	0.94	37.60	17.36	2.6	0.9	0.57	0.91	0.90	-5.21	21.28
DEM-ES100-h2-3	25	0.45	0.94	0.93	40.62	17.59	2.0	0.8	0.57	0.91	0.90	-3.19	26.67
DEM-ES100-h2-A	**25**	**0.46**	**0.96**	**0.94**	**40.57**	**16.99**	**2.5**	**1.03**	**0.58**	**0.91**	**0.90**	**-4.86**	**25.91**
ES-0.4-CD-H	**25**	**0.53**	**1.04**	**-**	**40.65**	**16.52**	**5.7**	**5.7**	**0.61**	**0.92**	**-**	**-10.58**	**15.09**

Table 5.8: Summary of the soil properties before and after a heterogeneous erosion (Scenario #1 is identified as 'h1' in the table and Scenario #2, identified as 'h2').
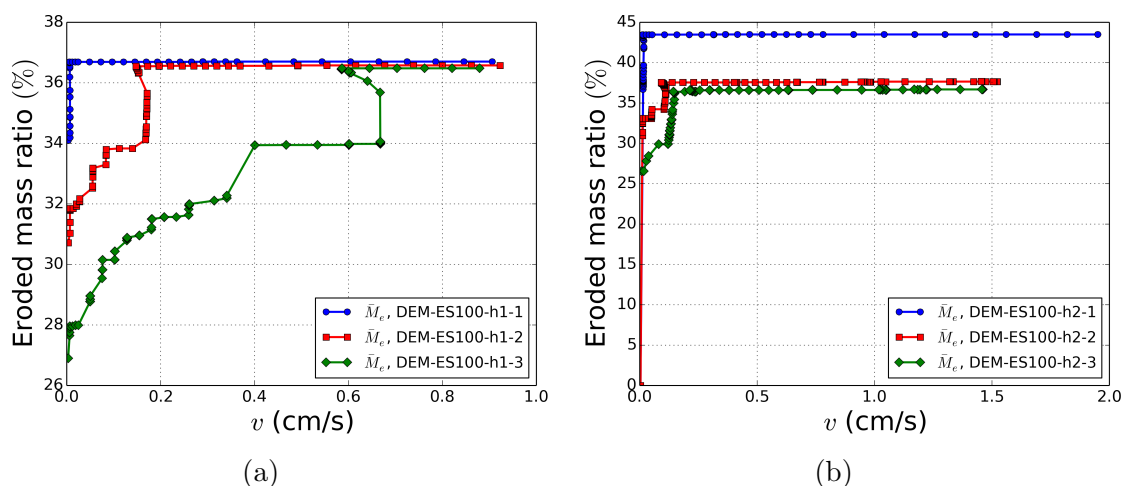
Figure 5.16: Eroded mass with the increase in flow velocity, v; (a) Scenario # 1 and (b) Scenario #2.

soil compacts (ϵ_v=1.2 % in scenario #1 and ϵ_v=1.3 % in scenario #2) and the void ratio decreases slightly from 0.57 to 0.54 in scenario #1 and from 0.58 to 0.56 in scenario #2
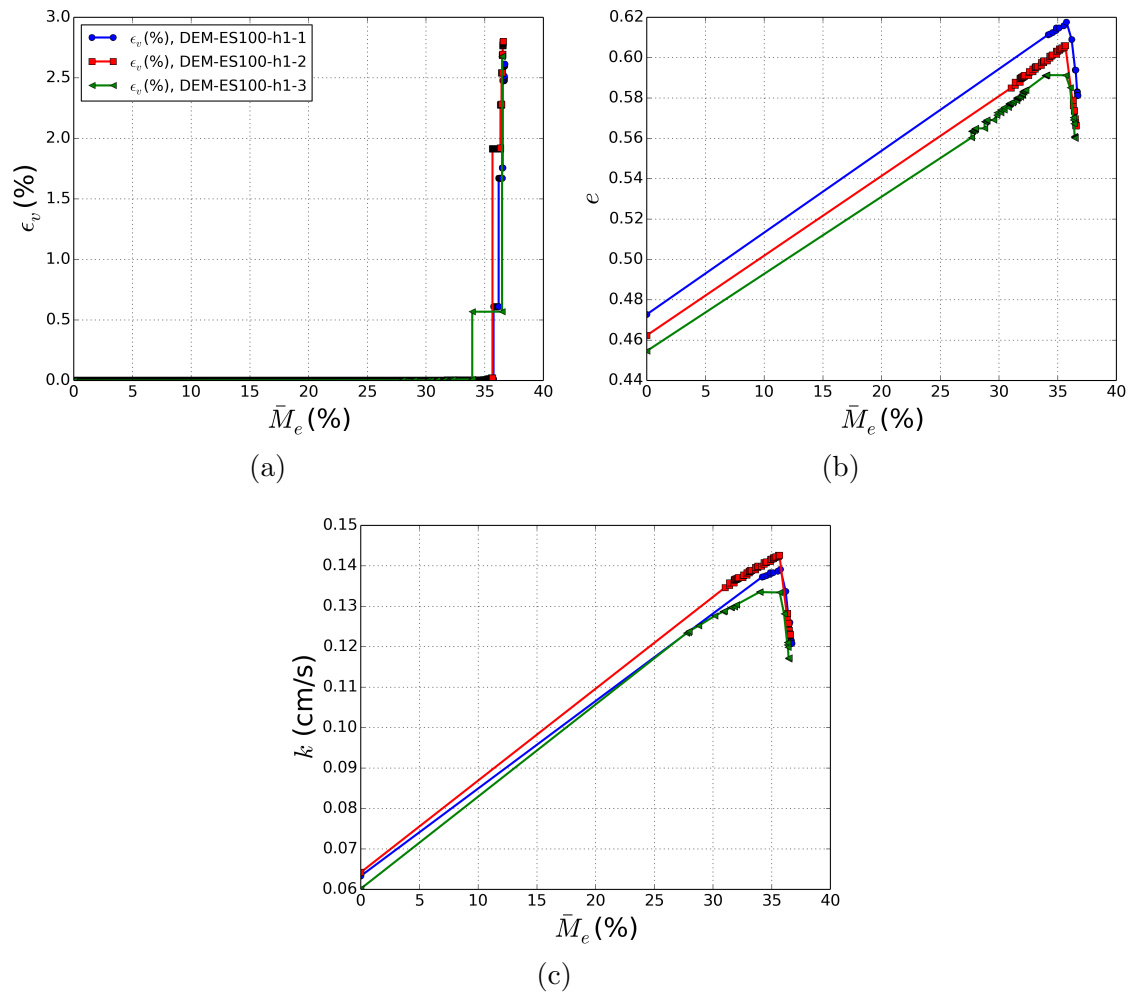
Figure 5.17: The variation in the (a) volumetric deformation, (b) global void ratio and (c) hydraulic conductivity with the erosion of particles in Scenario # 1.
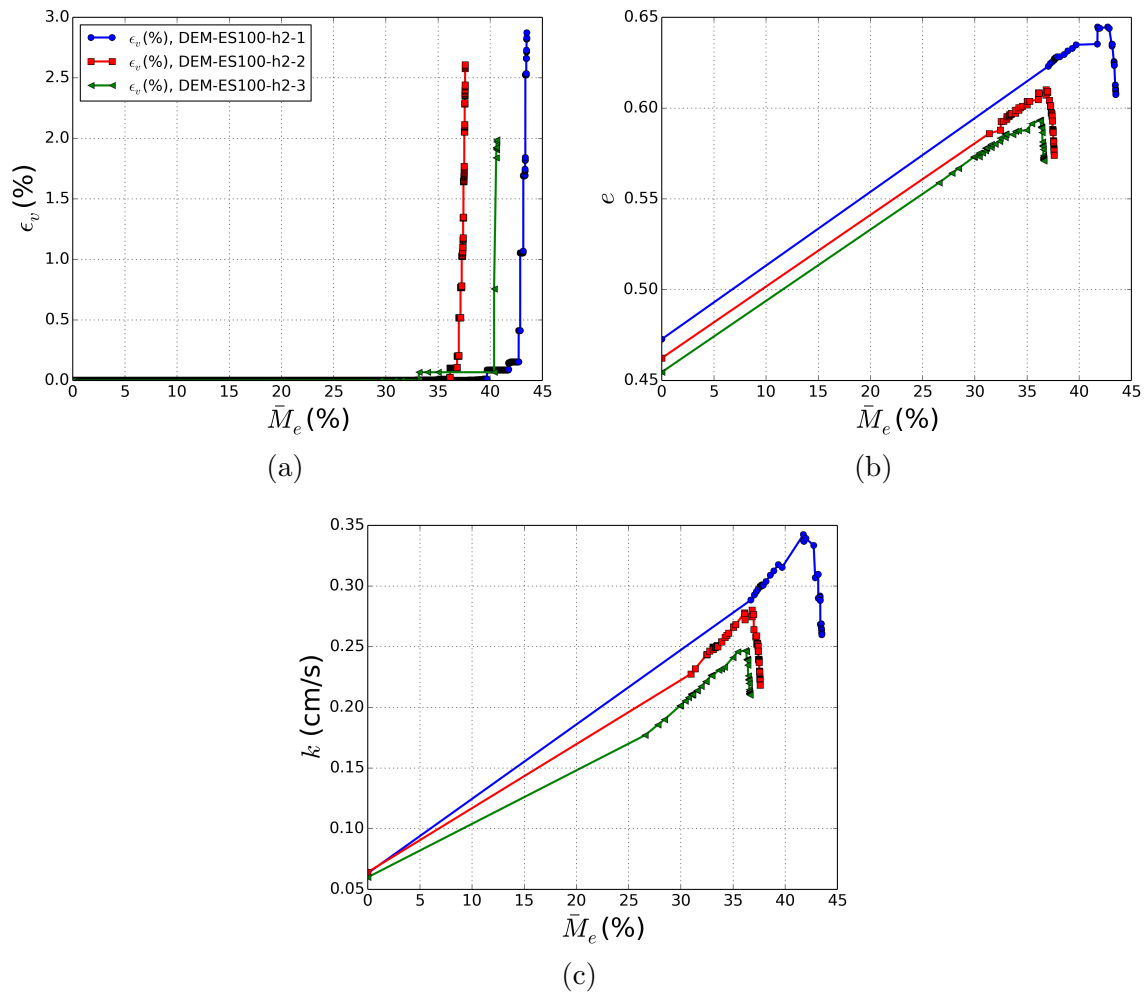
Figure 5.18: The variation in the (a) volumetric deformation, (b) global void ratio and (c) hydraulic conductivity with the erosion of particles in Scenario # 2.

(Table 5.9). Also the inter-granular and the equivalent inter-granular void ratios decrease slightly as a result of this compaction. Thus, the soil skeleton becomes slightly denser.

However, the void ratios of the samples given in Tables 5.8 and 5.9 are only true

Soil sample	P_c=5kPa			P_c=100kPa				
	e_{er}	e_{ger}	e_{eqer}	ϵ_v (%)	ϵ_a (%)	e'_{er}	e'_{ger}	e'_{eqer}
DEM-ES100-h1-1	0.58	0.92	0.91	1.2	0.4	0.56	0.90	0.88
DEM-ES100-h1-2	0.57	0.90	0.89	1.3	0.4	0.54	0.88	0.86
DEM-ES100-h1-3	0.56	0.89	0.89	1.2	0.4	0.54	0.87	0.85
DEM-ES100-h1-A	**0.57**	**0.90**	**0.90**	**1.2**	**0.4**	**0.54**	**0.88**	**0.86**
DEM-ES100-h2-1	0.61	0.91	0.91	1.3	0.5	0.59	0.89	0.88
DEM-ES100-h2-2	0.57	0.91	0.90	1.3	0.4	0.56	0.88	0.87
DEM-ES100-h2-3	0.57	0.91	0.90	1.3	0.4	0.56	0.91	0.90
DEM-ES100-h2-A	**0.58**	**0.91**	**0.90**	**1.3**	**0.43**	**0.56**	**0.89**	**0.88**

Table 5.9: Response of the eroded soil samples due to the increase in the confining pressure from 5 kPa to 100 kPa in each case of heterogeneous erosion.

if considering a homogeneous soil. In a heterogeneous case, we distinguish between two different values of the void ratio for each section of the soil sample. Table 5.10 gives the values of the void ratio in the upper and lower parts for scenario #1 and at the center and the boundaries of the soil in scenario #2. It is clear that due to the removal of fine particles from the upper part or from the boundaries, the void ratio is higher there. Hence, the soil is divided into two zones, one denser than the other.

Drained triaxial compression tests are then simulated to characterize the effect of a heterogeneous erosion on the soil properties (even if we still use the expression "soil properties", as the medium is heterogeneous these properties cannot be considered actually as material or intrinsic properties). Figures 5.19 and 5.20 show the responses of the numerical soil samples before and after erosion in comparison with the experimental data and the numerical homogeneous erosion. The numerical heterogeneous soils show a loose behavior characterized by a lower stiffness and a more contractant behavior. This is similar to the homogeneous case. Nevertheless, the shear strength in all numerical samples is similar. Table 5.11 gives the peak and residual friction angles before and after erosion. The average peak friction angle increases slightly from 29.96 ° before erosion to 32.08 ° in scenario #1 and to 30.36° in scenario #2 which is close to that of the homogeneous case (30.50°). Also, the dilatancy angle, ψ_{max}, is given in Table 5.11. It increases slightly after erosion. This is similar to the experimental results. Moreover, similarly to the homogeneously eroded soil, the heterogeneous soil exhibits the same residual state as the non-eroded soil. Thus, induced heterogeneities do not explain the decrease in the shear

	P_c=5kPa	P_c=100kPa
Soil sample	e_{er}	e_{er-c}
DEM-ES100-h1-1 (top)	0.72	0.69
DEM-ES100-h1-1 (bottom)	0.47	0.45
DEM-ES100-h1-2 (top)	0.69	0.67
DEM-ES100-h1-2 (bottom)	0.45	0.43
DEM-ES100-h1-3 (top)	0.69	0.67
DEM-ES100-h1-3 (bottom)	0.45	0.43
DEM-ES100-h1-A (top)	**0.69**	**0.67**
DEM-ES100-h1-A (bottom)	**0.45**	**0.43**
DEM-ES100-h2-1 (boundaries)	0.61	0.61
DEM-ES100-h2-1 (center)	0.56	0.54
DEM-ES100-h2-2 (boundaries)	0.59	0.56
DEM-ES100-h2-2 (center)	0.54	0.52
DEM-ES100-h2-3 (boundaries)	0.59	0.56
DEM-ES100-h2-3 (center)	0.54	0.52
DEM-ES100-h2-A (boundaries)	**0.60**	**0.58**
DEM-ES100-h2-A (center)	**0.55**	**0.53**

Table 5.10: The void ratio of the different sections of the heterogeneous eroded soil samples.

strength in the experimental results.

(a)

(b)

(c)
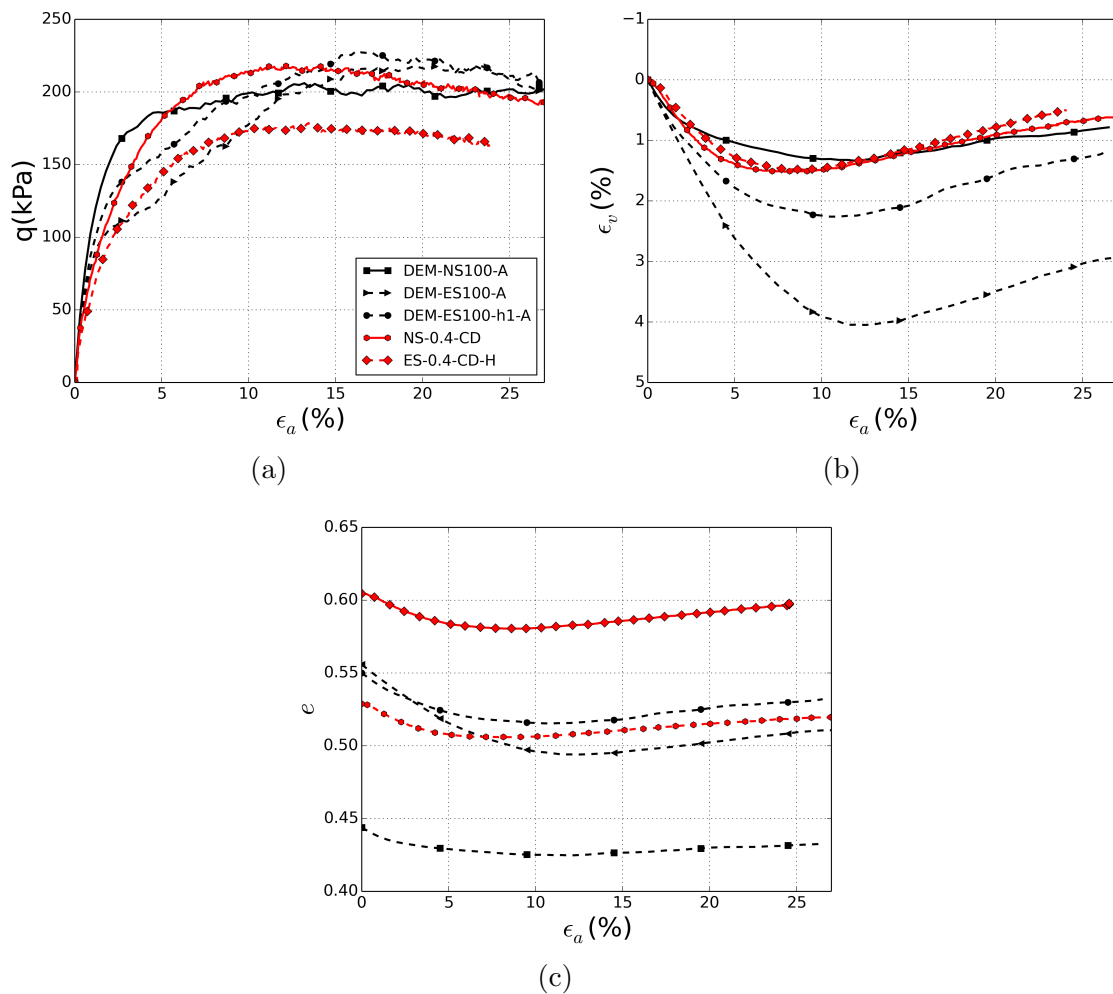
Figure 5.19: Comparison between experimental and DEM soil response to drained triaxial compression test before and after erosion in the case of Scenario #1.
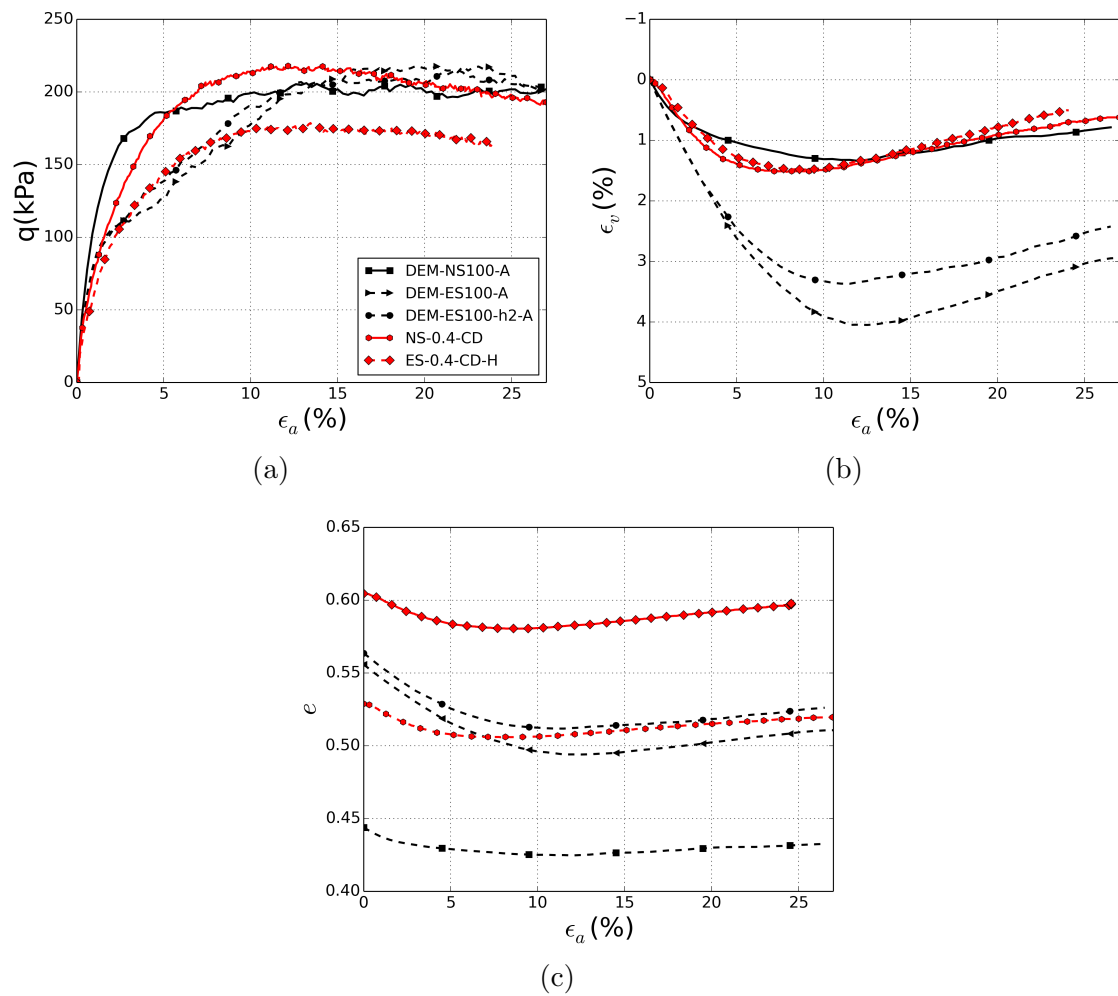
Figure 5.20: Comparison between experimental and DEM soil response to drained triaxial compression test before and after erosion in the case of Scenario #2.

	Before suffusion			After suffusion		
Soil sample	φ_p (°)	φ_0 (°)	ψ_{max} (°)	φ_p (°)	φ_0 (°)	ψ_{max} (°)
DEM-ES100-h1-1	29.41	29.41	1.16	30.63	30.63	1.72
DEM-ES100-h1-2	30.25	30.25	33.46	1.34	29.96	3.08
DEM-ES100-h1-3	29.86	29.86	2.53	31.85	29.46	2.30
DEM-ES100-h1-A	**29.96**	**29.96**	**1.68**	**32.08**	**30.80**	**2.37**
DEM-ES100-h2-1	29.41	29.41	1.16	29.42	29.42	2.19
DEM-ES100-h2-2	30.25	30.25	1.34	30.87	30.87	2.06
DEM-ES100-h2-3	29.86	29.86	2.53	30.30	30.30	1.10
DEM-ES100-h2-A	**29.96**	**29.96**	**1.68**	**30.36**	**30.36**	**1.78**
ES-0.4-CD-H	**31.4**	**29.2**	**1.90**	**27.8**	**26.7**	**2.34**

Table 5.11: Peak and residual friction angles and dilatancy angles before and after suffusion.

5.4.2   Fine and coarse fraction with different mechanical properties

Experimental results show that the erosion of fine particles lead to the decrease in the shear strength of the eroded soil sample. However, numerically, the shear stength of the soil is not highly influenced after erosion. In fact, in the numerical model, the granular assembly is made up of spheres unlike the real angular grains. To overcome the excessive rolling of such shapes, rolling resistance is taken into account in the contact law. The same rolling friction is used for fine and coarse particles (η_r=0.2). However, if smaller particles are more angular than the coarser particles, the rolling friction of the smaller ones should be larger. Thus, in these conditions, the erosion of fine particles could result in a decrease in the shear strength as for the experimental results.

Table 5.12 gives the parameters used in the DEM model. The rolling friction coefficient is higher for smaller particles (η_r=0.5) than for the coarser ones (η_r=0.2). Three samples with the simplified PSD have been generated randomly and confined up to 5 kPa. The percentage of rattlers is still the same as in the previous case (about 97% of fine particles). The void ratio did not change after increasing η_r for the fine fraction (e=0.47).

The calibration of x gives a value of 0.7 to obtain similar eroded mass as the experimental data. However, as we are using new parameters different than the calibrated ones, the comparison with the experimental results is only qualitative.

Figure 5.21 shows the eroded mass in each soil sample at different flow velocities.

E_c (kPa)	α_s	φ_c during compaction (°)	φ_c after compaction (°)	α_r	η_r (big particles)	η_r (small particles)
$2\ 10^8$	0.2	18	30	7.5	0.2	0.5

Table 5.12: Summary of the used DEM parameters in the case of different rolling resistances for fine and coarse particles.

The average eroded mass is 35.01%. Volumetric deformation, changes in the void ratio and the hydraulic conductivity are displayed in Figures 5.22a, 5.22b and 5.22c. The average volumetric deformation is 2.9%, which is still underestimated by the model, but closer to the experimental response compared to the homogeneous case. Consequently, the computed relative variation of the inter-granular void ratio is also closer to the experimental one: numerically $\Delta e_g / e_{g0} = -6.20$ % compared to the experimental data, -10.58% (Table 5.13). As a conclusion, considering higher rolling friction for fine particles makes the volumetric deformation and the change in the intergranular void ratio during erosion closer to the experimental data, and it is even slightly better than in the heterogeneous case.

Drained triaxial compression tests are then simulated. Before starting the triaxial compression test, the confining pressure is increased from 5 kPa to 100 kPa. Table 5.14 gives the variation in the density indices of the soil and the deformation during this phase. The void ratio decreased from 0.56 to 0.55. The inter-granular and the equivalent inter-granular void ratios remain almost unchanged (e_g=e_{eq} =0.90 before erosion; e_g=0.89 and e_{eq}=0.87 after erosion).

	Before suffusion			After suffusion								
Soil sample	FC_0 (%)	e_0	e_{g0}	e_{eq0}	M_e (%)	FC_f (%)	ϵ_v (%)	ϵ_a (%)	e_{er}	e_{ger}	e_{eqer}	$\Delta e_g/e_{g0}$ (%)	$\Delta e/e_0$ (%)
DEM-ES100-R-1	25	0.47	0.98	0.96	41	17.95	3.8	1.8	0.59	0.90	0.90	-8.16	25.53
DEM-ES100-R-2	25	0.47	0.95	0.93	28.73	19.16	1.5	0.7	0.55	0.92	0.92	-3.16	17.02
DEM-ES100-R-3	25	0.47	0.96	0.94	35.30	17.89	3.4	1.6	0.55	0.89	0.89	-7.29	22.22
DEM-ES100-R-A	**25**	**0.47**	**0.96**	**0.95**	**35.01**	**18.33**	**2.9**	**1.37**	**0.56**	**0.90**	**0.90**	**-6.20**	**21.62**

Table 5.13: Summary of the soil properties before and after erosion in the case of different rolling resistances for fine and coarse particles.
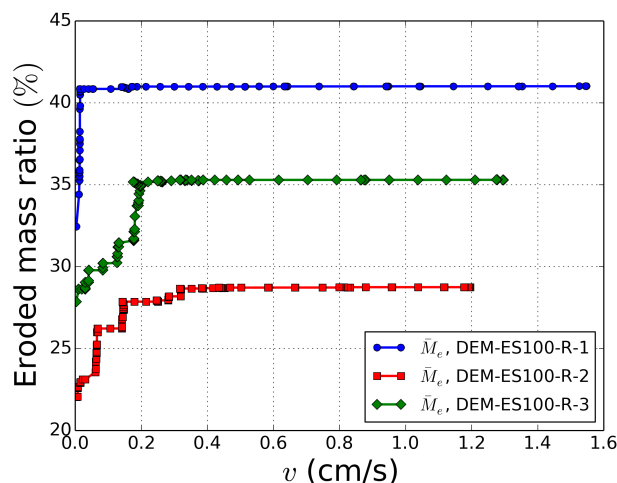
Figure 5.21: Eroded mass with the increase in flow velocity, v, in the case of different rolling resistances for fine and coarse particles.

Once the soil is confined up to 100 kPa, the drained triaxial compression test is carried out. Figure 5.23 shows the response of the numerical soil before and after erosion compared to the experimental data. Even if smaller particles have a higher rolling resistance than the coarser ones, their removal did not influence the shear strength. The peak and residual friction angles remain almost the same after erosion (Table 5.15). Moreover, the eroded soil exhibits a slightly higher dilatancy angle, $\psi_{max} = 2.60°$, compared to the non-eroded soil sample ($\psi_{max} = 1.62°$).

In fact, even if smaller particles have higher rolling resistance, about 97% of them are rattlers and mainly inactive particles are removed. The soil skeleton did not compact significantly after erosion. Thus, the shear strength after erosion was not highly influenced by the removal of inactive particles. It is expected that if more fine particles participate in the force chain network (or if the soil is initially denser so that less fine particles are rattlers), the effect of higher rolling resistance would be more important and maybe the removal of fine particles may decrease the shear strength of eroded soil samples.
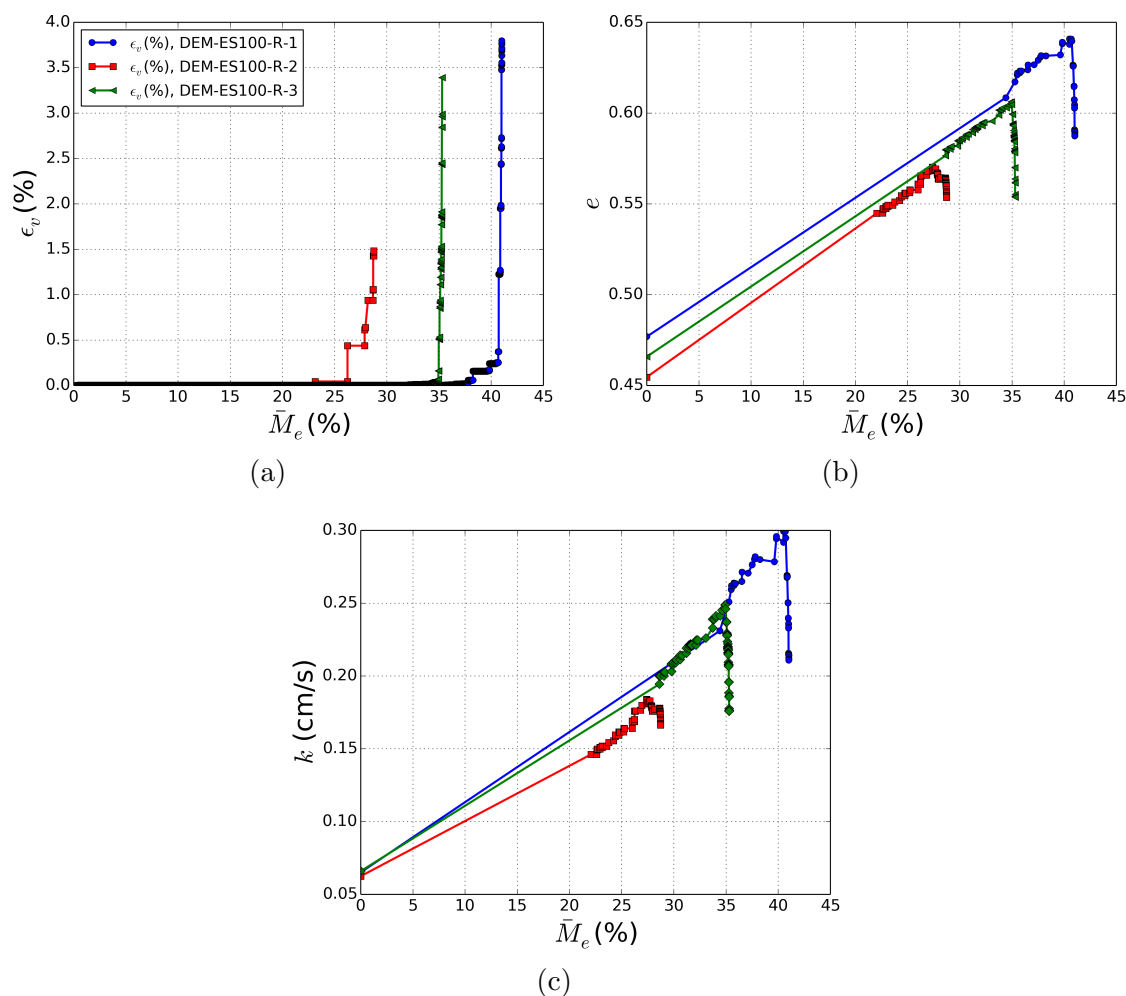
Figure 5.22: The variation in the (a) volumetric deformation, (b) global void ratio and (c) hydraulic conductivity with the erosion of fine particles in the case of different rolling resistances for fine and coarse particles .

Soil sample	P_c=5kPa			P_c=100kPa				
	e_{er}	e_{ger}	e_{eqer}	ϵ_v (%)	ϵ_a (%)	e'_{er}	e'_{ger}	e'_{eqer}
DEM-ES100-R-1	0.59	0.90	0.90	1.3	0.4	0.56	0.91	0.89
DEM-ES100-R-2	0.55	0.92	0.92	1.4	0.5	0.54	0.90	0.88
DEM-ES100-R-3	0.55	0.89	0.89	1.3	0.4	0.54	0.87	0.85
DEM-ES100-R-A	**0.56**	**0.90**	**0.90**	**1.3**	**0.43**	**0.55**	**0.89**	**0.87**

Table 5.14: Response of the soil samples due to the increase in the confining pressure from 5 kPa to 100 kPa in the case of different rolling resistances for fine and coarse particles.

Soil sample	Before suffusion			After suffusion		
	φ_p (°)	φ_0 (°)	ψ_{max} (°)	φ_p (°)	φ_0 (°)	ψ_{max} (°)
DEM-ES100-R-1	32.26	29.91	2.25	30.95	30.95	1.76
DEM-ES100-R-2	33.30	30.45	1.60	32.29	30.62	2.26
DEM-ES100-R-3	32.32	31.38	1.01	33.31	31.34	3.79
DEM-ES100-R-A	**32.18**	**30.63**	**1.62**	**32.19**	**31.15**	**2.60**

Table 5.15: Peak and residual friction angles before and after suffusion in the case of different rolling resistances for fine and coarse particles.


(a)

(b)

(c)
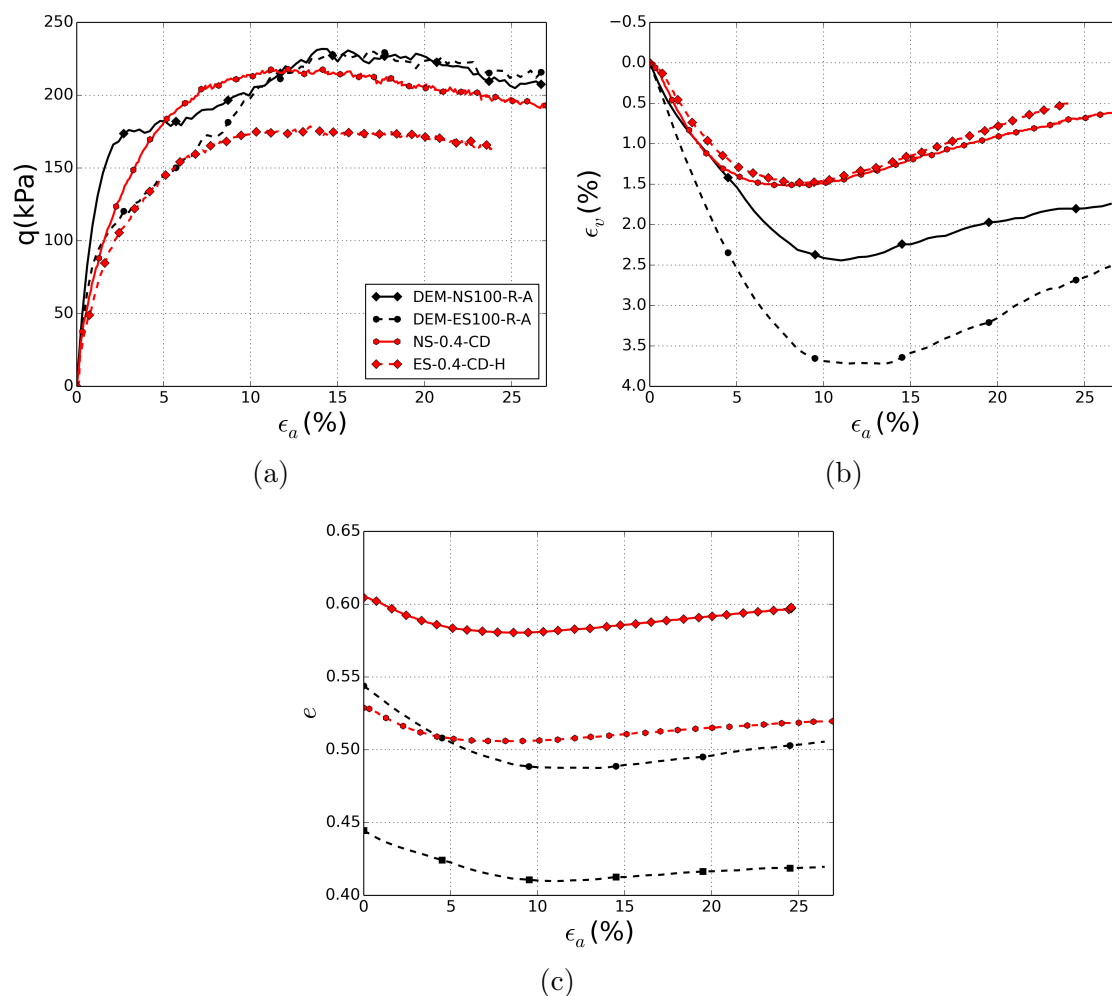
Figure 5.23: Comparison between experimental and DEM soil response to drained triaxial compression test before and after erosion in the case of different rolling resistances for fine and coarse particles.

5.4.3   Influence of the global density

So far, the effect of suffusion on the soil shear strength is not important in the numerical soil samples compared to the experimental ones. It has been stated earlier that this may be related to a different microstructure between numerical and experimental soil samples. The micro-structural analysis of the numerical soil has shown that about 97 % of fine particles are rattlers under a confining pressure of 5 kPa. Moreover, the threshold fines content for this soil is around 40 %, slightly higher than the experimental value (35 %). Hence, probably, the experimental soil has more active fines whose loss might have led to a significant effect on the shear strength. This could be confirmed since it was shown that as the density increases (leading to more active fine particles), the reduction of the soil shear strength with the erosion is more important (Chapter 4). Therefore, as an attempt to investigate the effect of density (or the erosion of more active particles) on the shear strength, a numerical simulation was performed on a soil sample prepared at a higher density.

The dense soil sample was prepared by setting the contact friction angle of soil particles to 10° during compaction under a confining pressure of 5 kPa. The resulting specimen thus contains 93.29 % of rattlers which is a lower fraction compared to the previous looser specimens (97 %).

Although at higher densities the eroded mass decreases, in this case we tried to erode a fraction of particles similar to the previous cases to make the comparison possible. Note, in this case we consider the homogeneous erosion and same mechanical properties for both fine and coarse particles. For that purpose, x was calibrated giving a value of 0.75 for which 33.73% by mass of fine particles were eroded. Notice that, also more active particles were eroded in this case ($\bar{M}ea = 0.82\%$). Table 5.16 gives the characteristics of the eroded dense soil. Figure 5.24 shows the evolution of the eroded mass with Darcy's flow velocity and the variation in the volumetric deformation, void ratio and hydraulic conductivity with the eroded mass. For low flow velocities, the soil did not lose fine particles. As the flow velocity increases, more fine particles were detached and transported including active particles. Hence, the eroded mass increases progressively with the flow velocity (Figure 5.24a). However, Figure 5.24b shows negligible deformations with the erosion of fine particles. Therefore, in this case, erosion did not influence the stability of the soil skeleton. Moreover, as given in Table 5.16, the relative change in the inter-granular void ratio is negligible which confirms that the soil preserves its soil skeleton during erosion. However, since the soil lost fine particles, the void ratio increases and consequently the permeability increases slightly too (Figures 5.24c and 5.24d).

Once the erosion process is terminated, the soil is then confined under 100 kPa. Similarly

Soil sample	Before suffusion				After suffusion							$\Delta e_g/e_{g0}$ (%)	$\Delta e/e_0$ (%)
	FC_0 (%)	e_0	e_{g0}	e_{eq0}	M_e (%)	FC_f (%)	ϵ_v (%)	ϵ_a (%)	e_{er}	e_{ger}	e_{eqer}		
DEM-dense_eroded	25	0.39	0.85	0.81	33.73	18.36	≈ 0	≈ 0	0.51	0.85	0.84	≈ 0	30.77

Table 5.16: Summary of the soil properties before and after erosion in the case of an initially dense soil.
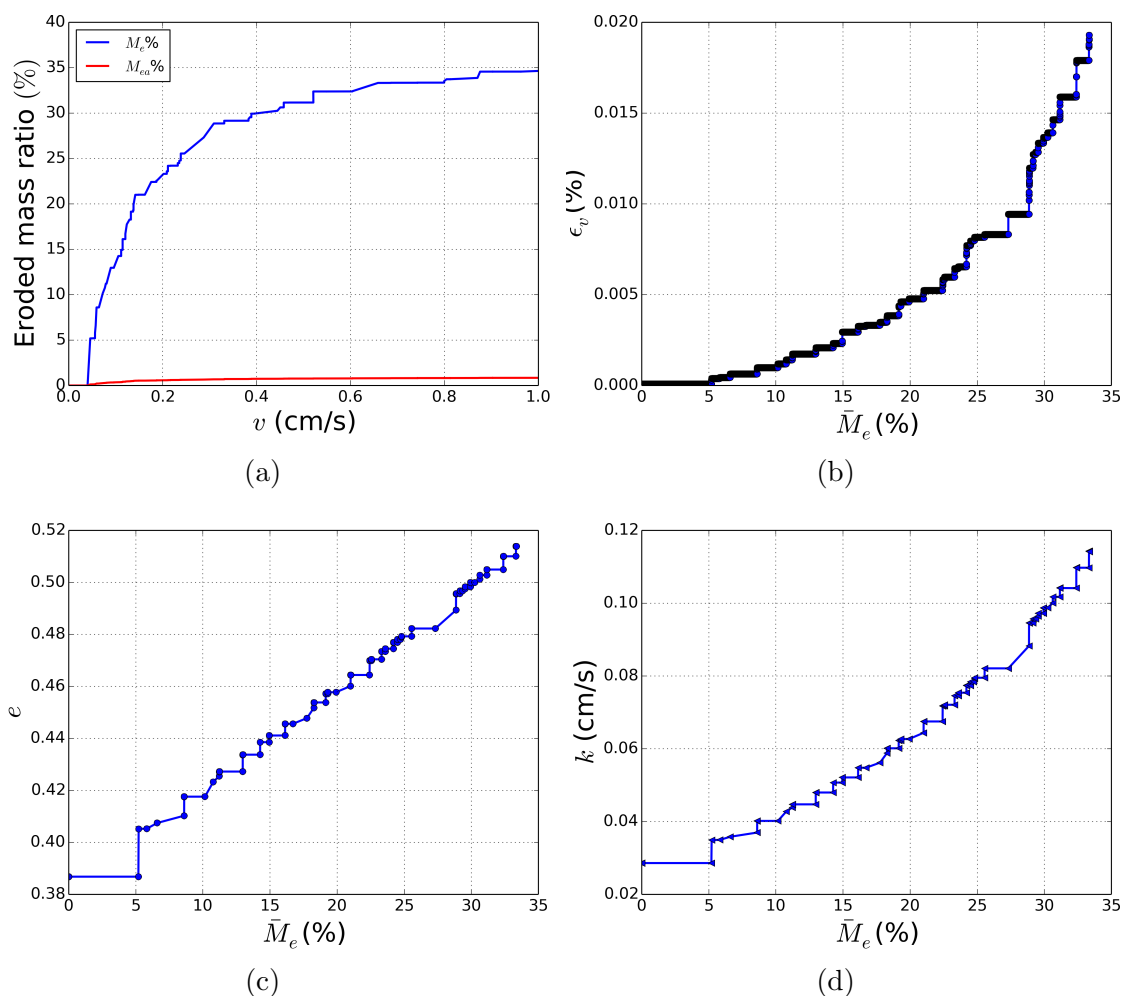
Figure 5.24: The variation in the (a) eroded mass with Darcy's velocity, (b) volumetric deformation, (c) global void ratio and (d) hydraulic conductivity with the erosion of particles for the case of an initially dense soil.

to the previous sections, the soil during this phase shows small defromations (ϵ_v =0.7 %, ϵ_a =0.2 % as given in Table 5.17). Consequently, the void ratio, the inter-granular and equivalent inter-granular void ratios decrease slightly too. Thus, the soil densifies slightly in this phase. Nevertheless, such modifications seem to be negligible in this case.

Therafter, a drained triaxial compression test is carried out. Figure 5.25 shows the

Soil sample	P_c=5kPa			P_c=100kPa				
	e_{er}	e_{ger}	e_{eqer}	ϵ_v (%)	ϵ_a (%)	e'_{er}	e'_{ger}	e'_{eqer}
DEM-dense_eroded	0.51	0.85	0.84	0.7	0.2	0.49	0.84	0.81

Table 5.17: Response of the soil samples due to the increase in the confining pressure from 5 kPa to 100 kPa in the case of an initially dense soil.

response of the non-eroded and eroded soil samples. A significant decrease in the shear strength after erosion can be observed in Figure 5.25a. The peak friction angle decreases

from 38.26 ° to 31.01 ° (Table 5.18). Hence the effect of erosion on the shear strength is more pronounced for higher densities. Moreover, Figure 5.25b shows that the soil becomes more contractant. Concerning the critical state, both eroded and non-eroded soil samples reached the same deviator stress at large deformations. The residual friction angle is almost the same (30.14 ° for the non-eroded model and 31.01 ° for the eroded one). However, even if the shear strength at the critical state was not affected, Figure 5.25c shows that the two samples have different void ratios at the critical state.

Finally, the parametric study shows that the average global compaction of the granular

(a)

(b)

(c)
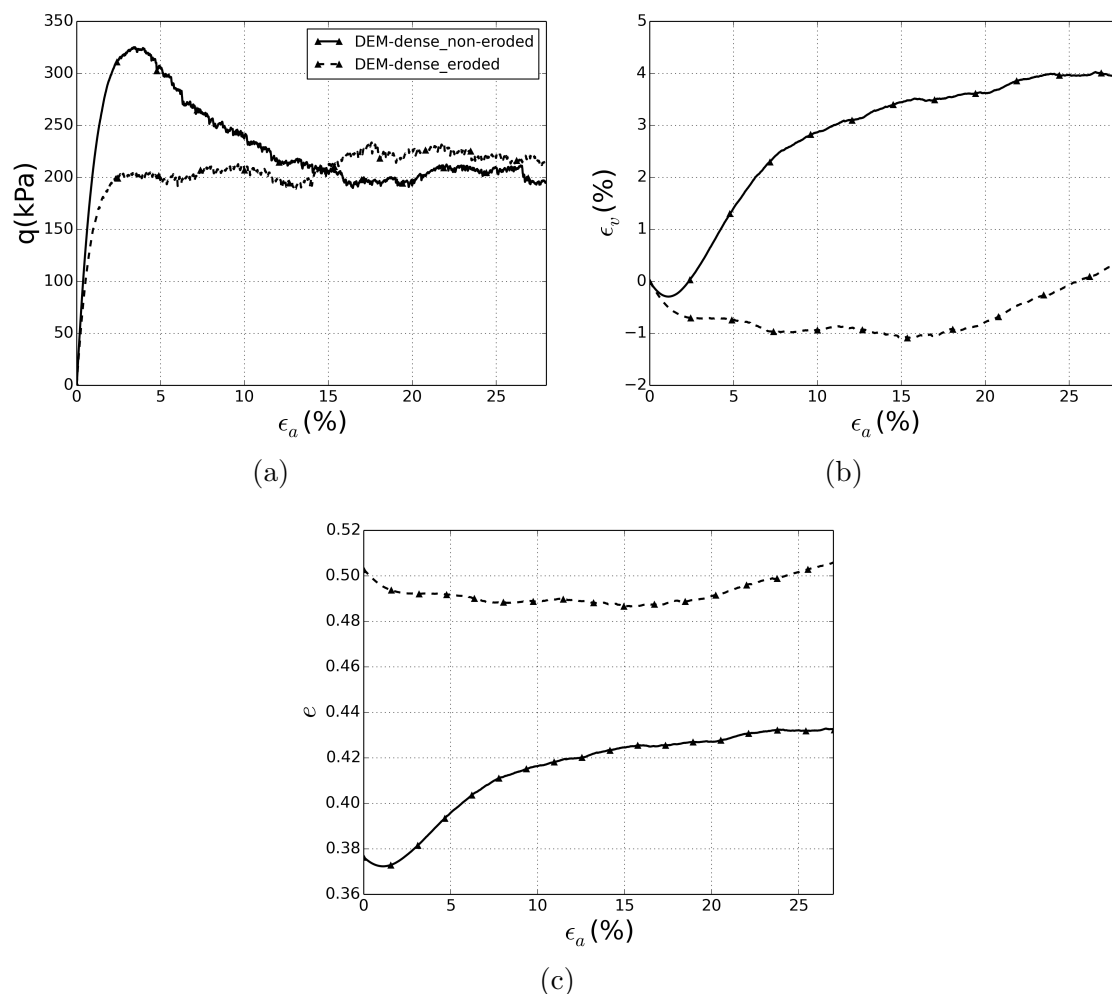
Figure 5.25: Comparison between experimental and DEM soil response to drained triaxial compression test before and after erosion.

skeleton during the suffusion development could be slightly more important in case of heterogeneous erosion or if the fine fraction presents higher mechanical properties than the coarse fraction. In this way the response of the model during suffusion gets closer to the experimental results. Although the combination of a heterogeneous erosion with higher mechanical properties for the fine fraction has not been tested, it may even accentuate this trend. Nevertheless, it seems that the influence of the factors discussed above on the degradation of the mechanical properties after suffusion are of second importance. However, the initial density of the sample seems to play a major role. The numerical model and the experimental data (see Chapter 4) seem to present a similar trend. For

Soil sample	Before suffusion			After suffusion		
	φ_p (°)	φ_0 (°)	ψ_{max} (°)	φ_p (°)	φ_0 (°)	ψ_{max} (°)
DEM-dense_eroded	38.26	30.14	12.42	31.01	31.01	3.73

Table 5.18: Peak and residual friction angles and dilatancy angles before and after suffusion in the case of a dense granular assembly.

a low initial density the medium tends to compact quite easily during suffusion and the mechanical response to a drained triaxial compression is weakly impacted, whereas for a high initial density, the granular assembly, more stable, presents lower volumetric deformation during the suffusion process but the mechanical properties of the eroded medium are much more degraded.

5.5 Conclusion

In this chapter the numerical extraction procedure as defined in Chapter 3 was applied on wider gradations similar to that used experimentally in Chapter 4. Two particle size distributions were considered. One of them is the same PSD used experimentally while the second is a simplified gradation to reduce the computational time. The soil was first calibrated to fit the experimental data. Thereafter, suffusion tests were simulated followed by drained triaxial compression tests to characterize the mechanical behavior of eroded soils.

The suffusion-like simulations reproduced qualitatively the experimental behavior of the soil during erosion. The void ratio and the hydraulic conductivity increased with the eroded mass. Due to the removal of fines, soil particles rearrange themselves to reach a new equilibrium state causing the soil to compact. Despite this global compaction the void ratio and hydraulic conductivity increase with the eroded mass. However, the soil deformation was underestimated numerically. This was attributed to the different initial microstructures from the experimental one resulting in too much rattlers. Therefore, since the majority of the eroded fines were rattlers, their effect on the soil structure was negligible. The accurate description of the initial soil microstructure seems to constitute a key factor for the improvement of the predicted soil response during the suffusion development.

Drained triaxial compression tests were then performed to study the effect of erosion on the mechanical properties of the soil. Although the numerical soil samples behave similarly to the experimental one during erosion, once sheared the behavior is different in some points. The numerical soil samples did not show a decrease in the shear strength as the experimental results, and presented a more important initial contraction at the shearing initiation. Nevertheless, the dilatative response after this initial contraction is slightly more marked for the eroded samples than the non-eroded one, as observed experimentally. In addition, the loss of rigidity, initial rigidity and in the hardening phase, is in quite good agreement with the experimental data; the general shift of the void ratio for the eroded soils, towards a globally more porous state is also satisfactorily described all along the compression, and more particularly at large strains.

Since the suffusion-like simulation results in a homogeneous eroded soil unlike the experimental specimens, an attempt to study the effect of such induced heterogeneities was followed. Two cases were considered, either by eroding fine particles from the upper part of the soil samples; or by eroding fine particles from the lateral boundaries. Another parametric study was done by considering different rolling properties of fine and coarse particles. Assuming that fine particles are more resistant to rolling (so that their erosion may influence more the shear strength), the rolling friction, η_r, of fine particles was set higher than that of coarse particles. Both approaches (heterogeneous erosion or different rolling properties) lead to a more sensitive response of the model in terms of global volumetric deformation to the suffusion development. The simulated compaction was more important and get closer to the experimental one even if the correction is not enough to fit satisfactorily the experimental data. However, despite this slight improvement, the responses of the eroded numerical samples to the drained compression are almost unchanged: the shear strength is still not affected by the erosion and the initial contractancy is still more important than the experimental results.

The main problem seems to be due to the fact that the numerical model has many rattlers and their removal in any created scenario does not affect the shear strength as is the experimental case. Therefore, a final attempt was to increase the density so that the number of rattlers decrease. Moreover, this allows to study the effect of density as it was done experimentally. A suffusion-like simulation has been done on a dense specimen followed by a drained triaxial compression. In this case, more active particles were eroded during suffusion. However, the soil did not deform. Once sheared, the peak shear strength decreases significantly and the soil becomes less dilatant due to the higher global void ratio which governs the behavior of the soil. Hence, there is a much more marked degradation of the mechanical properties by suffusion for the denser material. The looser granular assembly initially considered seems to be much less affected.

Finally, although, the numerical model did not perfectly reproduce the experimental results due to the different initial microstructures, but qualitatively it has led to some common conclusions. It was found that, similarly to the experimental results, the eroded mass increases with the hydraulic loading creating a more open microstructure, even if, with the increase in the eroded mass, the soil compresses. Furthermore, it was shown that, for higher densities, erosion of fine particles leads to less deformations. Once sheared, initially denser soils suffer from a larger reduction in the peak shear strength. However, loose samples that compress more during erosion, tend to conserve their mechanical properties.

Conclusions and Perspectives

This research was devoted to the study of the internal erosion process by suffusion. The importance of this work lies in its application for the safety and durability of hydraulic earth structures such as dams and levees.

The objectives of this study were to improve the chracterization of the suffusion development and more particularly its impact on the mechanical properties of cohesionless soils. To achieve these objectives, we have followed an approach which consisted of the following steps:

- definition of a DEM model to analyze the microstructure of granular assemblies and to describe quantitatively the soil's macroscopic behavior;

- investigation of the role of fine particles with respect to a given soil microstructure (i.e. without taking into account an erosion process);

- definition of a simplified kinetics of grain extraction to describe the suffusion process;

- performing experimental tests using a newly developed suffusion apparatus and a triaxial compression apparatus;

- numerical simulations with the discrete model calibrated on the soil used experimentally;

The numerical results were used in complementary with the experimental data to give a global conclusion on how the soil's mechanical properties change with suffusion. The major contributions and conclusions obtained from this study are summarized in this chapter. Moreover, perspectives and recommendations for future research work are also presented.

1. Major contributions

Discrete numerical model to describe quantitatively the soil macroscopic behavior

A discrete numerical model was defined to study the soil mechanical behavior using spherical particles and contact rolling resistance. In this model, five parameters are involved (contact stiffness, tangential stiffness, rolling stiffness, contact rolling moment and contact friction angle). It was shown that if contacts are sufficiently stiff, the macroscopic plastic properties of the granular assembly depends on the plastic parameters at the microscopic scale, and mainly on the plastic rolling moment reflecting the particle's

shape. Moreover, the macroscopic behavior is greatly affected by the initial density as a real soil. Therefore, a new numerical method of compaction was proposed, which involves the introduction of inter-particle adhesion forces or by the lubrication of contacts, to reach a wide range of initial densities from very loose to very dense. Using a simple elasto-plastic constitutive relation requiring few paramters to be calibrated, the model succeeded in describing quantitatively the mechanical behavior of soil. Finally, a calibration process has been suggested to identify the parameters of the contact law and the initial numerical porosity to be used to model a cohesionless soil.

The role of fine particles in the microscopic and macroscopic behavior of a polydisperse granular soil

Since the evolution of the soil properties with suffusion is directly related to the role of fine particles, an analysis of polydisperse granular assemblies with different fines contents was considered (Chapter 2). Idealized samples with isotropic fabric and spherical particles were studied using the defined DEM model. Analysis of the microstructure of soils with different fines contents is done by studying the impact on the void ratio (global, inter-granular and equivalent inter-granular void ratios). Furthermore, the consequences on the contacts formed between particles were investigated. From such an analysis, an "active" fines content FC_{active} was distinguished from FC_{th}. Therefore, if erosion takes place for FC around FC_{active} and if active fine particles are eroded, the macroscopic behavior of the soil should be affected significantly as fine particles will be involved in the strong contact force network, unlike the case of soil gradations with lower fines contents.

A simplified kinetics of grain extraction

A numerical approach was presented to describe the erosion of soil by suffusion. A simplified extraction procedure was defined based on the discrete element method with a one-way fluid-solid coupling. The proposed method consisted in splitting the suffusion process in detachment and migration steps considered sequentially from an equilibrium state of the granular assembly reached under a prescribed stress state. The detachment criterion is based on checking the equilibrium of solid particles under the combined action of inter-particle contact forces and fluid forces. A particle out of equilibrium is considered as detached. The possibility of these particles to be transported through the pore network is then examined by following a transport criterion deduced from the constriction size distribution. A detached particle is removed from the soil sample if its diameter is smaller than xD_{c35} (D_{c35} is the constriction size for which 35 % of the constrictions of the granular assembly are finer than this size), where x stands for the collective passing of fine particles through a given constriction and is calibrated to fit the eroded mass collected experimentally. By taking into account the hydraulic loading and the constrictions of the interstitial space, the definition of this extraction procedure constitutes an original contribution with a reasonable computational cost.

Experimental suffusion tests using a newly developed permeameter

A new suffusion apparatus and technique developed at IRSTEA have been used to investigate the seepage-induced internal instability in cohesionless soils. The experiments

were based on an imposed uni-directional multi-stage flow. A novel feature of this apparatus and technique was the freezing procedure which can be performed in the erosion cell, and the possibilty to preserve the microstructure of the eroded soil allowing their transfer into the triaxial cell without any disturbances. A series of suffusion tests was conducted. The data measured for each test were: the hydraulic gradient, the hydraulic conductivity, the eroded mass, and the final volume change. Moreover, the final density, the global void ratio, the inter-granular void ratio and the final fines content were calculated to take into account modifications in the soil microstructure. The objectives of these tests were to study the effect of the flow rate and the initial density on the erosion process as well as to investigate its consequences on the mechanical properties of soils.

Induced modifications by suffusion in the soil microstructure

Experimental and numerical suffusion tests were done on soil samples with different gradations (particularly in the numerical tests where narrow gradations, in addition to wide gradations, were also used to reduce the computational time). Although the numerical approach did not fully describe the experimental results, some interesting conlusions were obtained:

- for a given density, the eroded mass increases with the hydraulic loading (characterized experimentally by the Darcy's velocity). Depending on the state of the eroded particles (i.e. active or inactive), the soil may either deform and compact significantly modifying the coarse soil skeleton (if active particles are eroded) or it may keep its matrix integrity with only a slight compaction (in the case of erosion of inactive particles);
  As the initial state of the eroded soil particles, or more generally speaking the initial soil microstructure, constitutes a key factor in the overall soil deformation induced by suffusion, it seems necessary to take it into account to model (with a discrete numerical model as in this work, or with any other modeling approaches) the soil response to a suffusion process. Let us recall that a variable of density or porosity does not define completely the soil microstructure since different microstructures are possible for a given density, even for a sand (Benahmed et al. (2004));
  Despite the compaction induced by suffusion, the soil becomes globally looser and more permeable (for all the studied cases: narrow and wider gradations and different initial densities). The departure of eroded particles leads to an increase in the global void ratio which cannot be completely compensated by the sample compaction;

- for a given initial gradation, when different initial density states are considered, it is found that the soil compaction becomes less pronounced during suffusion in case of a higher initial density. In other words, the denser soil skeleton is capable of withstanding the erosion of fine particles without buckling. Moreover, as will be stated later, the mechanical properties may be modified although the deformations during suffusion are negligible;

- for a narrow initial grading (Chapter 3), suffusion development could lead to highly porous medium possibly without impacting the coarse skeleton and thus without clear deformations observed at the macroscopic scale.

Effects of suffusion on the macroscopic constitutive behavior

After the erosion process, soil samples were subjected to monotonic triaxial compression tests to characterize the impact of suffusion on the mechanical behavior of the soil. Drained and undrained triaxial compression tests were carried out in the experimental approach and only drained triaxial compression tests were simulated in the numerical approach.

- for a given density, the experimental results show that the peak and residual friction angles identified in drained condition decrease with the eroded mass. This seems to be accompanied by a slight increase of the dilatancy angle, but no clear evolution of the latter with the eroded mass has been identified. The interpretation of these results may be related to the combined effect of the void ratio, the inter-granular void ratio and the final fines content which controls the overall behavior of the soil. However, the impact on the dilatancy angle is different in the numerical and experimental results. Numerically, there is a consistency in the results whereby the loss in the peak shear strength (for sufficiently initially dense materials) is accompanied by a reduction in the dilatancy angle. Despite this difference, the numerical model and the experimental data are in agreement with the reduction of the initial rigidity of the soil and the softer stress-strain behavior in the hardening regime. Moreover, there is a shift at large deformation (critical state) induced by the erosion towards higher void ratios, but lower inter-granular void ratios. However, experimental and numerical results differ about the impact on the shear strength at large strains. Numerically, the deviator stress at the critical state is not impacted whereas experimental results show a reduction of the latter as the eroded mass increases. This difference may be related to the model considering a microstructure which is not sufficiently representative of the real one as already discussed (with probably an overestimation of the number of rattlers among the fine fraction);

- when different initial densities are considered, the impact of the suffusion appears as dependent on the density: as the initial density increases, the loss in the shear strength increases too. Looser samples that deform more significantly during suffusion, are more prone to conserve their initial mechanical properties;

- for a narrow initial grading (Chapter 3), suffusion may not impact the coarse skeleton and thus no clear deformations are observed at the macroscopic scale. In such cases, the eroded medium would present a kind of atypical dual behavior: a typical dense mechanical behavior at low deformations when sheared, and a very loose behavior at large deformations. Nevertheless, these numerical results have been obtained from a soil grading which is marginal with respect to those usually impacted by suffusion and therefore should be carefully considered;

- the consequences of the erosion of inactive particles seems to depend on the initial soil gradation. Soils with a narrow gradation (Chapter 3) showed that if mainly inactive particles are eroded, almost no deformation occurs during suffusion; however the soil shear strength can be greatly affected. Using a wider gradation (Chapter 5), it was noticed that eroding mainly inactive particles had almost no influence on the soil shear strength. In other words, for the narrow gradation, the inactive particles in the initial state probably participate in the force transfer from time to time, along a compression loading path, and play a key role, at least occasionally;

- it was shown numerically that, for a given density, both homogeneous and heterogeneous erosion processes lead to a similar mechanical behavior; Similar conclusion was drawn if fine and coarse particles have different mechanical properties;

- it was shown experimentally that eroded and non-eroded soils have the same phase transformation/characteristic lines under undrained/drained conditions respectively. Moreover, the critical friction angle for non-eroded soil samples in drained and undrained conditions is the same. Similarly, eroded soil samples exhibit the same critical state/failure line in drained and undrained conditions. Hence, there is a consistency between the drained and undrained results respectively. However, the critical state line of the tested eroded soils in $q - p'$ diagram is lower than that of the non-eroded soils;

- an approach to predict the mechanical response of eroded soils was proposed. A parameter, δ, representing the void volumetric variation between the eroded and the non-eroded soil samples was defined. This parameter helps to predict whether the eroded soil will be more resistant or not compared to the non-eroded soil. When δ is greater than 0, the shear strength of the eroded soils would be lower than that of the non-eroded soil. When δ is close to or smaller than 0, the soil would behave like the non-eroded one.

- critical state points in $e - \log p'$ and $e_g - \log p'$ planes show an interesting trend regarding the critical state of eroded and non-eroded soils. The location of the critical state points of eroded samples above that of non-eroded ones in $e - \log p'$ implies that the shear resistance at the critical state for a given void ratio increases with the increase of erosion and the loss of the fine particles. Whereas, in $e_g - \log p'$ plane, the critical state points of eroded samples are situated below that of the non-eroded ones indicating that for a given inter-granular void ratio, the shear resistance at the critical state decreases with erosion of fine particles; i.e. the decrease of the fines content. These results are in agreement with studies done on samples reconstituted with different fines contents.

2. Perspectives

This study has opened new research paths that can be interesting. In what follows, recommendations for future research work are presented which concerns both numerical and experimental approaches.

Perspectives for improving the numerical model

- The DEM model defined in Chapter 2 succeeded in reproducing the experimental data. However, it had some limitations related to the description of the dependency of volumetric strains on the mean pressure. These limitations were due to the difference in the relative variation of the initial porosity after compaction between experimental and numerical tests and to the different particles' shapes. To better reproduce the dependency of dilatancy on the mean pressure, an additional law describing the dependency of the contact friction angle with the normal contact force may be required.

- Another limitation of the numerical model is that it could not describe accurately the microstructure of the experimental soil even though the macroscopic behavior was well reproduced. In other words, it was noticed that the threshold fines content in the numerical soil is higher than the experimental value which might have resulted in a very high number of rattlers in the numerical granular assembly. Consequently, numerical soils reconstituted at the same fines content as the experimental soil, did not give quantitatively the same results obtained in the laboratory erosion tests. The soil's deformation and the change in both the inter-granular and the global void ratios were underestimated. Therefore, the defined model still needs to be improved so that it would be possible to create the same microstructure of a given soil. For that purpose we propose the following solutions:

  - use a more complex particle's shape instead of spheres, such as polyhedral shape. Particles with edges will tend to make more contacts with other particles and thus maybe the number of rattlers will decrease. However, studies in the literature show that using such shapes requires a higher computational cost;

  - add gravity forces after reconstituting the soil sample so that some rattlers become in contact with other particles; in the case of periodic boundaries, after compaction at a low confining pressure, the periodic cell should be fixed. Then, add the gravity forces, and run few iterations. Thereafter, remove the gravity forces and increase the confinement until the target value;

  - as the soil samples were created experimentally with the moist tamping technique, the use of an inter-granular adhesion during the preparation phase of the numerical granular assembly could be tested;

- the numerical extraction procedure is based on simple assumptions concerning the detachment and migration of particles. As the focus in this research was not to describe accurately the suffusion process, adopting such assumptions was needed to keep a limited computational time knowing that only a complete hydromechanical coupling approach is needed for this description. Thus, it is recommended to perform suffusion simulations using a complete fluid-solid coupling. These simulations serve to better understand how the microstructure of the soil is modified during suffusion development. Moreover, it can describe the filtration process that was ignored in our study. So far, few attempts are found in this direction; for example Tejada et al. (2016) investigated the effects of the intermittent blockage of constrictions and its consequences on the particle transport using a complete coupled hydromechanical approach (DEM-PFV) based on the discrete element method. In addition to that, the ongoing PhD of Antoine WAUTIER at IRSTEA concerns the modeling of suffusion in granular materials in order to improve the understanding of elementary mechanisms at the microscopic scale. For that purpose, Antoine also uses the complete DEM-PFV method.

- usually soils are found under complex stress states. In our study, the erosion process was initiated in soil samples at an isotropic stress state. Thus, it would be interesting to investigate how the stress state influences the suffusion development; Our proposed model makes it helpfull now to simulate such different stress states. A triaxial compression can be carried out up to a given stress deviator. Then, suffusion simulations can be performed. Results should be validated by experimental data;

- besides the simplicity of using a discrete element method, it is not possible to model the behavior of soils at a large scale. Therefore, using a DEM model, it would be interesting to define a relation between suffusion and the mechanical properties of soil. Developing such a relation requires, though, a sufficient data; i.e. performing many simulations on different gradations, stress states, densities,... It can serve to develop a clear suffusion law that can be used in continuum approaches where it would be possible to model the macroscopic behavior of soils at the scale of engineering structures;

Perspectives for improving the experimental approach

- using the newly developed apparatus, suffusion tests were carried out on unconfined soils or soils not subjected to any stresses. Similarly to the previous recommendation in the previous section, it would be interesting to study effects of suffusion on soils under different stress states. However, as we are using a rigid wall permeameter, it is not possible to apply any confining pressure on the sample. Nevertheless, the apparatus could be equipped with an axial loading system (Sail et al. (2011)). This allows studying the effect of the axial effective stress on the suffusion process;

- the suffusion apparatus used at its initial version was not provided with means to measure the volumetric deformation during suffusion tests. Only at the end of each test, the height of the sample was measured and the final volumetric deformation was calculated. However, it is of great interest to have all the data for each hydraulic loading stage. For that purpose, a new approach is now adopted by Ph.D student, C.D. Nguyen at IRSTEA, who is using a non-contact measurement transducer to measure accurately the settlement of specimens during suffusion;

- the interpretation of the experimental results in this study was difficult as we did not have any clear information about the soil microstructure induced by erosion. Hence, microscopic observations of the eroded soil fabric are necessary to better undestand the mechanical behavior of eroded soils. For that purpose, x-ray tomographies can be used to investigate the micro-structural changes of eroded soils by suffusion. This will give access to the following data: distribution of fine particles in the pore space (and better discription of the induced heterogeneities), filtration zones, and calculation of the constriction size distribution. This work is presently tackled by C.D. Nguyen, Ph.D student in IRSTEA, who has performed x-ray tomographies on eroded soil samples at 3SR laboratory. Such microstructural study may open to more deep analysis and description of the suffusion process;

Improvement of the suffusion-like model with a probabilistic approach for the particle transportation

A limitation of the particle extraction process that we defined to mimic the suffusion development is related to the particle transport criterion based on D_{c35} (which stands for a characteristic constriction size of the pore space). This assumption is not totally clearly justified and a better description of the ability of detached particles to be transported could be given by a probabilistic approach (see for example Reboul (2008)). For that purpose we initiated the development of a probabilistic transport criterion to be embedded in the defined kinetic extraction and we give below the ideas about this probabilistic approach.

The problem of the suffusion process or the migration of particles through a porous medium has been studied so far by several researchers. Continuum models have been proposed, based on phenomelogical laws, but they cannot describe accurately such a particle-scale mechanism. In addition to that, DEM models have been also defined for that purpose, sometimes embedding a coupling with a fluid model. However, using the DEM is always limited to a reasonable number of discrete elements to avoid an unaffordable computational time. Thus, it would be interesting to have an alternative approach based on a probabilistic scheme of the migration of fine particles in a granular assembly. In what follows, the general idea for developing a future probabilistic method is presented.

The transfer process in granular materials is governed by the way pores are connected. In other words, it is related to the topological properties of the soil. The constrictions are the determining entities in such processes (Vogel & Roth (2001)). Indeed, the largest constriction size defines the size of the particle above which the granular medium will act as a filter. Conversely, a population of particles smaller than the minimum constriction size will successfully percolate through the medium. To carry out a topological study on granular media, the void space is usually represented as a set of pores linked together via constrictions. Thus, constrictions determine the pore network connectivity. Based on that, a topological study of a simulated packing of spheres was performed.

The movement of a particle of a given size through the pore network is modeled. The transport model is constructed based on the geometrical data of the pore space given by the DEM model. The pore space of a granular medium presents multiple paths that fine particles can displace through. An approach to account for the migration of particles is to model the granular medium by a network of constrictions and to identify the potential paths of migration as a succession of constrictions. Therefore, all the migration paths (successive constrictions) are first identified. The migration paths considered are assumed to be in the downward direction (considering a downward flow direction), i.e. the connectivity of two pores is taken into account if the second constriction is below the first one; so that we assume that migrating particles do not move upwards or horizontally in the pore space. The calculation process is as follows:

- first all the sizes of the constrictions are calculated;

- two constrictions connecting a common pore to two other pores are considered part of a migration path, such that one of them is below the other;

- as we are using periodic boundaries, we can make use of that by developing infinite migration paths;

- for a given particle with a given diameter, it is now possible to determine, for each migration path, the free distance that this particle can cross before being blocked by a smaller constriction. Figure 6 gives the probability density function of particles having different radii (0.2 mm and 0.25 mm) to traverse a free distance (L_{free}) in a sample of height H.

- knowing the free distances that particles of a given size can cross, the probability density function can be plotted; thus, for a particle at a given location in the soil sample, it is possible to know the probability that it leaves the sample;
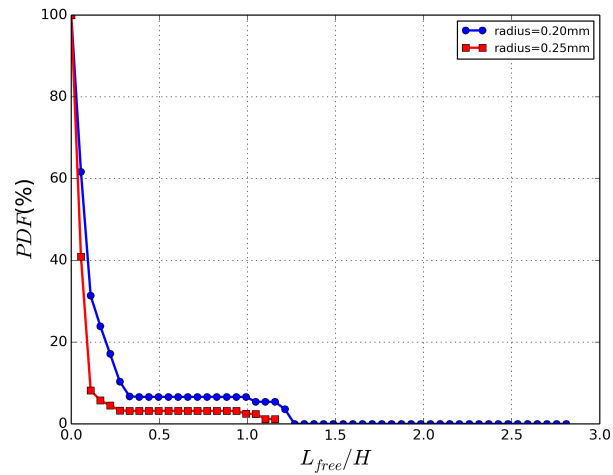
Figure 6: The probability density function for a given particles' radius to traverse a free distance in a sample of height H.

These steps form the basis of a probabilistic method which is still in progress to improve the transport criterion.

Résumé étendu en français

Contexte général

L'érosion interne dans les sols est un phénomène défini comme la migration des particules du sol en son sein induite par un écoulement de fluide. Il s'agit donc d'un processus multi-disciplinaire régi par les principes de la mécanique des sols et de l'hydraulique. L'érosion interne pose des problèmes importants dans différents domaines d'ingénierie. La production de sable est un problème majeur de l'ingénierie pétrolière où la migration des particules fines peut conduire au colmatage du puit d'extraction, de sorte qu'elle peut réduire la production de pétrole (Papamichos et al. (2001)). En géotechnique, la migration des particules fines peut entraîner l'effondrement des ouvrages en sol telles que les barrages en remblai et les digues. Les inondations provoquées par ces effondrements peuvent provoquer des catastrophes causant de graves dégâts aux infrastructures et présentant un risque important pour la vie humaine et animale (par exemple, l'effondrement du barrage de Teton (Seed & Duncan (1987))). L'analyse statistique montre que l'érosion interne est la principale cause d'environ la moitié des effondrements des barrages en remblai (Foster et al. (2000)).

L'érosion interne se présente sous de nombreuses formes différentes. Cette étude se concentre sur le processus de suffusion impliquant l'érosion sélective des particules fines dans la matrice des particules grossières. Un tel mécanisme à l'échelle des particules est caractérisé par le détachement et la migration des particules fines sous l'effet de l'écoulement interstitiel laissant derrière le squelette granulaire grossier. Ces modifications de la micro-structure du sol peuvent entraîner des déformations à l'échelle macroscopique et influencer de manière significative le comportement mécanique du sol. Un aspect peu étudié dans le domaine géotechnique porte sur les effets de la suffusion sur la résistance au cisaillement du sol. Une analyse plus approfondie de ce sujet peut faciliter une meilleure compréhension des mécanismes et processus impliqués et conduira à une conception, un entretien et une protection plus adéquats des nombreux ouvrages hydrauliques vis-à-vis des dégradations par érosion de suffusion.

Cette étude s'appuie sur une approche numérique basée sur la méthode des éléments discrets (DEM) et sur une approche expérimentale utilisant un dispositif de suffusion nouvellement développé. La recherche d'une relation claire entre l'érosion des particules fines et les propriétés mécaniques des sols constituera l'objectif principal de ce travail.

Objectifs

L'objectif principal de cette étude est de décrire les changements dans les propriétés mécaniques des sols érodés par suffusion. Pour y parvenir, des approches numériques et expérimentales sont envisagées:

- un modèle DEM est défini pour tenter de décrire quantitativement les modifications de la micro-structure du sol par un écoulement d'eau interstitiel;

- puisque l'évolution des propriétés du sol avec la suffusion est directement liée au rôle des particules fines (potentiellement érodables) dans les sols, le rôle des particules fines par rapport à une micro-structure du sol donnée (c'est-à-dire sans tenir compte d'un processus d'érosion) est également étudié;

- une cinétique simplifiée d'extraction des grains mimant le processus de suffusion pour pouvoir réaliser des simulations quantitatives avec des coûts de calcul réalistes est proposée;

- des essais expérimentaux ont été effectués pour valider le modèle numérique (si possible). Les essais de laboratoire sont utilisés pour construire une conclusion globale vis-à-vis de l'effet de la suffusion sur les propriétés mécaniques du sol en plus des résultats numériques;

- toutes les données obtenues sont consacrées à conclure sur l'impact de la suffusion sur les propriétés macroscopiques du sol;

Les résultats numériques ont été utilisés en complément des données expérimentales pour donner une conclusion globale sur la façon dont les propriétés mécaniques du sol changent avec la suffusion. Les principales contributions et conclusions tirées de cette étude sont résumées ci-dessous.

Un modèle numérique discret pour décrire quantitativement le comportement macroscopique d'un sol granulaire

Un modèle numérique discret a été défini pour étudier le comportement mécanique du sol en utilisant des particules sphériques associée à une résistance au roulement aux contacts. Dans ce modèle, cinq paramètres mécaniques sont impliqués (rigidités normales et tangentielles au contact, rigidité de roulement, seuil de moment plastique et angle de frottement aux contacts). Il a été montré que si les contacts sont suffisamment rigides (y compris la rigidité de roulement), les propriétés plastiques macroscopiques de l'assemblage granulaire dépendent uniquement des paramètres plastiques à l'échelle microscopique, et principalement du moment de roulement plastique reflétant la forme de la particule. De plus, le comportement macroscopique est fortement influencé par la densité initiale au même titre qu'un sol réel. Par conséquent, pour atteindre une large gamme de densités initiales de très lâche à très dense, une nouvelle méthode de compactage numérique a été proposée, qui implique l'introduction de forces d'adhésion inter-particules ou la lubrification des contacts, pour atteindre une large gamme de densités initiales de très lâche à très dense. Enfin, un processus d'étalonnage a été proposé pour identifier les

paramètres de la loi de contact et la porosité numérique initiale à utiliser pour modéliser un sol non-cohésif.

Le rôle des particules fines dans le comportement microscopique et macroscopique d'un sol granulaire polydisperse

Puisque l'évolution des propriétés du sol avec la suffusion est directement liée au rôle des particules fines, une analyse des assemblages granulaires polydisperses avec différentes teneurs en fines a été considérée. Des assemblages granulaires isotropes et des particules sphériques ont été étudiés en utilisant le modèle DEM tel que défini précédemment. L'analyse de la micro-structure des assemblages considérés porte sur l'évolution de l'indice des vides (global, inter-granulaire et inter-granulaire équivalent) et des types de contacts formés entre particules en fonction de la teneur en fine. A partir de cette analyse, on a distingué une teneur en fine "active", FC_{active} (pour laquelle des particules fines commencent à être impliquées dans le réseau de contacts forts participant à la résistance au cisaillement du sol), de la teneur seuil en fine, FC_{th} (pour laquelle le maximum de densité globale est obtenue, les fines remplissent exactement les espaces inter-granulaires). Par conséquent, si une érosion a lieu pour une teneur en fines proche de FC_{active} et si les particules fines actives sont érodés, le comportement macroscopique du sol devrait être affecté de manière significative car les particules fines seront impliquées dans le réseau de force de contact fort, contrairement au cas des gradations de sols comportant une teneur en fines plus faible.

Une cinétique simplifiée d'extraction des grains

Une méthodologie numérique est présentée pour décrire l'érosion du sol par suffusion, elle repose sur une procédure d'extraction simplifiée définie sur la base de la méthode des éléments discrets avec un couplage fluide-solide partiel. La méthode proposée consiste à diviser le processus de suffusion en deux étapes: une première étape de détachement et une seconde étape de migration considérées consécutivement à partir d'un état d'équilibre de l'ensemble granulaire sous un état de contrainte prescrit. Le critère de détachement est basé sur la vérification de l'équilibre des particules solides sous l'action combinée des forces de contact inter-particules et des forces fluides. Une particule hors d'équilibre est considérée comme détachée. La possibilité de transport des particules détachées à travers le réseau de pores du sol est ensuite examinée en suivant un critère de transport déduit de la distribution de taille de constriction. Une particule détachée est retirée de l'échantillon de sol si son diamètre est inférieur à xD_{c35} (D_{c35} est la taille de constriction pour laquelle 35% des constrictions de l'assemblage granulaire sont plus fines que celle-ci), où x permet de tenir compte du passage collectif de particules fines à travers une constriction donnée. Le paramètre x peut être calibré pour s'adapter à la masse érodée collectée expérimentalement. En prenant en compte le chargement hydraulique et les constrictions de l'espace interstitiel, la définition de cette procédure d'extraction constitue une contribution originale avec un coût de calcul raisonnable.

Des essais de suffusion en laboratoire en utilisant un perméamètre nouvellement développé

Un nouvel dispositif de suffusion et une technique développés à IRSTEA ont été utilisés pour étudier l'instabilité interne de la fraction fine d'un sol pulvérulent sous l'effet d'un écoulement interstitiel. Les expériences d'érosion par suffusion ont été menées en imposant un flux d'eau vertical descendant dans l'échantillon de sol contrôlé en vitesse. Une caractéristique originale de la technique mise en oeuvre consiste à congeler l'échantillon érodée dans la cellule de suffusion pour le transférer dans la cellule triaxiale tout en préservant la micro-structure du sol érodé. Une série de tests de suffusion a été menée. Les données mesurées pour chaque essai sont: le gradient hydraulique, la conductivité hydraulique, la masse érodée et le changement de volume final. De plus, la densité finale, l'indice des vides global, l'indice des vides intergranulaire et la teneur finale en fines ont été calculés pour tenir compte des modifications de la microstructure du sol. Ces essais ont permis d'étudier l'effet du débit et de la densité initiale sur le processus d'érosion ainsi que les conséquences de ce dernier sur les propriétés mécaniques des sols.

Conséquences de la suffusion sur l'état du sol et sa microstructure

Les essais en laboratoire de suffusion ont été réalisés à différentes densités initiales du sol alors que différentes granulométries initiales ont été considérées pour les simulations numériques. Bien que l'approche numérique n'a pas permis de décrire complètement les résultats expérimentaux, quelques conclusions intéressantes ont été obtenues:

- pour une densité donnée, la masse érodée augmente avec la sollicitation hydraulique (caractérisée expérimentalement par la vitesse de Darcy). Selon l'état des particules érodées (actives ou inactives), le sol peut soit se déformer et se compacter en modifiant significativement le squelette du sol grossier (si les particules actives sont érodées), soit garder son intégrité avec un léger compactage (dans le cas d'érosion de particules inactives);

  Malgré le compactage induit par la suffusion, le sol devient globalement plus lâche et plus perméable (pour tous les cas étudiés: granulométries étroites et plus étalée et densités initiales différentes). Le départ des particules érodées conduit à une augmentation de l'indice de vides global qui ne peut être complètement compensé par le compactage de l'échantillon;

- pour une granulométrie initiale donnée, lorsque l'on considère des états de densité initiale différents, on constate que le compactage du sol devient moins prononcé pendant la suffusion dans le cas d'une densité initiale plus élevée. En d'autres termes, le squelette du sol plus dense est capable de résister à l'érosion des particules fines sans subir de déformation excessive (résultant d'un flambement des chaînes de force).

- pour une granulométrie initiale étroite, le développement de la suffusion pourrait conduire à un milieu très poreux, sans impact sur le squelette grossier et donc sans déformations visibles à l'échelle macroscopique.

Impacts de la suffusion sur le comportement constitutif macroscopique

Après le processus d'érosion, les échantillons de sol ont été soumis à des essais de compression triaxiale monotone pour caractériser l'impact de la suffusion sur le comportement mécanique du sol. Des essais de compression triaxiale drainée et non drainée ont été réalisés dans l'approche expérimentale et seuls des essais de compression triaxiale drainée ont été simulés dans l'approche numérique.

- pour une densité donnée, les résultats expérimentaux montrent que les angles de frottement maximums et résiduels identifiés à l'état drainé diminuent avec la masse érodée. Cela semble s'accompagner d'une légère augmentation de l'angle de dilatance, mais aucune évolution claire de ce dernier avec la masse érodée n'a été identifiée.

  L'interprétation de ces résultats peut être liée à l'effet combiné de l'indice de vides, de l'indice de vides inter-granulaire et de la teneur finale en fines qui contrôle le comportement global du sol. Cependant, l'impact sur l'angle de dilatance est différent dans les résultats numériques et expérimentaux. Numériquement, il y a une cohérence dans les résultats où la perte de la résistance au cisaillement maximale (pour des matériaux suffisamment denses au départ) s'accompagne d'une réduction de l'angle de dilatance. Malgré cette différence, le modèle numérique et les données expérimentales concordent avec la réduction de la rigidité initiale du sol et le comportement moins raide dans la partie d'écrouissage.

  De plus, il y a un décalage à grande déformation (état critique) induit par l'érosion vers des indices des vide globaux plus élevés, mais des indices des vides inter-granulaires plus faibles. Cependant, les résultats expérimentaux et numériques diffèrent quant à l'impact sur la résistance au cisaillement pour les grandes déformations. Numériquement, le déviateur de contrainte à l'état critique n'est pas impacté alors que les résultats expérimentaux montrent une réduction de ce dernier à mesure que la masse érodée augmente. Cette différence peut être liée au modèle qui ne considère pas une micro-structure suffisamment représentative du sol réel (avec probablement une surestimation du nombre de particules flottantes au sein de la fraction fine);

- lorsque l'on considère des densités initiales différentes, l'impact de la suffusion apparaît comme dépendant de la densité: à mesure que la densité initiale augmente, la perte de la résistance au cisaillement augmente également. Les échantillons plus lâches qui se compactent plus significativement lors de la suffusion, peuvent conserver leurs propriétés mécaniques initiales;

- Pour une granulométrie initiale étroite, la suffusion n'impacte pas le squelette grossier et ainsi aucune déformation n'est observée à l'échelle macroscopique. Dans de tels cas, le milieu érodé présenterait une sorte de double comportement atypique: un comportement mécanique typiquement dense à faible déformation en cisaillement, et un comportement très lâche à grandes déformations. Néanmoins, ces résultats numériques ont été obtenus d'une granulométrie dite stable contrairement à celles habituellement sujettes à la suffusion et qui doivent donc être soigneusement pris en compte;

- les conséquences de l'érosion des particules inactives semblent dépendre de la granulométrie initiale du sol. Les sols avec une granulométrie étroite ont montré que si se sont les particules inactives qui sont principalement érodées, alors quasiment aucune déformation ne se produit pendant la suffusion; Cependant, la résistance au cisaillement du sol peut être grandement influencée. En utilisant une granulométrie plus étalée, on a remarqué que l'érosion principalement des particules inactives n'avait que très peu d'influence sur la résistance au cisaillement du sol. En d'autres termes, pour la granulométrie étroite, les particules inactives à l'état initial participent probablement au transfert de force de temps en temps, le long d'un chemin de compression, et jouent un rôle clé, au moins occasionnellement;

- il a été montré numériquement pour les micro-structures considérées que, pour une densité donnée, les processus d'érosion homogènes et hétérogènes conduisent à un comportement mécanique semblable; Une conclusion similaire a été tirée si les particules fines et grossières ont des propriétés mécaniques différentes;

- il a été montré expérimentalement que les sols érodés et non érodés ont les mêmes lignes de transformation de phase/caractéristiques pour des compressions dans des conditions non drainées/drainées, respectivement. De plus, les échantillons de sol érodés présentent la même ligne d'état critique dans les conditions de compression drainées et non drainées, tout comme les échantillons non érodés. Par conséquent, il y a une cohérence entre les résultats drainés et non drainés, respectivement. Cependant, la ligne d'état critique des sols érodés dans le diagramme $q - p'$ est inférieure à celle des sols non érodés;

- une approche pour prédire la réponse mécanique des sols érodés a été proposée. Un paramètre, δ, représentant la variation volumétrique des vides entre les échantillons de sol érodés et non érodés a été défini. Ce paramètre permet d'estimer si le sol érodé sera plus résistant ou non par rapport au sol non érodé. Lorsque δ est supérieur à 0, la résistance au cisaillement des sols érodés serait plus faible que celle du sol non érodé. Lorsque δ est proche ou plus petit que 0, le sol érodé se comporte comme le sol non érodé.

- Les points d'état critique dans les plans $e - \log p'$ et $e_g - \log p'$ montrent une tendance intéressante concernant l'état critique des sols érodés et non-érodés. L'emplacement des points d'état critique des échantillons érodés au-dessus de ceux non-érodés dans le plan $e - \log p'$ implique que la résistance au cisaillement à l'état critique pour un indice de vide global donné augmente avec l'augmentation de l'érosion et la perte de les particules fines. Tandis que, dans le plan $e_g - \log p'$, les points critiques des échantillons érodés sont situés en dessous de ceux des échantillons non érodés, ce qui indique que pour un indice de vide inter-granulaire donné, la résistance au cisaillement à l'état critique diminue avec l'érosion des particules fines; c'est-à-dire la diminution de la teneur en fines. Ces résultats sont en accord avec des études antérieures effectuées sur des échantillons reconstitués avec différentes teneurs en fines.

References

Aboul Hosn, R., Sibille, L., Benahmed, N., & Chareyre, B. (2017). Discrete numerical modeling of loose soil with spherical particles and interparticle rolling friction. *Granular matter, doi:10.1007/s10035-016-0687-0*, *19:4*.

Aparicio, N., & Cocks, A. (1995). On the representation of random packings for sintering simulations. *Acta Metallurgica et Materilia*, *43*, 3873-3884.

Bardet, J. (1994). Observations on the effects of particle rotations on the failure of idealized granular materials. *Mechanics of Materials.*, *18*, 159-182.

Benahmed, N., Canou, J., & Dupla, J.-C. (2004). Structure initiale et propriétés de liquéfaction statique d'un sable. *Compte Rendu Mecanique*, *332*, 887-894.

Benahmed, N., Nguyen, T., Hicher, P., & Nicolas, M. (2015). An experimental investigation into the effects of low plastic fines content on the behaviour of sand/silt mixtures. *European Journal of environmental and civil engineering*, *19*, 109-128.

Bendahmane, F., Marot, D., , & Alexis, A. (2008). Experimental parametric study of suffusion and backward erosion. *J. Geotech. Geoenviron. Eng.*, *134(1)*, 57-67.

Bonelli, S. (2012). *Erosion in geomechanics applied to dams and levees.* ISTE-Wiley.

Bowling, S., Khaeawneh, M., Kaewkuekool, S., & Cho, B. (2009). A logistic approximation to the cumulative normal distribution. *Journal of Industrial Engineering and Management.*, *2*(1), 114-127.

Burenkova, V. (1993). Assessment of suffusion in noncohesive and graded soils. In *1st conf geo-filters, karlsruhe, germany, balkema, rotterdam, the netherlands.*

Calvetti, F., Combe, G., & Lunier, J. (1997). Experimental micromechanical analysis of a 2d granular material: relation between structure evolution and loading path. *Mech. Cohes.-Fric. Matter.*, *2*(2), 121-163.

Calvetti, F., Viggiani, G., & Tamagnini, C. (2003). A numerical investigation of the incremental behavior of granular soils. *Riv.Ital.Geotech*, *3*, 11-29.

Catalano, E., Chareyre, B., & Barthélémy, E. (2014). Pore-scale modeling of fluid-particles interaction and emerging poromechanical effects. *International Journal for Numerical and Analytical Methods in Geomechanics*, *38*(1), 51-71. doi: 10.1002/nag.2198

Chang, C., & Hicher, P. (2005). An elastoplastic model for granular materials with analytical consideration. *International journal of solids and structures.*, *42(2)*, 4258-4277.

Chang, D., & Zhang, L. (2011). A stress-controlled erosion apparatus for studying internal erosion in soils. *Geotechnical Testing Journal.*, *34*, 1-11.

Chang, D., & Zhang, L. (2013a). Critical hydraulic gradients of internal erosion under complex stress states. *J. Geotech. Geoenviron. Eng.*, *139(9)*, 1454-1467.

Chang, D., & Zhang, L. (2013b). Extended internal stability criteria for soils under seepage. *Soils and Foundations.*, *53*(4), 569-583.

Chang, D., Zhang, L., & Xu, T. (2012). Laboratory investigation of initiation and development of internal erosion in soils under complex stress states. In *Icse6 paris* (p. 895-902).

Chapuis, R. (1992). Similarity of internal stability criteria for granular soils. *Canadian Geotechnical Journal.*, *29*(4), 711-713. doi: 10.1139/t92-078

Chareyre, B. (2003). *Modélisation du comportement d'ouvrages composites sol-géosynthétique par élements discrets-application aux ouvrages en tranchées en tête de talus.* (Unpublished doctoral dissertation). Université Joseph Fourier., Grenoble, France.

Chareyre, B., Briançon, L., & Villard, P. (2002). Theoretical versus experimental modeling of the anchorage capacity of geotextiles in trenches. *Geosynth. Int.*, *9(2)*, 97-123.

Chareyre, B., Cortis, A., Catalano, E., & Eric, B. (2012). Pore-scale modeling of viscous flow and induced forces in dense sphere packings. *Transport in porous media.*, *92*, 473-493.

Chareyre, B., & Villard, P. (2005). Dynamic spar elements and discrete element methods in two dimensions for the modeling of soil-inclusion problems. *Journal of Engineering Mechanics*, *131*(7), 689–698. Retrieved from https://yade-dem.org/wiki/File:Chareyre%26Villard2005_licensed.pdf doi: 10.1061/(ASCE)0733-9399(2005)131:7(689)

Chen, Y., Ishibashi, I., & Jenkins, J. (1988). Dynamic shear modulus and fabric: part i, depositional and induced fabric. *Geotechnique*, *38*, 25-32.

Combe, G. (2001). *Origines géométrique du comportement quasi-statique des assemblages granulaires denses: étude par simulations numériques* (Unpublished doctoral dissertation). Ecole nationale des ponts et chaussées.

Crawford-Flett, K. (2014). *An improved hydromechanical understanding of seepage-induced instability phenomena in soil.* (Unpublished doctoral dissertation). The University Of British Columbia.

Cundall, P. (1988). Computer simulations of dense sphere assemblies. *Micromechanics of granular materials.*, *4*, 113-123.

Cundall, P., & Strack, O. (1979). A discrete numerical model for granular assemblies. *Géotechnique*, *29*(1), 47-65.

Dai, B., & Yang, J. (2013). On the physical meaning of the equivalent skeleton void ratio for granular soil with fines. In *Aipp conference proceedings* (p. 257-260).

Dluzewski, J., & Hrabowski, W. (1998). Slope failure at dychow dam - analytical and numerical study of the accident. In *Proccedings of the international symposium on new trends and guidelines on dam safety: New trends and guidelines on dam safety* (p. 925-932). Balkema, Barcelona..

Dutt, M., Hancock, B., Bentham, C., & Elliot, J. (2005). An implementation of granular dynamics for simulating frictional elastic particles based on the dl_poly code. *Computer Physics Communications*, *166*, 26-44.

El Shamy, U., & Denissen, C. (2010). Microscale characterization of energy dissipation mechanisms in liquefiable granular soils. *Computers and Geotechnics*, *37*, 846-857.

Ergun, S. (1952). Fluid flow through packed columns. *Chemical Engineering Science.*, *48*, 89-94.

Estrada, N., Azéma, E., Radjaï, F., & Taboada, A. (2013). Comparison of the effects of rolling resistance and angularity in sheared granular media. *Powder and grains*, *hal-00842799*, 891-894.

Fannin, R., & Moffat, R. (2006). Observations on internal stability of cohesionless soils. *Géotechnique.*, *56*(7), 497-500. doi: 10.1680/geot.2006.56.7.497.

Fell, R., & Fry, J. (2007). The state of the art of assessing the likelihood of internal erosion of embankment dams, water retaining structures and their foundations. *Internal Erosion of Dams and Their Foundations(Taylor & Francis, London)*, 1-23.

Fell, R., MacGregor, P., Stapleton, D., & Bell, G. (2005). *Geotechnical engineering of dams.* Taylor & francis Group, plc, London.

Foster, M., Fell, R., & Spannagle, M. (2000). The statistics of embankment dam failures and accidents. *Canadian Geot.*, *37(5)*, 1000-1024.

Frost, J. (1989). *Studies on the monotonic and cyclic behavior of sands.* (Unpublished doctoral dissertation). West Lafayette: Purdue University.

Gilabert, F., Roux, J.-N., & Castellanos, A. (2007). Computer simulation of model cohesive powders: Influence of assembling procedure and contact laws on low consolidation states. *Physical Review E*, *75, 011303*.

Glowinski, R., Pan, T., Hesla, T., Joseph, D., & Periaux, J. (2001). A fictious domain approach to the direct numerical simulation of incompressible viscous flow past moving rigid bodies: Application to particulate flow. *Journal of computational physics.*, *169*(2), 363-426.

Hama, N. (2016). *Comportement mécanique des sols granulaires et critères de stabilité: application à l'érosion interne.* (Unpublished doctoral dissertation). Université du Havre, 2016.

Hicher, P. (2012). Modelling the behaviour of soil subjected to internal erosion. In *Proceedings of the 6th international conference on scour and erosion.*

Huang, X., Hanley, K., O'Sullivan, C., & Kwok, C. (2014). Exploring the influence of interparticle friction on critical state behavior using DEM. *Int. J. Numer. Anal. Meth. Geomech*, *38(12)*, 1276-1297.

Hvorslev, J. M. (1949). *Subsurface exploration and sampling of soils for civil engineering purposes.* Vicksburg: Waterways Experiment Station.

Indraratna, B., Israr, J., & Rujikiatkamjorn, C. (2015). Geometrical method for evaluating the internal instability of granular filters based on constriction size distribution. *J. Geotech. Geoenviron. Eng.*, *141*(10,04015045).

Indraratna, B., Raut, A., & Khabbaz, H. (2007). Constriction-based retention criterion for granular filter design. *Journal of Geotechnical and Geoenvironmental engineering.*, *133 (3)*, 266-276.

Ishihara, K., Tatsuoka, F., & Yasuda, S. (1975). Undrained deformation and liquefaction of sand under cyclic stresses. *Soils and Foundations.*, *15(1)*, 29-44.

Israr, J., & Rujikiatkamjorn, C. (2016). Laboratory investigation of the seepage induced response of granular soils under static and cyclic loading. *Geotechnical testing journal.*, *39(5)*, 795-812.

Istomina, V. (1957). *Filtration stability of soils.* Gostroizdat, Moscow, Leningrad (in Russia).

Iwashita, K., & Oda, M. (2000). Micro-deformation mechanism of shear banding process based on modified distinct element method. *Powder Technology*, *109(1-3)*, 192-205.

Jerier, I., Richefeu, V., Imbault, D., & Donzé, F.-V. (2010). Packing spherical discrete elements for large scale simulations. *Computer Methods in Applied Mechanics and Engineering.*, *199*(25-28), 1668-1676.

Jiang, M., Konrad, J., & Leroueil, S. (2003). An efficient technique for generating homogeneous specimens for DEM studies. *Computers and Geotechnics*, *30(7)*, 579-597.

Jodrey, W., & Troy, E. (1985). Computer simulation of close random packing of equal spheres. *Physical review A*, *32*, 2347-2351.

Jodrey, W., & Troy, E. (2000). Computer simulations of steepest descent ballistic deposition. *Colloids and Surfaces A: Physicochemical and Engineering Aspects.*, *165*, 405-422.

kafui, K., Thorton, C., & Adams, M. (2002). Discrete particle-continuum fluid modeling of gas-solid fluidized beds. *Chemical Engineering Science.*, *57*(13), 2395-2410.

Ke, L., & Takahashi, A. (2012a). Influence of internal erosion on deformation and strength of gap-graded non-cohesive soil. In *International conference of scour and erosion, icse.*

Ke, L., & Takahashi, A. (2012b). Strength reduction of cohesionless soil due to internal erosion induced by one-dimensional upward seepage flow. *Soils and Foundations.*, *52*, 698-711.

Ke, L., & Takahashi, A. (2014a). Experimental investigations on suffusion characteristics and its mechanical consequences on saturated cohesionless soil. *Soils and Foundations.*, *54*, 713-730.

Ke, L., & Takahashi, A. (2014b). Triaxial erosion test for evaluation of mechanical consequences of internal erosion. *Geotechnical Testing Journal.*, *37*, 1-18.

Kenney, T. (1977). Residual strength of mineral textures. In *The 9th icsmfe* (Vol. 1).

Kenney, T., Chiu, E., & Ofoegbu, C., G. Ume. (1985). Controlling constriction sizes of granular filters. *Canadian Geotechnical Journal.*, *22*, 32-43.

Kenney, T., & Lau, D. (1985). Internal stability of granular filters. *Canadian Geotechnical Journal.*, *22(2)*, 215-225. doi: 10.1139/t85-029

Kenney, T., & Lau, D. (1986). Internal stability of granular filters. *Reply. Canadian Geotechnical Journal.*, *23(3)*, 420-423. doi: 10.1139/t86-068

Kezdi, A. (1979). Developments in geotechnical engineering. In *Soil physics (selected topics), elsevier science ltd. amesterdam, netherlands.*

Kovacs, G. (1981). *Seepage hydraulic.* Elsevier Scientific Publishing Co, Amsterdam.

Kozicki, J., & Tejchman, J. (2011). Numerical simulations of sand behaviour using DEM with two different descriptions of grain roughness. In *Ii international conference on particle-based methods – fundamentals and applications, particles.*

Kozicki, J., Tejchman, J., & Leśniewska, D. (2013). Study of some micro-structural phenomena in granular shear zones. In *Powder and grains, aip conference proceeding* (Vol. 1542, p. 495-498).

Lade, P. (1992). Static instability and liquefaction of loose fine sandy slopes. *Journal of Geotechnical Engineering.*, *118(1)*, 51-71.

Lade, P., & Ibsen, L. (1997). A study of the phase transformation and the characteristic lines of sand behavior. In *In international symposium on deformation and progressive failure in geomechanics, pages 353-359, nagoya, japan.*

Lee, S., Hashash, Y., & Nezami, E. (2012). Simulation of triaxial compression tests with polyhedral discrete elements. *Computers and Geotechnics*, *43*, 92-100.

Li, M. (2008a). *Seepage induced instability in widely graded soils.* (Unpublished doctoral dissertation). The University of British Columbia.

Li, M. (2008b). *Seepage induced instability in widely graded soils.* (Unpublished doctoral dissertation). The University of British Columbia.

Li, M., & Fannin, J. (2008). Comparison of two criteria for internal stability of granular soil. *Canadian Geotechnical Journal.*, *45*, 1303-1309.

Locke, M., & Indraratna, B. (2001). Time-dependent particle transport through granular filters. *Journal of Geotechnical and Geoenvironmental Engineering.*, *127*, 521-529.

Lominé, F., Sholtés, L., Sibille, L., & Poullain, P. (2013). Modeling of fluid-solid interaction in granular media with coupled lattice boltzmann/discrete element methods: application to piping erosion. *International Journal of Numerical and Analytical Methods in Geomechanics.*, *37*(6), 577-596.

Luong, M. (1982). Stress-strain aspects of cohesionless soils under cyclic and transient loading. In *In international symposium on soils under cyclic and transient loading, pages 315-324, swansea, wales.*

Maeda, K., Muir Wood, D., & Kondo, A. (2012). Micro and macro modeling of internal erosion and scouring with fine particle dynamics. In *Icse6.*

Marot, D., Bendahmane, F., Rosquoet, F., & Alexis, A. (2009). Internal flow effects on isotropic confined sand-clay mixtures. *Soil & sediments Contamination*, *18*, 294-306.

Marot, D., Le, V., Garnier, J., Thorel, L., & Audrain, P. (2012). Study of scale effect in an internal erosion mechanism. *European Journal of Environmental and Civil Engineering.*, *16*, 1-19.

Marot, D., Regazzoni, P., & Wahl, T. (2011). Energy based method for providing soil surface erodibility rankings. *Journal of Geotechnical and Geoenvironmental Engineering.*, *137*, 1290-1294.

Moffat, R., & Fannin, R. (2006). A large permeameter for study of internal stability in cohesionless soils. *Geotechnical Testing Journal*, *29*(4), 273-279.

Moffat, R., & Fannin, R. (2011). A hydromechanical relation governing internal instability in cohesionless soils. *Canadian Geotechnical Journal*, *48*(3), 413-424. doi: 10.1139/ T10-070

Moffat, R., Fannin, R., & Garner, S. (2011). Spatial and temporal progression of internal erosion in cohesionless soil. *Canadian Geotechnical Journal*, *48*, 399-412. doi: 10.1139/T10-071

Mueller, G. (2005). Numerically packing spheres in cylinders. *Powder Technology.*, *159*, 105-110.

Muir Wood, D., & Maeda, K. (2007). Changing grading of soil: effect on critical states. *Acta Geotechnica.*, *3*, 3-14.

Muir Wood, D., Maeda, K., & Nukudani, E. (2008). Discrete element modelling of soil erosion. In *Fourth international conference on scour and erosion.*

Muir Wood, D., Maeda, K., & Nukudani, E. (2010). Modelling mechanical consequences of erosion. *Geotechnique.*, *60(6)*, 447-457.

Naieni, S., & Bazier, M. (2004). Effect of fines content on steady-state strength of mixed and layered samples of a sand. *Soil Dynamics and earthquake engineering.*, *24*, 181-187.

Nguyen, C., Benahmed, N., Andò, E., Sibille, L., & Philippe, P. (2017). Experiment investigation of micro-structural changes of eroded soil by suffusion using x-ray tomography. In *The ph.d. student's day - ed 353, aix-marseille university.*

Nguyen, T. (2014). *Etude experimentale du comportement instable d'un sable silteux: application aux digues de protection.* (Unpublished doctoral dissertation). Universite d'Aix-Marseille.

Oda, M. (1977). An experimental investigation into the effects of low plastic fines content on the behavior of sand/silt mixtures. *European Journal of Environmental and Civil Engineering.*, *19*(1), 109-128.

Oda, M., & Iwashita, K. (2000). Study on couple stress and shear band development in granular media based on numerical simulation analyses. *International Journal of Engineering Sciences*, *38(15)*, 1713-1740.

Oda, M., Konishi, J., & Nemat-Nasser, S. (1982). Experimental micromechanical evaluation of strength of granular materials: Effects of particle rolling. *Mechanics of Materials*, *1(4)*, 269-283.

Papamichos, E., Vardoulakis, I., Tranvoll, J., & SKaejrstein, A. (2001). Volumetric sand production model and experiment. *Int. J. Numer. Analyt. Meth. Geomech.*, *25*.

Perzlmier, S. (2007). *Hydraulic criteria for internal erosion in cohesionless soil. in internal erosion of dams and their foundations.* Editors R. Fell and J.J. Fry. Taylor & Francis.

Plassiard, J.-P., Belheine, N., & Donzé, F.-V. (2009). A spherical discrete element model: calibration procedure and incremental response. *Granular Matter*, *11(5)*, 293-306.

Polito, C. (1999). *The effects of non-plastic fines on the liquefaction of sandy soils.* (Unpublished doctoral dissertation). Virginia Polytechnic Institute and State University.

Potapov, A., Hunt, M., & Campbell, C. (2001). Liquid-solid flows using smoothed particle hydrodynamics and the discrete element method. *Powder Technology.*, *116*(2-3), 204-213.

Radjaï, F., & Dubois, F. (2011). *Discrete-element modeling of granular materials.* ISTE Ltd and John Wiley & Sons.

Rahman, M., & Lo, S. (2007). Liquefaction potential and undrained fragility of silty soils. In *The 16th south east asian geotechnical conference.*

Raut, A. (2006). *Mathematical modelling of granular filters and constriction-based filter design criteria.* (Unpublished doctoral dissertation). University of Wollongong., Wollongong, Australia.

Raut, A., & Indraratna, B. (2008). Further advancement in filter criteria through constriction-based techniques. *Journal of Geotechnical and Geoenvironmental Engineering*, *134(6)*, 833-887.

Reboul, N. (2008). *Transport de particules dans les milieux granulaires.* (Unpublished doctoral dissertation). Ecole Centrale de Lyon.

Reboul, N., Vincens, E., & Combou, B. (2010). A computational procedure to assess the distribution of constrictions sizes for an assembly of spheres. *Comput. Geotech.*, *37*, 195-206.

Reddi, L., Lee, I., & Bonala, M. (2000). Comparison of internal and surface erosion using flow pump test on a sand-koalinite mixture. *Geotech. Testing J., 23*(1).

Richards, K., & Reddy, K. (2007). Critical appraisal of piping phenomena in earth dams. *Bull. Eng. Geol. Environ., 66*, 381-402.

Roux, J.-N., & Chevoir, F. (2005). *Discrete numerical simulation and the mechanical behavior of granular materials. Bulletin des laboratoires des ponts et chaussées – n 254.*

Roux, J.-N., & Combe, G. (2010). How granular materials deform in quasistatic conditions. In *Iutam-isimm symposium on mathematical modeling and physical instances of granular flow. aip publishing.* (Vol. 1227(1), pp. 260–270).

Sail, Y., Marot, D., Sibille, L., & Alexis, A. (2011). Suffusion tests on cohesionless granular matter. *European Journal of Environmental and Civil Engineering., 15*, 799-817.

Salot, C., Gotteland, P., & Villard, P. (2009). Influence of relative density on granular materials behavior: DEM simulations of triaxial tests. *Granular Matter, 11(4)*, 221-236.

Sanchez, R., Strutynsky, A., & Silver, M. (1983). *Evaluation of the erosion potential of embankment core materials using the laboratory triaxial erosion test procedure.* Technical report GL-83-4, Army Engineer Water-ways Experiments Station, Geotechnical Lab, Vicksburg, MS.

Sari, H., Chareyre, B., Catalano, E., Philippe, P., & Vincens, E. (2011). Investigation of internal erosion process using a coupled dem-fluid method. In *Ii international conference on particle-based methods − fundamentals and applications, particles.*

Schneider, H. R., Chameau, J.-L., & Leonards, G. A. (1989). Chemical impreganation of cohesionless soils. *Geotechnical Testing Journal., 12*(3), 204-210.

Scholtès, L., Hicher, P., & Sibille, L. (2010). Multiscale approaches to describe mechanical responses induced by particle removal in granular materials. *Comptes Rendus Mécanique., 338*, 627-638.

Seed, H., & Duncan, J. (1987). The failure of teton dam. *Engineering Geology., 24*(1-4), 173-205.

Shire, T., & O'Sullivan, C. (2013). Micromechanical assessment of an internal stability criterion. *Acta Geotechnica, DOI:10.1007/s11440-012-0176-5, 8*, 81-90.

Shire, T., O'Sullivan, C., & Hanley, K. (2015). The influence of finer fraction and size-ratio on the micro-scale properties of dense bimodal materials. In *Geomechanics from micro to macro* (p. 231-236). London.

Shire, T., O'Sullivan, C., Hanley, K., & Fannin, R. (2014). Fabric and effective stress distribution in internally unstable soils. *Journal of Geotechnical and Geoenvironmental Engineering., 140(12), 04014072.*.

Sibille, L. (2016). Erosion interne et rupture dans les sols grenus, habilitation á diriger des recherches. universités grenoble alpes, grenoble, france.

Sibille, L., Marot, D., & Sail, Y. (2015). A description of internal erosion by suffusion and induced settlements on cohesionless granular matter. *Acta Geotechnica.*, *10(6)*, 735-748.

Sibille, L., Villard, P., Darve, F., & Aboul Hosn, R. (2017). Quantitative prediction of discrete element models on complex loading path. *Under preparation.*.

Silveira, A. (1965). An analysis of the problem of washing through in protective filters. In *Proceedings of the sixth international conference on soil mechanics and foundation engineering, vol. 2; 1965.*

Skempton, A., & Brogan, J. (1994). Experiments on piping in sandy gravels. *Geotechnique*, *44 (3)*, 449-460.

Slangen, P. (2015). *On the influence of effective stress and micro-structure on suffusion and suffosion.* (Unpublished doctoral dissertation). The University Of British Columbia.

Stewart, R., & Watts, B. (2000). The wac bennett dam sinkhole incident. In *Proceedings 53rd canadian geotechnical conference, montreal, canada.*

Suhr, B., & Six, K. (2016). On the effect of stress dependent interparticle friction in direct shear tests. *Powder Technology*, *294*, 211-220.

Szarf, K., Combe, G., & Villard, P. (2011). Polygons vs. clumps of discs: A numerical study of the influence of grain shape on the mechanical behaviour of granular materials. *Powder Technology*, *208(2)*, 279-288.

Tejada, I., Sibille, L., & Chareyre, B. (2016). Role of blockages in particle transport through homogeneous granular assemblies. *EPL*, *115*(5), 54005. doi: 10.1209/0295-5075/115/54005

Terzaghi, K. (1939). Soil mechanics: a new chapter in engineering science. *J. Instn. Civ. Engrs*, *12*, 106-141.

Terzaghi, K., & Peck, R. (1948). *Soil mechanics in engineering practice.* 1st edition John Wiley and Sons, New York.

Thevanayagam, S. (1998). Effects of fines and confining stress on undrained shear strength of silty sands. *Journal of Geotechnical and Geoenvironmental Engineering.*, *124(6)*, 479-491.

Thevanayagam, S. (2000). Liquefaction potential and undrained fragility of silty soils. In *Proceedings of the 12th world conference on earthquake engineering.* (p. Paper 2383). New Zealand.

Thornton, C. (2000). Numerical simulations of deviatoric shear deformation of granular media. *Géotechnique*, *50(1)*, 43-53.

Thornton, C., & Antony, S. (1998). *Philos. trans.* R. Soc. London A 356.

Ting, J., Corkum, B., Kauffman, C., & Greco, C. (1989). Discrete numerical model for soil mechanics. *J Geotech Eng*, *115(3)*, 379-398.

Tong, A.-T., Catalano, E., & Chareyre, B. (2012). Pore-scale flow simulations: Model predictions compared with experiments on bi-dispersed granular assemblies. *Oil & Gas Science and Technology – Revue IFP Energies nouvelles*, *67(5)*, 743-752.

Vallejo, L. (2001). Intergranular of the limits in shear strength in binary granular mixtures. *Ganadian Geotechnical Journal.*, *38*, 1097-1104.

Vincens, E., Reboul, N., & Cambou, B. (2012). *The process of filtration in granular materials.* Bonelli, S. (Ed.), Erosion of Geomaterials, Chapter 3. ISTE-Wiley, London, UK, pp. 81-111.

Vincens, E., Witt, K., & Homberg, U. (2014). Approaches to determine the constriction size distribution for understanding filtration phenomena in granular materials. *Acta Geotechnca, online first published 2014. DOI: 10.1007/s11440-014-0308-1*.

Vogel, H.-J., & Roth, K. (2001). Quantitative morphology and network representation of soil pore structure. *Advances in Water Resources.*, *24*, 233-242.

Voivret, C., Radjai, F., Delenne, J. Y., & El Youssoufi, M. S. (2009). Multiscale force networks in highly polydisperse granular media. *Physical review letters.*, *102*, 178001.

Šmilauer, V., et al. (2015a). Reference manual. In *Yade Documentation 2nd ed.* The Yade Project. (http://yade-dem.org/doc/) doi: 10.5281/zenodo.34045

Šmilauer, V., et al. (2015b). *Yade Documentation 2nd ed.* The Yade Project. (http://yade-dem.org/doc/) doi: 10.5281/zenodo.34073

Wan, C. (2006). *Experimental investigations of piping erosion and suffusion of soils in embankment dams and their foundations.* (Unpublished doctoral dissertation). School of civil and environmental engineering, University of new south wales.

Wan, C., & Fell, R. (2004). Investigation of the rate of erosion of soils in embankment dams. *Journal of Geotechnical and Geoenvironmental Engineering.*, *130(4)*, 373-380.

Wan, C., & Fell, R. (2008). Assessing the potential of internal instability and suffusion in embankment dams and their foundations. *J. Geotech. Eng. ASCE.*, *134*(3), 401-407.

Wang, X., & Li, J. (2014). Simulation of triaxial response of granular materials by modified DEM. *Science China: Physics, Mechanics and Astronomy.*, *57(12)*, 2297-2308.

Wautier, A., Bonelli, S., & Nicot, F. (2017). Micromechanical modelling of suffusion: Towards the stability analysis of hydraulic structures. In *Proceedings of the 11th international workshop on bifurcation and degradation in geomaterials, limassol, cyprus.*

Westman, A., & Hugill, H. (1930). The packing of particles. *Journal of American Ceramic Society.*, *13(10)*, 767-779.

White, D. (2002). *An investigation into the behavior of pressed-in piles.* (Unpublished doctoral dissertation). University Of Cambridge.

Widuliński, L., Kozicki, J., & Tejchman, J. (2009). Numerical simulations of triaxial test with sand using DEM. *Archives of Hydro-Engineering and Environmental Mechanics*, *56(3-4)*, 149-171.

Xiao, M., & Shwiyhat, N. (2012). Experimental investigation of the effects of suffusion on physical and geomechanic characteristics of sandy soils. *Geotechnical Testing Journal.*, *35*, 1-11.

Yin, Z., Zhao, J., & Hicher, P. (2014a). A micromechanics-based model for sand-silt mixtures. *International journal of solids and structures.*, *51*, 1350-1363.

Yin, Z., Zhao, J., & Hicher, P. (2014b). A micromechanics-based model for sand-silt mixtures. *International journal of solids and structures.*, *51*, 1350-1363.

Zeghal, M., & El Shamy, U. (2004). A continuum-discrete hydromechanical analysis of granular deposit liquefaction. *Int. J. Numer. Anal. Meth. Geomech.*, *28*, 1361-1383. doi: 10.1002/nag.390

Zhang, L., & Chen, Q. (2006). Seepage failure mechanism of the gouhou rockfill dam during reservoir water infiltration. *Soils and Foundations*, *46*, 557-568.